2016-01-01

A Cracking Methodology to Assess Fracture and Fatigue Properties of Asphalt Concrete Mixtures using Overlay Tester

Victor M. Garcia
University of Texas at El Paso, vmgarcia5@miners.utep.edu

A CRACKING METHODOLOGY TO ASSESS FRACTURE AND FATIGUE PROPERTIES OF ASPHALT CONCRETE MIXTURES USING OVERLAY TESTER

VICTOR M GARCIA

Master's Program in Civil Engineering

APPROVED:

Soheil Nazarian, Ph.D., Chair

Imad Abdallah, Ph.D., Co-Chair

Calvin Stewart, Ph.D.,

Charles Ambler, Ph.D.
Dean of the Graduate School

Dedication

I dedicate this thesis work to my grandmother, Margarita Fuentes de Villota, and my parents, Victor Garcia and Teresa Villota. Their values and sacrifice have resonated onto blessings and opportunities for my family, and myself.

A CRACKING METHODOLOGY TO ASSESS FRACTURE AND FATIGUE PROPERTIES OF ASPHALT CONCRETE MIXTURES USING OVERLAY TESTER

by

VICTOR M GARCIA, BSCE, EIT

THESIS

Presented to the Faculty of the Graduate School of

The University of Texas at El Paso

in Partial Fulfillment

of the Requirements

for the Degree of

MASTER OF SCIENCE

Department of Civil Engineering

THE UNIVERSITY OF TEXAS AT EL PASO

August 2016

Acknowledgements

First and above all, I praise God, the almighty for providing me this opportunity and granting me the capability to proceed successfully. This thesis appears in its current form due to the assistance and guidance of several people whom I would like to offer my sincere gratitude.

I would like to express my gratitude to Dr. Soheil Nazarian and Dr. Imad Abdallah for their invaluable guidance and mentorship during my undergraduate and graduate years at the Center for Transportation Infrastructure Systems (CTIS). As a young civil engineering student they gave me the opportunity to join the research team at CTIS and acquire research experience and opportunities that cemented my passion for geotechnical/pavement engineering. I greatly appreciate them for allowing me the opportunity to work on of TxDOT Project 0-6815 upon which this thesis work is founded on. I would like to extend my gratitude to Robert Lee and Gisel Carrasco from the Texas Department of Transportation (TxDOT) - Flexible Pavement Branch for their guidance and support during the research work performed under this project. Further, I would like to express my appreciation to Dr. Soheil Nazarian, Dr. Imad Abdallah, and Dr. Calvin Stewart for serving as committee members for this these defense, and for their valuable feedback and support.

I also appreciate the financial support from the National Science Foundation under Grant #10-60-113 and thank Dr. Carlos Ferregut for giving me the opportunity to join the NSF program at UTEP. Gratitude is also extended to Luisa Mendoza for her assistance with the NSF scholarship.

My deepest gratitude is also expressed to my colleagues from CTIS, especially Jose Garibay, Jose Rodriguez, Mauricio Valenzuela, Carlos Anguiano, Daniel Arguelles, Paulette Lugo and Luiza Barros for the great experiences and support during my time at CTIS. Another teammate and good friend I would like to acknowledge is my project colleague Alejandro Miramontes.

I warmly thank and profoundly appreciate my parents and lovely sisters, Christina and Elizabeth Garcia for their unconditional support and continuous encouragement. This accomplishment would not have been possible without them.

Abstract

Several highway agencies have either implemented or considered implementing performance tests to predict the cracking potential of asphalt concrete (AC) mixtures in the laboratory setting. One such test, the Overlay Tester (OT) test, measures the number of cycles to failure of the AC specimens by simulating the opening and closing of the cracks induced by daily temperature variations and high tensile strain generated by the traffic load. The variability of the OT test results is expressed as a major concern in reliably characterizing the cracking potential of the AC mixes.

The performance of the OT test, in general, and current performance index, in particular, were evaluated in this study. The consistency of the current performance index and potential parameters that can be measured from the OT was comprehensively investigated with two different AC mix types. A cracking methodology and performance indices were implemented considering the crack initiation and propagation phases of the OT test. The consistency and repeatability of the proposed performance indices, critical fracture energy and crack progression rate, seem to be better than the acceptable repeatability level defined as a coefficient of variation (COV) of less than 20%. The proposed cracking methodology and preliminary failure limits seem to characterize and discriminate satisfactorily the cracking resistance of several AC mix types commonly used in Texas. A parametric study using synthetic specimens was conducted on key variables (e.g., glue type and gluing method) considered in the current OT specifications (Tex-247-F) to improve the specimen preparation and testing processes. The improved OT test method was preliminarily validated with OT tests on field cores from pavement sections with known field performance. Given its promise in this study, the improved OT test method is recommended as a routine test during the mix-design process of AC mixes.

Table of Contents

List of Tables

List of Figures

Chapter 1: Introduction

The accumulation of damage due to premature cracking of hot mix asphalt (HMA) layers is a major concern with the performance of flexible pavements. An AC layer must have a balance of both good rut and crack resistance properties to perform well in the field *(Zhou et al., 2006)*. With the adaption of the Hamburg wheel-tracking device (HWTD) over the past decade, many AC mixes have been modified to improve their rutting potential. The use of stiffer binders may improve the rutting resistance of AC mixes but they may also reduce the mix flexibility and cracking resistance of the HMA mixes *(Zhou et al. 2005)*. This distress is even further aggravated by the current sustainable measures such as the inclusion of reclaimed asphalt pavement (RAP) and recycled asphalt shingles (RAS). The implementation of performance tests during the mix design stage in the laboratory setting is crucial to balance the mixes' rutting and cracking potentials and to minimize the premature failure of flexible pavements.

Several performance crack tests have been proposed for routine application to assess the cracking resistance of AC mixtures in the laboratory setting (*Monismith and Coetzee, 1980; Buttlar and Roque, 1994; Witczak et al., 2002; Wagoner et al., 2005; Perez-Jimenez et al., 2011; Al-Qadi et al., 2015*). The indirect tensile (IDT) test, the semi-circular bending (SCB) test, the disk-shape compact tension (DCT) test and four point bending test are some examples of available tests to evaluate the fatigue and cracking characteristics of mixes. One such popular test, the overlay tester (OT), measures the number of cycles to failure of specimens by simulating the opening and closing of joints and/or cracks induced by daily temperature variations and tensile strain generated by the traffic load. Although the OT seems to simulate effectively the cracking mechanism of the AC mixes, the repeatability of the number of cycles to failure used as a

performance index is expressed as a major concern in reliably characterizing these mixes. The use of OT to measure the resistance to cracking reliably and in a robust manner is needed for all mixture types and AC specifications.

A great deal of effort has been directed toward improving the characterization of the cracking potential of AC mixes *(Monismith and Deacon, 1969; Jacobs et al., 1996; Medani and Molenaar, 2000; Marasteanu et al., 2002; Daniel and Kim., 2002; Ghuzlan and Carpenter, 2003; Wagoner et al., 2005; Hajj et al., 2008; Elseifi et al., 2012; Jimenez et al., 2012; Yi-Qiu et al., 2012).* This study was performed to investigate the consistency of the number of cycles to failure as a cracking parameter and evaluate the performance of the OT to implement an improved cracking methodology and potential cracking parameters that can reliably predict and screen the well and poor performing mixes. The cracking properties of an AC mix can be characterized in two stages: a) crack initiation and b) crack propagation. A cracking methodology and performance indices were implemented for the OT considering these two stages. The proposed cracking methodology and performance indices were investigated using several AC mixes to examine its applicability and effectiveness on all types of AC mixes. The improved OT test method was preliminarily validated with OT tests on field cores from pavement sections with known field performance. The ultimate goal is to implement a consistent and reliable crack test that can be routinely performed to assess the cracking potential of AC mixes during the mix-design process.

1.1 BACKGROUND

Premature cracking occurs due to the tensile stresses imposed by traffic loads exceeding the tensile strength of the AC layers. The moisture damage and climatic effects also significantly influence the performance of the AC layers in the field. Premature cracking continues to be a recurring problem for the pavement community especially with the aging of the surface layer in

the existing pavements and the intricacy of the new mix designs that utilize more additives and recycled materials. Agencies in the US and worldwide have implemented testing procedures and empirical relationships to predict the cracking properties of AC mixes from conventional material parameters, such as the tensile strength and modulus *(Wagoner et al., 2005)*. At present, a single widely accepted laboratory test that can be performed routinely to evaluate the cracking susceptibility has not been established. A testing procedure and thorough specifications are required during the mix design to ensure the desired cracking performance of flexible pavements.

The OT was first introduced by Germann and Lytton *(1979)* to predict the reflective cracking resistance of asphalt overlays on long beam specimens. Zhou and Scullion *(2003)* upgraded and standardized the original OT test procedure. They proposed to modify the specimen's dimensions for testing laboratory prepared specimens and field cores. The results from the modified test setup were validated with field observations and OT results from field cores. Zhou and Scullion *(2005)* evaluated the data obtained from the OT test using two approaches. First approach was based on the change in the response of material to constant displacement (called "loading shape method"). The other alternative was based on the reduction in the maximum load. In the loading shape method, three distinct phases were observed: (I) crack initiation and steady propagation, (II) late crack propagation, and (III) failure. The other alternative was based on the reduction in the maximum load. In the loading shape method, three distinct phases were observed: (I) crack initiation and steady propagation, (II) late crack propagation, and (III) failure. For the reduction in the maximum load method, the number of cycles was established as the performance parameter. The number of cycles is currently obtained at the 93% reduction in load from the maximum load of the first cycle. This criterion was proposed based on the performance of 200 specimens from different AC mixes. They concluded that asphalt mixtures that achieve a 93% load

reduction after 300 load cycles were resistant to cracking. Zhou et al. (2005) recommended using the OT test in conjunction with the Hamburg wheel tracking device to design asphalt mixes with adequate reliability against rutting and cracking resistance.

Several traditional cracking models have been used to explain the crack growth mechanism in AC layers *()*. Linear fracture mechanics and continuum damage mechanics frameworks have been explored to characterize the crack growth mechanisms *(Jacobs et al., 1995; Zhang et al., 2001; Roque et al., 2002; Ghuzlan and Carpenter, 2003; Zhou et al., 2009; Koohi et al., 2012).* Zhou et al. *(2009)* further modified the OT to measure the fatigue cracking resistance of mixes based on the principles of fracture mechanics. A backcalculation method was proposed to estimate the crack length and fracture parameters A and n. Hu et al. *(2012)* presented the required modifications to the present OT to measure the cracking properties. The enhancement was incorporated to characterize the Mode I (bending or tensile mode) type of fracture in the asphalt mixtures due to repeated loads and to measure the modulus of asphalt mixtures under tensile mode. The backcalculated crack length depended on the calibration with actual measurements using digital image correlation (DIC) technique that might increase the variability in the estimated parameters due to different mixture types, binder types and volumetric properties.

Zhou and Scullion *(2003)* performed a sensitivity study to analyze the influence of the operational parameters such as the test temperature, opening displacement, air voids, asphalt performance grade, and asphalt content, on the variability of the results. They found the OT results are sensitive to key components of the mixtures such as the grade of asphalt binder, asphalt binder content, air voids, and aggregate properties. Walubita et al. *(2012)* studied comprehensively a number of parameters that could influence the repeatability of the OT results, especially for coarse and dense-graded mixes. They noted that one of the key problems contributing to the reported high

variability in the OT test results was related to non-adherence to the specifications and OT test procedures. They also concluded that, aside from the AC mix response behavior, the variability in the OT test might be a function of the sample fabrication and test setup. Recommendations were given for the gluing method, sample drying method, curing time prior to testing, and the sample conditioning time to reduce the variability in the results.

The specimen preparation process require cutting and gluing. The preparation of OT specimens may be a source of variability to the OT results if a detailed preparation process is not consistently followed. Garcia and Miramontes (*2015*) evaluated several key steps outlined on the current Tex-248-F overlay tester test procedure using synthetic specimens to minimize the uncertainties from the material-related variability. Recommendations for the amount of glue, glue curing time and amount of torque were provided. Although those studies helped to improve the OT procedure, the variability of the number of cycles measured with the OT test to reliably determine the cracking resistance of AC specimens in the laboratory setting is still a concern.

Walubita et al. *(2013)* proposed a monotonic test protocol with OT to screen and rank mixes similar to Fenix and indirect tensile tests. The fracture energy and fracture energy index were recommended to distinguish the fracture resistance of the AC mixes. A parametric sensitivity analysis was carried out to compare the variability as compared to the repeated load OT test. They concluded that the fracture energy index could be used to rank the mixtures with less variability in comparison to the standard OT procedure.

The OT test has shown promising potential to predict the cracking potential of AC mixes in the lab and satisfactory correlation with the field performance of those AC mixes (*Bennert and Maher, 2008; Bennert et al., 2009; and Hajj et al., 2010*). A recent study by Walubita et al. (*2012*) documented that the COV for OT results is roughly 30%, especially for dense-graded mixes which

in fact have been used extensively on flexible pavements. Garcia and Miramontes (*2015*) investigated the variability of the number of cycles to failure using a large amount of OT results from a commonly used dense-graded mix. The variability of the number of cycles to failure was significantly high in this study. The high variability of the number of cycles to failure measured with the OT test has been the difficulty to reliably adopt the OT test as a routine cracking performance test.

Monismith and Cotzee (1980) commented that the reflection cracking mechanism is affected mainly by the stress concentrations at the bottom of the AC layer that might lead to crack initiation and propagation. The crack initiation and propagation depend on the material, geometry and load levels. At low load/ displacement levels, the energy is expended in nucleating cracks rather than propagating them. At high load/displacement levels, plastic deformation takes place rapidly leading to failure (Pugno et al., 2006). The loading conditions of the OT and response of AC specimens under the OT test must be further analyzed to delineate the cracking mechanism of OT test and potential performance indicators that can improve the applicability and repeatability of OT to all types of AC mixtures.

In summary, there has been extensive research effort to characterize the crack initiation and the crack propagation of AC specimens using OT. The direct measurement of fracture and fatigue parameters has become important in evaluating the cracking potential of AC mixtures. At present, no single widely accepted laboratory test has been established. The development of a valid performance test suitable for characterizing cracking potential of AC mixes is considered as indispensable step to improve the performance of flexible pavements.

1.2 STUDY METHODOLOGY AND OBJECTIVES

The main goal of this thesis study is to propose an improved test methodology for OT so that in a timely manner and with less variability in the results not only rank the cracking potential of all AC mixes but also provide parameters that can assess the cracking properties of the AC mixes. A systematic study was conducted to gain in depth understanding of the key issues related to OT. To achieve the goal of this study, the technical objectives can be summarized in the following items:

- Conduct a critical evaluation of OT test to evaluate the variability of the number of cycles to failure and the current performance of OT with additional emphasis given to dense-graded mixes due to the high variability reported in the past studies.
- Investigate various promising fracture and cracking parameters that can be measured from OT to develop a cracking methodology that considers the crack initiation and propagation phases of OT.
- Evaluate a large amount of different AC mix types to assess the effectiveness of the proposed methodology in predicting and screening the well and poor performing mixes.
- Propose an improved OT method and specifications that address the following constraints:
  - repeatable to an acceptable level,
  - can provide fatigue and cracking properties,
  - practical, reliable, and easily implementable, and
  - applicable for all AC mix types.

Chapter 2: Critical Evaluation of Overlay Tester and Current Performance Index

2.1 OVERLAY TESTER

Detailed information about the OT test procedure is outlined in the TxDOT test procedure Tex-248-F, which is similar to the ASTM WK26816 protocol. The test is conducted in a displacement-controlled mode at a repeated loading rate of one cycle per 10 sec. The sliding platen moves in a cyclic triangular waveform to a constant maximum displacement of 0.025 in. (635 µm) at a test temperature of 77ºF (25ºC). The primary output of the OT test is the number of cycles of applied load. Zhou et al. (2006) defined the specimen as failed when the maximum load the specimen experienced at a given cycle was 93% less than the maximum peak load from the first cycle. As such, the number of cycles to failure is the number of cycles when the failure criterion is achieved. Alternatively, the test is discontinued when a preset number of cycles is reached. They suggested a pass/fail limit of 300 or more number of cycles for AC mixtures with satisfactory cracking performance.

Figure 2.1 shows the key components of an OT specimen mounted onto the base plates. The OT specimens are nominally 6 in. (150 mm) long, 3 in. (75 mm) wide and 1.5 in. (38 mm) thick. The specimens are trimmed from the standard 6 in. (150 mm) diameter by 4.5 in. (114 mm) thick specimens compacted with a Superpave gyratory compactor (SGC) in accordance with the Tex-241-F (ASTM D-6925) protocol to a nominal target air voids of 7±1.0%. The OT specimens can also be prepared from field cores or slabs. The specimens are glued to the two horizontal platens with half of the length of the specimen resting on each platen. The accumulation of the glue in the gap between the base plates (marked as “a” in Figure 2.1) and the uniformity of the

glued area (marked as “b”) could be potential sources of variability. As described by Garcia and Miramontes (2015), a linear variable differential transformer (LVDT) was added to the test setup (marked as “c”) to ensure that the specimens do not experience significant bending since the OT load is applied eccentric to the neutral axis of the specimen.

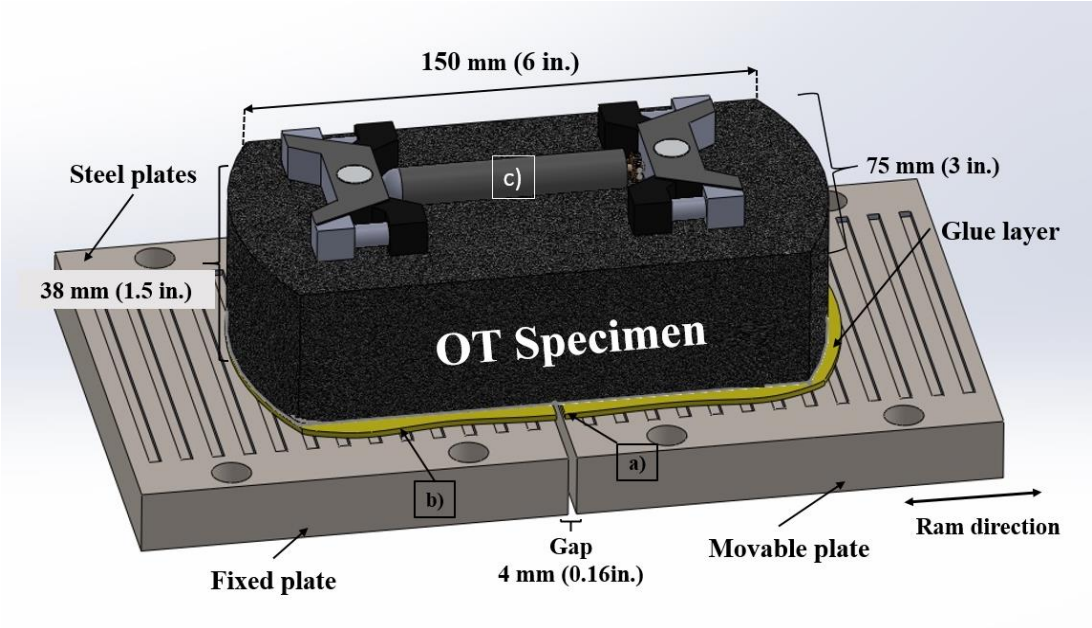

Figure 2.1 OT Schematic Layout and Sample Setup

During the OT test, the device automatically records the time histories of the applied load, the actuator displacement, the top LVDT displacement (if installed), the number of cycles, and the test temperature. Figure 2.2a shows the typical data obtained from the OT test. The displacement and load acquired for each cycle can be plotted against one another to inspect the hysteretic behavior (load-displacement curve) of the mix as shown in Figure 2.2b. The first cycle provides the maximum load where the initial damage occurs. The remaining cycles represent the crack propagation phase until the failure limit of 93% of maximum load is reached as shown in Figure 2.2c.

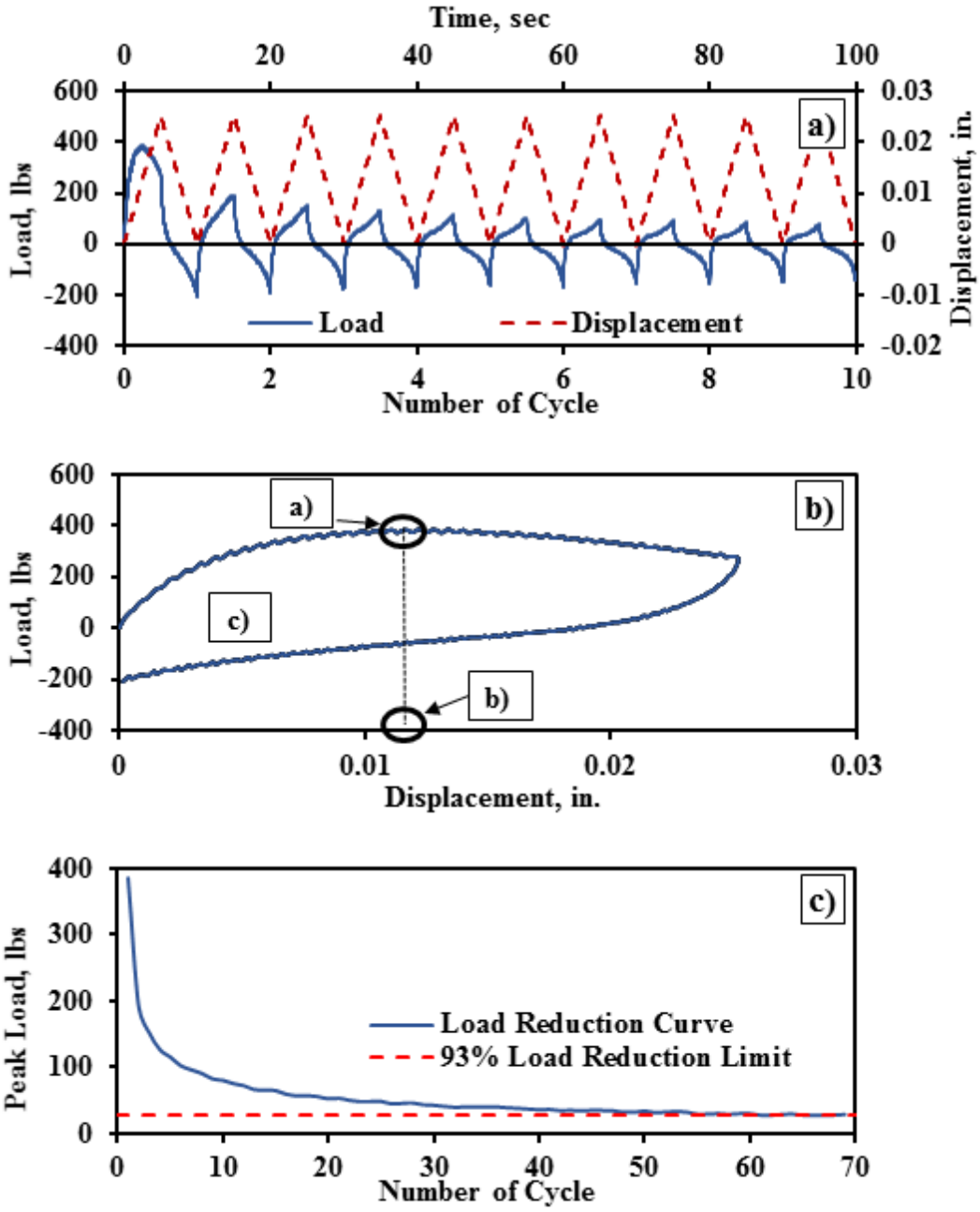

Figure 2.2 Interpretation of OT Results: a) Typical OT Data and b) Load-Displacement Response Curve (Hysteresis Loop), and c) Load Reduction Curve

2.2 PERFORMANCE OF NUMBER OF CYCLES TO FAILURE

The main challenge to the widespread implementation of the OT test has been the high variability of the number of cycles to failure that is used as a performance index. To evaluate this

phenomenon, OT tests were carried out on two AC mixes following the latest Tex-247-F version. The two mix types were a stone matrix asphalt (SMA-F) with crumb rubber and a dense-graded (Type-C) mixes. Table 2.1 presents further information of the AC mixes.

Table 2.1 Characteristics of AC Mixes

Designation	Mix Type	Location	Mix-design Characteristics	Perceived Performance
Type-C	Type-C	El Paso	4.6% PG 64-22 + 20% RAP + 2% WMA + Limestone/Dolomite/Gravel (NMAS 12.7 mm)	Marginal
SMAR-F	SMA-F	El Paso	7.8% PG 64-22 + 18.5% CR + 15% RAP + Limestone/Dolomite (NMAS 9.5 mm)	Poor

Note: NMAS= nominal maximum aggregate size, WMA= warm mix asphalt additive, CR = crumb rubber, RAP = reclaimed asphalt pavement

Five replicate specimens were tested for each AC mix type such that the specimens' air voids were the only parameter that varied. Three parameters were measured and reported from the OT tests: (1) the maximum load from the first cycle, (2) the maximum load from last cycle, and (3) the number of cycles to failure. The average, median, standard deviation and coefficient of variation (COV) of the results are reported in Table 2.2. The COV values for the number of cycles to failure for the SMAR-F and Type-C mixes were 37% and 44%, respectively. In the contrary, the maximum loads from the first and last cycles are less variable as compared to the number of cycles to failure.

Table 2.2 Summary of OT Test Results

Mix	Parameter	Maximum Load, lbs	Load of Last Cycle, lbs	Number of Cycles
SMAR-F	Average	409	26	69
	Std Dev	32	2	26
	COV	**8%**	**10%**	**37%**
Type-C	Average	409	34	334
	Std Dev	89	5	131
	COV	**22%**	**14%**	**39%**

To better understand the performance of the OT tests, the load-displacement curves (a.k.a. hysteresis loops) and the maximum peak load versus the number of cycles curve (referred to as load reduction curve hereafter) were investigated. The results from the SMAR-F mix are presented as an example. The results from the Type-C mix are reported in Appendix A.

The hysteresis loops of the first cycle for the five replicate specimens from the SMAR-F mix are shown in Figure 2.3a. The similar patterns from the first hysteresis loops points out to the consistency of the raw data, despite the high variability in the number of cycles to failure. Similarly, the consistency of the load reduction curves for that mix is presented in Figure 2.3b.

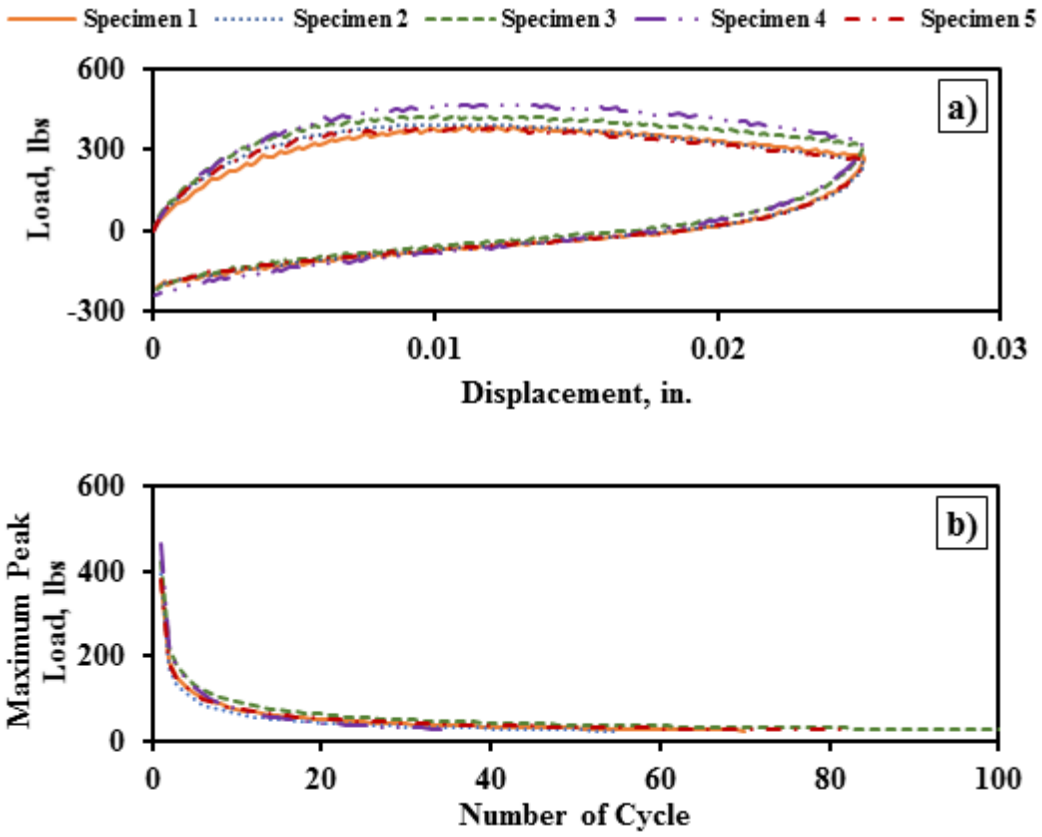

Figure 2.3 Test Response Curves from SMAR-F: a) First Hysteresis Loops and b) Maximum Peak Load versus Number of Cycles

2.3 ALTERNATIVE APPROACH TO COMPUTE NUMBER OF CYCLES TO FAILURE

For further exploring the raw data from OT, the differences in the maximum loads from consecutive cycles as a function of the number of cycles are shown in Figure 2.4a. The results up to cycle number 50 are presented to provide a better visualization of the trends. The numbers of cycles to several predefined load differences (1 lb, 2 lbs, 3 lbs, 5 lbs, 8 lbs, and 10 lbs) are illustrated in Figure 2.4b.

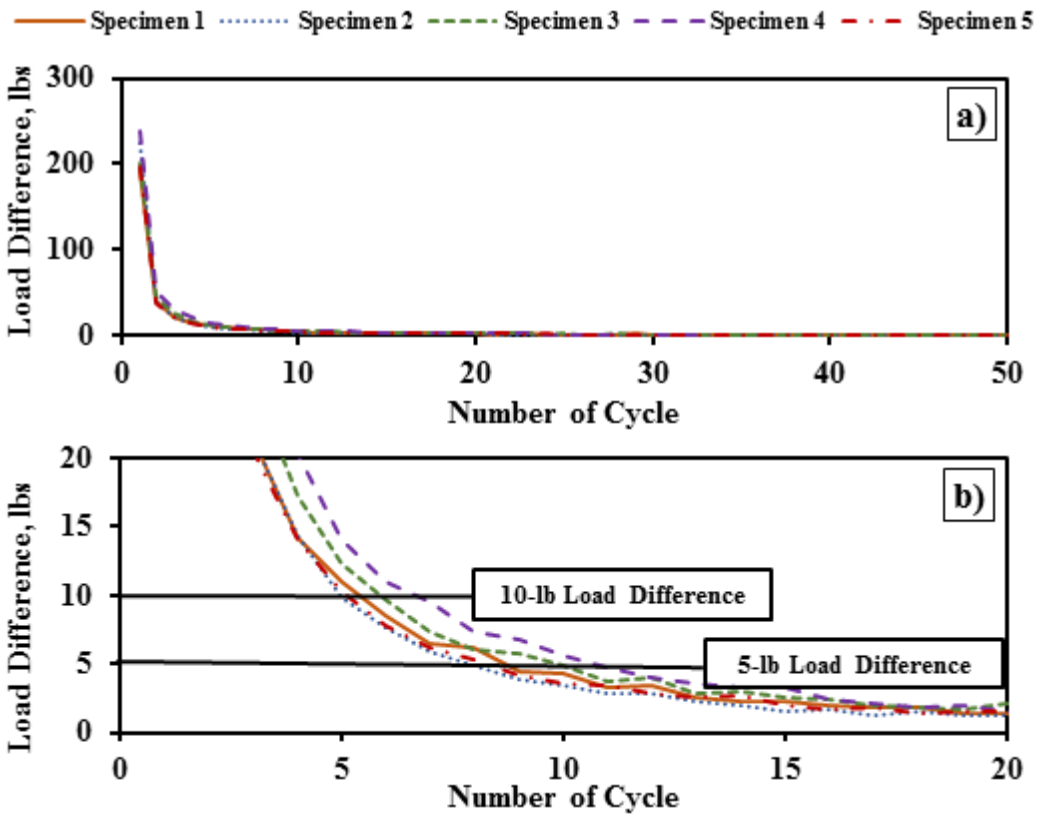

Figure 2.4 Load Difference of Consecutive Cycles Approach: a) Load Difference versus Number of Cycles and b) Number of Cycles at Predefined Load Difference

The summary of the results for the two AC mixes is presented in Table 2.3. A large difference between the number of cycles to failure (93% criterion) and the number of cycles corresponding to even the load difference of 1 lb is evident in Table 2.3. This may be considered as a reason for the excess variability of the number of cycles to failure when one considers the limitations of the instrumentation used in the OT devices. A load cell with a capacity of either

5000 lbs or 2000 lbs is often installed in the OT devices. Considering an optimistic precision of 0.1% for the load cell, the reported loads are within 2 lbs to 5 lbs of the actual values. Considering that the test has to continue until the maximum load decreases by 93%, the level of uncertainty in the measured loads is up to 10% of the actual value. The OT could report any value as the number of cycles to failure from cycle number twenty seven and forty onwards for SMAR-F and Type-C, respectively. The precision of the load cell may introduce a considerable level of variability to consistently compute the number of cycles to failure using the current failure criterion.

Table 2.3 Consistency of Number of Cycles to Failure using Load Difference Method

Mix	Parameters	Number of cycles to Failure	Number of Cycles Corresponding to Load Difference of					
			1 lb	2 lb	3 lb	5 lb	8 lb	10 lb
SMAR-F	Average	69	27	17	14	10	8	7
	Std. Dev	26	2	1	1	1	1	1
	COV	**37%**	**7%**	**8%**	**9%**	**10%**	**12%**	**13%**
Type-C	Average	334	40	25	19	13	9	8
	Std. Dev	146	2	1	1	0	0	0
	COV	**44%**	**5%**	**4%**	**4%**	**4%**	**3%**	**3%**

2.4 LOADING CONDITIONS FROM CYCLIC AND MONOTONIC OT TEST METHODS

The typical hysteresis loops from several cycles of an OT test are shown in Figure 2.5. The hysteresis loop of the first cycle is significantly different from the hysteresis loops of the other cycles. The shape of the first hysteresis loop suggests that the specimen is in a post failure state, meaning that a considerable deformation level was applied during the first cycle damaging severely the specimen. The hysteresis loops from the remaining cycles resemble the pattern of a material that is experiencing a highly nonlinear over-strained state. The level of damage induced during the first cycle of the OT test and residual strength from the consecutive cycles may be controlled by the cracking and fatigue properties of the AC specimens. The number of cycles to

failure measured from the OT may not reliably capture the cracking and fracture properties of AC mixes under the cyclic loading conditions of the OT test.

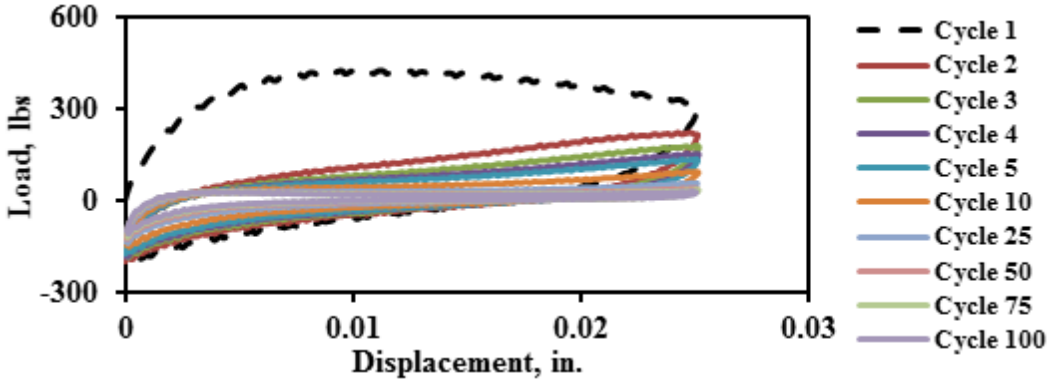

Figure 2.5 Shape of Hysteresis Loops from OT Test

To further evaluate the impact of the cyclic nature of the OT test, a set of monotonic OT tests was conducted. The monotonic OT test method consists of applying unidirectional deformation to cause the total failure of the specimen. The loading rate for the monotonic tests was adjusted to that used for the cyclic OT tests to consistently compare the cyclic and monotonic behaviors of the materials. With a maximum opening displacement of 0.125 in. (3.175 mm), the loading period for the cyclic OT is 25 seconds. The five load-displacement curves from the cyclic and monotonic OT test performed on a SMAR-F mix were averaged and compared in Figure 2.6a. The results from Type-C are presented in Appendix A. Similar trends are observed between the averaged curves from the monotonic and cyclic OT tests for both mixes. An expanded version of Figure 2.6a with errors bars depicting one standard deviation bounds is presented in Figure 2.6b.

Walubita et al. (2012) defined two main stages from the load-displacement curve of a monotonic OT test: crack initiation and propagation. The crack initiation stage is assumed to occur from the beginning of test up to the corresponding maximum load of the load-displacement response curve (where the initial damage of the specimens is assumed to occur). The similarity of the load-displacement curves from the monotonic and cyclic OT tests also suggests that the cyclic

OT test is composed of two main stages when the crack initiation clearly happens during the first cycle. This preliminary study provided an insight as to the possibility of using an alternative interpretation method for the current OT tests to assess the cracking resistance of AC mixes with better consistency and acceptable variability in the results.

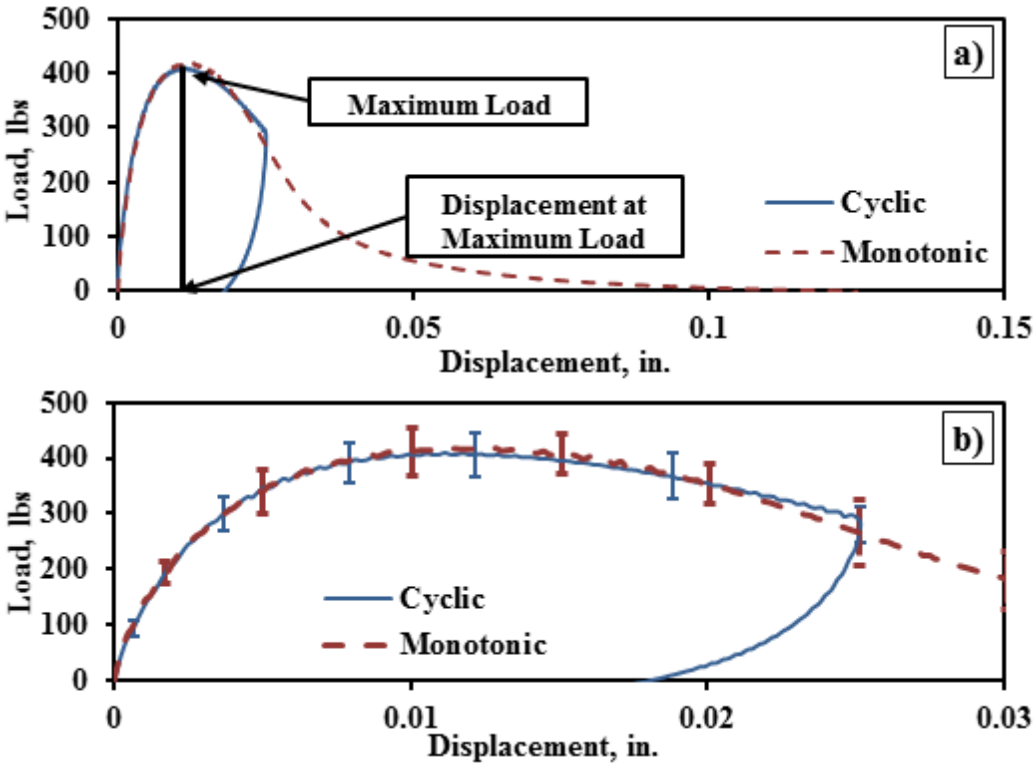

Figure 2.6 Comparison of Monotonic and Cyclic OT Tests: a) Displacement up to 0.125 in. and b) Displacement up to 0.03 in

2.5 SURROGATE PARAMETERS AND TEST RESPONSE CURVES

Response curves from the OT tests such as the hysteresis loop of the first cycle and the load reduction curve presented promising alternatives to current failure criterion. Alternative parameters and approaches for the OT were considered to implement potential performance indices that can predict the fatigue and cracking properties of mixes with more certainty.

The first focus was given to the hysteresis loop of the first cycle. Figure 2.7 illustrates alternative parameters investigated in this study. These parameters can be described in the following manner:

1) **Maximum load** - the highest load obtained from the first cycle. This load may result in the initial damage to the OT specimen.
2) **Displacement at maximum load** - the displacement at which the maximum load is reached during the first cycle.
3) **Initial slope** - obtained from the linear portion of the hysteresis loop of the first cycle.
4) **Displacement at zero load** - the displacement when the compression load starts to be measured during the unloading time.

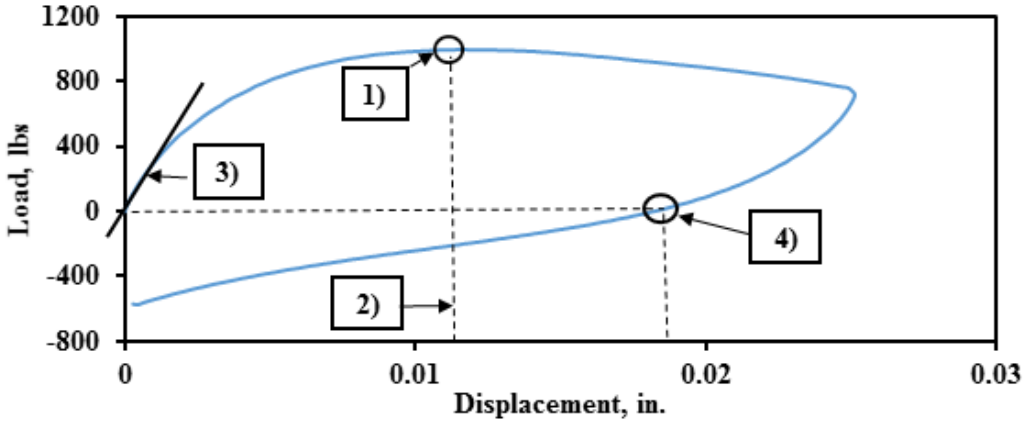

Figure 2.7 Graphical Representation of Alternative Parameters

Energy-based analysis methods and fracture mechanics principles were also utilized to better understand the initial cracking process of the AC specimens. The hysteresis loop from the first cycle was used for this purpose, as shown in Figure 2.8. The following parameters were calculated:

1) **Loading area (Work of Fracture)** – the area below the loading curve of the hysteresis loop up to the maximum displacement (0.025 in.)

2) **Unloading area (Released Work)** – the area below the unloading curve of the hysteresis loop from the maximum displacement to the displacement at zero load.

3) **Compressive area (Work of Healing) –** the area of the unloading curve of the hysteresis loop from the displacement at zero load to the zero displacement. The reasons for the specimens experiencing compressive loads is unexplained at this time.

4) **Total area (Dissipated Work) –** the sum of the areas at each stage of the hysteresis loop. The compressive area is added to the difference between the loading and unloading area.

These parameters for the SMAR-F and Type-C mixes along with their corresponding variabilities are reported in Table 2.4. The number of cycles to failure was also added to the table for comparison purposes. A COV equal or less than 20% was considered an acceptable level of repeatability for a performance index. Most parameters yielded COVs close to or less than 20%, except for the number of cycles to failure.

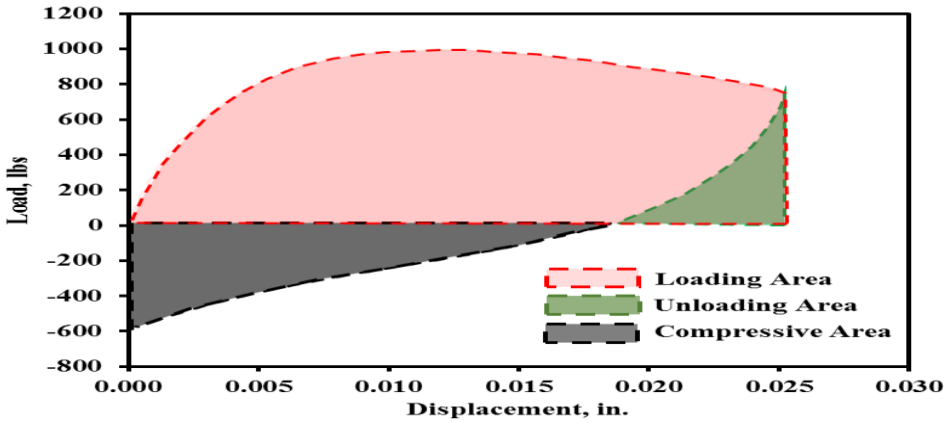

Figure 2.8 Graphical Representation of Alternative Parameters to Calculate Energy

The dissipated work and the work of fracture parameters were considered for further implementation in order to estimate the cracking resistance of AC mixtures during the initial damage of the specimen (i.e., the crack initiation stage). Both parameters showed low COVs.

Table 2.4 Consistency of Alternative Parameters

Parameter	SMAR-F			Type-C		
	Average	Std Dev	COV	Average	Std Dev	COV
Maximum load, lbs	409	35	**9%**	409	99	**24%**
Displacement at maximum load, in.	0.012	0.001	**11%**	0.014	0.001	**8%**
Initial slope, lbs/in.	98866	19455	**20%**	103774	15660	**15%**
Displacement at zero load, in.	0.018	0.001	**5%**	0.021	0.000	**2%**
Work of Fracture, lbs-in.	8.6	0.8	**10%**	9.8	0.3	**3%**
Unloading area, lbs-in.	-0.5	0.1	**22%**	-0.4	0.1	**13%**
Work of Healing, lbs-in.	1.5	0.1	**9%**	2.8	0.1	**4%**
Dissipated Work, lbs-in.	9.6	0.8	**8%**	12.2	0.4	**3%**
Number of cycles	69	26	**37%**	334	146	**44%**

The second area investigated was related to the load reduction curves. As shown in Figure 2.9, the five load reduction curves from the SMAR-F followed a similar load drop even though the number of cycles reported by the OT presented high variability. In the figure, the values in parentheses correspond to the numbers of cycles to failure. The high consistency of the load reduction curves was also considered promising to assess the cracking resistance of AC mixtures during the propagation of the crack with more certainty.

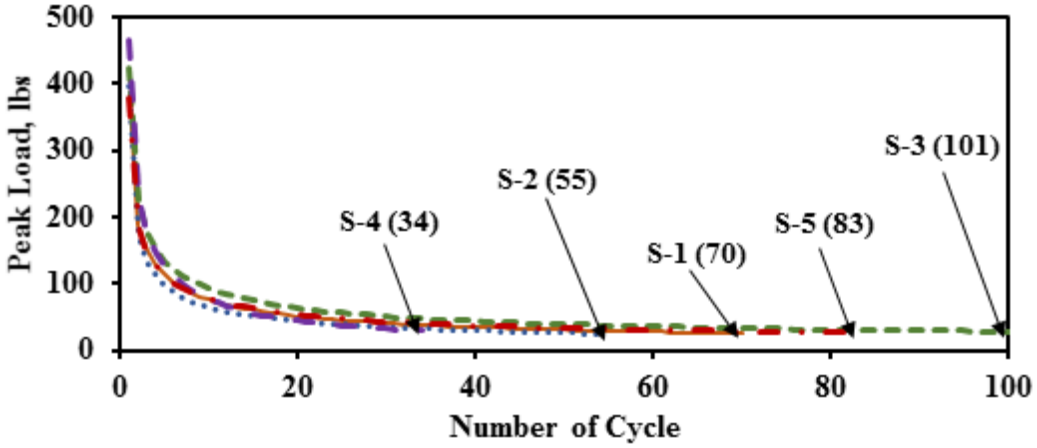

Figure 2.9 Performance of Load Reduction Curve and Corresponding Number of cycles to Failure

The typical applied displacement and resulted load measured with the OT are depicted in Figure 2.10. The shape of the load versus time curve clearly reflects that the maximum peak load happen at the end of the loading period except for the maximum load reported during the first cycle. The crack initiation stage happens during the first cycle which load response is different as compared to the rest of the cycles. The load responses for the second cycle and onwards suggest that the specimen is being damaged further and the residual strength of the specimen is being diminished gradually. The maximum peak load of each cycle may be interpreted as the force that drives the crack through the specimen. The dissipation of this crack driving force throughout the cyclic applied deformation may be used to assess the flexibility of the AC mixes to attenuate the propagation of the crack. Computing a parameter to quantify the load reduction curve seems to be a potential approach to assess cracking resistance of AC mixtures during the crack propagation stage.

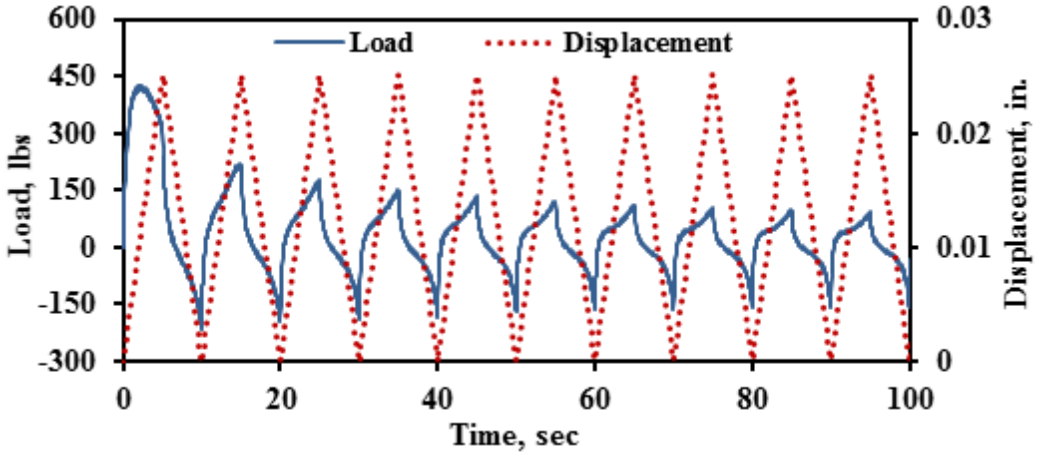

Figure 2.10 Applied Displacement and Measured Load versus Time

Chapter 3: Assessment of a Cracking Methodology

3.1 INTRODUCTION

A crack resistant mix should ideally exhibit the following two characteristics:

1. The mix should be tough enough so that it would not permit easily the initiation of a crack. This means that during the first cycle of OT test, the peak load should be as high as possible, and the displacement at peak should be as large as possible so that the magnitude of a computed modulus or energy-based parameter will be high enough, and
2. The mix should be flexible enough so that it would attenuate the rate of the propagation of the crack after it is initiated. This means, the rate of loss of load and dissipation of the residual strength should be rather gradual through the application of the cyclic deformation.

Potential parameters that can be measured from the OT test were evaluated and documented on Chapter 2. Additionally, two main stages were clearly delineated from the OT test based on the hysteretic behavior and load response of the AC specimens under the OT. An approach that considers the two stages of the OT test was considered to develop a cracking methodology.

3.2 ALTERNATIVE DATA INTERPRETATION ASSESSMENT

3.2.1 Crack Initiation (Critical Fracture Energy)

The area under the hysteresis loop was considered as crucial to compute the fracture parameters that characterize the crack initiation stage of the OT. The critical fracture energy, G_c, represents the energy required to initiate a crack. The dissipated energy is considered as the energy released during the loading and unloading stages of each cycle (in this case the first cycle). The

required areas to calculate the two fracture parameters are illustrated in Figure 3.1. Equation 3.1 can be used to calculate the dissipated and fracture energy.

$$G = \frac{W}{A} \qquad (3.1)$$

where G= Energy (lbs-in./in.^{2}), W = portion of the hysteresis loop, A = area of the cracked section which is considered as the specimen thickness multiplied by the width of the specimen (1.5 in. x 3.0 in.)

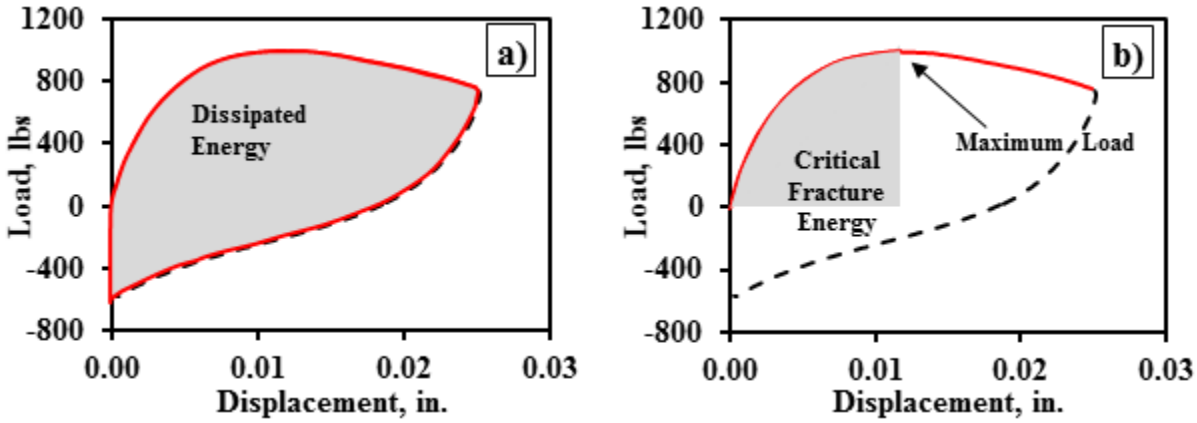

Figure 3.1 Portion of Hysteresis Loop to Calculate: a) Dissipated and b) Critical Fracture Energy

One concern with the dissipated energy in the context of the OT is that it includes the compressive area (negative portion of the hysteresis loop). This compressive area is not a natural healing strength from the AC specimen and it is understood to be induced by the mode of testing (displacement control) and the OT specimen's setup. More emphasis was directed to the critical fracture energy, G_c, which is explainable with the fracture mechanics principle of the OT test.

3.2.2 Crack Propagation (Crack Progression Rate)

For the crack propagation stage of the OT test, the crack driving force (maximum peak load) for each loading cycle was considered. Figure 3.2 presents the variation of the crack driving forces against the number of cycles (hereafter refer as to "load reduction curve"). In the example shown in Figure 3.2, the specimen reached the 93% load reduction criterion after 30 cycles. The

crack propagation was quantified by first fitting a power equation to the load reduction curve. The curve fitting, which normally yields R^2 values close to unity, is meant to smooth the uncertainties in the load measurements. The power coefficient (b-coefficient) of the power equation is interpreted as the crack progression rate. Instead of the number of cycles measured with the 93% failure criterion, the crack progression rate will assess the cracking properties of specimens during the propagation of the crack.

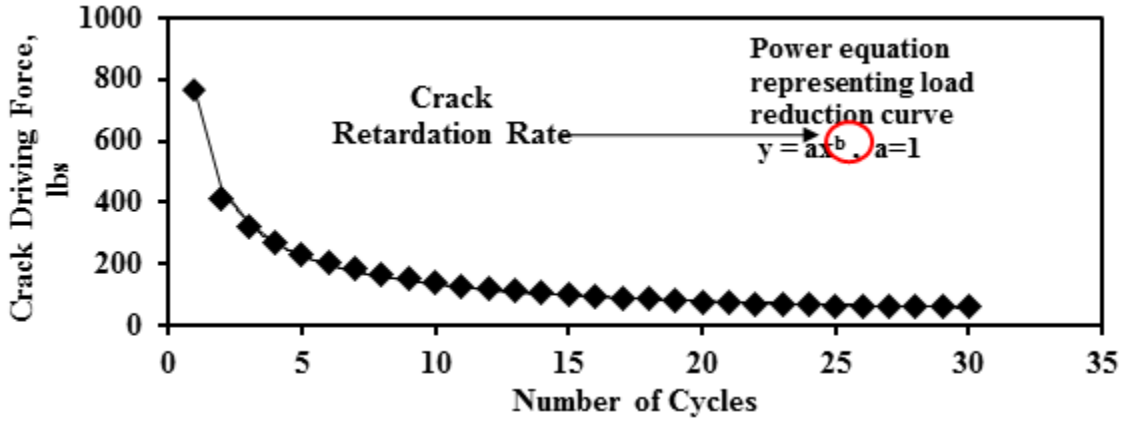

Figure 3.2 Graphical Representation of Crack Progression Rate

To compare the results more consistently, the load reduction curve is normalized by the maximum load of the first cycle. Figure 3.3 shows the average normalized load reduction curves obtained for SMAR-F and Type-C mixes. The corresponding crack progression rates for each load reduction curve are added to that figure. Errors bars representing one standard deviation are added to the load reduction curves on Figure 3.3. Under the curve-fitting scheme the constant associated with the power curve is equal to unity, while the power term is always negative. The absolute value of the crack progression rate will be used for practical purposes. The crack progression rates were 0.68 and 0.41 for SMAR-F and Type-C, respectively.

The average, standard deviation and coefficient of variation of the proposed parameters measured from SMAR-F and Type-C mixes are reported in Table 3.1. The proposed parameters presented COV values less than 25%, while the COV for the number of cycles to failure was

between 35% and 45%. Although the repeatability of the proposed parameters was better than that of the number of cycles to failure, a larger number of specimens should be evaluated to delineate the consistency of those parameters.

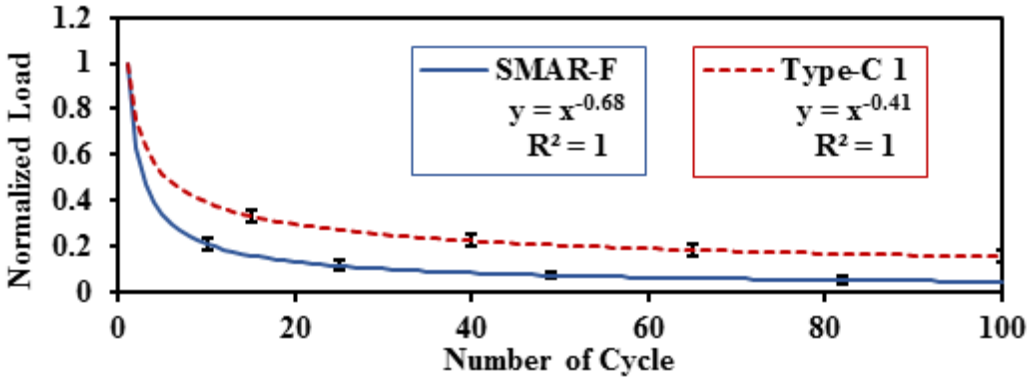

Figure 3.3 Load Reduction Curve and Corresponding Crack Progression Rate

Table 3.1 Performance of Proposed Parameters and Number of Cycles to Failure

Mix	Parameters	Max Load, lbs	Critical Fracture Energy, in.-lbs/in.^{2}	Crack Progression Rate	R^2	Number of Cycles to Failure
SMAR-F	Average	409	0.91	0.68	1.0	69
	Std Dev	32	0.15	0.07	0.0	23
	COV	**8%**	**17%**	**10%**	**NA**	**34%**
Type-C	Average	409	1.36	0.41	1.0	334
	Std Dev	99	0.20	0.11	0.0	146
	COV	**24%**	**15%**	**26%**	**NA**	**44%**

3.2.3 Repeatability of Proposed Performance Indices

The repeatability of the proposed parameters was further evaluated using 60 OT test results collected from a multi-laboratory study between UTEP and TxDOT. The sample size for each laboratory was 30 specimens. For this study, a dense-graded type-C mix was used because of the concerns with the variability of the OT results for dense-graded mixes reported in past studies. The specimens were compacted and prepared at TxDOT's facility to minimize the variability due to

the specimen preparation process. The specimens were tested within a period of 5 days after the day of molding.

The averages, standard deviations and COV values for the proposed parameters and the number of cycles to failure results from each laboratory are presented in Table 3.2. On average, the results obtained from both institutions were similar meaning that the OT tests are reproducible among different laboratories. As reflected in Table 3.2, all parameters, except the number of cycles, yielded relatively low COVs. Using the crack progression rate of the normalized load reduction curve and the critical fracture energy, instead of the number of cycles seems promising as an alternative for estimating the resistance of the AC specimens to cracking under OT.

Table 3.2 Results from a Multi-laboratory Study between UTEP and TxDOT

Institution	Parameter	Max Load, lbs	Critical Fracture Energy, in.-lb/in.^{2}	Crack Progression Rate	Number of Cycles
UTEP	Average	847	1.8	0.68	66
	Std. Dev	53	0.2	0.17	48
	COV	**6%**	**13%**	**25%**	**73%**
TxDOT	Average	902	2.2	0.70	60
	Std. Dev	63	0.3	0.15	40
	COV	**7%**	**12%**	**21%**	**68%**

3.3 DESIGN INTERACTION PLOT FOR CRACKING PROPERTIES

A data interpretation method that involves the two phases of the OT test, crack initiation and propagation, is proposed. The surrogate parameter for quantifying the crack initiation is the critical fracture energy. The higher the value is, the more energy the AC mix will require initiating the crack. The crack progression rate, the power term obtained from the fitting of a power curve to the normalized load reduction curve, is used as a surrogate for characterizing the resistance to cracking during the propagation of the crack. The greater the absolute value of the crack progression rate, the faster the crack propagates through the AC specimen and shorter the fatigue

live for that AC mixture will be. To better understand the cracking properties of mixtures using the proposed parameters, a design interaction plot was created as shown in Figure 3.4. The critical fracture energy (Crack Initiation Resistance) and crack progression rate (Crack Propagation Resistance) were plotted against one other. Using the design interaction plot, the cracking resistance of AC mixtures was subjectively divided into the following four categories:

- **Tough-Crack Resistant:** Good resistance during crack initiation (Tough) and propagation (Flexible). AC mixes with acceptable cracking resistance should be in this quadrant.
- **Tough-Crack Susceptible:** AC mixtures with good resistance to crack initiation (Tough) and susceptible to crack propagation (Brittle).
- **Soft-Crack Resistant:** Susceptible to crack initiation (Soft) but good resistance to attenuate the propagation of the crack (Flexible)
- **Soft-Crack Susceptible:** AC mixtures with significantly poor resistance to crack initiation and propagation.

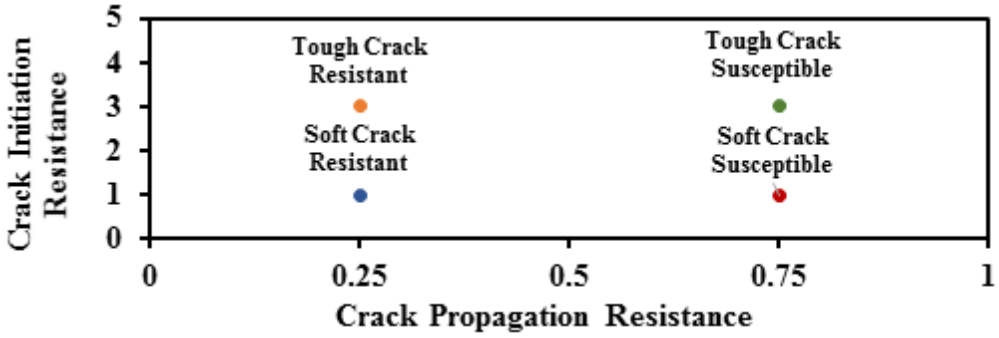

Figure 3.4 Design Interaction Plot for Cracking Resistance of AC Mixes

A preliminary threshold for the crack progression rate was proposed based on the current pass/fail criteria of the number of cycles to failure. The crack progression rate corresponding to the current criterion of 93% load reduction in 300 cycles corresponds to 0.47. As a preliminary failure limit, a crack progression rate of 0.5 was used to delineate the well and poor cracking resistant mixes. Figure 3.5 shows the performance of the SMAR-F and Type-C mixes in the design

interaction plot with the preliminary failure limit. Type-C will be considered a good cracking resistant mix based on the preliminary failure criteria. Conversely, SMAR-F did not pass the preliminary failure criterion.

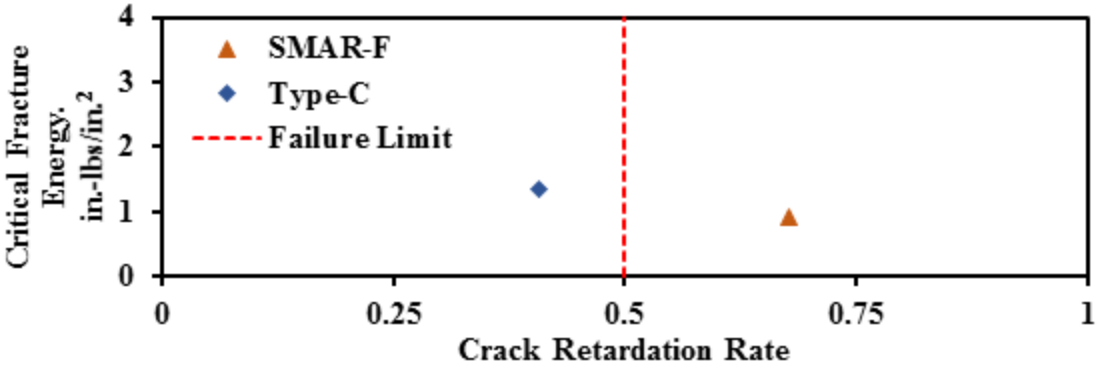

Figure 3.5 Performance of AC Mixes using Proposed Parameters

3.4 EFFECTIVENESS OF PROPOSED METHODOLOGY FOR TYPICAL AC MIXTURES

The potential of the proposed method was evaluated using the data from over 350 tests of 120 different mix designs and 10 different AC mix types performed by TxDOT in the previous years. Table 3.3 provides the AC mixes that were included in this study. This database contained relevant information about the mixes such as the date of test, performance grade of the binder, asphalt content, anti-stripping content, and asphalt source. Only the data from 2012 onwards that correspond to the latest Tex 248-F test protocol was considered. The critical fracture energy and crack progression rate were calculated for all OT tests. As an example, the analysis and results for the SP-C mixes are shown. The results from other mixes are presented in Appendix B.

Table 3.3 Summary of OT Data Used for Evaluation

Mix Type	Mix Designs	Sample Size
Thin Overlay Mix (TOM)	19	54
Crack Attenuating Mix (CAM)	18	53
Permeable Friction Course (PFC-F)	3	9
Stone Matrix Asphalt (SMA-D)	18	50
Stone Matrix Asphalt (SMA-F)	7	20
Superpave-C (SP-C)	17	50
Superpave-D (SP-D)	15	43
Type B (Fine Base)	3	8
Type C (Coarse Surface)	12	35
Type D (Fine Surface)	12	35
TOTAL	**124**	**357**

3.4.1 Normalized Load Reduction Curves

The average load reduction curves were generated and plotted along with the representative average and median curve for SP-C mixes. The curve associated to the 93% load drop criteria was also plotted as shown in Figure 3.6a. For this mix type, the curves associated with the individual mixes were equally distributed around the 93% load drop curve meaning that some of these mixes would have performed satisfactorily while some would have exhibited poor cracking performance. Figure 3.6b shows the average trend for all the SP-C mixes with error bars representing one standard deviation. The abscissa of Figure 3.6b was converted to logarithmic scale. Three representative curves associated with 100, 300 and 1000 cycles to reach a load reduction of 93% are also shown in Figure 3.6b. Based on the average curve that is above the 100 cycles' line, the cracking susceptibility of the SP-C mixes will be significantly high with mixes mostly failing the failure criterion.

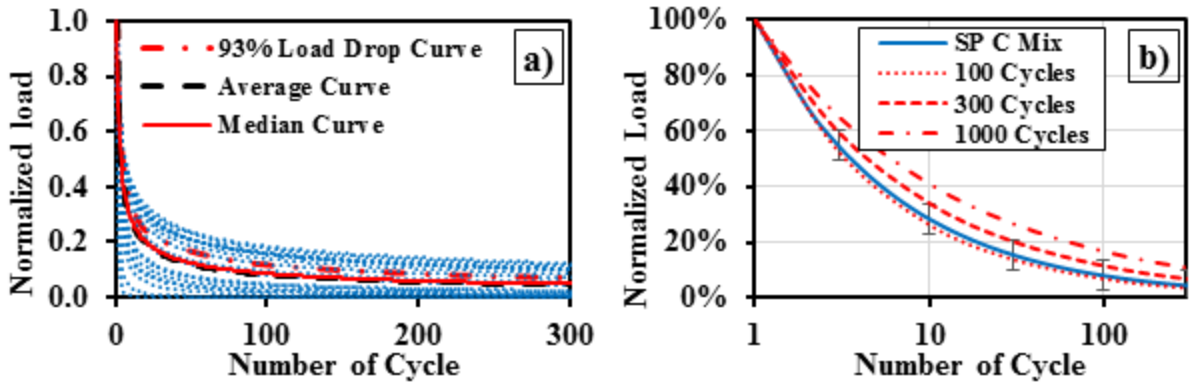

Figure 3.6 Performance of SP-C Mixes: a) Normalized Load Reduction Curves and b) Average

To comparatively evaluate the performance of the different mixes, the average normalized load reduction curves for all mix types are superimposed on to the failure criterion in Figure 3.7. The average curves for the CAM, TOM, SMA-D, SMA-F and PFC-C mixes always lie above the failure criterion curve. Type D mixes were considered the worst mix with poorly performance as per current criterion. The other mixes sometimes passed and sometimes failed the current criterion.

Figures 3.8 presents the average trends for each AC mix type as well as the three representative failure criteria. Errors bars are added to the average curves to demonstrate the uncertainties associated with different AC mixes.

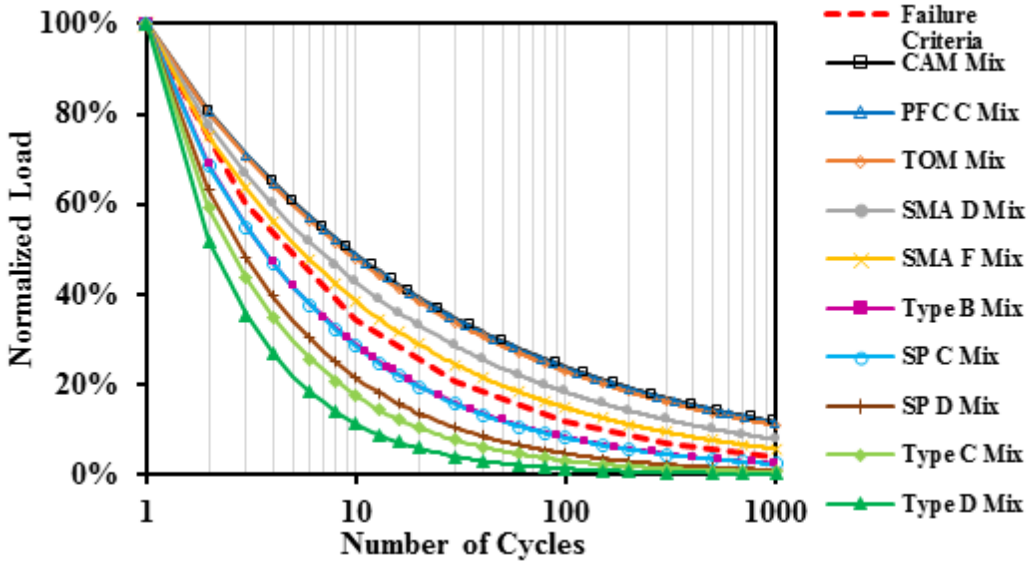

Figure 3.7 Average Normalized Load Reduction Curves for All AC mixes

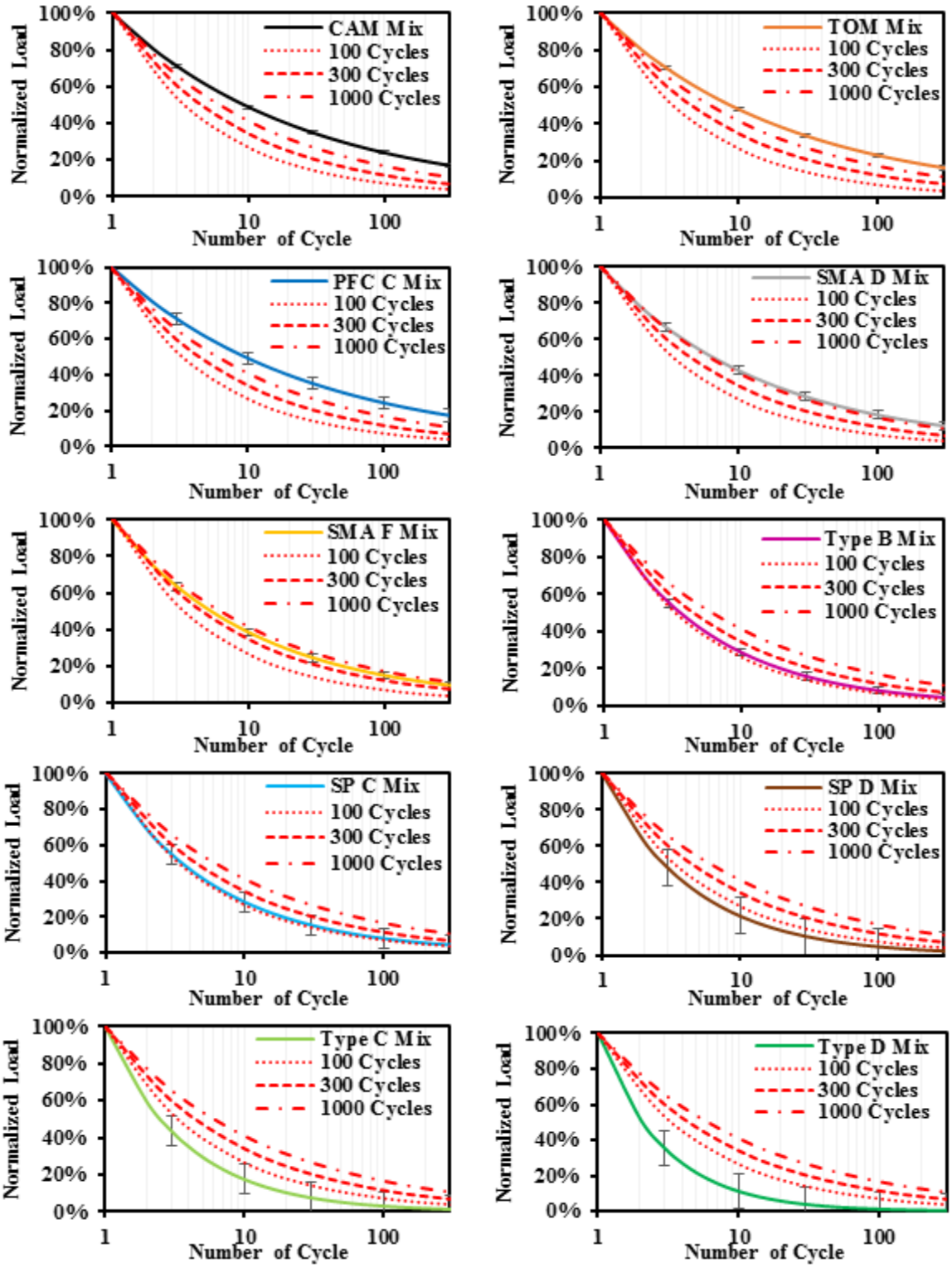

Figure 3.8 Normalized Load Reduction Curves for AC Mixes

3.4.2 Performance of AC Mixes on Design Interaction Plot

The design interaction plot composed of the critical fracture energy and crack progression rate was also used to evaluate the cracking performance of the AC mixes. The design interaction plot for the SP-C mixes is presented in Figure 3.9. Lines corresponding to the average and median power parameter for the SP-C mixes are added to Figure 3.9. The failure limit is also presented. The label of each data point represents the corresponding number of cycles using the 93% load reduction criterion. The data points for the SP-C mixes were divided in two categories: good crack retardants (green dots) and poor crack retardants (red squares). The design interaction plots for the rest of the AC mixes are presented in Appendix B.

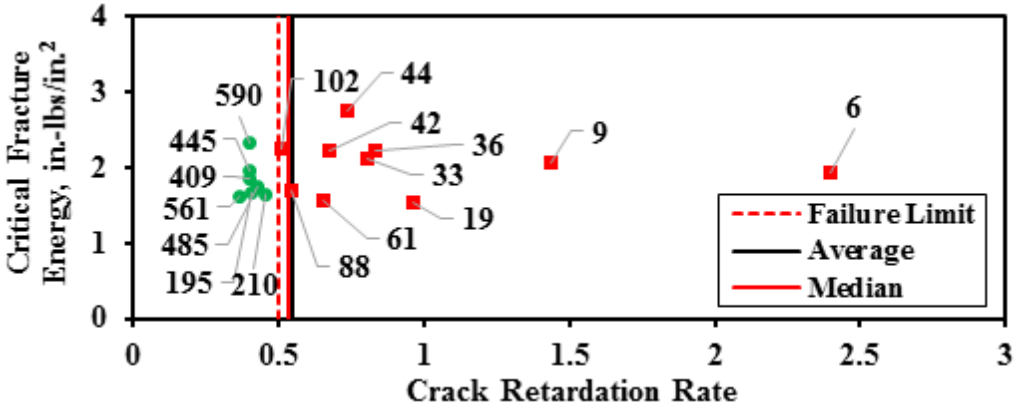

Figure 3.9 Design Interaction Plot of Cracking Performance for SP-C Mixes

The performance of all mixes was evaluated using the critical fracture energy and crack progression rate parameters. The distribution of those parameters for each AC mix is presented in Figure 3.10. According to this methodology, the best mixes are CAM and TOM since they required more energy to initiate a crack (high critical fracture energy) and they were very flexible (lowest crack progression rate) after the crack was initiated. The PFC mixes presented high flexibility after crack initiation, but the energy required to initiate a crack was low. SMA-D mixes presented good flexibility after the initiation of the crack; however, the critical fracture energy was relatively low. SMA-F mixes presented high critical fracture energy and good crack progression

rate. SP-C mixes are more prone to fail based on the crack progression rate. Type-B mixes are closed to the failure criteria for the crack progression rate. On average, the Type C, Type D and SP-D mixes are ranked the worst because of the high crack progression rate.

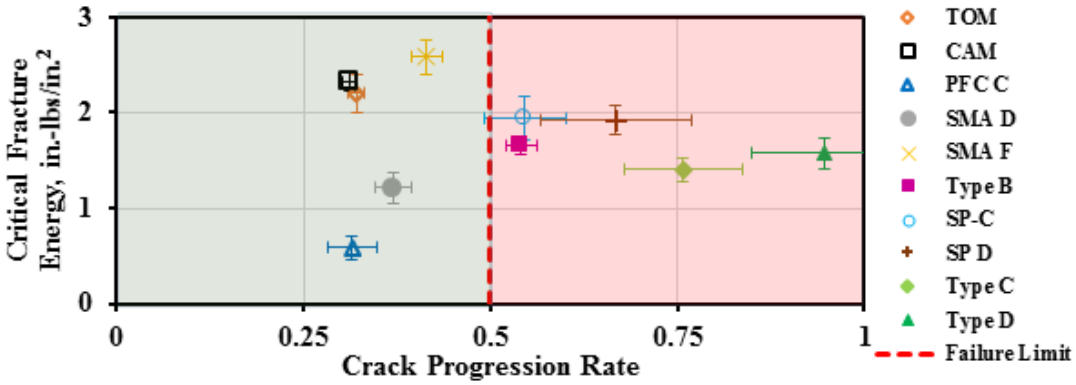

Figure 3.10 Cracking Performance of AC Mixes on Design Interaction Plot

3.4.3 Typical Variability of Current and Improved OT Methods

One of the main objectives of this study was to improve the repeatability of the cracking parameters used to characterize the performance of specimens under the OT test. Each mix contained a number of sets of triplicate specimens. The average and COV of the implemented parameters and the number of cycles to failure were calculated for each set of specimens. The medians of the averages and COVs of all sets of specimens for a mix are shown in Table 3.4. The detailed results for each mix are shown in Appendix B.

The typical COVs for the crack progression rate are less than 20%. In contrast, the typical COVs of the number of cycles to failure for mixes that were not close to the 1000 cycles are greater than 20%. The COVs of some mixes such as TOM, CAM and PFC-F that tend to last more than 1000 cycles before reaching the 93% reduction in load are not reported due to the 1000 cycle setup limit of the OT machine.

The COVs of the fracture energies is typically less than 20% except for the PFC that had a COV of 25% due to the small sample size and low data quality. This inconsistency of the hysteresis

loops for PFC mix was investigated and a set of triplicate specimens is presented in Figure 3.11 as an example. It was clear from the figure that the loops were atypical, especially for Specimen 1 which curve did not started from zero and the maximum opening displacement was higher than 0.025 in.. The hysteresis loop for Specimen 2 and 3 had different initial slopes while the consistency of triplicate specimens for the rest of the AC mixes was reasonably well. Typically, this data will be discarded. However, since only a small sample size was received, all specimens were included. Further investigation on a larger sample size of PFC mixes would be desirable to properly compute the typical repeatability and performance of this AC mix.

Table 3.4 Median Repeatability of OT Results for AC Mixes

Mix	**Critical Fracture Energy, in.-lbs/in.^{2}**		**Crack Progression Rate**		**Number of cycles to Failure**	
	Median	**COV**	**Median**	**COV**	**Median**	**COV**
TOM	2.2	**8%**	0.32	**4%**	1000	**NA**
CAM	2.3	**4%**	0.31	**3%**	1000	**NA**
PFC	0.5	**25%**	0.31	**11%**	1000	**NA**
SMA-D	1.2	**14%**	0.36	**7%**	847	**20%**
SMA-F	2.6	**7%**	0.41	**5%**	182	**23%**
Type-B	1.7	**5%**	0.50	**6%**	117	**27%**
SP-C	2.0	**11%**	0.53	**10%**	94	**31%**
SP-D	1.9	**9%**	0.67	**15%**	47	**30%**
Type-C	1.4	**8%**	0.73	**10%**	46	**27%**
Type-D	1.6	**9%**	0.95	**10%**	20	**32%**

Chapter 4: Assessment of OT Test Specifications

4.1 Evaluation of Specimen Preparation Process

One challenge associated with the OT tests is the specimen preparation process. Specimen preparation requires cutting and gluing. Considering the variables studied by Walubita et al. *(2012)* and Garcia and Miramontes *(2015)*, further investigations were carried out on variables such as glue type, weight on top of the specimens and gluing method using synthetic specimens. A synthetic specimen with a durometer 90A, which corresponds to a soft material, was used to evaluate the specimen preparation process. The outcomes of this evaluation are reported next.

4.1.1 Glue Type

To reduce the probability of failure of the OT specimens at the specimen-plate interface, a strong bond between the specimen and the OT plates is required. The current test procedure calls for using a 2-part, 2-ton epoxy for gluing the specimens to the OT test plates. The required epoxy type can potentially acquire a strength of 2500 psi when completely cured. While maintaining all the other operational parameters constant, the epoxy was replaced with a similar epoxy with a strength of 4400 psi for comparison purposes. Figure 4.1 presents the typical performance of the 2500-psi and 4400-psi epoxies under OT monotonic loading. Monotonic loads were applied to exert greater displacements than normally used in the OT tests. The maximum load for the 4400-psi epoxy is greater than that of the 2500-psi epoxy. The hysteresis loop obtained from the 4400-psi epoxy demonstrated a more linear behavior and a higher maximum load that can thus be interpreted as less internal damage to the bond between the specimen and the plates. Implementing a stronger epoxy to achieve a strong bond between the specimens and the OT plates is

recommended to minimize the probability of failure of the OT specimens at the specimen-plate interface.

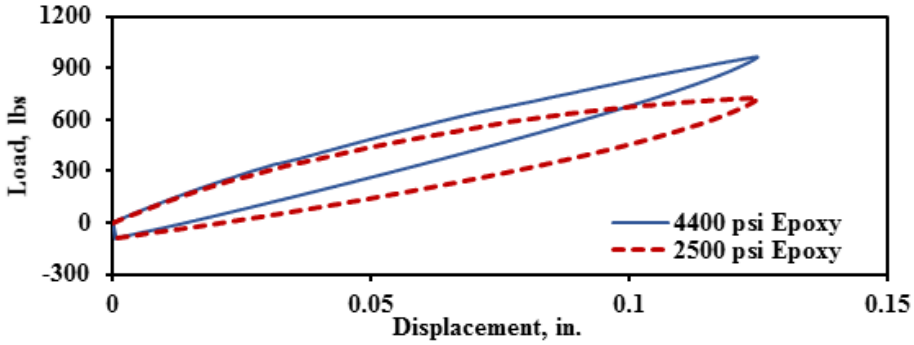

Figure 4.1 Comparison of Two Epoxies with Different Strengths

4.1.2 Weight on Top

A private communication with the company that manufactures the epoxy recommended having an epoxy thickness greater than what is currently used for attaching the specimens to the OT plates. To increase the thickness of the epoxy layer, the synthetic specimen was prepared using a 5-lb instead of a 10-lb weight. The 4400-psi epoxy was used in this comparison. Figure 4.2 presents the load-displacement response curves using 5-lb and 10-lb weights on top of the OT specimens. The slopes of the two load-displacement curves changed after a displacement of around 0.03 in. was reached. This means that for the opening displacement used during the cyclic OT test method, similar performance may be obtained when using 5-lb or 10-lb weights. Despite similar maximum loads from both testing options, a 5-lb weight is recommended to comply better with the manufacturer's recommendation and to minimize glue squeezed out from the sides of the specimens.

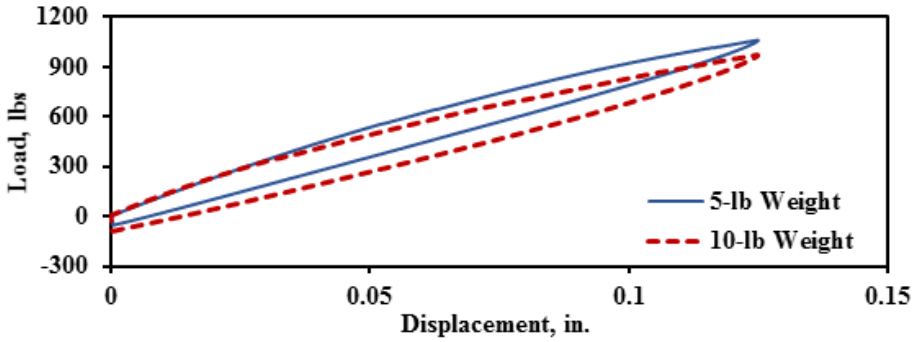

Figure 4.2 Load-displacement Response Curves with 5-lb and 10-lb Weight

4.1.3 Gluing Method

The earlier version of the gluing method (called the "Version 2009" hereafter) of OT test protocol consisted of covering the gap between the base plates with adhesive tape to prevent the accumulation of epoxy. The adhesive tape and the accumulated hardened epoxy were removed with a hacksaw. This process was perceived as operator-dependent and a possible factor affecting the consistency of the OT results. In the current (called the "Version 2014") protocol, the spacer bars are used instead of adhesive tape to remove the excess epoxy that accumulates between the OT plates after mounting the specimen. This new method seems more practical because the accumulated epoxy along the gap is removed easily while the epoxy is still fresh. The uniformity of the glued area due to the use of the tape and the ease of removing the epoxy between the base plates with the space bars are both desirable. Thus, an alternative method was considered that could potentially provide both benefits. In the alternative method (called the "Proposed Gluing Method"), the tape is covered with a thin layer of grease and placed on the specimen to cover the gap area along the specimen. The space bars are placed between the base plates to prevent the accumulation of epoxy. The removal of the tape and the space bars after the specimen is mounted to the base plates are easy and the glued portion as well as the gap portion of the specimen is uniform.

The other issue observed was that the weight placed on top of the specimens to ensure intimate contact between the specimen and the plates caused some epoxy to squeeze out. The squeezed out epoxy accumulates and hardens along the contact area between the perimeter of the specimen and the plates. This additional epoxy is not always uniform. To achieve uniformity, the epoxy along the perimeter of the specimens was removed with a razor immediately after the weight was applied to the specimen. This step was only used for the proposed gluing method.

The three gluing methods were compared using the synthetic specimen 90A (Very Soft) under an opening displacement of 0.025 in. and loading time of 5 sec, as specified by the cyclic OT test protocol. Figure 4.3 illustrates typical load-deformation curves obtained from the three gluing methods. The differences in the maximum loads and the shapes of the hysteresis loops indicate that the method of gluing will impact the OT results. The load-displacement response from the proposed gluing method is slightly different than both the 2009 and 2014 versions. The slopes of the loading portion of the last two versions are steeper than the proposed protocol because the proposed protocol visually provided the most uniform gap. The application of tape and space bars seems to improve the consistency of the glued area.

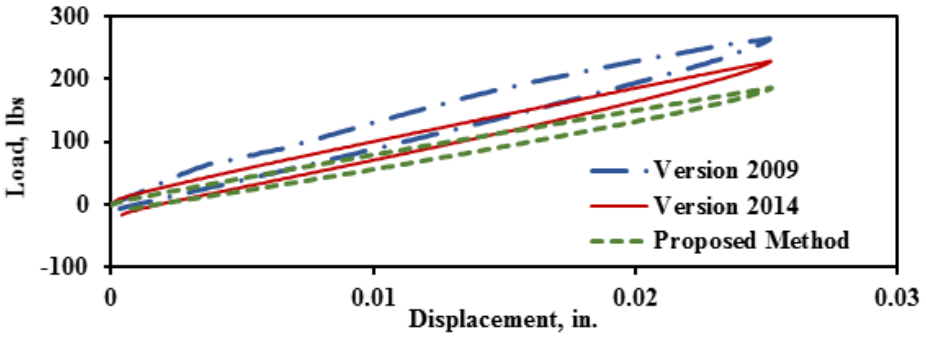

Figure 4.3 Comparison of Hysteresis Loops from Three Gluing Methods

This comparison indicates that the glued area must be consistent to improve the consistency and performance of the OT. Based on these preliminary results, the proposed gluing method was implemented to provide a more consistent bond between the specimen and steel plates, and to

minimize the influence of the glued area. Figure 4.4 presents the materials required to glue and mount the specimens to the OT plates under the proposed process. The following steps are proposed for gluing the OT specimens as per the proposed gluing method:

1. Ensure the base plates and spacer bars are clean and free of any dirt or epoxy from any previous uses.
2. Mount and secure the base plates to the mounting jig. Insert the spacer bar between the plates. Apply a small amount of petroleum jelly on the spacer bar to facilitate its removal (Figure 4.4b).
3. Draw a line along the middle of the trimmed specimen to guide the placement of the tape (Figure 4.4c).
4. Place a piece of 4-mm-wide tape along the middle of the trimmed specimen to cover the gap. Apply a small amount of petroleum jelly between the tape and the specimen to facilitate the tape removal once the specimen is mounted onto the base plates (Figure 4.4d).
5. Prepare two containers each containing 8 g of the two-part epoxy (Figure 4.4e). Prepare the epoxy only for one specimen in one batch.
6. Evenly spread the glue in each container on one side of the trimmed specimen (see Figures 4.4f and 4.4g).
7. Glue the specimen to the base plates while ensuring that the specimen is centered and aligned with the edges of the base plates.

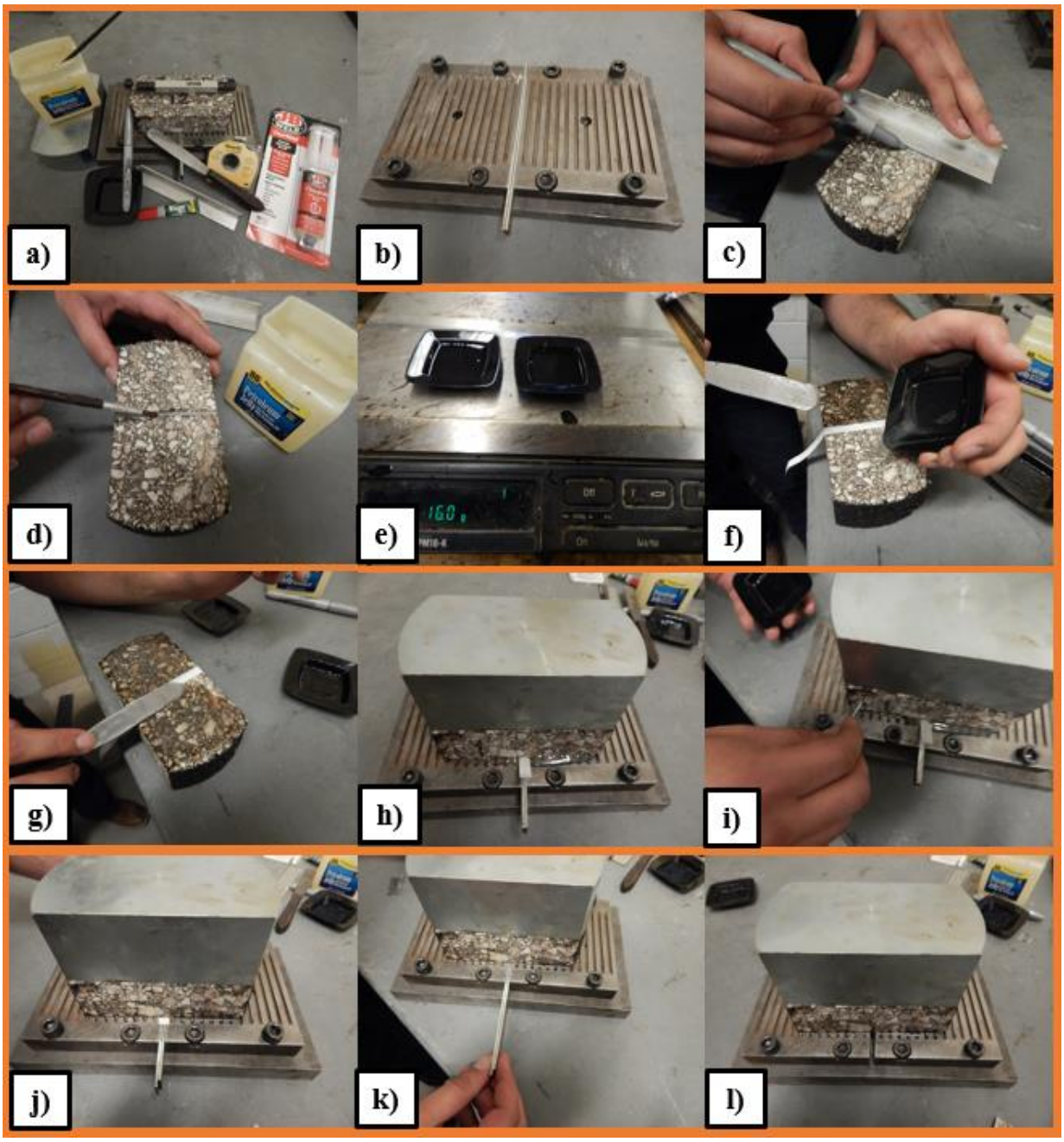

Figure 4.4 Key Steps of OT Specimen Gluing Procedure

8. Add a 5-lb weight on top of the specimen to ensure intimate contact between the specimen and the base plates (Figure 4.4h).
9. Remove the excess glue accumulated on the perimeter of the mounted specimen with a razor (Figure 4.4i).

10. Remove the tape and then the spacer bar carefully to prevent the specimen from moving (Figures 4.4j and 4.4k).
11. Allow the epoxy to cure for sufficient bonding strength as per the manufacturer's recommendations, usually overnight (Figure 4.4l).

This process that is slightly different than the current specification tends to provide more repeatable results. Figure 4.5 demonstrates the repeatability of the proposed gluing method with the synthetic specimen. The load-displacement curves from the three trials are very similar.

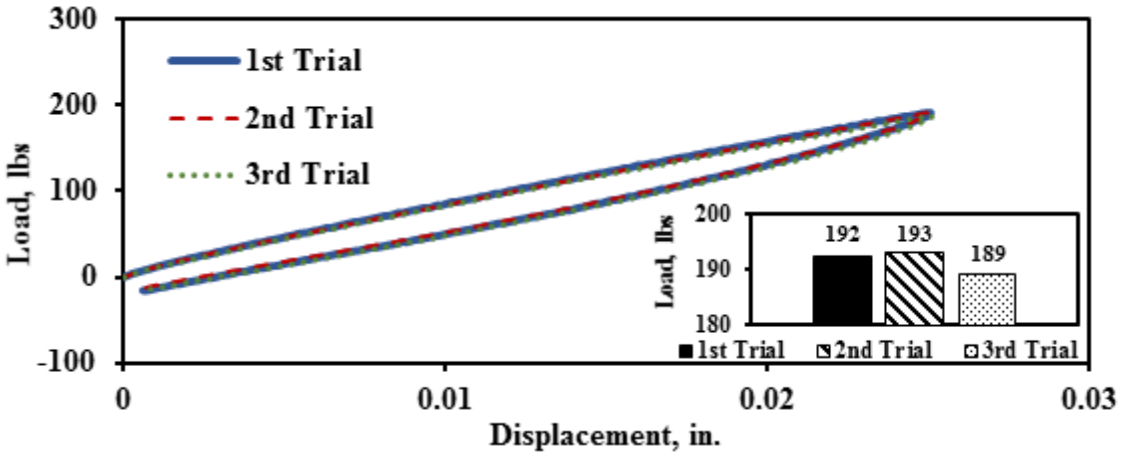

Figure 4.5 Consistency of Modified Gluing Method

As compared to the last two gluing methods, the proposed gluing method helps to delimitate the contact area between the specimens and the OT plates by removing the glue on the sides of the specimens. Similarly, the application of the tape and space bars as proposed improves the removal of the glue accumulated between the OT plates. The specimen preparation process is further explained in Appendix C.

4.1.4 Influence of Gluing Methods on OT Performance

In addition to the study carried on the specimen preparation process using synthetic specimens, OT tests were also carried out with AC specimens to comparatively evaluate the

performance of the OT results using the proposed specimen preparation vs. the Version 2014 method. Type-C mix was investigated under this study. Five similar specimens were tested for each testing option such that the specimens' air voids were the only parameter that varied. The performance of the OT results using the version 2014 preparation method was evaluated first. The load-displacement curves for the first and second loading cycles from this activity are shown in Figures 4.6a and 4.6b, respectively. Three out of the five specimens performed similarly. Figure 4.6c displays the displacement time histories captured by an LVDT placed on top of the specimens. The displacement recorded by the LVDT was also not fully consistent. The differences in the maximum load and hysteresis loop may be caused by the inconsistency of the specimen glued area.

Figures 4.7a and 4.7b show the load-displacement curves for the first and second loading cycles when the specimens were prepared using the proposed specimen preparation, respectively. These load-displacement curves are more repeatable and consistent than those shown in Figures 4.6a and 4.6b. The specimen with the higher maximum load for the first cycle also exhibited higher maximum load for the second cycle. Figure 4.7c shows the displacement time histories captured by an LVDT placed on top of the specimens. The displacements recorded by the LVDT were still less consistent than the load-displacement curves. This may be due to geometric dissimilarity of the applied load since, strictly speaking, the specimens are not subjected to a pure tension.

Table 4.1 summarizes the statistical information of a number of parameters measured from the OT tests performed using the proposed and version 2014 specimen preparations. Apart from the number of OT cycles, the proposed parameters were documented. The COV values obtained from the proposed specimen preparation were relatively smaller as compared to the similar results from the version 2014. The number of cycles to failure presented unacceptable COV values for Version 2014 and Proposed Method results.

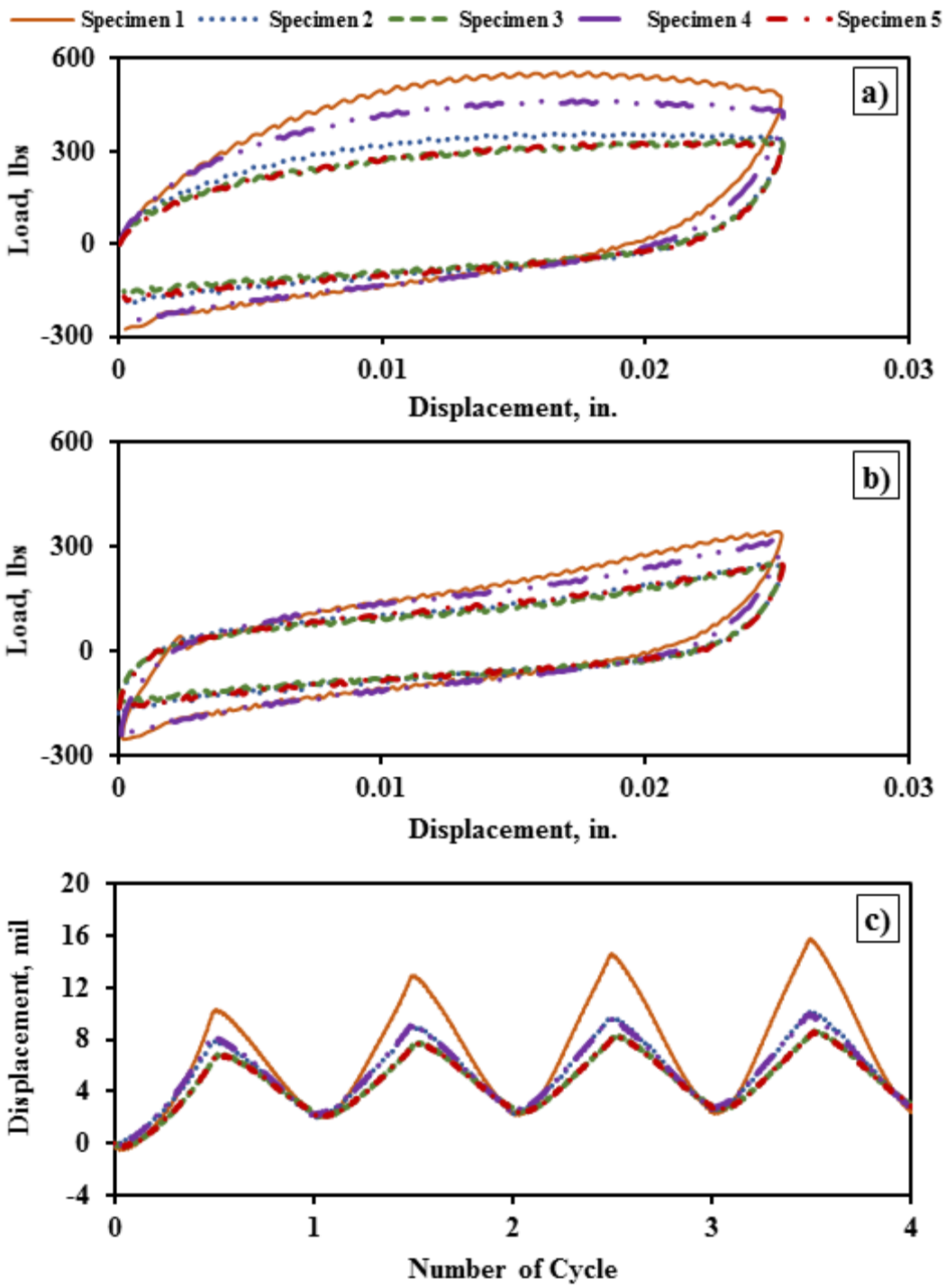

Figure 4.6 Results for Version 2014 Gluing Method a) First Cycle Hysteresis Loop, b) Second Cycle Hysteresis Loop, and c) Displacement of Top LVDT.

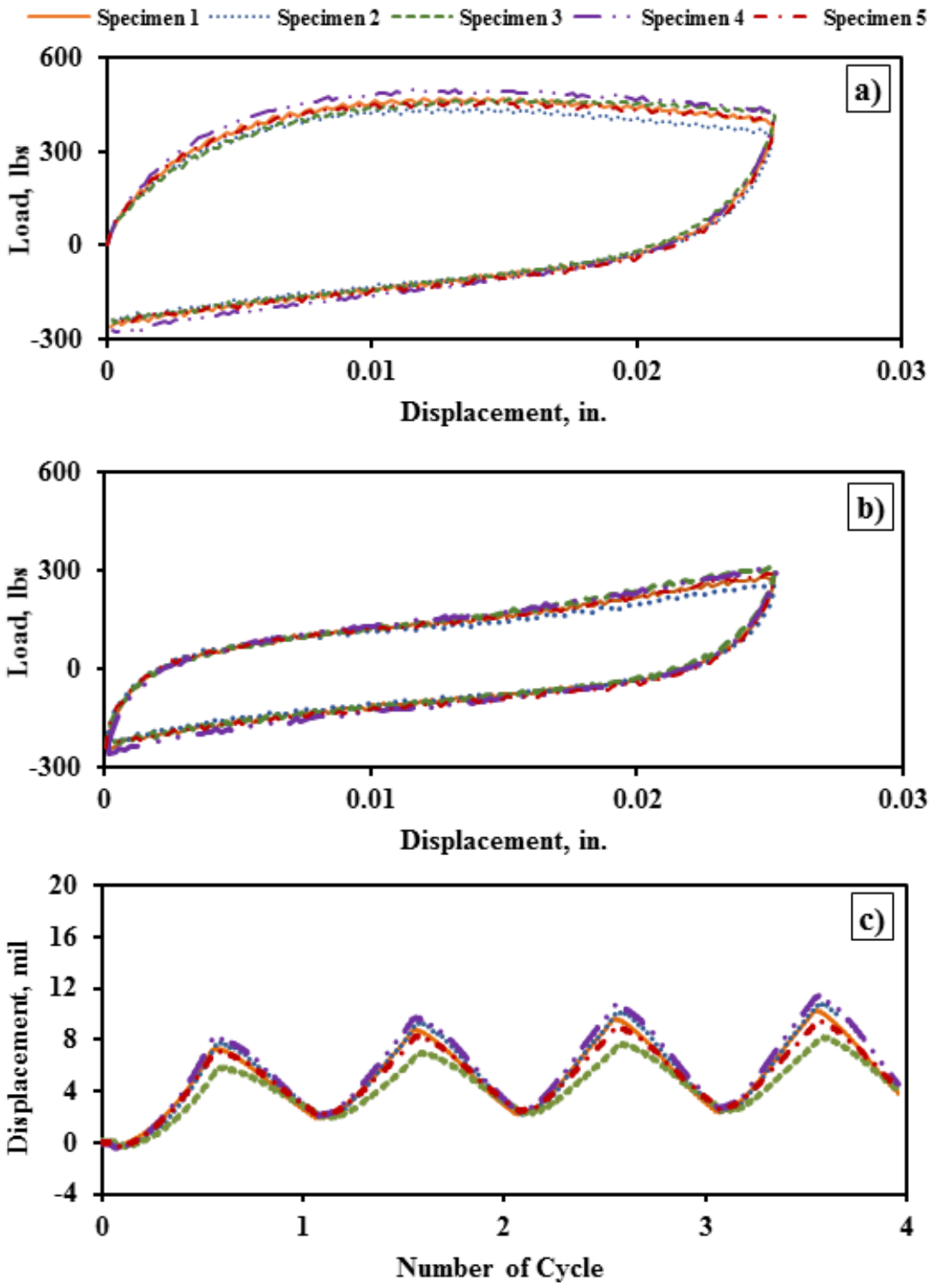

Figure 4.7 Results for Proposed Gluing Method a) First Cycle Hysteresis Loop, b) Second Cycle Hysteresis Loop, and c) Displacement of Top LVDT.

Table 4.1 Summary of Results Obtained from both Gluing Methods

Gluing Method	Parameter	Max Load, lbs	Critical Fracture Energy, in.-lbs/in.^{2}	Crack Progression Rate	Number of Cycles to Failure
Version 2014	Average	409	1.36	0.41	334
	Std Dev	99	0.20	0.11	146
	COV	**24%**	**15%**	**26%**	**44%**
Proposed Method	Average	467	1.10	0.45	350
	Std Dev	19	0.10	0.03	94
	COV	**4%**	**9%**	**6%**	**27%**

Despite the decrease in the variability in the number of cycles to failure from the proposed specimen preparation, the stated goal of acceptable variability, defined as COV ≤ 20%, could not be achieved. The proposed specimen preparation method seems to improve the consistency of the OT and the repeatability of the proposed parameters, critical fracture energy and crack progression rate.

4.2 RIGOROUS EVALUATION OF IMPROVED OT METHOD

4.2.1 Experimental Study Plan and AC Mixtures Characteristics

On the basis of the objectives of this evaluation, an experimental program was developed. The scope of the experimental program contains AC mix-level testing of plant-produced and laboratory-compacted specimens. Six different AC mix types including a thin overlay mix (TOM), a stone mastic asphalt (SMA), dense-graded and dense-graded superpave (SP) mixes were included in the experimental design plan. Various aspects in terms of the AC mix types were considered in developing the experimental design plan. As a minimum, a Type-C or D (typically poor crack resistant) and a SMA (consider good crack resistant) mixes were included to evaluate at least two commonly used dense-graded mixes, with known poor and good cracking

performance. More emphasis was given to the dense-graded and dense-graded SP mixes due to the variability concerns reported on past studies. Additionally, the selected AC mixes were chosen based on the perceived field performance reported by the districts and/or the members of the project committee. Table 4.2 lists these AC mixes and reports information such as the AC mix designation, mix type, location, mix-design characteristics and perceived performance. More information of the AC mixes used during this study is presented in *Appendix C*.

Table 4.2 Characteristics of AC Mixes

Designation	Mix Type	Location	Mix-design Characteristics	Perceived Performance
TOM	TOM	Austin	6.5% PG 76-22 + Sandstone/Limestone/Dolomite (NMAS 4.76)	Very Good
SMA-D	SMA-D	Lubbock	6.3% PG 70-28 + 0.4% AS + 0.3% FC + Sandstone/Limestone/Dolomite/Gravel (NMAS 9.5 mm)	Very Good
SP-C	SP-C	LaSalle	6.3% PG 64-22 + 30% RAP + 0.5% WMA + Gravel/Limestone/Dolomite (NMAS 9.5 mm)	Good
Type-C	Type-C	El Paso	4.6% PG 64-22 + 20% RAP + 2% WMA + Limestone/Dolomite/Gravel (NMAS 12.7 mm)	Marginal
SP-D 1	SP-D	Abilene	5.3% PG 64-22 + 1% AS + 8% RAP + 2% RAS + Limestone/Dolomite (NMAS 9.5 mm)	Poor
SP-D 2	SP-D	Corpus Christi	5.4% PG 64-22 + 0.4% WMA + 15% RAP + NP (NMAS 9.5 mm)	Poor
Type-D	Type-D	Brownwood	5.1% PG 64-22 + 15% RAP + 2% RAS + Limestone/Dolomite (NMAS 4.76 mm)	Poor

The results from the Type-C mix were also included during the analysis of the results. Five replicate specimens were tested for each mix to further evaluate the repeatability of the improved OT method and specimen preparation process. The preparation, molding, and trimming of the specimens took two days. The specimens were molded utilizing a gyratory compactor and trimmed using a double-blade masonry saw. All specimens were dried using a CoreDry^{TM} and air-dried to room temperature to prevent moisture intrusion and aging. The specimens were glued to the steel plates on the third day. The specimens' air voids were the only parameter that varied during the preparation process of specimens. The proposed parameters and the current performance index were computed and documented during evaluation. The average, standard deviation, and

coefficient of variation (COV) are reported for each parameter. The results from the TOM mix are thoroughly explained followed by a summary of the results from the other AC mixes. Detailed results for all mixes are presented in *Appendix C.*

4.2.2 Current and Proposed OT Test Results and Discussions

The hysteresis loops were first evaluated. The hysteresis loops from the first and second cycles of the TOM mixes are presented in Figures 4.8a and 4.8b, respectively. These hysteresis loops were consistent among the five tested OT specimens. The repeatability of the hysteresis loops from the first cycle suggests that the parameters measured from the first cycle hysteresis loop (maximum load and critical fracture energy) should also be consistent.

The displacement time histories captured by the LVDT placed on top of the specimens were also inspected. Even though the displacement time histories of the top LVDT were smaller in magnitude as compared to the displacement of the actuator LVDT (25 mil), the five specimens were in tension since the beginning of the test as shown in Figure 4.8c.

The variability of the load reduction curves was also analyzed to estimate the certainty of the crack progression rate. The normalized load reduction curves presented in Figure 4.9 are also consistent for TOM mix. The average crack progression rate for TOM was 0.25 with a COV of 4%.

The critical fracture energy and crack progression rate for each OT specimen of the TOM mix are shown in Figure 4.10. The cluster of the data points demonstrates the potential of the proposed OT method to provide repeatable results.

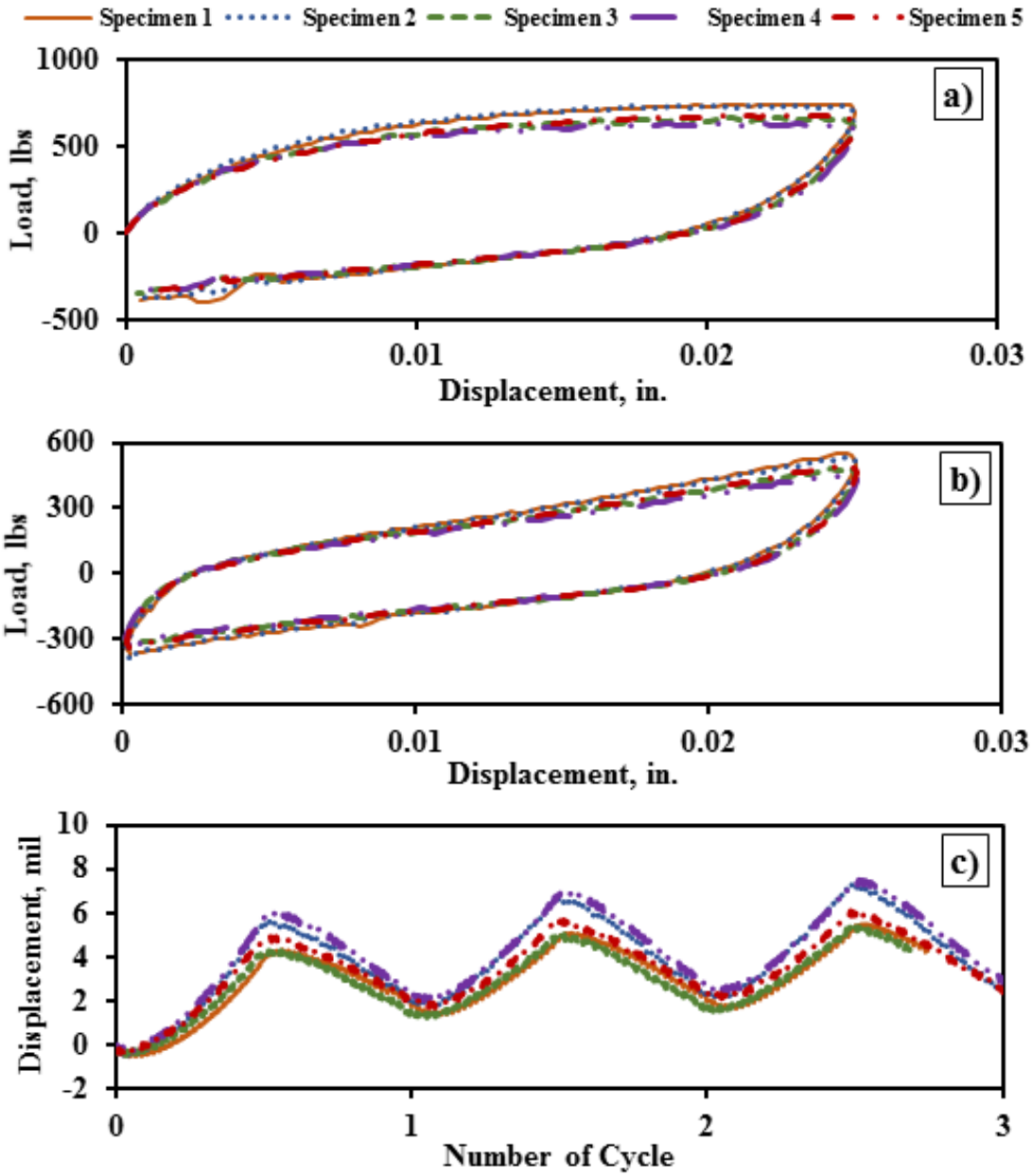

Figure 4.8 Results for TOM Mix: a) First Cycle Hysteresis Loop, b) Second Cycle Hysteresis Loop, and c) Displacement of Top LVDT

The average of the first hysteresis loops for each AC mixture is presented in Figure 4.11. Type-D and SP-D-1 mixtures exhibited similar maximum loads that are greater than the maximum loads from the other AC mixtures tested. Since a mix with greater critical fracture energy will resist the initiation of the crack better than a mix with lower critical fracture energy, Type-D and SP-D mixes should retard the initiation of the crack better than the other AC mixtures. However,

a good crack resistant mix must ideally also retard the crack propagation to perform adequately in the field. Thus, the inclusion of the crack progression rate is very important to properly characterize the potential of AC mixtures to cracking under the OT test.

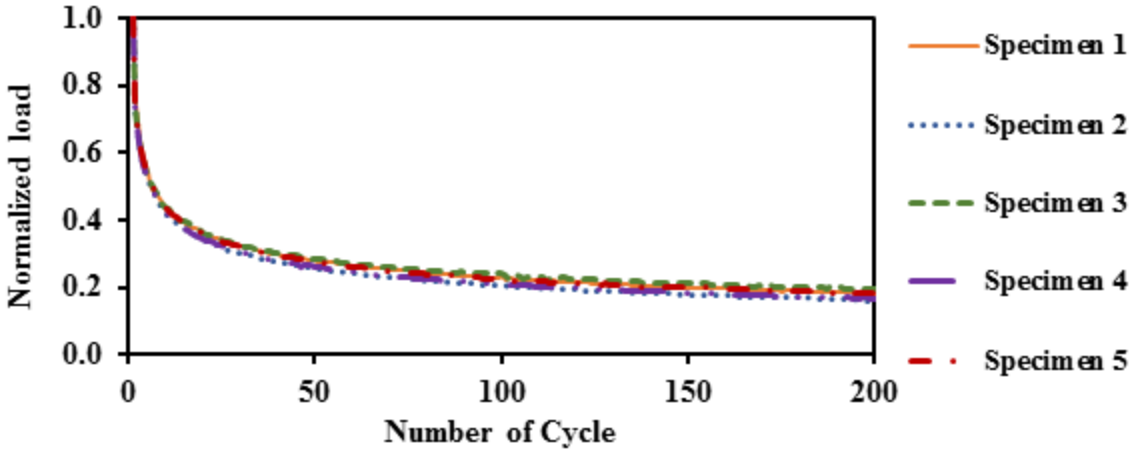

Figure 4.9 Load Reduction Curves for TOM Mix

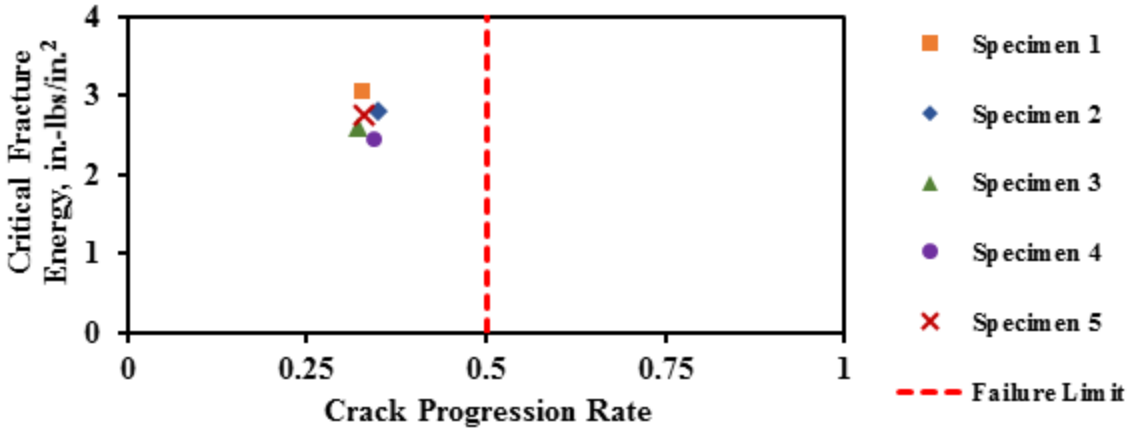

Figure 4.10 Performance of TOM Results on Design Interaction Plot

The average normalized load reduction curve of each mixture is presented in Figure 4.12. Based on these curves, the performance of the AC mixtures was satisfactorily delineated according to the perceived performance. The TOM, SMA-D and SP-C mixtures passed the failure criterion. The load reduction curve for the Type C mix is close to the load reduction curve corresponding to the failure limit, meaning that this Type-C mix has a marginal performance. Type-D, SP-D-1, and SP-D-2 did not pass the failure criterion, signifying that these mixtures are not flexible enough to attenuate the propagation of the crack.

The design interaction plot of the critical fracture energy and crack progression rate for the mixes is presented in Figure 4.13. Using the preliminary failure threshold for the crack progression rate, two zones were identified in the design interaction plot: good crack retardants (green) and poor crack retardants (red). According to this methodology, TOM is the best mix since it requires some energy to initiate a crack (exhibits high critical fracture energy) and it is flexible (exhibits low crack progression rate) after the crack has initiated. SMA-D mix can be ranked as the second best with the lowest crack progression rate (high flexibility after the crack has initiated) and low critical fracture energy (poor resistance to initiate a crack).

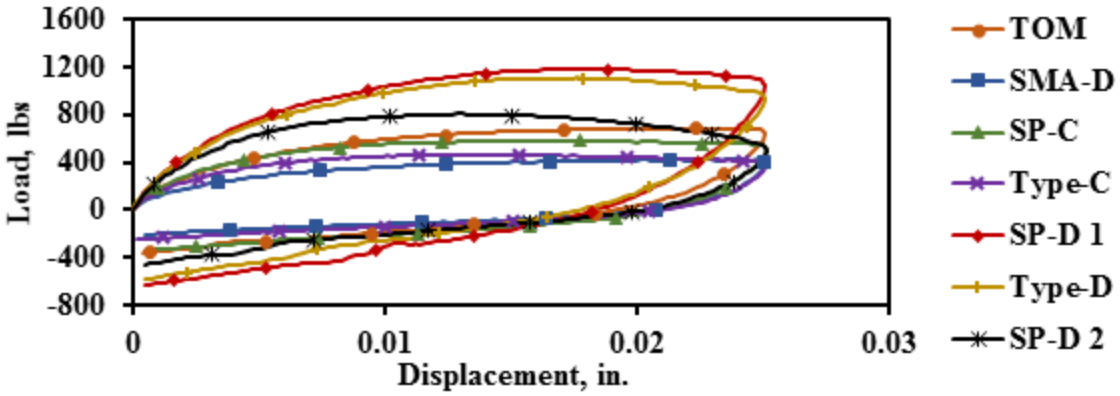

Figure 4.11 Average First Hysteresis Loop of AC Mixtures

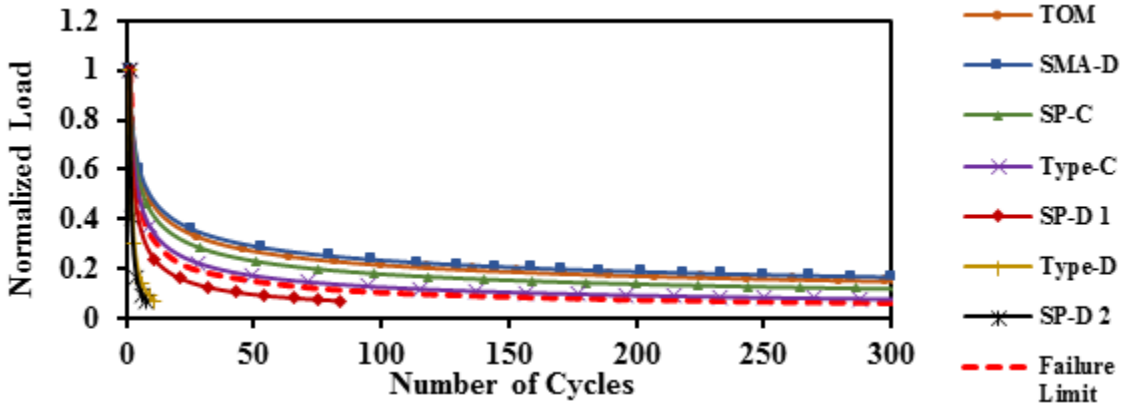

Figure 4.12 Average Normalized Load Reduction Curve of AC Mixtures

The critical fracture energy for SP-C mix is similar to that of SMA-D. However, the crack progression rate is higher for the SP-C mixture than the SMA-D mix. Type-C mix will satisfactorily resist the propagation of the crack, but the crack will initiate easily due to the low

critical fracture energy. Conversely, SP-D-1 will resist more at the crack initiation stage, but the crack will easily propagate due to the high crack progression rate. Type-D mix presented a poor crack progression rate but its high fracture energy makes the initiation of the crack relatively difficult. SP-D-2 can be ranked as the worst of the AC mixtures with the highest crack progression rate.

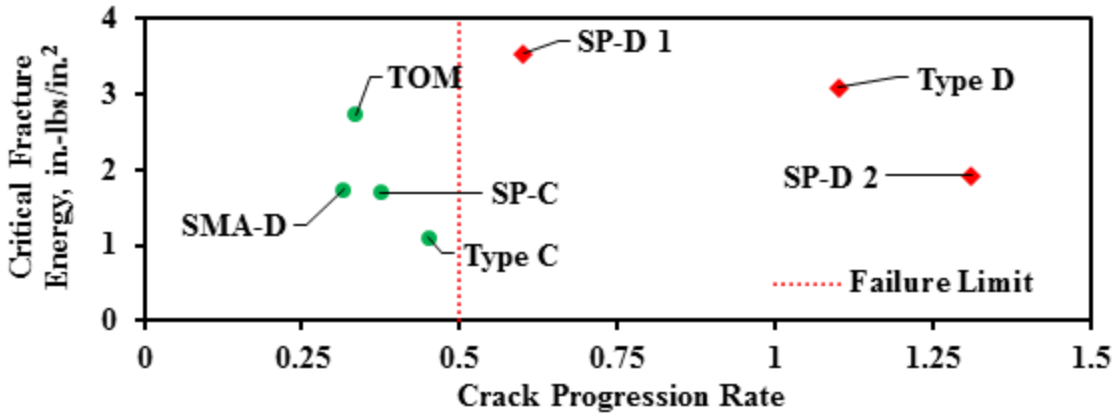

Figure 4.13 Cracking Performance of AC Mixtures using Improved OT Method

The statistical parameters of the proposed parameters and the number of cycles to failure are reported in Table 4.3. The COV values of the critical fracture energy and crack progression rate are less than 20%, except for the Type-D mixture that has a COV of 33% for the crack progression rate. The COV values for the number of cycles to failure ranged between 27% and 85%. It can be observed from the results of Type-D mix presented in *Appendix C* that one outlier is presented on the five OT results, which explains the high COV values.

The improved OT method based on the critical fracture energy and the crack progression rate seems to rank the resistance of the AC mixes during the crack initiation and propagation stages reasonably well.

Table 4.3 Consistency of Proposed Parameters and Number of Cycles to Failure

AC Mix	Parameters	Max Load, lbs	Critical Fracture Energy, in.-lbs/in.^{2}	Crack Progression Rate	Number of cycles to Failure
TOM	Average	689	2.7	0.33	1000
	Std Dev	44	0.2	0.01	0
	COV	**6%**	**7%**	**3%**	**NA**
SMA-D	Average	426	1.7	0.32	1000
	Std Dev	34	0.2	0.01	0
	COV	**8%**	**9%**	**4%**	**NA**
SP-C	Average	582.3	1.70	0.37	653
	Std Dev	39.6	0.13	0.03	326
	COV	**7%**	**8%**	**8%**	**50%**
Type C	Average	467	1.1	0.45	350
	Std Dev	19	0.1	0.03	94
	COV	**4%**	**9%**	**6%**	**27%**
SP-D 1	Average	1190	3.5	0.60	73
	Std Dev	42	0.2	0.04	26
	COV	**4%**	**5%**	**7%**	**35%**
Type D	Average	1116	3.1	1.10	21
	Std Dev	47	0.3	0.36	18
	COV	**4%**	**10%**	**33%**	**85%**
SP-D 2	Average	809	1.9	1.31	14
	Std Dev	28	0.2	0.26	6
	COV	**3%**	**10%**	**20%**	**40%**

4.3 PRELIMINARY DESIGN LIMITS FOR CRITICAL FRACTURE ENERGY

The current TxDOT AC mix design specifications present specific limits for performance tests such as the HWTD, OT and IDT tests especially for the dense-graded and super pave (SP) mixes. The design limits for the IDT are used to ensure that the stiffness properties of the mixes will not compromise the cracking performance in the field. Currently, the maximum allowable IDT strength is 200 psi and the minimum is set as 85 psi for dense-graded AC mixes. IDT tests were conducted on the AC mixes to correlate the tensile strength and the critical fracture energy measured from the IDT and OT tests, respectively. The results from the IDT tests are reported in

Appendix C. Five replicate IDT specimens were used to estimate the tensile strength of the mixes. The IDT specimens' dimensions were 2 in. (52 mm) thick and 4 in. (110 mm) diameter. The tensile strength and critical fracture energy of the mixes are plotted against one another in Figure 4.14. Based on the R^2 value, a good correlation was found between the tensile strength and critical fracture energy. Preliminary limits for the critical fracture energy were selected based on this correlation. The upper limit (UL) was rounded to 3 to screen the AC mixtures with high brittleness potential. The lower limit (LL) was rounded to 1. The design interaction plot and design limits for the cracking parameters measured with the OT test is presented in Figure 4.15.

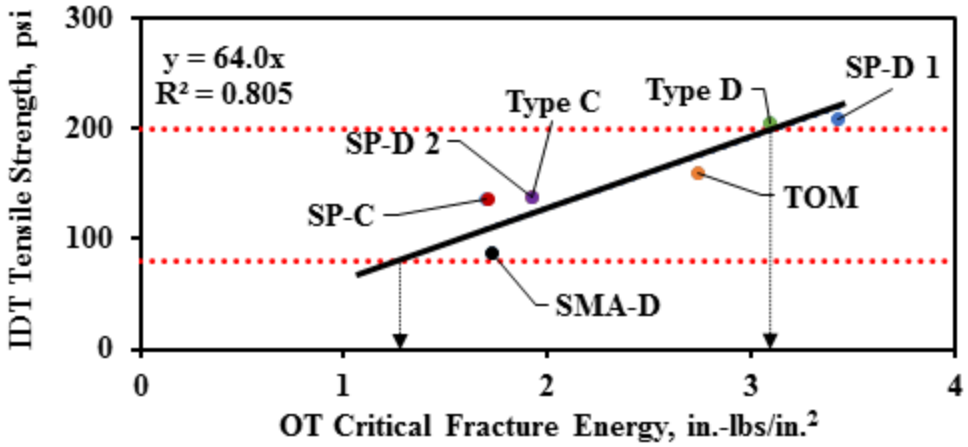

Figure 4.14 Correlation between IDT and OT Performance Indices

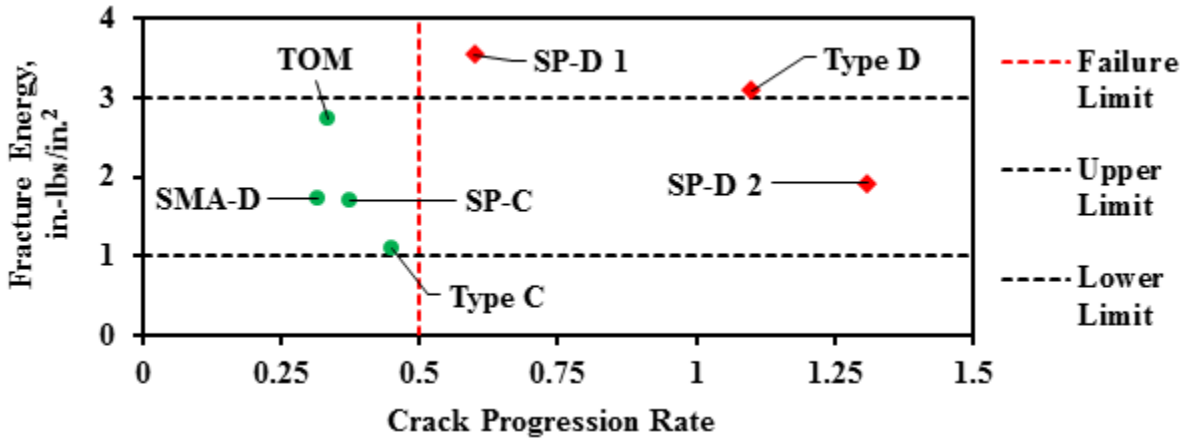

Figure 4.15 Design Interaction Plot for Cracking Resistance of AC Mixtures

Chapter 5: Validation of Improved OT Method

5.1 CRACKING PERFORMANCE OF FIELD SECTIONS

Field validation was conducted using distress surveys of seventeen pavement sections Table 5.1 presents the information about the sections. Most pavement sections are overlaid sections.

Table 5.1 Information of Seventeen Field Sections

Section ID	Mix Type	Construction Year	Binder Grade	Binder Content, %	RAP, %	RAS, %	ADT	Trucks Volume, %
1	SMA-D	2011	PG 70-28	6.3	20	0	3007	5.5
2	SMA-D	2011	PG 70-28	6.0	0	0	612	-
3	SMA-D	2011	PG 70-28	6.3	10	0	4837	3.2
4	SMA-D	2012	-	5.1	23	0	2103	22.3
5	SMA-D	2011	PG 70-28	6.3	0	0	4600	17.9
6	SMA-D	2012	-	6.3	18	0	337	2.0
7	CMHB-F	2013	PG 64-22	5.3	20	0	579	14.3
8	CMHB-F	2013	PG 64-22	5.3	20	0	372	12.8
9	Type-C	2013	PG 64-22	5.0	20	0	343	16.0
10	CMHB-F	2013	PG 70-22	5.0	20	0	-	-
11	Type-C	2012	PG 64-22	5.0	20	0	3288	1.0
12	Type-C	2011	PG 64-22	4.6	20	0	1545	4.2
13	Type-C	2011	PG 64-22	4.8	20	0	4127	7.8
14	Type-C	2012	PG 64-23	4.8	20	0	4270	4.0
15	TOM	2012	PG 76-22	6.5	0	0	929	12.0
16	TOM	2013	PG 76-22	6.5	0	0	3952	13.9
17	TOM	2013	PG 76-22	6.5	0	0	2620	4.4

Distress surveys have been conducted on nominally six-month intervals to document the conditions and performance of these sections. Four different cracking distresses have been documented during the distress surveys: alligator, block, transverse and longitudinal cracking. The distress severity of each field section has then been ranked as low, moderate and high. The field

sections were divided into three categories, good, satisfactory and poor performing, based on their service life and the distress severity. Table 5.2 provides the conditions and general performance of the field sections.

Table 5.2 Severity Rankings for Seventeen Field Sections

Section ID	Age (Months)	Type of Cracking Distress				General Performance
		Alligator	Block	Transverse	Longitudinal	
1	44	None	None	None	None	Good
2	44	None	None	None	None	Good
3	43	None	None	None	None	Good
4	36	None	None	None	None	Good
5	44	None	None	None	None	Good
6	43	None	None	None	None	Good
7	31	None	None	Low	None	Satisfactory
8	31	None	None	Low	None	Poor
9	36	None	None	Moderate	None	Poor
10	31	Low	None	Low	None	Poor
11	49	Moderate	None	Low	None	Satisfactory
12	58	Low	None	Moderate	None	Poor
13	59	Low	None	Low	Low	Poor
14	59	Moderate	None	Low	Low	Poor
15	47	None	None	None	None	Good
16	36	Low	None	Low	None	Satisfactory
17	36	None	None	Low	None	Satisfactory

These mixes were sampled during the construction stage of the field sections and subjected to the OT test in the laboratory. Initially, the OT data from replicate specimens was analyzed using the proposed OT test method to introduce the concept of designing crack resistant mixes using the critical fracture energy and crack progression rate parameters. The number of cycles was also computed from the OT data to compare the repeatability and consistency of this and the proposed parameters. The thickness of the AC layer for Sections 13, 14, 16, and 17 was less than the thickness required for an OT specimen, which might have introduced some uncertainties in the results obtained from the field cores. Densification, oxidation and layer thickness are considered

important factors that can influence the field core results. Additionally, the specimen preparation for the current and proposed OT methods is slightly different. This difference might have also affected the results from the field cores. With those caveats, a good, satisfactory and two poor performing sections are comprehensively described and presented to evaluate the performance of the OT test and the cracking life of AC mixes in the field. The results from all pavement sections are presented in *Appendix D*.

Section 1 is a moderately traveled roadway with two lanes per direction. This roadway was constructed and opened to traffic in 2011. The pavement structure consists of an AC layer made of type-D SMA, over a Type-B HMA layer with 20% reclaimed asphalt pavement (RAP). The base layer is cement-treated with 2% cement on top of a compacted natural soil subgrade. The ADT for this roadway in 2014 was 3007, about 5.5% of which were trucks. No cracking distresses were observed during the last survey performed on December 1, 2015.

The proposed design interaction (the average critical fracture energy vs. crack progression rate parameters) plot shown in Figure 5.1 can be used to estimate the cracking potential of the AC mix from this pavement section. The critical fracture energy was around 2.4, which is close to the upper limit. Based on this critical fracture energy, this AC mix would perform well in retarding the initiation of the crack. The crack progression rate was around 0.34, which is smaller than the failure limit of 0.50, meaning that the mix can be considered as a crack retardant mix. The field performance and initial OT test results for this section confirmed the effectiveness of the design interaction plot to predict the cracking potential of AC mixes.

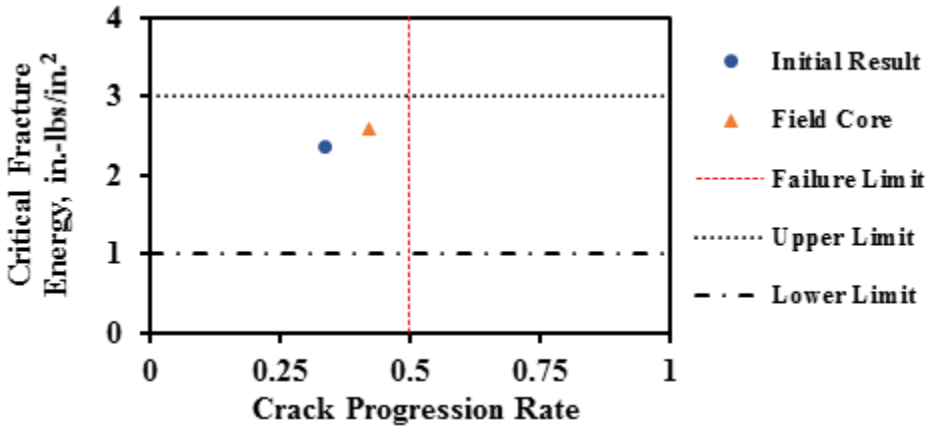

Figure 5.1 Cracking Potential for Section 1

For comparison purposes the means, standard deviations and COV values of the fracture energy and crack progression rates as well as the numbers of cycles to failure are shown in Table 5.3. The COV values for the critical fracture energy and crack progression rate are less than 5%, while the COV for the number of cycles to failure is greater than 20%. Based on the number of cycles to failure, this AC mix also should perform satisfactorily in terms of cracking. However, the high COV for the number of cycles to failure introduces some uncertainty in the application of this parameter as a performance index.

Table 5.3 Summary of Parameters for Section 1

Parameter	**Max Load, lbs**	**Critical Fracture Energy, in.-lbs/in.^{2}**	**Crack Progression Rate**	**Number of Cycles**
Average	719	2.4	0.34	847
Std. Dev.	26	0.1	0.01	217
COV	**4%**	**2%**	**4%**	**26%**

Two field cores were extracted from this section and subjected to OT tests. The initial and the field cores' OT results are also compared in Figure 5.1. The field core results are also located in the acceptable zone for a crack resistant mix. The crack progression rate for the field cores is greater as compared to that for the lab specimens that can be attributed to the stiffening of the mixes due to environmental conditions.

Similarly, the critical fracture energy is greater for the field cores. The magnitude of the fracture energy is directly related to the shape of the first hysteresis loop. The average first hysteresis loop for the initial and field core results are depicted in Figure 5.2. The hysteresis loop for the field cores resulted in greater critical fracture energy than the one from the initial test. As for the crack progression rate, the critical fracture energy can be affected by the aging effect and the densification of the field cores.

As a second example, Section 11 is a moderately traveled roadway with two lanes per direction with an ADT of 3288 of which only around 1% is truck traffic. The section was opened to traffic in 2012. The AC layer is a Type-C mix containing 20% RAP. The base is a cement-treated base with 3% percent cement. The subgrade is a compacted natural soil. The field cores and last survey were done around five years after the construction date. The last distress survey of this section reflected moderate alligator cracking and low transverse cracking. Alligator cracking with low severity was found on this section after less than to two years of service.

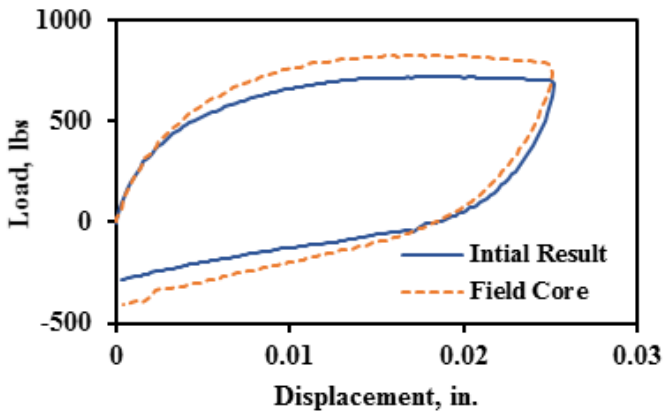

Figure 5.2 Comparison of Initial and Field Core Average Hysteresis Loops for Section 1

The average critical fracture energy and crack progression rate parameters are shown in Figure 5.3. The fracture energy was 1.6, which is considered a low value based on the established limits. The average absolute crack progression rate for this mix was 0.47, which is close to the proposed failure limit. Based on the proposed OT method, the cracking resistance of this mix is

considered marginal. The mix is expected to perform satisfactorily with a considerable potential to cracking in an early time.

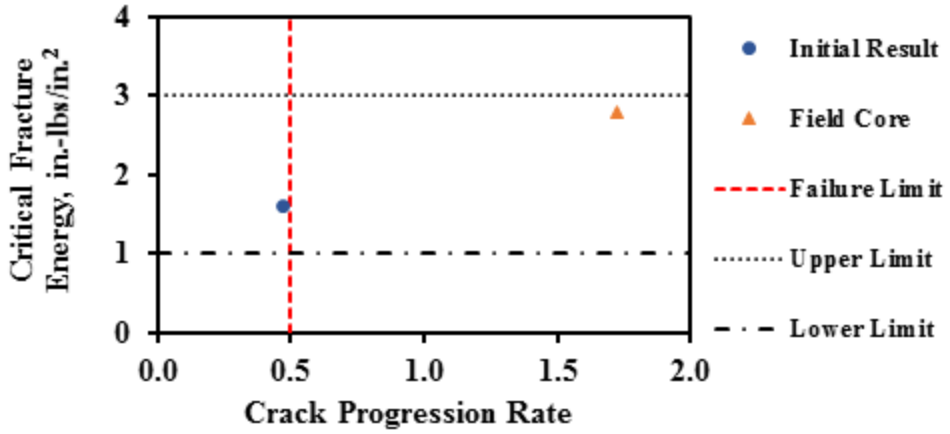

Figure 5.3 Cracking Potential for Section 11

The summary of the statistical parameters for the critical fracture energy, crack progression rate and number of cycles is presented in Table 5.4. The COVs for almost all parameters are within the acceptable levels of repeatability of 20% or less.

Table 5.4 Summary of Parameters for Section 11

Parameter	Max Load, lbs	Fracture Energy, in.-lbs/in.^{2}	Crack Progression Rate	Number of Cycles
Average	680	1.6	0.47	328
Std Dev	157	0.3	0.05	43
COV	**23%**	**20%**	**11%**	**13%**

The OT results from the two field cores are also included in Figure 5.3. The critical fracture energy is greater and the crack progression rate is significantly greater than the initial results. The average hysteresis loops from the initial mix and field cores are significantly different as shown in Figure 5.4. The results from the field cores indicate that the mix is significantly stiffer and more crack susceptible than the initial mix.

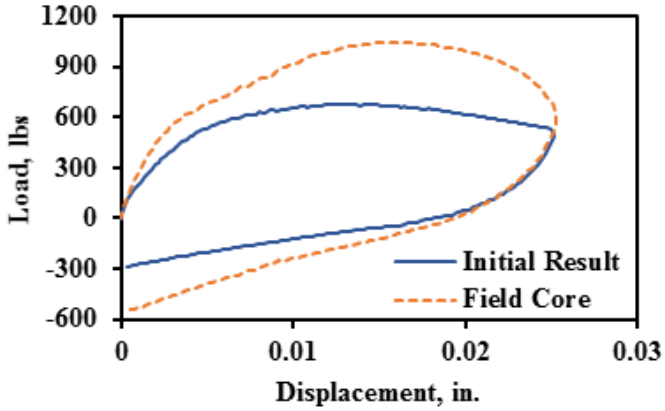

Figure 5.4 Comparison of Initial and Field Core Average Hysteresis Loops for Section 11

Section 9 corresponds to a poor performing section. This section was opened to traffic in 2013. The ADT for this section recorded in June 2015 was 343 with around 16% truck volume. The pavement section consisted of three layers on top of the existing natural compacted subgrade. The AC mixture collected and investigated from this section is Type C with 20% RAP. A warm mix asphalt (WMA) layer existed underneath the AC layer. The last distress survey conducted in March 2016 documented this section with moderate transverse cracking. A distress survey about six months after the construction revealed several 4-ft long transverse cracks.

The average critical fracture energy and absolute crack progression rate from the initial tests, as shown in Figure 5.5, indicate a marginally unacceptable mix as per the proposed criteria. The current criterion of the number of cycles yielded a COV of 31% (see Table 5.5). As per Table 5.5, the COVs for the critical fracture energy and the crack progression rate were less than 20%.

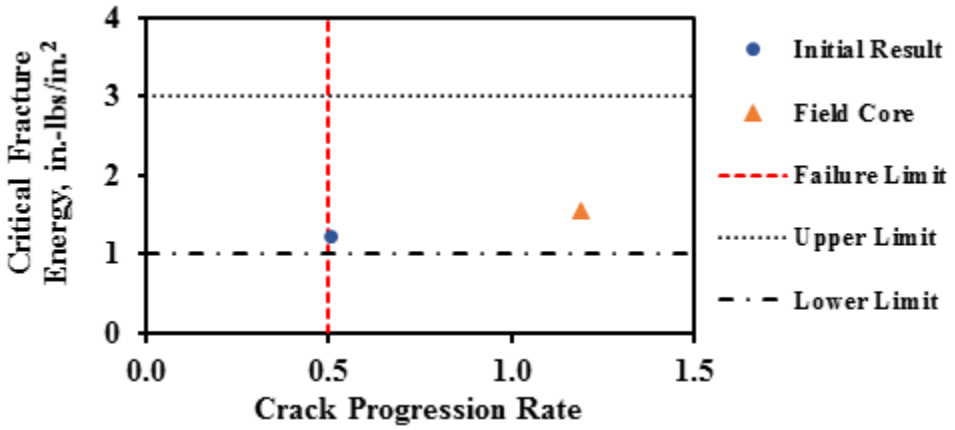

Figure 5.5 Cracking Potential for Section 9

Table 5.5 Summary of Parameters from Section 9

Parameter	Max Load, lbs	Critical Fracture Energy, in.-lbs/in.^{2}	Crack Progression Rate	Number of Cycles
Average	563	1.2	0.50	155
Std. Dev.	22	0.03	0.06	48
COV	**4%**	**3%**	**11%**	**31%**

Two field cores were extracted from this section, but only one was subjected to the OT test. A crack was found on the second field core. As shown in Figure 5.5, the cracking susceptibility of the mix placed in the field is significantly greater than the initial result. The critical fracture energy from the core was also greater than the initial result.

Figure 5.6 presents the comparison of the average hysteresis loops of the initial result and the field core. Similar to the previous case, the hysteresis loop for the field core is different from the one of the initial results.

Section 12, which is the second example of a poor performing mix, is a roadway with two lanes in each direction. This section was constructed in 2011. Based on the field measurements carried out in January 2013, the ADT for this section is 1848 with around 12% truck volume. The pavement section consists of two layers on top of the subgrade. The AC layer was built with a Type C mix containing 20% RAP. The base layer was treated with 3% cement. Based on the last

distress survey conducted in March 2016, the section exhibited moderate transverse and minor alligator cracking. However, 6-ft long transverse cracks were observed on this section after less than one year of service. The accumulation of damage due to the traffic loading and the poor cracking performance of the AC mix have introduced more cracking damage to this section throughout its service life.

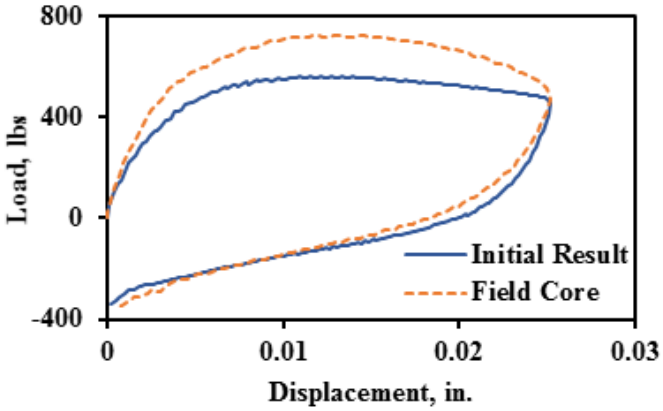

Figure 5.6 Comparison of Initial and Field Core Average Hysteresis Loops for Section 11

As shown in Figure 5.7, the average crack progression rate for this mix was initially 0.68, which would have been considered an unsatisfactory mix for crack propagation. Based on the critical fracture energy, the mix shows low resistance to crack initiation. From Table 5.6, the mix was also considered as a crack susceptible mix using the current failure criteria. Once again, the proposed cracking parameters exhibit smaller COVs than the number of cycles to failure.

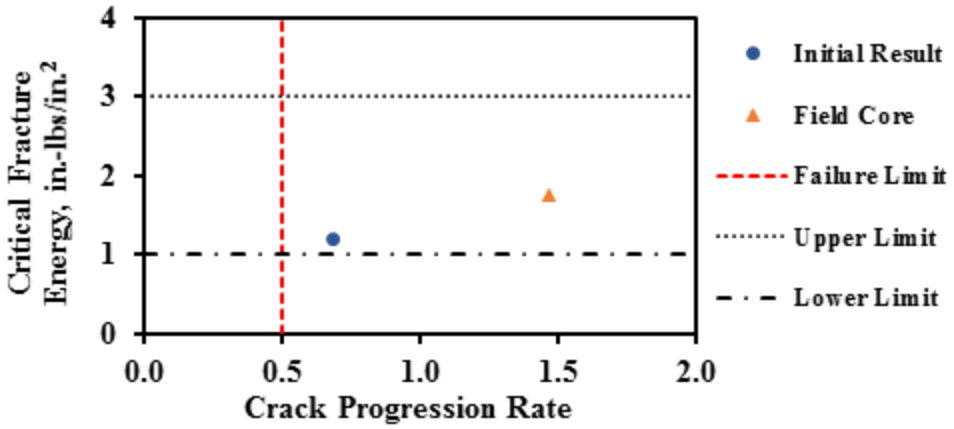

Figure 5.7 Cracking Potential for Section 12

Table 5.6 Summary of Parameters from Section 12

Parameter	Max Load, lbs	Critical Fracture Energy, in.-lbs/in.^{2}	Crack Progression Rate	Number of Cycles
Average	818	1.2	0.68	90
Std. Dev	132	0.1	0.07	32
COV	**16%**	**7%**	**11%**	**35%**

The OT tests were conducted on extracted field cores from this section. As shown in Figure 5.7, the two field cores exhibit more crack susceptibility (higher absolute value of crack progression rate) and greater critical fracture energy than the initial result.

5.2 COMPARISON BETWEEN OT TEST RESULTS DURING MIX DESIGN AND FIELD CORES

In this section, the OT performance parameters from the 17 field sections during the construction stage of the pavements are compared to the general performance of the pavements. General information related to the field performance, the current age and the OT results from the initial tests of the sections are presented in Table 5.7. The well performing sections are defined as those sections that had a service life of more than 40 months with no or minimal visible cracks. Most of the sections with good performance presented a crack progression rate less than 0.5 and a critical fracture energy value greater than 1.5, except for section 4 and 17 which have critical fracture energy values of 1.27 and 0.8 respectively. The ages for the sections with satisfactory performance were between 30 and 50 months with low severity visible cracks. The sections with satisfactory performance had crack progression rates between 0.35 and 1.0, and critical fracture energies between 0.8 and 1.9. For the sections with poor performance, the crack progression rate is generally greater than 1.0. With the ages of 30 to 60 months, most of the poor performing sections exhibited premature cracking within the first year after construction.

The combination of the crack progression rate and the critical fracture energy are promising parameters in predicting the cracking susceptibility of AC mixes during the design of the pavement section. Based on the design interaction plot shown in Figure 5.8a, the initial OT results satisfactorily predicted the observed performance of a large number of field sections. Additionally, the results from the field cores in Figure 5.8b satisfactorily delineate most of the well and poor performing AC mixes. A few of the predicted crack-susceptibility of the mixes from the OT tests do not agree with the field performance. Aside from the possible need to refine the limits, one should not forget that the OT acceptance criteria ascertains the suitability of the mixes without considering how strong or weak the pavement structure underneath that mix is. Comparisons of the initial and field cores' results with the performance of the sections are shown in Figure 5.9. Error bars for the initial results demonstrate the uncertainty in terms of one standard deviation from the OT tests. The data labels provide the average relative densities of the field cores. Most of the field cores had a relative density between 95% and 97%, especially for the well performing sections. The relative densities of the field cores from the satisfactory and poor performing sections varied substantially.

Figure 5.9a shows the critical fracture energies for the initial result and field cores as a function of the general performance of the pavement sections. The critical fracture energies from the field cores are normally greater or similar to those from the initial results. The differences in the critical fracture energies from the two sets of specimens (i.e., lab-prepared and filed cores) are not well understood but may be partially due to the oxidation and densification of the AC layers. Even though the same mix with the same lift thickness was supposed to be placed on Sections 7 and 8, the field cores from Section 7 were 1 in. thicker than Section 8. This may explain the difference in the field performance of these two sections.

Table 5.7 Comparison of Initial OT Results with Field Performance

Section ID	Age (Months)	Performance	Crack Progression Rate	Critical Fracture Energy, in.-lbs/in.^{2}
1	44	Good	0.34	2.37
2	44	Good	0.30	2.67
3	43	Good	0.30	2.67
4	36	Good	0.38	1.27
5	44	Good	0.67	2.57
6	43	Good	0.28	1.63
7	31	Satisfactory	0.95	0.84
8	31	Poor	0.95	0.84
9	36	Poor	0.50	1.23
10	31	Poor	0.61	0.79
11	49	Satisfactory	0.47	1.61
12	58	Poor	0.90	1.47
13	59	Poor	1.13	1.40
14	59	Poor	1.13	1.40
15	47	Good	0.33	0.80
16	36	Satisfactory	0.38	1.82
17	36	Satisfactory	0.38	1.82

The same information but for the crack progression rates is shown in Figure 5.9b. The crack progression rates for the sections with good performance almost always lie below the proposed delineation limit. Similarly, almost all sections that have performed poorly lie above the proposed delineation limit. While for well performing sections the results from the initial results and the extracted cores are similar, that is not the case for the poorly performing sections. This trend for the satisfactory mixes is not consistent.

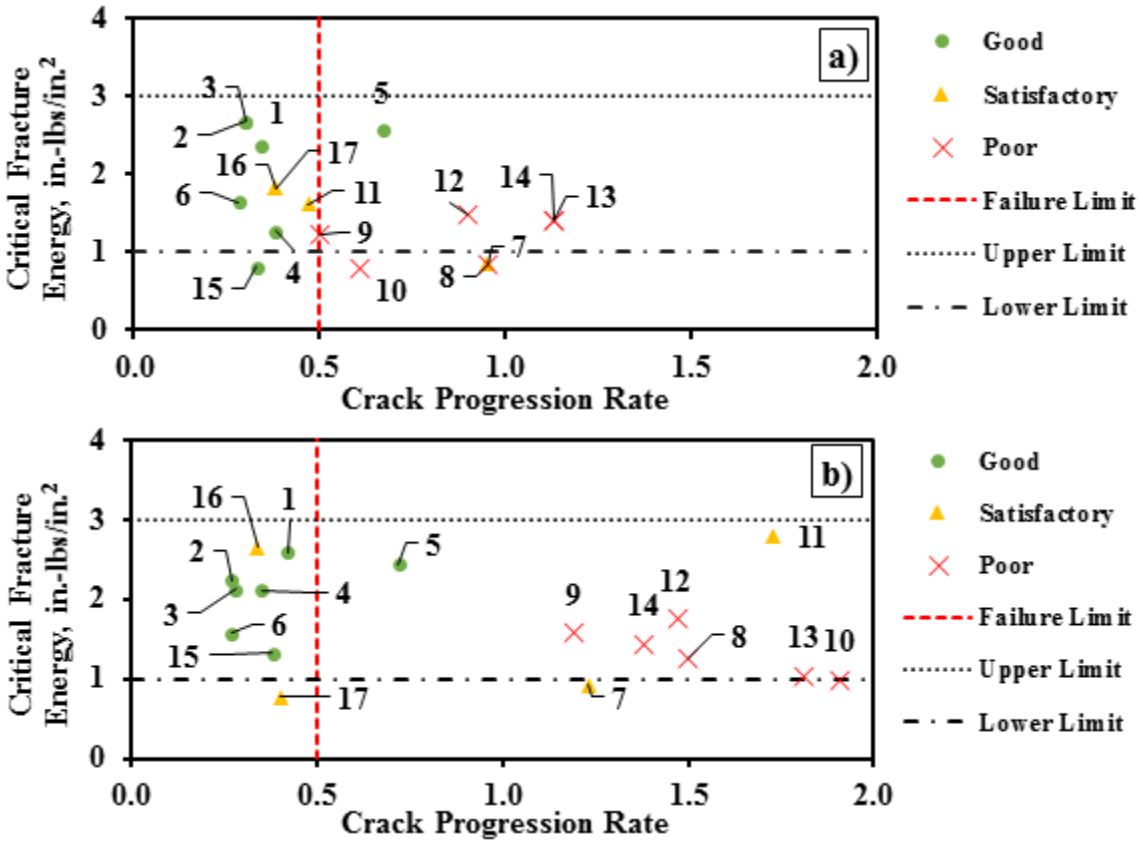

Figure 5.8 Design Interaction Plot for: a) Initial Results and b) Field Cores

The same comparisons but with the number of cycles to failure are shown in Figure 5.9c. The existing criterion based on the number of cycles also predicts the cracking performance of the sections similarly to the crack progression rate but with greater uncertainties as judged by the error bars. The patterns between the results from the initial results and the field cores are similar to those explained for the crack progression rate.

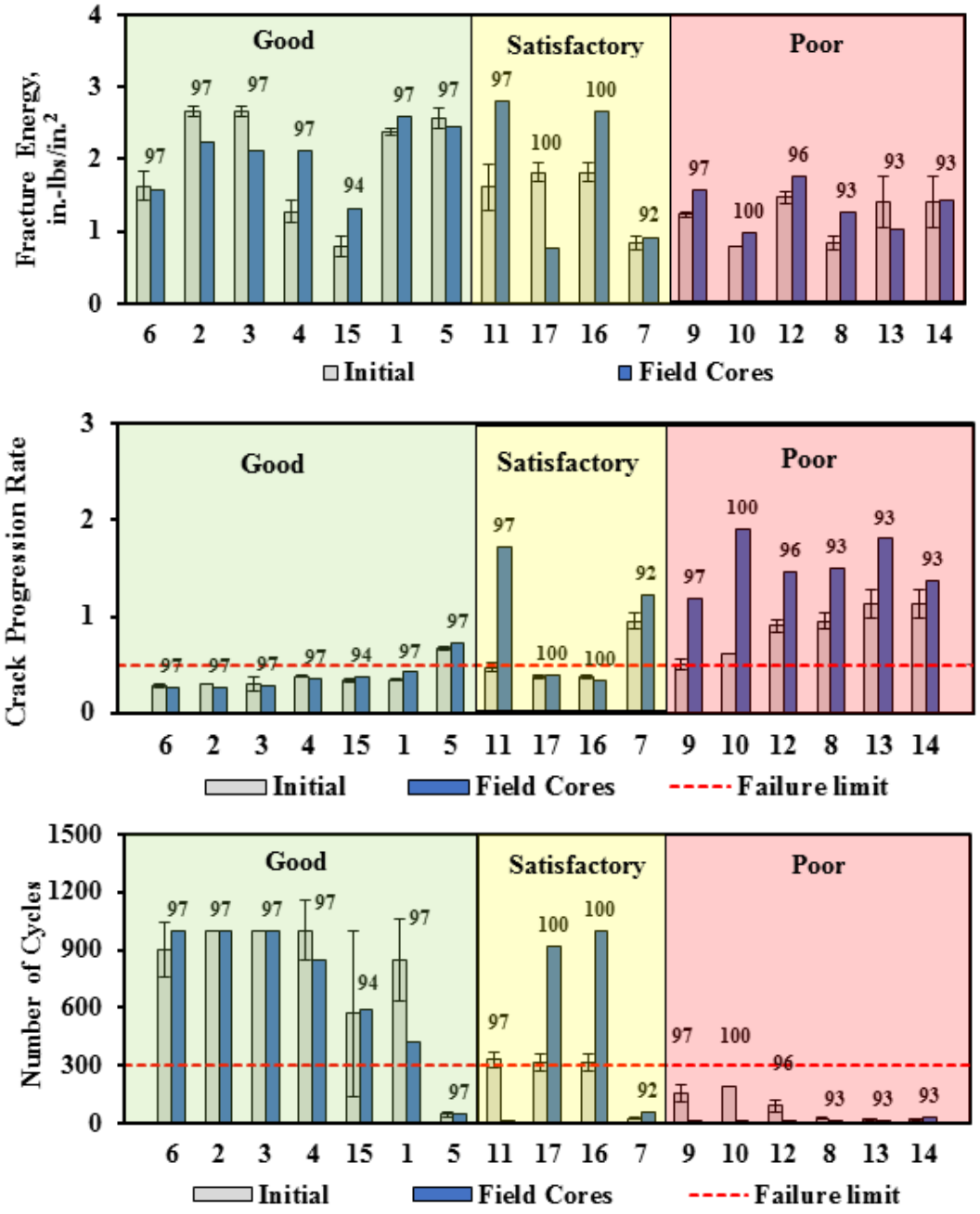

Figure 5.9 Performance of Cracking Indices: a) Critical Fracture Energy, b) Crack Progression Rate, and c) Number of cycles to Failure

Chapter 6: Key Remarks and Conclusions

A number of test methods have been proposed to assess the cracking resistance of the AC mixes during the mix-design process. At present, no single laboratory test has been established as the widely accepted standard cracking test that can be performed routinely to evaluate the cracking susceptibility of AC mixes. The main goal of this thesis study was to evaluate the performance of the current OT to propose an improved methodology to screen the cracking potential of well and poor performing AC mixes.

An improved cracking methodology based on the critical fracture energy and crack progression rate from the OT tests is proposed here. The proposed alternative methodology is able to delineate the performance of AC mixes and provide fracture and fatigue parameters to assess the cracking properties of the AC specimens during the crack initiation and propagation of the OT test.

6.1 Conclusions and Key Findings

From the findings of this study, the following major conclusions can be drawn:

1. The number of cycles to failure may not be the best parameter to be used as a performance index when the load reduction curves and hysteresis loops from replicate specimens seem more repeatable.
2. The comparison of the load-displacement curves from the cyclic and monotonic OT methods clearly demonstrated that the OT specimens are strained past their peak loads. Thus, the number of cycles to failure may not be a valid fatigue parameter to measure the fatigue properties of AC specimens.

3. The OT test was divided into two distinctive phases, crack initiation and propagation, to comprehensively predict the fracture and fatigue properties of AC mixes. An analysis methodology that considers these two phases is proposed.
4. The critical fracture energy from the first cycle of the cyclic OT method can be used to estimate the resistance of AC mixes to initiating a crack.
5. The crack progression rate that is defined as the rate of decrease in the measured load with the number of cycles can be used to characterize the crack propagation.
6. The critical fracture energy and the crack progression rate seemed to be more repeatable than the number of cycles to failure.
7. A design interaction plot to interpret the cracking properties of AC mixes was created using the proposed fracture and fatigue parameters.
8. The preliminary failure limit for the crack progression rate was added to delineate between good and poor crack retardant AC mixes.
9. Several AC mixes were evaluated using the alternative cracking methodology for the OT. The proposed methodology delineated the cracking performance of the AC mixes reasonably well.
10. A modified gluing method that can provide a consistent glued area and clean gap between the OT plates was implemented to minimize the variability and uncertainties related to the specimen preparation process.
11. The improved OT methodology was validated using cracking performance data and field cores from seventeen pavement sections. Most pavement sections with OT results that pass the proposed failure criteria seem to perform satisfactorily for at least five years with minor or no cracking damage.

6.2 RECOMMENDATIONS

The following recommendations are suggested to finalize the evaluation of the proposed OT method and continue validating the preliminary design limits for the critical fracture energy and crack progression rate:

- The field sections considered in this study have been in service for five years or less. The present criteria can only ascertain the suitability of the mix independent of the pavement structure or the function that the designer expect for the mix to perform and the stresses to carry. Further evaluation of these sections and extraction of field cores in the future are strongly recommended to better refine the acceptance criteria of the proposed OT method.
- The proposed OT test may be performed on aged and unaged specimens. However, a protocol must be identified to properly account for the densification, oxidation and aging of the field cores relative to the lab specimens.
- The implemented cracking methodology and parameters presented high repeatability and consistency. A parametric study is recommended to evaluate the sensitivity of the proposed performance indices to changes in parameters such as the asphalt content, asphalt grade, recycle material content and additives.
- By addressing the sensitivity of this cracking methodology to different AC mix designs, the improved OT method can be further implemented as a routine crack tests to design the cracking resistance of all types of AC mixes.

References

1. Al-Qadi, I. L., Ozer, H., Lambros, J., Khatib, A. E., Singhvi, P., Khan, T., Rivera-Perez, J., and Doll, B. (2015) "Testing Protocols to Ensure Performance of High Asphalt Binder Replacement Mixes using RAP and RAS." Research Report No. FHWA-ICT-15-017. Illinois Center for Transportation, Illinois.
2. Bennert, T. and Ali, M., "Field and Laboratory Evaluation of a Reflection Crack Interlayer in New Jersey," Journal of the Transportation Research Board, No. 2084, 2008, pp. 112–123, Transportation Research Board of the National Academies, Washington, D.C.
3. Bennert, T., Worden, M., and Turo, M., "Field and Laboratory Forensic Analysis of Reflection Cracking on Massachusetts Interstate 495," Journal of the Transportation Research Board, No. 2126, 2009, pp. 27–38. Transportation Research Board of the National Academies, Washington, D.C.
4. Buttlar, W. G. and R. Roque (1994). "Development and Evaluation of the Strategic Highway Research Program Measurement and Analysis System for Indirect Tensile Testing at Low Temperature." Journal of the Transportation Research Record No. 1454, pp. 163-171.
5. Daniel, J. S. and Y. R. Kim. (2002). "Development of a Simplified Fatigue Test and Analysis Procedure Using a Viscoelastic Continuum Damage Model," Journal of the Association of Asphalt Paving Technologists, Vol. 71, pp. 619–650.
6. Elseifi, M., L. Mohammad, H. Ying, and S. Cooper III. (2012). "Modeling and Evaluation of the Cracking Resistance of Asphalt Mixture Using Semi-Circular Bending Test at Intermediate Temperature," Journal of the Association of Asphalt Paving Technologists, Vol. 81, pp. 277–302.
7. Garcia, V. and Miramontes, A. (2015) "Understanding Sources of Variability of Overlay Test Procedure". No. 16-2317, Journal of the Transportation Research Board, No. 2507, 10-18, Transportation Research Board of the National Academies, Washington D.C.
8. Germann, F. P., and Lytton, R. L. (1979). "Methodology for Predicting the Reflection Cracking Life of Asphalt Concrete Overlays." Report No. FHWA/TX-79/09+207-5, Texas Transportation Institute, College Station, Texas.
9. Ghuzlan, K. A., and Carpenter, S. H. (2003). "Traditional fatigue analysis of asphalt concrete mixtures." 82nd Annual Meeting of Transportation Research Board, CD-ROM, Washington D.C.
10. Hajj, E., Sebaaly, P., and Loria L. (2008) "Reflective cracking of flexible pavements phase II: review of analysis models and evaluation tests." Research Report No. 13JF-1, Nevada Department of Transportation.
11. Hajj, E., Sebaaly, P., Porras, J., and J. Azofeifa., "Reflection Cracking of Flexible Pavements Phase III: Field Verification," Research Report No. 13KJ-1, Nevada Department of Transportation, Research Division, University of Nevada, Reno. 2010.
12. Hu S., Zhou, F., Scullion, T., and Leidy, J. (2012). "Calibrating and Validating Overlay Tester–Based Fatigue Cracking Model with Data from National Center for Asphalt

Technology." Transportation Research Record, Journal of the Transportation Research Board, No. 2296, 57–68, Transportation Research Board of the National Academies, Washington, D.C.

13. Jacobs, M. M. J., Hopman, P. C., and Molenaar, A. A. A. (1995). "The crack growth mechanism in asphaltic mixes." HERON, 40, (3), ISSN 0046-7316.
14. Jacobs, M. M. J., Hopman, P.C., and Molenaar, A. A. A. (1996). "Application of Fracture Mechanics Principles to Analyze Cracking in Asphalt Concrete." Journal of the Association of Asphalt Paving Technologists, Vol. 65, pp. 1–39
15. Jimenez, F. P., Valdes, G. A., Botella, R., Miro, R., and Martinez, A. (2012). "Approach to fatigue performance using Fenix test for asphalt mixtures." Construction and Building Materials, 26, 372–380.
16. Koohi, Y., Luo, R., Lytton, R. L., and Scullion, T. (2012). "New methodology to find the healing and fracture properties of asphalt mixes using overlay tester." Journal of Materials in Civil Engineering, ASCE, doi. 10. 1061/ (ASCE) MT.
17. Marasteanu, M. O., J. F. Labuz, S. Dai, and X. Li. (2002). "Determining the Low Temperature Fracture Toughness of Asphalt Mixtures." Transportation Research Record: Journal of the Transportation Research Board, No. 1789, pp. 191–199. Transportation Research Board of the National Academies, Washington, D.C.
18. Medani, T. O., and Molenaar, A. A. A. (2000). "Estimation of fatigue characteristics of asphalt mixes using simple tests." HERON, 45, (3), ISSN 0046-7316.
19. Monismith, C. L. and Deacon, J. A. (1969). Fatigue of Asphalt Paving Mixtures, ASCE Transportation Engineering Journal, Vol. 95:2, pp. 317–346.
20. Monismith, C. L. and N. F. Coetzee (1980). "Reflection Cracking: Analysis, Laboratory Studies and Design Consideration," Proceedings of Association of Asphalt Paving Technologists, Vol. 49, pp. 268–313.
21. Pérez-Jimenez, F., Valdés, G. A., Botella, R., Miro, R., and Martínez, A. (2011). "Approach to fatigue performance using Fenix test for asphalt mixtures." Journal of Construction and Building Materials.
22. Pugno, N., Ciavarella, M., Cornetti, P. and Carpinteri, A. (2006). "A generalized Paris' law for fatigue crack growth." Journal of the Mechanics and Physics of Solids, 54, 1333–1349.
23. Roque, R., Birgisson, B., Sangpetngam, B., and Zhang, Z. (2002). "Hot mix asphalt fracture mechanics: A fundamental crack growth law for asphalt mixtures." 81st Annual Meeting of Transportation Research Board, CD-ROM, Washington D.C.
24. Wagoner, M. P., Buttlar, W. G., Paulino, G. H., and Blankenship, P. (2005). "Investigation of the fracture resistance of hot-mix asphalt concrete using a disk-shaped compact tension test." Transportation Research Record, Journal of the Transportation Research Board, No. 1929, 183–192, Transportation Research Board of the National Academies, Washington, D.C.
25. Walubita, L. F., A. N. M. Faruk, G. Das, H. A. Tanvir, J. Zhang, and T. Scullion (2012). "The Overlay Tester: A Sensitivity Study to Improve OT Repeatability and Minimize

Variability in the OT Test Results". Research Report FHWA/TX-12/0-6607-1. Texas Transportation Institute, Texas A&M University System, College Station, Texas.

26. Walubita, L. F., Faruk, A. N. M., Alvarez, A. E., and Scullion, T. (2013). "The Overlay Tester (OT): using the fracture energy index concept to analyze the OT monotonic loading test data." Construction and Building Materials, 40, 802-811.
27. Witczak, M. W., Pellinen, T.K., and El-Basyouny. (2002) "Pursuit of the Simple Performance Test for Asphalt Concrete Fracture/Cracking." Journal of the Association of Asphalt Paving Technologists, Vol 71, pp 767-778.
28. Yi-qiu, T., Lei, Z., Meng, G., Li-yan, S. (2012). "Investigation of the deformation properties of asphalt mixtures with DIC technique." Construction and Building Materials, 37, 581–590.
29. Zhang, Z., Roque, R., Birgisson, B., and Sangpetngam, B. (2001). "Identification and verification of a suitable crack growth law." 80th Annual Meeting of Transportation Research Board, CD-ROM, Washington D.C.
30. Zhou, F., S. Hu, T. Scullion, M. Mikhail, and L. F. Walubita. (2005). "A Balanced HMA Mix Design Procedure for Overlays." Journal of the Association of Asphalt Paving Technologists, Vol. 74, pp. 443-484.
31. Zhou, F., Hu, S., and Scullion, T. (2006). "Integrated asphalt (overlay) mixture design, balancing rutting and cracking requirements." FHWA/ TX-06/0-5123-1, Texas Transportation Institute, College Station, Texas.
32. Zhou, F., Hu, S., and Scullion, T. (2007). "Development and verification of the overlay tester based fatigue cracking prediction approach." FHWA/ TX-07/9-1502-01-8, Texas Transportation Institute, College Station, Texas.
33. Zhou, F., Hu S., and T. Scullion. (2009) "Overlay tester: a simple and rapid test for HMA fracture properties." Texas Transportation Institute, USA.
34. Zhou, F., and Scullion, T. (2003). "Upgraded overlay tester and its application to characterize reflection cracking resistance of asphalt mixtures" FHWA/ TX-04/0-4467-1, Texas Transportation Institute, College Station, Texas
35. Zhou, F. and T. Scullion. (2005) "Overlay Tester: A Rapid Performance Related Crack Resistance Test," Texas Transportation Institute, the Texas A&M University System, Report FHWA/TX-05/0-4667-2, College Station, Texas.
36. Zhou, F. and T. Scullion, (2006). Overlay Tester: A Simple and Rapid Screening Test for Characterizing Crack Resistance of HMA Mixes, Proceedings of 10th International Conference on Asphalt Pavement, Quebec, Canada, August 12-17, 2006.

Appendix A: Evaluation of OT Test and Current Performance Index

	AGGREGATE BIN FRACTIONS							"RECYCLED MATERIALS"			
	Bin No.1	Bin No.2	Bin No.3	Bin No.4	Bin No.5	Bin No.6	Bin No.7	Bin No.8	Bin No.9	Bin No.10	
Aggregate Source:	Limestone_Dolom	Igneous	Limestone_Dolom					Fractionated RAP			Material Type
Aggregate Pit:	avispa	vado	screenins	filler				txdot			Material Source
Aggregate Number:	2407220	2411613	2407220								RAS Type
Sample ID:	3/8	3/8 SAC A	crusher fines								Sample ID

Ratio of Recycled to Total Binder, % *(based on binder percent (%) entered below in this worksheet)*
7.7

Recycled Asphalt Binder (%)

															4.0						Combined Gradation							
Hydrated Lime?:															14.4	% of Tot. Mix		% of Tot. Mix		% of Tot. Mix	Total Bin	Lower & Upper Specification Limits			Restricted Zone			Individual % Retained	Cumulative % Retained	Sieve Size
Individual Bin (%):	25.0	Percent	36.0	Percent	23.0	Percent	1.0	Percent		Percent		Percent		Percent	15.0	% of Aggreg		% of Aggreg		% of Aggreg	100.0%									
Sieve Size:	Cum.% Passing	Wtd Cum. %	Cum.% Passing	Wtd Cum. %	Cum.% Passing	Wtd Cum. %	Cum.% Passing	Wtd Cum. %	Cum.% Passing	Wtd Cum. %	Cum.% Passing	Wtd Cum. %	Cum.% Passing	Wtd Cum. %	Cum.% Passing	Wtd Cum. %	Cum.% Passing	Wtd Cum. %	Cum.% Passing	Wtd Cum. %	Cum. % Passing	Lower	Upper	Within Spec's	Lower	Upper	Within Spec's			
3/4"	100.0	25.0	100.0	36.0	100.0	23.0	100.0	1.0							100.0	15.0					100.0	100.0	100.0	Yes				0.0	0.0	3/4"
3/8"	93.0	23.3	95.0	34.2	100.0	23.0	100.0	1.0							93.0	14.0					95.4	95.0	100.0	Yes				4.6	4.6	3/8"
No. 4	21.0	5.3	23.0	8.3	99.0	22.8	100.0	1.0							62.0	9.3					46.6	40.0	50.0	Yes				48.8	53.4	No. 4
No. 8	4.0	1.0	3.0	1.1	78.7	18.1	100.0	1.0							28.0	4.2					25.4	17.0	27.0	Yes				21.2	74.6	No. 8
No. 16	1.8	0.5	2.0	0.7	46.0	10.6	100.0	1.0							23.0	3.5					16.2	12.0	22.0	Yes				9.2	83.8	No. 16
No. 30	1.7	0.4	1.7	0.6	30.0	6.9	100.0	1.0							17.0	2.6					11.5	8.0	20.0	Yes				4.7	88.5	No. 30
No. 50	1.5	0.4	1.5	0.5	19.8	4.6	100.0	1.0							13.0	2.0					8.4	6.0	15.0	Yes				3.1	91.6	No. 50
No. 200	1.0	0.3	1.0	0.4	12.5	2.9	100.0	1.0							8.5	1.3					5.8	5.0	9.0	Yes				2.7	94.2	No. 200

(Bold Italic) Not within specifications *(Bold Italic)* Not within specificaitons- Restricted Zone *(Italic)* Not cumulative

Lift Thickness, in:	2.00	Binder Substitution?	No	Binder Originally Specified:		Substitute Binder:
Asphalt Source:	Western refining PG 64-22	Binder Percent, (%):	7.8	Asphalt Spec. Grav.:	1.001	
Antistripping Agent:		Percent, (%):		% Crumb Rubber:	18.5	

Figure A1 SMAR-F Mix Design Summary Sheet

	AGGREGATE BIN FRACTIONS							"RECYCLED MATERIALS"			
	Bin No.1	Bin No.2	Bin No.3	Bin No.4	Bin No.5	Bin No.6	Bin No.7	Bin No.8	Bin No.9	Bin No.10	
Aggregate Source:	Limestone_Dolom	Igneous	Limestone_Dolom	Limestone_Dolom	Gravel			Fractionated RAP			Material Type
Aggregate Pit:	Butterfield	Padre Canyon	Butterfield	Butterfield				txdot			Material Source
Aggregate Number:	2407220	2411613	2407220	2407220							RAS Type
Sample ID:	3/4	3/8 SAC A	3/8	fines	sand						Sample ID

Ratio of Recycled to Total Binder, % *(based on binder percent (%) entered below in this worksheet)*
21.7

Recycled Asphalt Binder (%)

															5.0						Combined Gradation							
Hydrated Lime?:															20.0	% of Tot. Mix		% of Tot. Mix		% of Tot. Mix	Total Bin	Lower & Upper Specification Limits			Restricted Zone			Individual % Retained	Cumulative % Retained	Sieve Size
Individual Bin (%):	7.0	Percent	25.4	Percent	12.0	Percent	31.0	Percent	4.7	Percent		Percent		Percent	19.9	% of Aggreg		% of Aggreg		% of Aggreg	100.0%									
Sieve Size:	Cum.% Passing	Wtd Cum. %	Cum.% Passing	Wtd Cum. %	Cum.% Passing	Wtd Cum. %	Cum.% Passing	Wtd Cum. %	Cum.% Passing	Wtd Cum. %	Cum.% Passing	Wtd Cum. %	Cum.% Passing	Wtd Cum. %	Cum.% Passing	Wtd Cum. %	Cum.% Passing	Wtd Cum. %	Cum.% Passing	Wtd Cum. %	Cum. % Passing	Lower	Upper	Within Spec's	Lower	Upper	Within Spec's			
1"	100.0	7.0	100.0	25.4	100.0	12.0	100.0	31.0	100.0	4.7					100.0	19.9					100.0	100.0	100.0	Yes				0.0	0.0	1"
3/4"	90.0	6.3	100.0	25.4	100.0	12.0	100.0	31.0	100.0	4.7					100.0	19.9					99.3	95.0	100.0	Yes				0.7	0.7	3/4"
3/8"	15.0	1.1	68.0	17.3	82.0	9.8	100.0	31.0	100.0	4.7					93.0	18.5					82.4	70.0	85.0	Yes				16.9	17.6	3/8"
No. 4	1.0	0.1	5.0	1.3	22.0	2.6	99.0	30.7	98.0	4.6					67.5	13.4					52.7	43.0	63.0	Yes				29.7	47.3	No. 4
No. 8	*1.8*	0.1	1.0	0.3	4.2	0.5	73.0	22.6	98.0	4.6					44.0	8.8					36.9	32.0	44.0	Yes				15.8	63.1	No. 8
No. 30	0.7	0.0	0.7	0.2	2.5	0.3	33.9	10.5	81.0	3.8					19.0	3.8					18.6	14.0	28.0	Yes				18.3	81.4	No. 30
No. 50	0.6	0.0	0.5	0.1	2.0	0.2	27.0	8.4	44.0	2.1					15.9	3.2					14.0	7.0	21.0	Yes				4.6	86.0	No. 50
No. 200	0.4	0.0	0.4	0.1	1.0	0.1	12.3	3.8	1.0	0.0					7.3	1.5					5.6	2.0	7.0	Yes				8.4	94.4	No. 200

(Bold Italic) Not within specifications *(Bold Italic)* Not within specificaitons- Restricted Zone *(Italic)* Not cumulative

Lift Thickness, in:	2.00	Binder Substitution?	Yes	Binder Originally Specified:	PG 70-22	Substitute Binder:	PG 64-22	
Asphalt Source:	Western refining	Binder Percent, (%):	4.6	Asphalt Spec. Grav.:	1.001			
Antistripping Agent:		Percent, (%):						

Figure A2 Type-C Mix-Design Summary Sheet

Table A1 Summary of Results for SMAR-F Mix

Specimen	Air Voids, %	Max Load, lbs	Load of Last Cycle, lbs	Number of OT Cycles
1	7.2	385	26	70
2	6.8	396	24	55
3	7.3	410	27	101
4	6.0	469	30	34
5	6.5	385	24	83
Average	6.8	409	26	69
Median	6.8	396	26	70
Std Dev	0.5	35	2	26
COV	**8%**	**9%**	**10%**	**37%**

Table A2 Summary of Results for Type-C Mix

Specimen	Air Voids, %	Max Load, lbs	Load of Last Cycle, lbs	Number of OT Cycles
1	6.8	358	25	375
2	6.1	334	23	404
3	6.1	467	32	363
4	7.1	330	23	449
5	7.5	556	38	79
Average	6.7	409	28	334
Median	6.8	358	25	375
Std Dev	0.6	99	7	146
COV	**9%**	**24%**	**23%**	**44%**

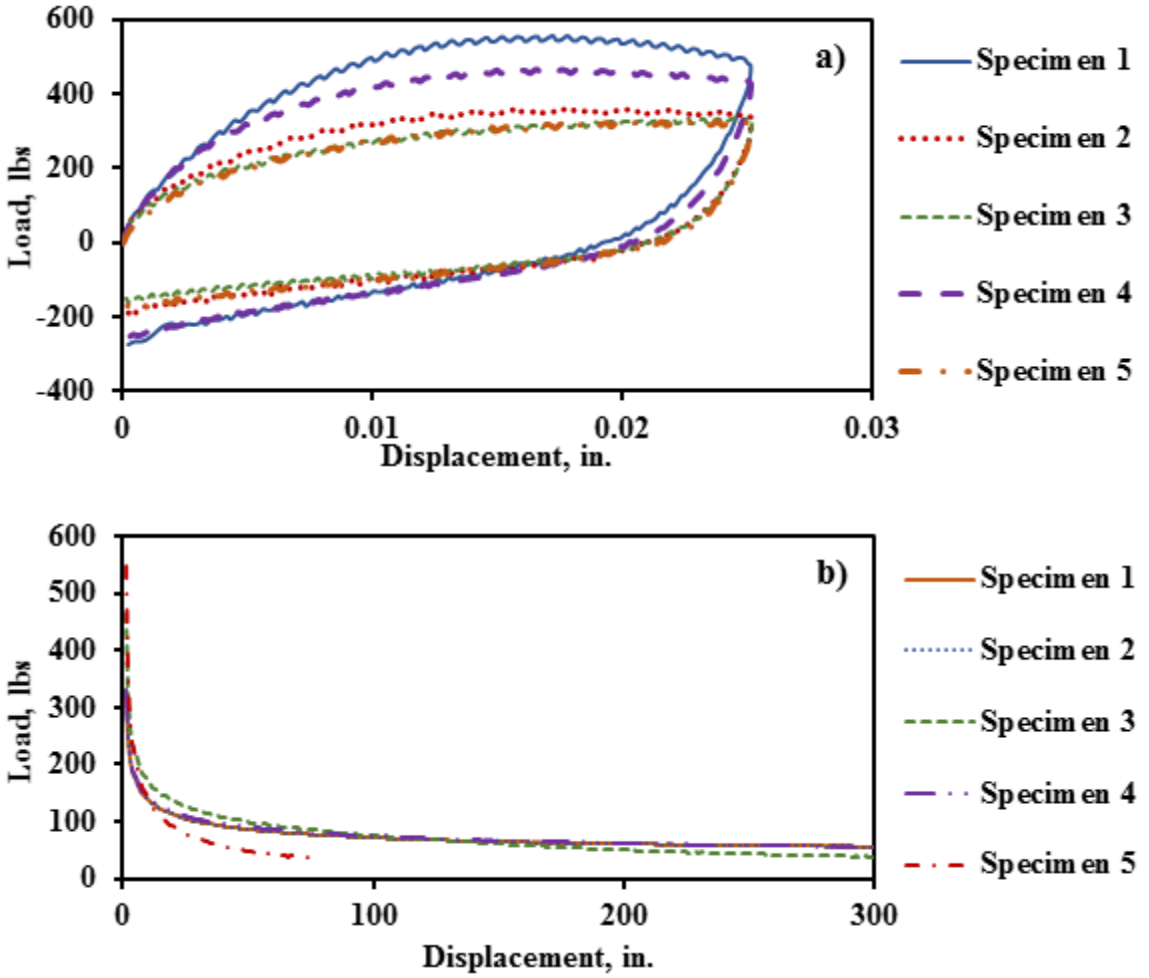

Figure A3 Test Response Curves from Type-C: a) First Hysteresis Loops and b) Maximum Peak Load versus Number of Cycles

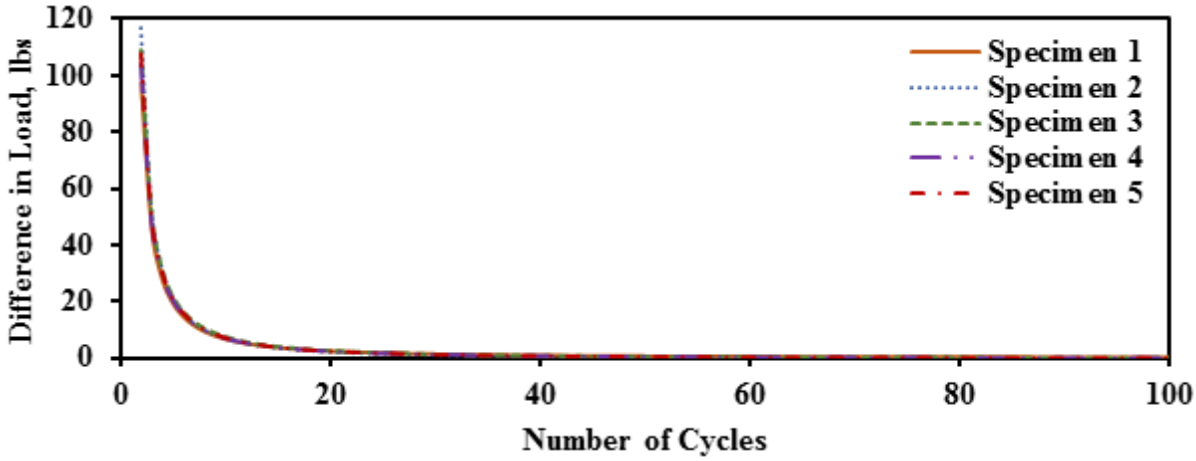

Figure A4 Load Difference of Consecutive Cycles versus Cycles for Type-C

Table A3 Number of Cycles to Failure using Load Difference Method (SMAR-F)

Specimen	Number of Cycles to Failure	Number of Cycles Corresponding to Load Difference of					
		1 lb	2 lb	3 lb	5 lb	8 lb	10 lb
1	70	27	17	14	10	7	6
2	55	24	16	12	9	7	6
3	101	39	25	19	13	10	9
4	34	27	19	15	11	9	8
5	83	26	17	13	9	7	6
Average	69	27	17	14	10	8	7
St Dev	26	2	1	1	1	1	1
COV	**37%**	**7%**	**8%**	**9%**	**10%**	**12%**	**13%**

Table A4 Number of Cycles to Failure using Load Difference Method (Type-C)

Specimen	Number of Cycles to Failure	Number of Cycles Corresponding to Load Difference of					
		1 lb	2 lb	3 lb	5 lb	8 lb	10 lb
1	375	38	23	18	12	9	8
2	404	38	24	18	13	9	8
3	363	43	26	20	14	10	8
4	449	40	25	19	13	9	8
5	79	55	35	24	17	12	6
Average	334	43	27	20	14	10	8
St Dev	146	7	5	3	2	1	1
COV	**44%**	**17%**	**18%**	**13%**	**13%**	**12%**	**12%**

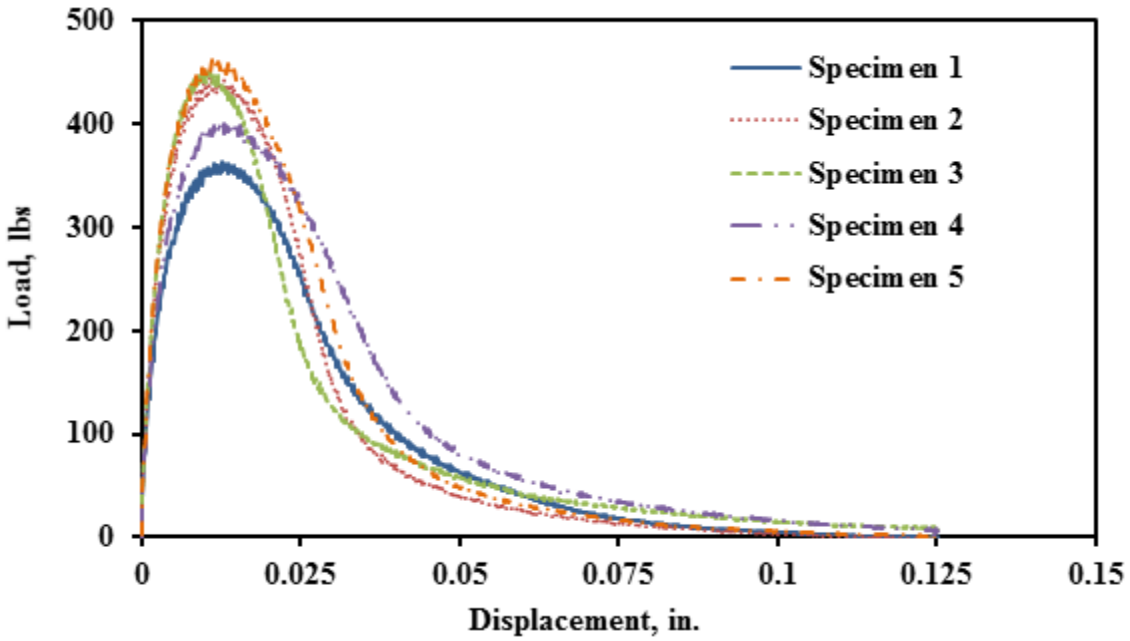

Figure A5 Monotonic OT Load-Displacement Response Curves for SMAR-F

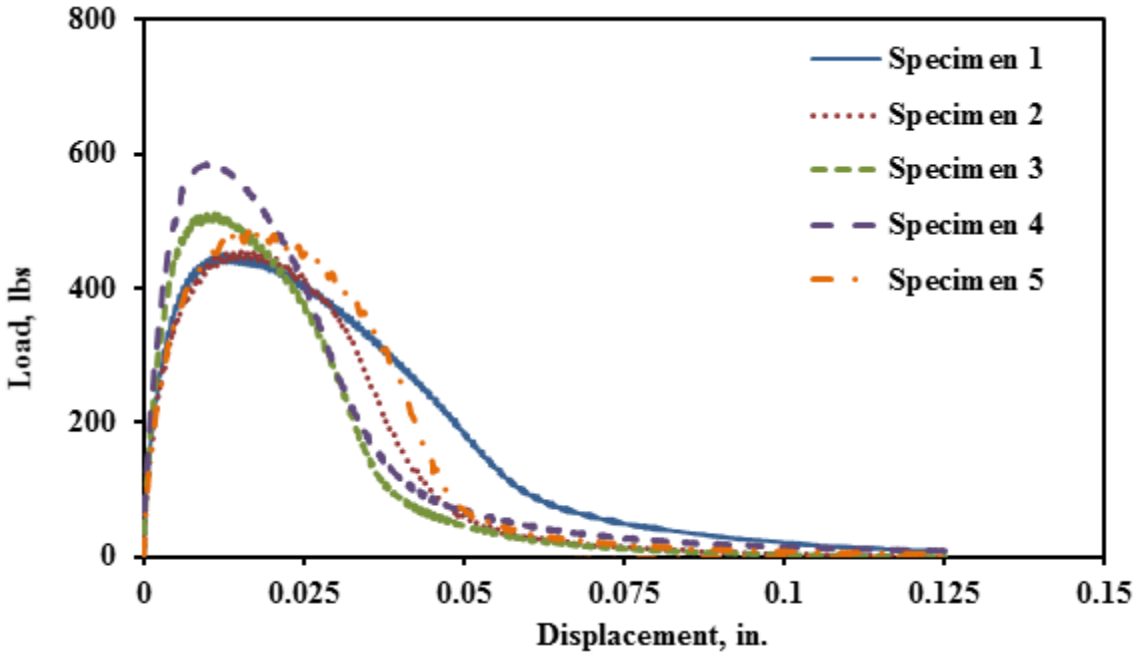

Figure A6 Monotonic OT Load-Displacement Response Curves for Type-C

Appendix B: Performance of Typical AC Mixtures using Proposed Cracking Methodology

Table B1 Summary of Proposed Parameters and Number of Cycles to Failure (SMAR-F)

Specimen	Air Voids, %	Max Load, lbs	Work of Fracture, in.-lbs	Critical Fracture Energy, in.-lbs/in.^{2}	Crack Progression Rate	R^2	Number of Cycles to Failure
1	7.6	385	4.0	0.9	0.65	0.999	70
2	7.9	396	3.3	0.7	0.72	0.997	55
3	7.4	410	4.8	1.1	0.61	0.999	101
4	7.6	469	4.9	1.1	0.79	1.000	34
5	7.2	385	3.4	0.8	0.63	0.998	83
Average	7.5	409	4.1	0.9	0.7	1.0	69
Std Dev	0.2	32	0.7	0.1	0.1	0.0	26
COV	**3%**	**8%**	**17%**	**17%**	**10%**	**NA**	**37%**

Table B2 Summary of Proposed Parameters and Number of Cycles to Failure (Type-C)

Specimen	Air Voids, %	Max Load, lbs	Work of Fracture, in.-lbs	Critical Fracture Energy, in.-lbs./in.^{2}	Crack Progression Rate	R^2	Number of Cycles to Failure
1	6.8	358	4.8	1.1	0.35	0.998	375
2	6.1	334	6.6	1.5	0.34	0.999	404
3	6.1	467	6.8	1.5	0.40	0.999	363
4	7.1	330	5.2	1.2	0.33	0.999	449
5	7.5	556	7.0	1.6	0.61	1.000	79
Average	6.7	409	6.1	1.4	0.41	0.999	334
Std Dev	0.6	89	0.9	0.2	0.11	0.000	146
COV	**8%**	**22%**	**15%**	**15%**	**26%**	**NA**	**44%**

Table B3 Results from Multi-laboratory Study (UTEP)

Specimen	Max Load, lbs	Work of Fracture, in.-lbs	Critical Fracture Energy, in.-lbs/in.^{2}	Crack Progression Rate	R^2	Number of Cycles to Failure
1	829	8.3	1.8	0.64	1.00	50
2	761	6.6	1.5	0.67	1.00	60
3	737	7.9	1.7	0.65	0.99	48
4	852	7.2	1.6	1.08	1.00	17
5	830	7.6	1.7	0.68	1.00	54
6	931	8.6	1.9	0.92	1.00	22
7	832	7.2	1.6	0.62	0.99	46
8	866	7.0	1.6	0.78	0.99	29
9	909	9.8	2.2	0.46	1.00	155
10	822	7.6	1.7	0.63	1.00	64
11	853	8.9	2.0	0.61	1.00	73
12	799	8.0	1.8	0.49	0.99	108
13	847	10.1	2.3	0.81	0.99	28
14	828	10.2	2.3	0.58	0.99	59
15	857	7.5	1.7	0.95	1.00	23
16	879	7.8	1.7	0.84	1.00	27
17	898	7.9	1.8	1.00	1.00	18
18	783	5.7	1.3	0.75	1.00	35
19	854	10.0	2.2	0.84	1.00	28
20	865	7.5	1.7	0.84	1.00	28
21	939	8.6	1.9	0.61	0.99	60
22	913	8.2	1.8	0.46	1.00	149
23	902	7.8	1.7	0.68	1.00	50
24	862	8.9	2.0	0.66	0.99	42
25	752	7.4	1.6	0.60	0.99	59
26	827	8.3	1.8	0.43	1.00	204
27	766	9.7	2.1	0.45	1.00	144
28	911	9.0	2.0	0.76	1.00	39
29	807	8.9	2.0	0.54	1.00	111
30	895	8.7	1.9	0.45	1.00	144
Average	847	8.2	1.8	0.68	1.00	66
Std Dev	53	1.1	0.2	0.17	0.00	48
COV	**6%**	**13%**	**13%**	**25%**	**0%**	**73%**

Table B4 Results from Multi-laboratory Study (TxDOT)

Specimen	Max Load, lbs	Work of Fracture, in.-lbs	Critical Fracture Energy, in.-lbs/in.^{2}	Crack Progression Rate	R^2	Number of Cycles to Failure
1	770	8.6	1.9	0.61	0.99	66
2	797	9.7	2.2	0.48	1.00	114
3	860	9.2	2.0	0.76	1.00	36
4	839	7.6	1.7	0.63	0.99	52
5	917	9.4	2.1	0.82	1.00	27
6	868	10.1	2.2	0.55	1.00	100
7	881	8.2	1.8	0.82	1.00	31
8	854	9.9	2.2	0.66	1.00	53
9	961	10.1	2.2	1.01	0.99	21
10	888	9.5	2.1	0.56	1.00	94
11	870	9.9	2.2	0.84	1.00	27
12	891	11.2	2.5	0.41	1.00	184
13	986	11.0	2.4	0.64	1.00	81
14	1003	12.2	2.7	0.69	1.00	66
15	982	9.2	2.0	0.86	0.98	21
16	886	9.3	2.1	0.84	1.00	27
17	805	9.6	2.1	0.52	1.00	144
18	885	9.9	2.2	0.68	0.99	40
19	1006	13.1	2.9	0.72	0.99	34
20	961	10.8	2.4	0.87	1.00	28
21	985	10.5	2.3	0.88	1.00	24
22	984	11.8	2.6	0.90	0.99	21
23	951	10.0	2.2	0.71	0.99	36
24	931	8.9	2.0	0.63	1.00	71
25	955	11.3	2.5	0.77	1.00	32
26	820	10.5	2.3	0.49	0.99	117
27	873	9.6	2.1	0.55	1.00	98
28	873	9.6	2.1	0.61	1.00	63
29	882	8.9	2.0	0.68	1.00	58
30	883	9.2	2.0	0.86	0.98	21
Average	902	10.0	2.2	0.70	1.00	60
Std Dev	63	1.2	0.3	0.15	0.00	40
COV	**7%**	**12%**	**12%**	**21%**	**0%**	**68%**

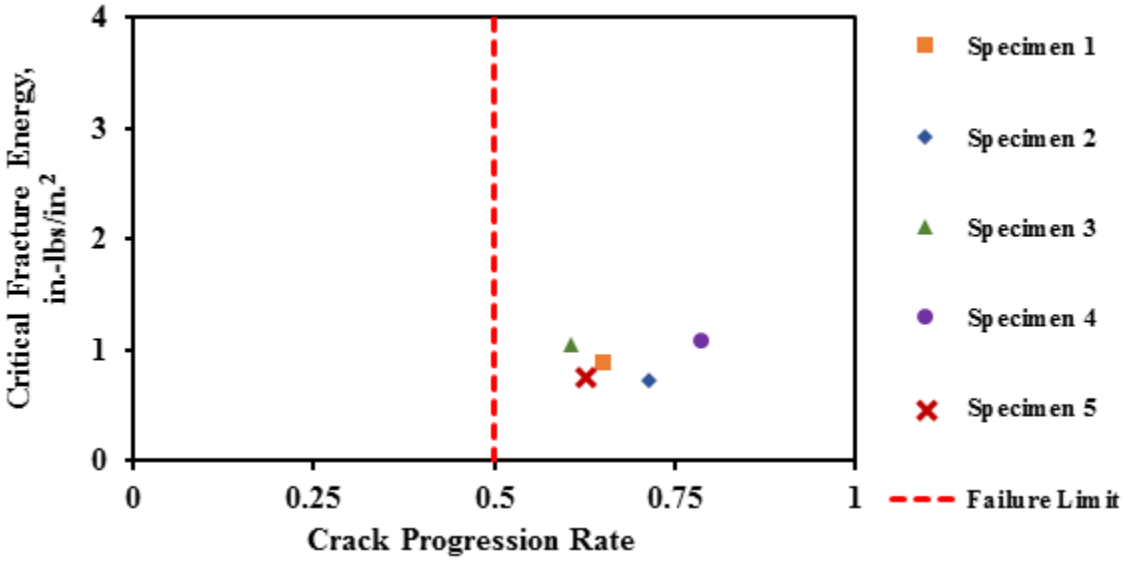

Figure B1 Performance of SMAR-F using Proposed Parameters

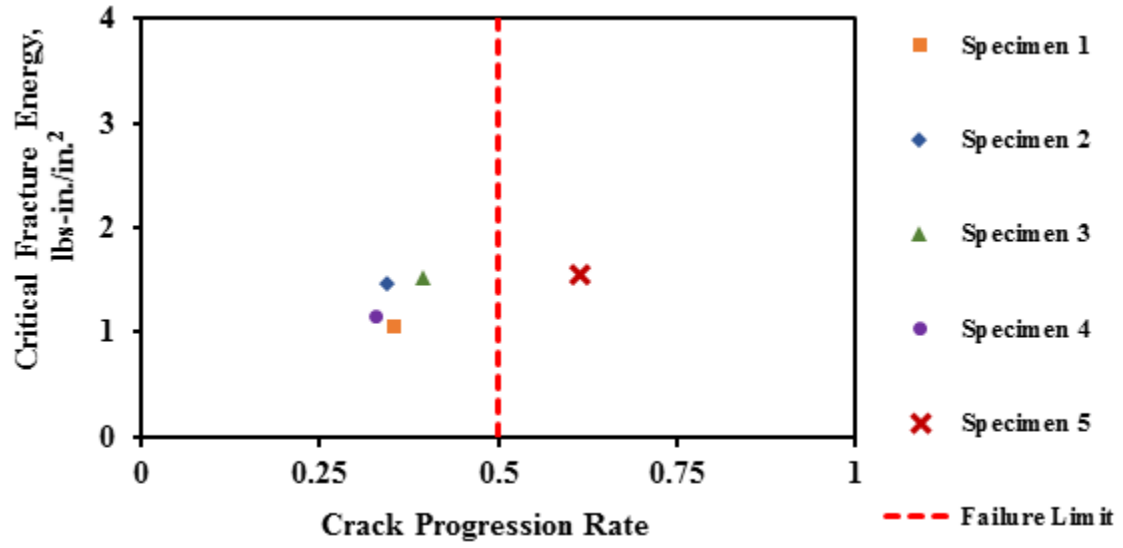

Figure B2 Performance of Type-C using Proposed Parameters

Table B5 Characteristics for TOM Mixes

Mix ID	Sample Size	Year	Aggregate Type	Asphalt Grade	Asphalt Source	Asphalt Content	Anti-Strip	Anti-Strip, %
1	3	2012	Sandstone	N/P	Valero	6.8	N/P	N/P
2	3	2012	Sandstone	PG76-22	Jebro	6.8	Liquid	0.3
3	3	2012	Limestones / Dolomites	PG76-22	Jebro	7.0	Liquid	0.3
4	3	2012	N/P	N/P	N/P	N/P	N/P	N/P
5	3	2014	Igneous	PG70-22	Valero	6.6	Lime	N/P
6	2	2014	LRA and Igneous	PG70-22	Valero	6.2	Lime	N/P
7	2	2014	Gravel	PG76-22	Lion	6.6	Lime	1
8	2	2015	N/P	PG76-22	Martin Asphalt	N/P	N/P	N/P
9	3	2015	N/P	PG70-22	N/P	N/P	N/P	N/P
10	3	2015	N/P	PG76-22	Valero	6.7	N/P	N/P
11	3	2015	Igneous	PG76-22	Lion	7	None	None
12	3	2015	Limestone	PG76-22	Heartland	6.6	Liquid	0.04
13	3	2015	Igneous	PG76-22	Valero	6.6	None	None
14	3	2015	N/P	PG76-22	N/P	N/P	N/P	N/P
15	3	2015	N/P	PG76-22	Lion	6.5	Lime	1
16	3	2015	Gravel	PG76-22	Lion	6.3	Lime	1
17	3	2015	Igneous	PG76-22	Lion	7.2	None	None
18	3	2015	N/P	PG70-22	N/P	N/P	N/P	N/P
19	3	2015	Limestone	N/P	N/P	N/P	N/P	N/P

N/P stands for Not Provided

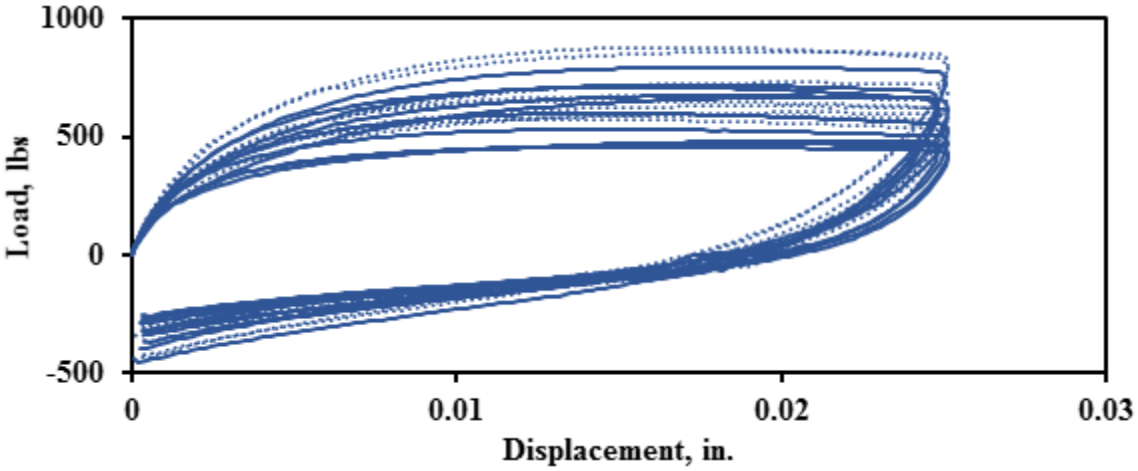

Figure B3 Average First Hysteresis Loops for TOM Mixes

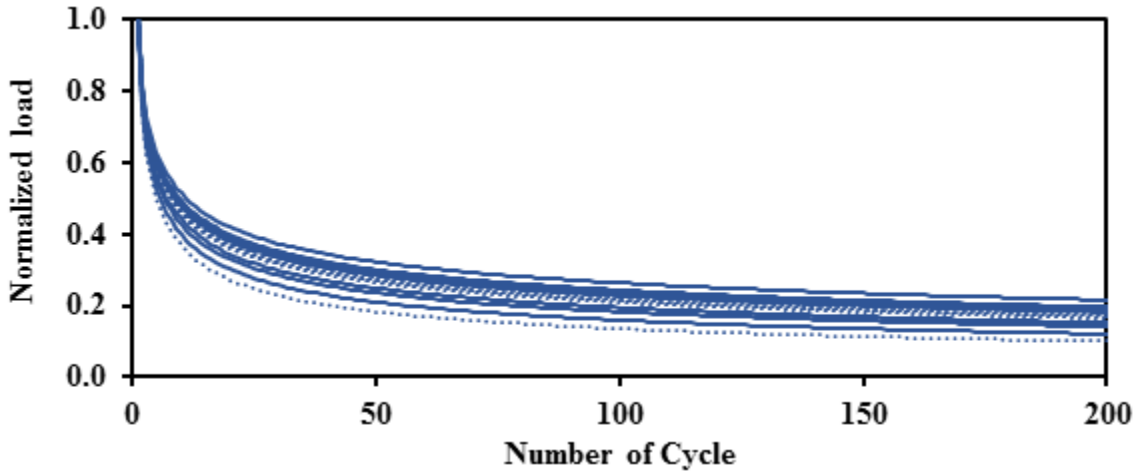

Figure B4 Average Normalized Load Reduction Curves for TOM Mixes

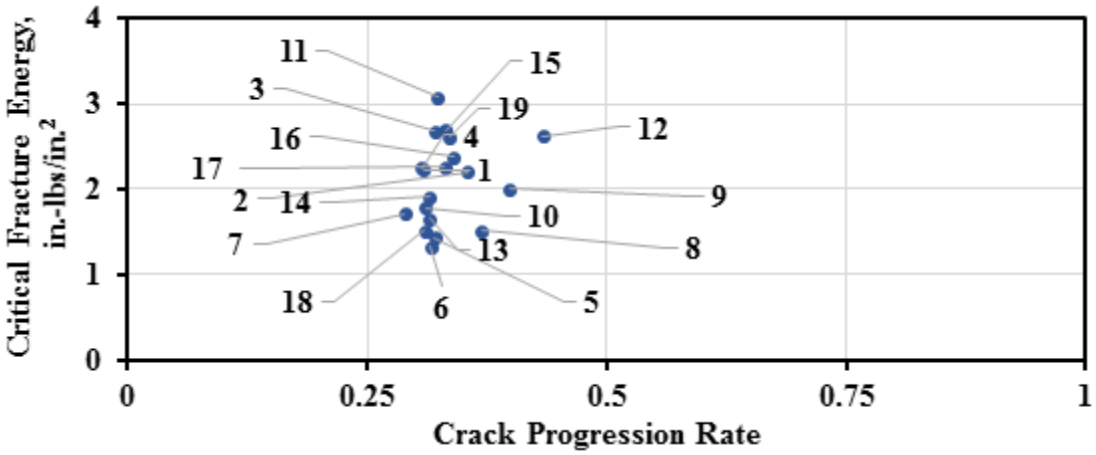

Figure B5 Cracking Performance of TOM Mixes on Design Interaction Plot

Table B6 Results from TOM Mixes

Mix ID	Parameter	Max Load, lbs	Work of Fracture, in.-lbs	Critical Fracture Energy, in.-lbs/in.^{2}	Crack Progression Rate	R^2	Number of Cycles to Failure
1	Average	674	10.0	2.2	0.31	1.0	1000
	Median	673	10.3	2.3	0.31	1.0	1000
	Std Dev	8	0.5	0.1	0.00	0.0	0
	COV	**1%**	**5%**	**5%**	**0.00**	**0%**	**NA**
2	Average	720	9.9	2.2	0.36	1.0	853
	Median	744	10.0	2.2	0.35	1.0	981
	Std Dev	69	0.4	0.1	0.00	0.0	195
	COV	**10%**	**4%**	**4%**	**0.01**	**0%**	**23%**
3	Average	670	12.05	2.68	0.32	1.00	1001
	Median	634	10.54	2.34	0.32	1.00	1001
	Std Dev	91	2.51	0.56	0.01	0.00	0
	COV	**14%**	**21%**	**21%**	**0.04**	**0%**	**NA**
4	Average	484	10.1	2.2	0.31	1.0	1001
	Median	455	9.8	2.2	0.29	1.0	1001
	Std Dev	61	1.2	0.3	0.03	0.0	0
	COV	**13%**	**11%**	**11%**	**0.09**	**0%**	**NA**
5	Average	532	6.5	1.4	0.32	1.0	1000
	Median	529	6.3	1.4	0.32	1.0	1000
	Std Dev	18	0.4	0.1	0.01	0.0	0
	COV	**3%**	**7%**	**7%**	**0.02**	**0%**	**NA**
6	Average	458	6.0	1.3	0.32	1.0	1000
	Median	458	6.0	1.3	0.32	1.0	1000
	Std Dev	65	0.2	0.0	0.03	0.0	0
	COV	**14%**	**3%**	**3%**	**0.08**	**0%**	**NA**
7	Average	470	7.7	1.7	0.29	1.0	1000
	Median	470	7.7	1.7	0.29	1.0	1000
	Std Dev	16	0.6	0.1	0.01	0.0	0
	COV	**3%**	**8%**	**8%**	**0.02**	**0%**	**NA**
8	Average	599	6.8	1.5	0.37	1.0	609
	Median	599	6.8	1.5	0.37	1.0	609
	Std Dev	9	0.0	0.0	0.00	0.0	20
	COV	**2%**	**0%**	**0%**	**0.00**	**0%**	**3%**
9	Average	711	9.0	2.0	0.40	1.0	405
	Median	721	9.0	2.0	0.39	1.0	322
	Std Dev	22	0.4	0.1	0.02	0.0	217
	COV	**3%**	**5%**	**5%**	**0.06**	**0%**	**54%**

Table B6 Results from TOM Mixes (Continued)

10	Average	593	8.0	1.8	0.31	1.0	1000
	Median	575	7.1	1.6	0.31	1.0	1000
	Std Dev	79	1.7	0.4	0.01	0.0	0
	COV	**13%**	**21%**	**21%**	**0.04**	**0%**	**NA**
11	Average	863	13.8	3.1	0.32	1.0	1000
	Median	852	13.1	2.9	0.33	1.0	1000
	Std Dev	22	1.5	0.3	0.01	0.0	0
	COV	**3%**	**11%**	**11%**	**0.03**	**0%**	**NA**
12	Average	882	11.8	2.6	0.43	1.0	396
	Median	971	12.2	2.7	0.45	1.0	131
	Std Dev	270	1.8	0.4	0.12	0.0	428
	COV	**31%**	**15%**	**15%**	**0.27**	**0%**	**108%**
13	Average	657	7.5	1.7	0.32	1.0	1000
	Median	664	8.2	1.8	0.31	1.0	1000
	Std Dev	14	1.5	0.3	0.02	0.0	0
	COV	**2%**	**20%**	**20%**	**0.05**	**0%**	**NA**
14	Average	674	8.6	1.9	0.31	1.0	1000
	Median	717	9.2	2.0	0.31	1.0	1000
	Std Dev	79	2.4	0.5	0.01	0.0	0
	COV	**12%**	**28%**	**28%**	**0.04**	**0%**	**NA**
15	Average	730	12.1	2.7	0.33	1.0	770
	Median	729	11.9	2.6	0.33	1.0	831
	Std Dev	13	0.8	0.2	0.00	0.0	100
	COV	**2%**	**7%**	**7%**	**0.01**	**0%**	**13%**
16	Average	605	10.7	2.4	0.34	1.0	949
	Median	585	11.0	2.4	0.34	1.0	1000
	Std Dev	58	1.3	0.3	0.02	0.0	72
	COV	**10%**	**12%**	**12%**	**0.06**	**0%**	**8%**
17	Average	632	10.2	2.3	0.33	1.0	1000
	Median	623	10.3	2.3	0.33	1.0	1000
	Std Dev	19	0.2	0.1	0.01	0.0	0
	COV	**3%**	**2%**	**2%**	**0.03**	**0%**	**NA**
18	Average	577	6.8	1.5	0.34	1.0	858
	Median	582	6.1	1.4	0.34	1.0	1000
	Std Dev	10	1.1	0.2	0.01	0.0	201
	COV	**2%**	**16%**	**16%**	**0.04**	**0%**	**23%**
19	Average	795	11.8	2.6	0.31	1.0	1000
	Median	797	12.4	2.7	0.31	1.0	1000
	Std Dev	38	0.9	0.2	0.01	0.0	0
	COV	**5%**	**8%**	**8%**	**0.02**	**0%**	**NA**

Table B7 Characteristics for CAM Mixes

Mix ID	Sample Size	Year	Aggregate Type	Asphalt Grade	Asphalt Source	Asphalt Content	Anti-Strip	Anti-Strip, %
1	3	2015	N/P	N/P	N/P	N/P	N/P	N/P
2	3	2015	N/P	PG70-22	N/P	7.1	N/P	N/P
3	3	2015	N/P	PG76-22	N/P	7.1	N/P	N/P
4	3	2015	Igneous	PG76-22	Jebro	7.2	Lime	1
5	3	2015	Limestone	PG76-22	Valero	N/P	Liquid	1
6	3	2015	N/P	PG76-22	N/P	6.8	N/P	N/P
7	3	2012	Gravel	N/P	Valero	7.5	Lime	1
8	3	2012	N/P	N/P	N/P	N/P	N/P	N/P
9	3	2012	N/P	N/P	N/P	N/P	N/P	N/P
10	3	2012	Igneous (Granite)	PG76-22	Martin Asphalt	7.2	N/P	N/P
11	3	2012	N/P	PG76-22	N/P	N/P	N/P	N/P
12	3	2012	Igneous (Granite)	N/P	Martin Asphalt	7.2	N/P	N/P
13	3	2012	Limestone	PG76-22T	Wright	7.3	Lime	1
14	3	2012	Limestone	PG76-22T	Wright	N/P	Lime	1
15	3	2012	N/P	N/P	N/P	7.3	Liquid	0.5
16	3	2012	N/P	PG76-22T	Wright	N/P	N/P	N/P
17	2	2012	N/P	N/P	Heartland	N/P	N/P	N/P
18	3	2012	N/P	N/P	Heartland	N/P	N/P	N/P

N/P stands for Not Provided

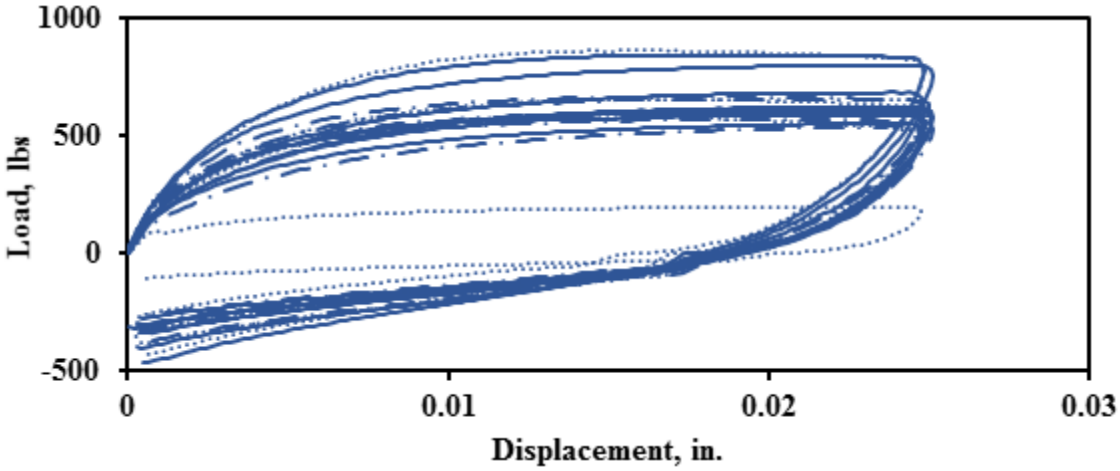

Figure B6 Average First Hysteresis Loops for CAM Mixes

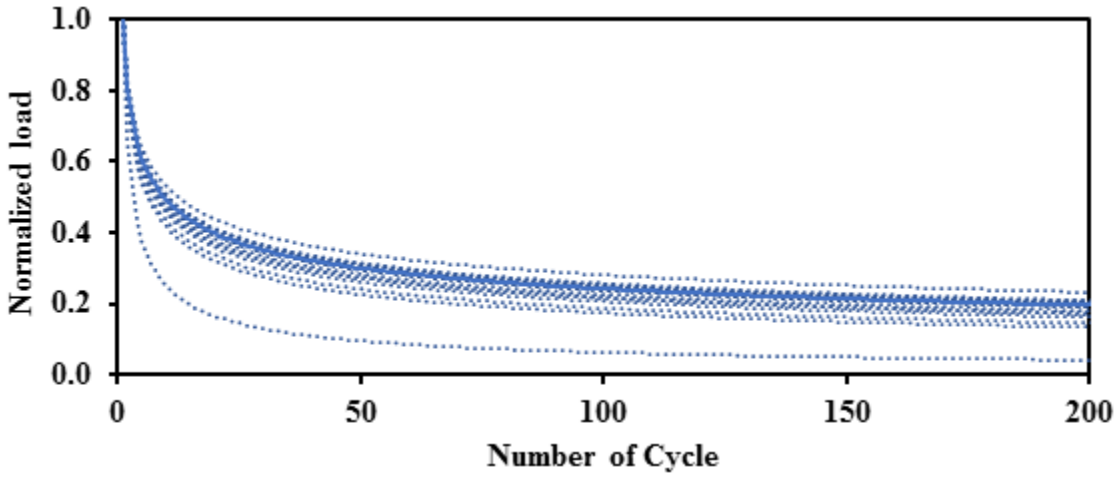

Figure B7 Average Normalized Load Reduction Curves for CAM Mixes

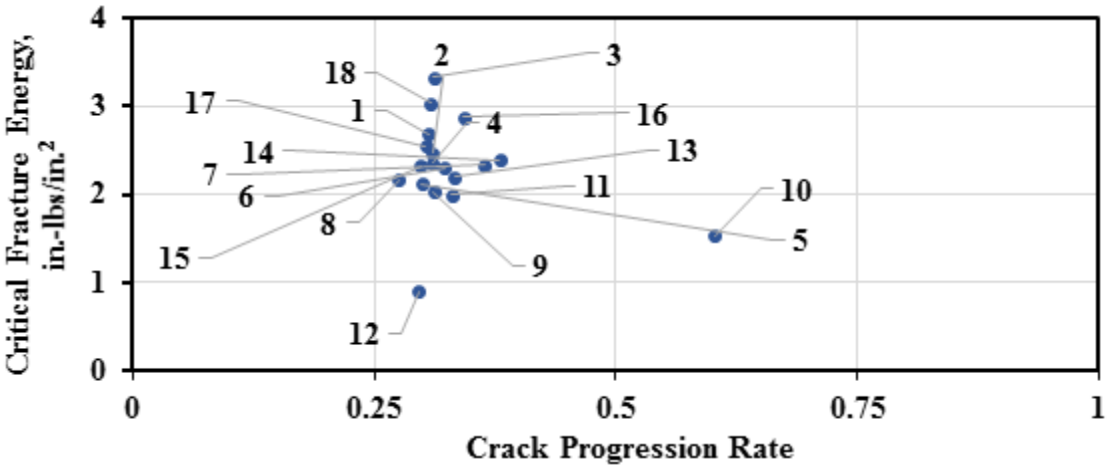

Figure B8 Cracking Performance of CAM Mixes on Design Interaction Plot

Table B8 Results from CAM Mixes

Mix ID	Parameter	Max Load, lbs	Work of Fracture, in.-lbs	Critical Fracture Energy, in.-lbs/in.^{2}	Crack Progression Rate	R^2	Number of Cycles to Failure
1	Average	617	12.1	2.7	0.31	1.0	1000
	Median	614	12.1	2.7	0.30	1.0	1000
	Std Dev	22	0.4	0.1	0.01	0.0	0
	COV	**4%**	**4%**	**4%**	**4%**	**0%**	**NA**
2	Average	622	11.1	2.5	0.31	1.0	1000
	Median	627	11.1	2.5	0.32	1.0	1000
	Std Dev	32	0.5	0.1	0.01	0.0	0
	COV	**5%**	**5%**	**5%**	**3%**	**0%**	**NA**
3	Average	800	14.96	3.32	0.31	1.00	907
	Median	808	15.41	3.42	0.31	1.00	1000
	Std Dev	16	0.65	0.15	0.01	0.00	132
	COV	**2%**	**4%**	**4%**	**3%**	**0%**	**15%**
4	Average	603	10.6	2.4	0.31	1.0	1000
	Median	567	10.5	2.3	0.30	1.0	1000
	Std Dev	72	0.2	0.1	0.02	0.0	0
	COV	**12%**	**2%**	**2%**	**5%**	**0%**	**NA**
5	Average	570	9.6	2.1	0.30	1.0	1000
	Median	581	9.8	2.2	0.30	1.0	1000
	Std Dev	36	0.4	0.1	0.01	0.0	0
	COV	**6%**	**4%**	**4%**	**2%**	**0%**	**NA**
6	Average	660	10.4	2.3	0.32	1.0	786
	Median	647	10.5	2.3	0.32	1.0	1000
	Std Dev	30	0.4	0.1	0.02	0.0	303
	COV	**5%**	**4%**	**4%**	**5%**	**0%**	**39%**
7	Average	670	10.5	2.3	0.36	1.0	245
	Median	697	10.3	2.3	0.37	1.0	228
	Std Dev	41	0.5	0.1	0.02	0.0	75
	COV	**6%**	**4%**	**4%**	**6%**	**0%**	**31%**
8	Average	542	9.7	2.2	0.28	1.0	1001
	Median	545	9.6	2.1	0.28	1.0	1001
	Std Dev	35	1.0	0.2	0.01	0.0	0
	COV	**7%**	**11%**	**11%**	**5%**	**0%**	**NA**
9	Average	602	9.2	2.0	0.31	1.0	1001
	Median	610	9.0	2.0	0.31	1.0	1001
	Std Dev	24	0.4	0.1	0.00	0.0	0
	COV	**4%**	**5%**	**5%**	**2%**	**0%**	**NA**

Table B8 Results from CAM Mixes (Continued)

10	Average	582	6.9	1.5	0.60	1.0	50
	Median	571	6.6	1.5	0.61	1.0	46
	Std Dev	22	0.4	0.1	0.02	0.0	9
	COV	**4%**	**6%**	**6%**	**3%**	**0%**	**18%**
11	Average	656	9.0	2.0	0.33	1.0	454
	Median	653	8.8	2.0	0.33	1.0	424
	Std Dev	19	0.3	0.1	0.01	0.0	93
	COV	**3%**	**3%**	**3%**	**3%**	**0%**	**21%**
12	Average	199	4.1	0.9	0.30	1.0	1000
	Median	200	4.1	0.9	0.30	1.0	1000
	Std Dev	2	0.1	0.0	0.00	0.0	0
	COV	**1%**	**3%**	**3%**	**0%**	**0%**	**NA**
13	Average	611	9.9	2.2	0.33	1.0	646
	Median	650	10.2	2.3	0.33	1.0	579
	Std Dev	57	0.5	0.1	0.01	0.0	98
	COV	**9%**	**5%**	**5%**	**3%**	**0%**	**15%**
14	Average	865	10.8	2.4	0.38	1.0	377
	Median	878	10.3	2.3	0.37	1.0	252
	Std Dev	19	0.7	0.2	0.03	0.0	254
	COV	**2%**	**7%**	**7%**	**8%**	**0%**	**67%**
15	Average	554	10.5	2.3	0.30	1.0	1001
	Median	548	10.5	2.3	0.30	1.0	1001
	Std Dev	22	0.3	0.1	0.01	NA	0
	COV	**4%**	**3%**	**3%**	**3%**	**NA**	**NA**
16	Average	850	12.9	2.9	0.34	1.0	441
	Median	845	12.7	2.8	0.35	1.0	272
	Std Dev	19	2.0	0.4	0.02	0.0	290
	COV	**2%**	**16%**	**16%**	**4%**	**0%**	**66%**
17	Average	591	11.5	2.5	0.30	1.0	1001
	Median	591	11.5	2.5	0.30	1.0	1001
	Std Dev	14	0.6	0.1	0.00	NA	0
	COV	**2%**	**6%**	**6%**	**0%**	**NA**	**NA**
18	Average	685	13.7	3.0	0.31	1.0	1001
	Median	694	13.6	3.0	0.31	1.0	1001
	Std Dev	17	0.3	0.1	0.00	0.0	0
	COV	**3%**	**2%**	**2%**	**1%**	**NA**	**NA**

Table B9 Characteristics for PFC Mixes

Mix ID	Sample Size	Year	Aggregate Type	Asphalt Grade	Asphalt Source	Asphalt Content	Anti-Strip	Anti-Strip, %
1	3	2015	N/P	PG76-22	N/P	N/P	N/P	N/P
2	3	2012	N/P	PG76-22	N/P	6.5	Liquid	0.75
3	3	2012	N/P	PG76-28	Valero	5.7	Lime	1
N/P stands for Not Provided								

Table B10 Results from PFC Mixes

Mix ID	Parameter	Max Load, lbs	Work of Fracture, in.-lbs	Critical Fracture Energy, in.-lbs/in.^{2}	Crack Progression Rate	R^2	Number of Cycles to Failure
1	Average	301	2.6	0.6	0.29	1.0	1000
	Median	291	2.4	0.5	0.29	1.0	1000
	Std Dev	15	1.1	0.2	0.01	NA	NA
	COV	**5%**	**42%**	**42%**	**3%**	**NA**	**NA**
2	Average	537	5.2	1.2	0.42	1.00	395
	Median	539	4.8	1.1	0.43	1.00	217
	Std Dev	35	0.6	0.1	0.05	NA	304
	COV	**7%**	**11%**	**11%**	**12%**	**NA**	**77%**
3	Average	188	0.5	0.1	0.31	1.0	1001
	Median	184	0.5	0.1	0.31	1.0	1001
	Std Dev	14	0.1	0.0	0.03	NA	NA
	COV	**7%**	**25%**	**25%**	**11%**	**NA**	**NA**

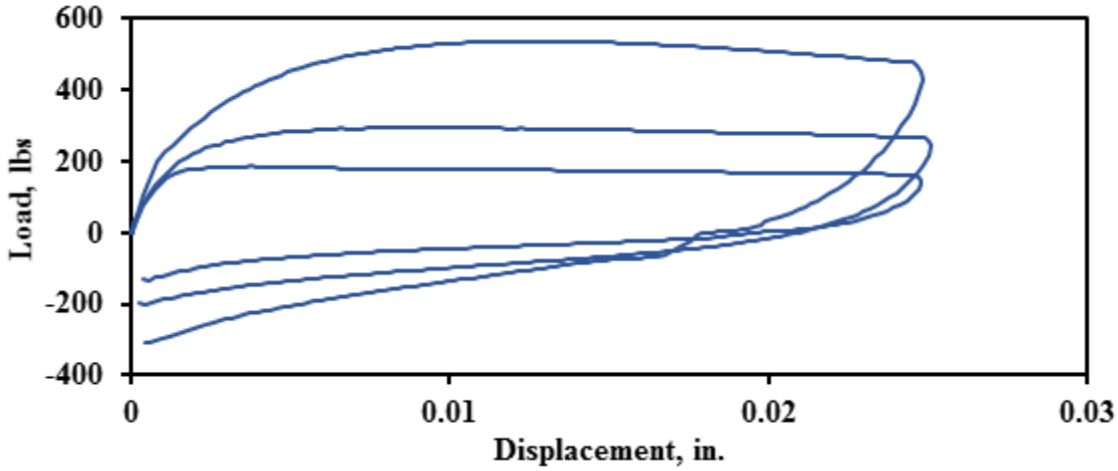

Figure B9 Average First Hysteresis Loops for PFC Mixes

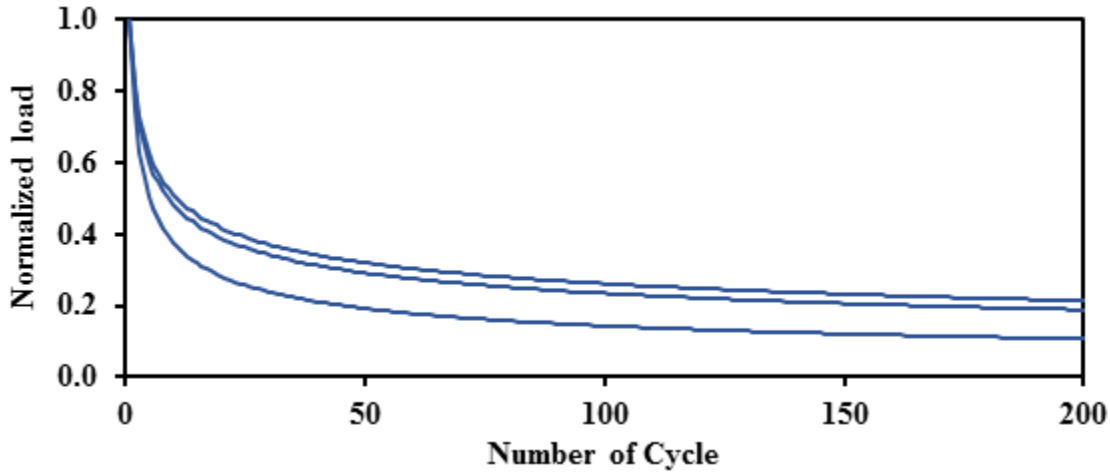

Figure B10 Average Normalized Load Reduction Curves for PFC Mixes

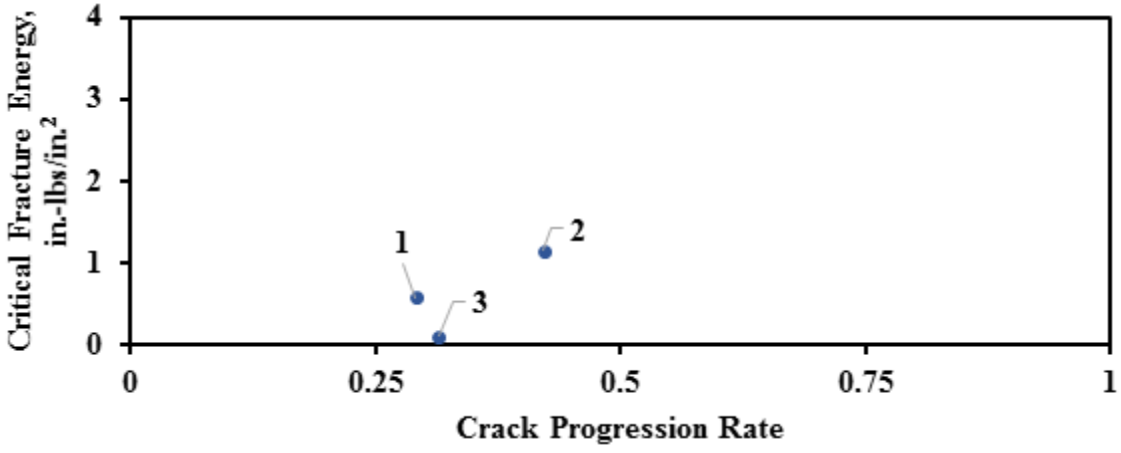

Figure B11 Cracking Performance of PFC Mixes on Design Interaction Plot

Table B11 Characteristics for SMA-D Mixes

Mix ID	Sample Size	Year	Aggregate Type	Asphalt Grade	Asphalt Source	Asphalt Content	Anti-Strip	Anti-Strip, %
1	3	2014	N/P	PG76-22	N/P	N/P	N/P	N/P
2	3	2014	N/P	PG76-22	Lion	6.1	Liquid	0.8
3	3	2014	N/P	PG76-22	Martin Asphalt	6.1	Lime	N/P
4	3	2014	Limestone	PG76-22	Lion	6	Liquid	0.8
5	3	2015	Igneous	PG76-22	Jebro	6.2	Lime	1
6	2	2015	N/P	N/P	N/P	N/P	N/P	N/P
7	3	2015	N/P	PG 76-22	Heartland	6	N/P	N/P
8	2	2015	Limestone	PG76-22	Valero	6.3	Lime	1
9	1	2015		PG76-22				
10	3	2015	Limestone and Gravel	PG70-28	N/P	6.2	N/P	0
11	3	2015	Limestone	PG76-22	Heartland	6	EVOTHERM	0.5
12	2	2015	N/P	PG76-22	N/P	N/P	N/P	N/P
13	3	2015	Limestone	PG76-22	Heartland	6.1	EVOTHERM	0.5
14	3	2015	N/P	PG76-22	N/P	N/P	N/P	N/P
15	3	2015	Limestone	PG70-28	Heartland	6.2	None	None
16	3	2015	Limestone and Gravel	PG70-28	Heartland	6.3	EVOTHERM	0.4
17	2	2015	N/P	PG76-22	N/P	N/P	N/P	N/P
18	3	2015	Limestone	PG70-28	Heartland	6.2	EVOTHERM	0.4
19	3	2015	Limestone and Gravel	PG 64-22	Valero	7.1	Lime	1

N/P stands for Not Provided

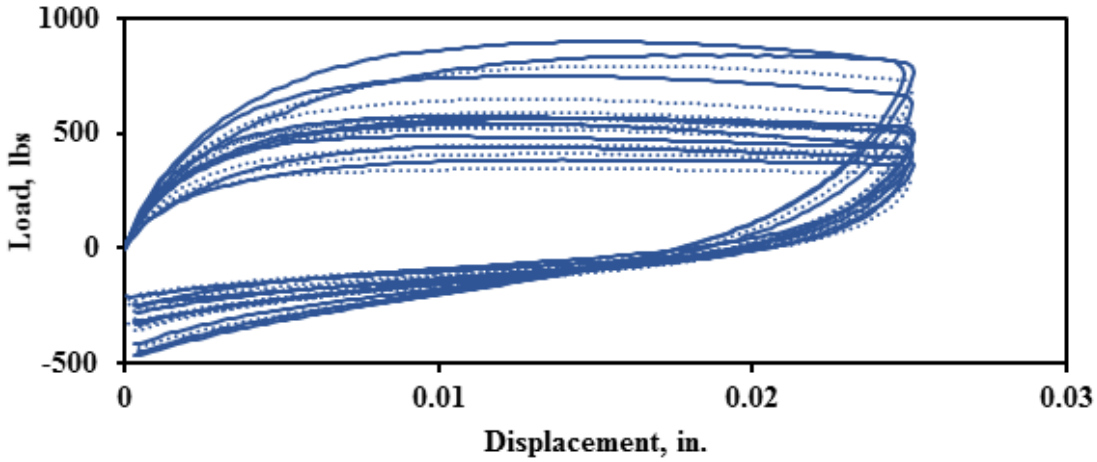

Figure B12 Average First Hysteresis Loops for SMA-D Mixes

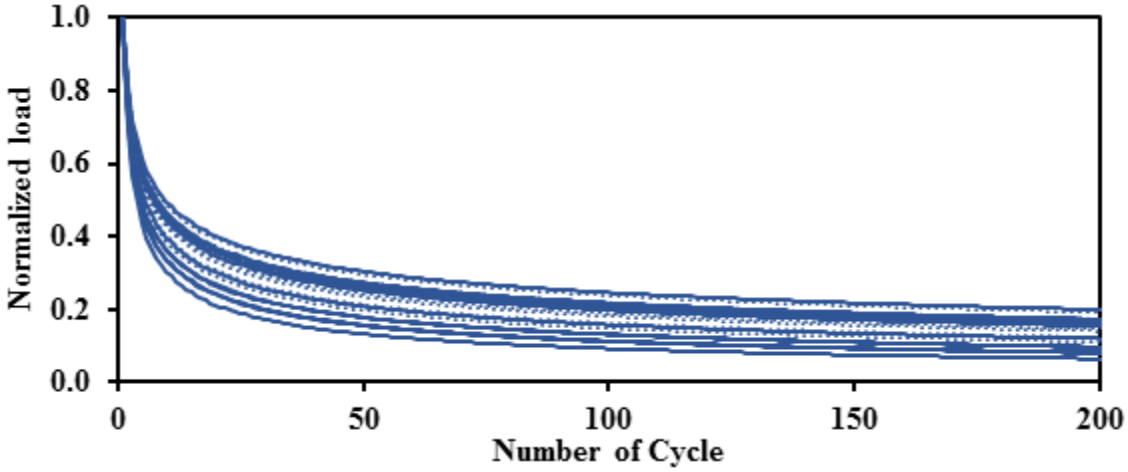

Figure B13 Average Normalized Load Reduction Curves for SMA-D Mixes

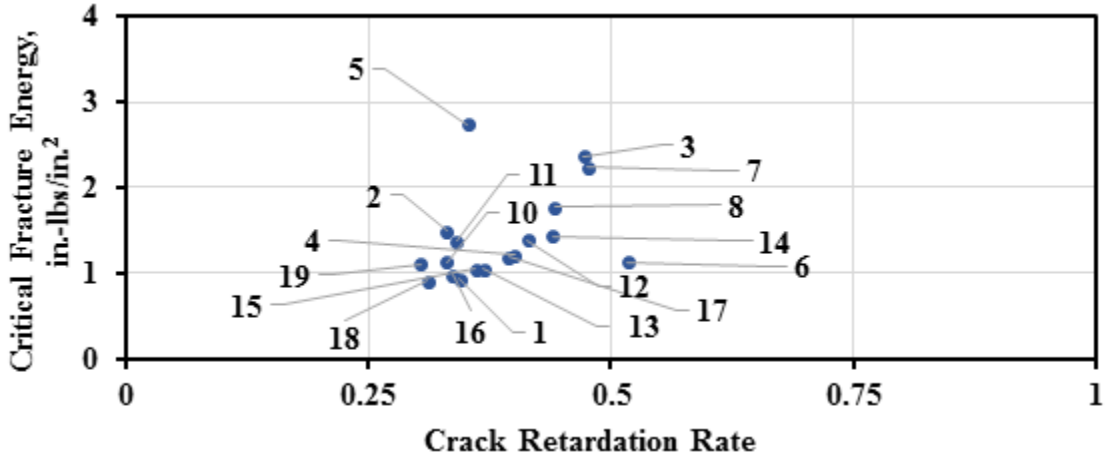

Figure B14 Cracking Performance of SMA-D Mixes on Design Interaction Plot

Table B12 Results from SMA-D Mixes

Mix ID	Parameter	Max Load, lbs	Work of Fracture, in.-lbs	Critical Fracture Energy, in.-lbs/in.^{2}	Crack Progression Rate	R^2	Number of Cycles to Failure
1	Average	489	4.2	0.9	0.34	1.0	906
	Median	477	4.1	0.9	0.34	1.0	1000
	Std Dev	23	0.4	0.1	0.02	0.0	133
	COV	**5%**	**10%**	**10%**	**6%**	**0%**	**15%**
2	Average	565	6.7	1.5	0.33	1.0	856
	Median	602	7.1	1.6	0.33	1.0	1000
	Std Dev	60	1.1	0.2	0.02	0.0	204
	COV	**11%**	**16%**	**16%**	**6%**	**0%**	**24%**
3	Average	897	10.67	2.4	0.47	1.00	426
	Median	902	10.39	2.3	0.41	1.00	382
	Std Dev	12	0.52	0.12	0.14	0.00	320
	COV	**1%**	**5%**	**5%**	**29%**	**0%**	**75%**
4	Average	573	5.5	1.2	0.40	1.0	519
	Median	590	5.9	1.3	0.40	1.0	336
	Std Dev	26	0.6	0.1	0.05	0.0	344
	COV	**5%**	**12%**	**12%**	**12%**	**0%**	**66%**
5	Average	840	12.3	2.7	0.35	1.0	538
	Median	850	12.1	2.7	0.31	1.0	430
	Std Dev	77	0.6	0.1	0.06	0.0	342
	COV	**9%**	**5%**	**5%**	**16%**	**0%**	**64%**
6	Average	541	5.1	1.1	0.52	1.0	254
	Median	541	5.1	1.1	0.52	1.0	254
	Std Dev	54	0.3	0.1	0.01	0.0	69
	COV	**10%**	**7%**	**7%**	**2%**	**0%**	**27%**
7	Average	796	10.0	2.2	0.48	1.0	256
	Median	794	10.2	2.3	0.49	1.0	136
	Std Dev	5	1.3	0.3	0.08	0.0	203
	COV	**1%**	**13%**	**13%**	**18%**	**0%**	**79%**
8	Average	748	8.0	1.8	0.44	1.0	295
	Median	748	8.0	1.8	0.44	1.0	295
	Std Dev	51	1.5	0.3	0.01	0.0	80
	COV	**7%**	**19%**	**19%**	**3%**	**0%**	**27%**
9	Average	410	5.1	1.1	0.33	1.0	1000
	Median	423	4.6	1.0	0.33	1.0	1000
	Std Dev	27	0.8	0.2	0.02	0.0	0
	COV	**7%**	**16%**	**16%**	**5%**	**0%**	**NA**

Table B12 Results from SMA-D Mixes (Continued)

10	Average	538	6.2	1.4	0.34	1.0	945
	Median	550	5.8	1.3	0.32	1.0	986
	Std Dev	52	1.3	0.3	0.03	0.0	68
	COV	**10%**	**20%**	**20%**	**9%**	**0%**	**7%**
11	Average	589	6.2	1.4	0.41	1.0	556
	Median	589	6.2	1.4	0.41	1.0	556
	Std Dev	8	0.1	0.0	0.00	0.0	10
	COV	**1%**	**2%**	**2%**	**1%**	**0%**	**2%**
12	Average	523	4.7	1.0	0.37	1.0	1000
	Median	508	4.0	0.9	0.37	1.0	1000
	Std Dev	65	1.1	0.3	0.01	0.0	0
	COV	**12%**	**24%**	**24%**	**3%**	**0%**	**NA**
13	Average	648	6.5	1.4	0.44	1.0	488
	Median	640	6.5	1.4	0.46	1.0	402
	Std Dev	47	0.2	0.0	0.05	0.0	235
	COV	**7%**	**3%**	**3%**	**11%**	**0%**	**48%**
14	Average	453	4.7	1.1	0.36	1.0	873
	Median	443	4.8	1.1	0.35	1.0	1000
	Std Dev	31	0.8	0.2	0.03	0.0	180
	COV	**7%**	**17%**	**17%**	**8%**	**0%**	**21%**
15	Average	387	4.4	1.0	0.34	1.0	1000
	Median	365	4.4	1.0	0.34	1.0	1000
	Std Dev	46	1.4	0.3	0.01	0.0	0
	COV	**12%**	**33%**	**33%**	**3%**	**0%**	**NA**
16	Average	569	5.4	1.2	0.39	1.0	708
	Median	569	5.4	1.2	0.39	1.0	708
	Std Dev	7	0.3	0.1	0.03	0.0	133
	COV	**1%**	**5%**	**5%**	**7%**	**0%**	**19%**
17	Average	346	4.1	0.9	0.31	1.0	1000
	Median	337	3.8	0.8	0.32	1.0	1000
	Std Dev	14	0.7	0.2	0.01	0.0	0
	COV	**4%**	**17%**	**17%**	**5%**	**0%**	**NA**
18	Average	448	5.0	1.1	0.30	1.0	1000
	Median	386	4.5	1.0	0.29	1.0	1000
	Std Dev	96	0.7	0.2	0.05	0.0	0
	COV	**21%**	**15%**	**15%**	**16%**	**0%**	**NA**

Table B13 Characteristics for SMA-F Mixes

Mix ID	Sample Size	Year	Aggregate Type	Asphalt Grade	Asphalt Source	Asphalt Content	Anti-Strip	Anti-Strip, %
1	3	2014	Igneous	PG76-22	Jebro	6.3	Lime	1
2	3	2014	Gravel	PG76-22	Jebro	6.3	Lime	1
3	3	2014	Limestone	N/P	Jebro	6.0	Lime	N/P
4	3	2014	Limestone	N/P	Jebro	6	Lime	1
5	3	2015	Limestone	PG76-22	Jebro	6.1	Lime	1
6	2	2015	Limestone	PG76-22	N/P	6.1	N/P	N/P
7	3	2015	N/P	N/P	N/P	6.2	N/P	N/P
N/P stands for Not Provided								

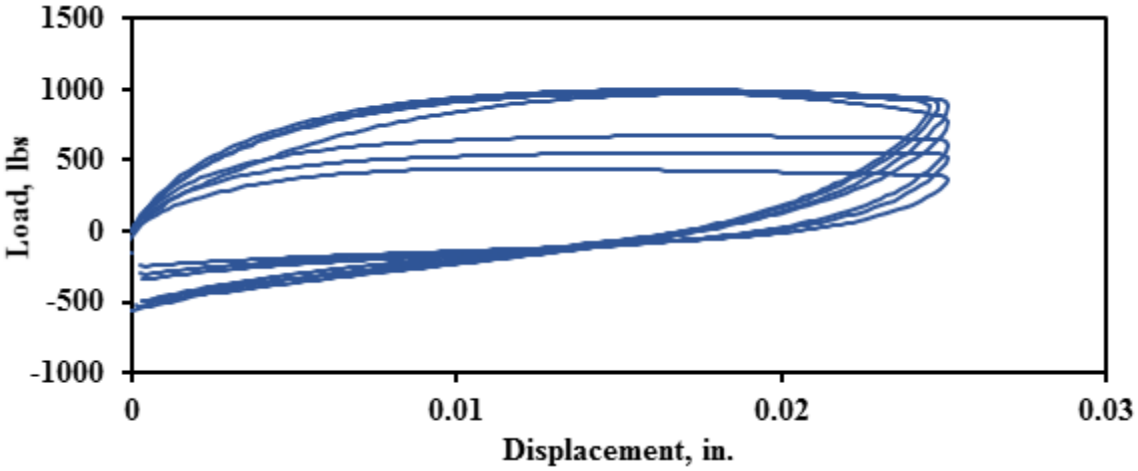

Figure B15 Average First Hysteresis Loops for SMA-F Mixes

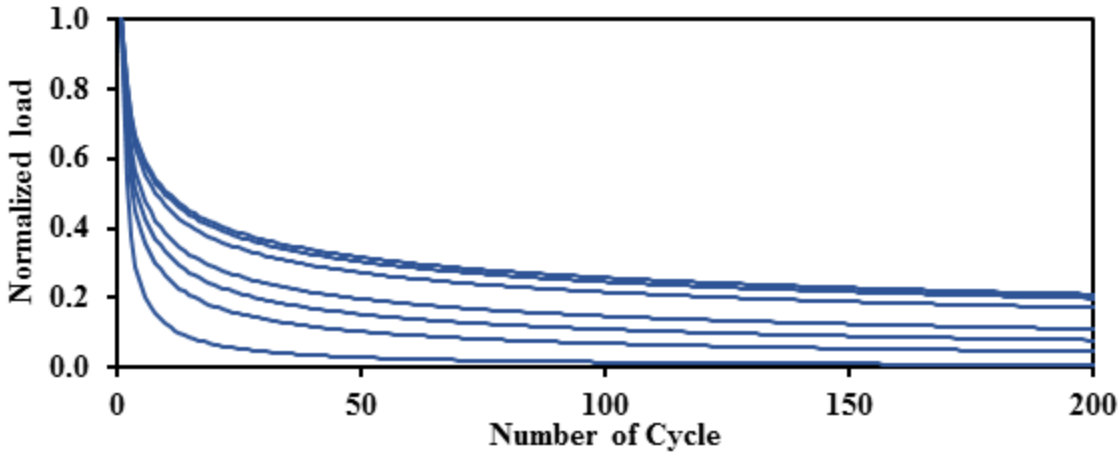

Figure B16 Average Normalized Load Reduction Curves for SMA-F Mixes

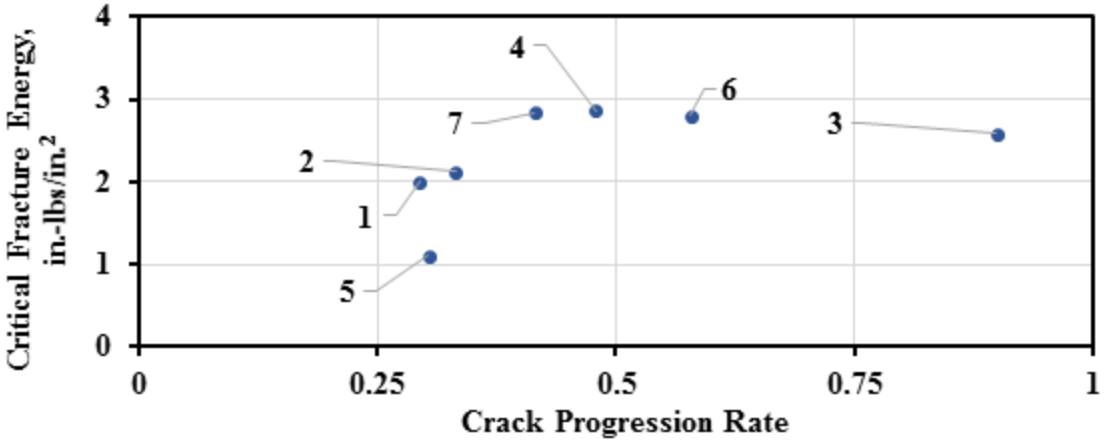

Figure B17 Cracking Performance of SMA-F Mixes on Design Interaction Plot

Table B14 Results from SMA-F Mixes

Mix ID	Parameter	Max Load, lbs	Work of Fracture, in.-lbs	Critical Fracture Energy, in.-lbs/in.^{2}	Crack Progression Rate	R^2	Number of Cycles to Failure
1	Average	555	9.0	2.0	0.29	1.0	1000
	Median	568	8.9	2.0	0.29	1.0	1000
	Std Dev	22	0.7	0.1	0.00	0.0	0
	COV	**4%**	**7%**	**7%**	**1%**	**0%**	**NA**
2	Average	672	9.6	2.1	0.33	1.0	927
	Median	668	9.0	2.0	0.33	1.0	1000
	Std Dev	9	0.8	0.2	0.01	0.0	103
	COV	**1%**	**9%**	**9%**	**3%**	**0%**	**11%**
3	Average	984	11.6	2.6	0.90	1.00	44
	Median	984	11.8	2.6	1.07	1.00	18
	Std Dev	61	0.83	0.18	0.25	0.00	38
	COV	**6%**	**7%**	**7%**	**27%**	**0%**	**86%**
4	Average	999	12.9	2.9	0.48	1.0	252
	Median	997	13.4	3.0	0.46	1.0	158
	Std Dev	20	0.9	0.2	0.11	0.0	205
	COV	**2%**	**7%**	**7%**	**22%**	**0%**	**81%**
5	Average	448	5.0	1.1	0.30	1.0	191
	Median	386	4.5	1.0	0.29	1.0	182
	Std Dev	96	0.7	0.2	0.05	0.0	62
	COV	**21%**	**15%**	**15%**	**16%**	**0%**	**32%**
6	Average	990	12.6	2.8	0.58	1.0	88
	Median	990	12.6	2.8	0.58	1.0	88
	Std Dev	74	0.1	0.0	0.01	0.0	5
	COV	**7%**	**1%**	**1%**	**1%**	**0%**	**6%**
7	Average	977	12.8	2.8	0.41	1.0	232
	Median	1000	13.3	3.0	0.41	1.0	223
	Std Dev	42	0.9	0.2	0.02	0.0	53
	COV	**4%**	**7%**	**7%**	**5%**	**0%**	**23%**

Table B15 Characteristics for Type-B Mixes

Mix ID	Sample Size	Year	Aggregate Type	Asphalt Grade	Asphalt Source	Asphalt Content	Anti-Strip	Anti-Strip, %
1	3	2015	Igneous	PG70-22	Heartland	5.3	Lime	1
2	3	2015	Limestone	PG70-28	Heartland	4.6	N/P	N/P
3	2	2015	Limestone	PG64-22	N/P	N/P	EVOTHERM	0.5
N/P stands for Not Provided								

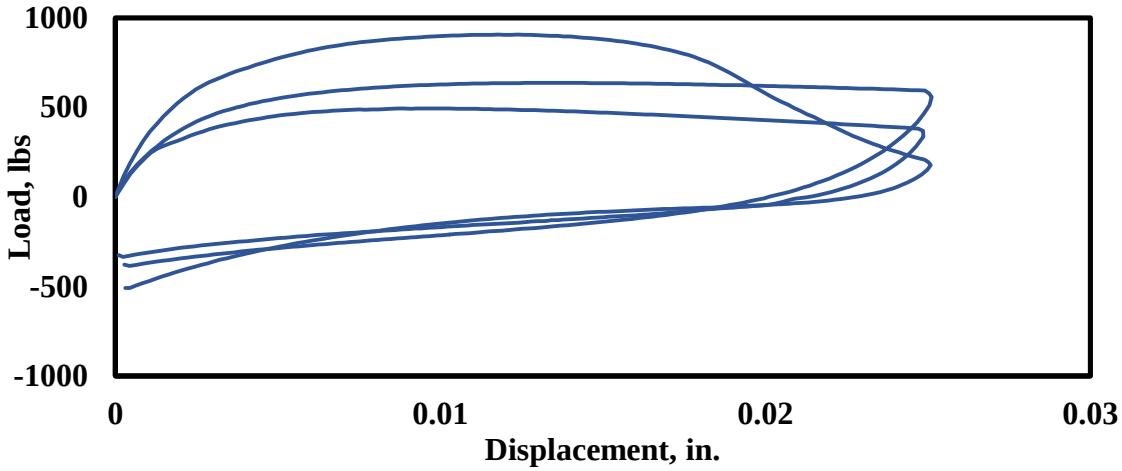

Figure B18 Average First Hysteresis Loops for Type-B Mixes

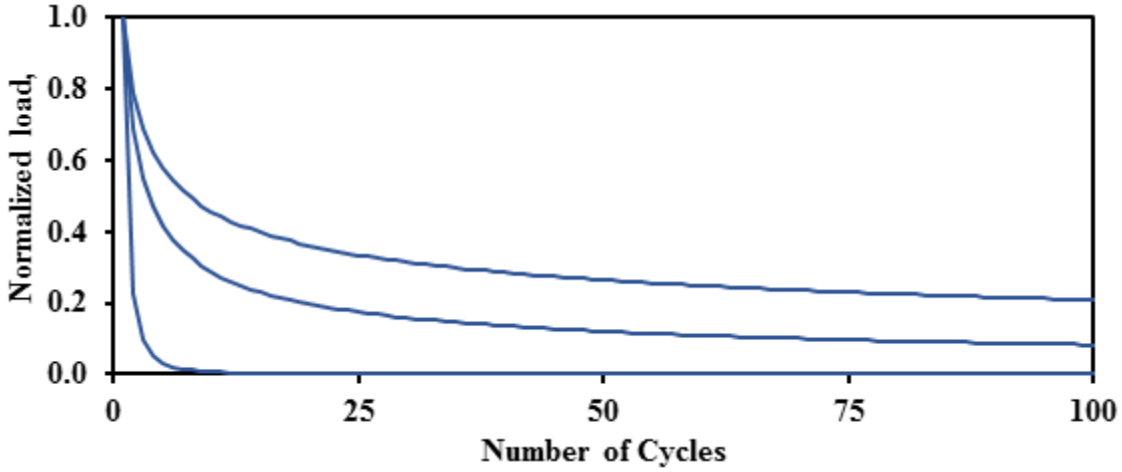

Figure B19 Average Normalized Load Reduction Curves for Type-B Mixes

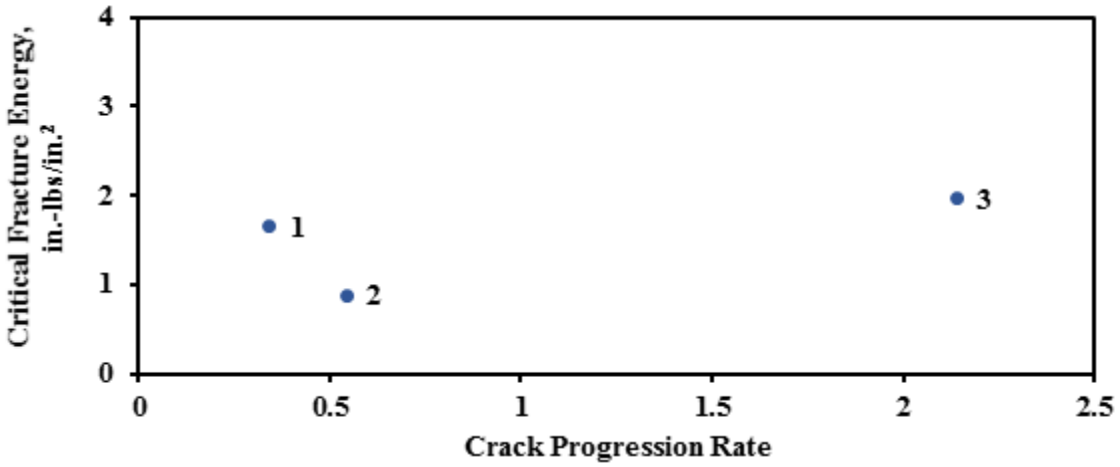

Figure B20 Cracking Performance of Type-B Mixes on Design Interaction Plot

Table B16 Results from Type-B Mixes

Mix ID	Parameter	Max Load, lbs	Work of Fracture, in.-lbs	Critical Fracture Energy, in.-lbs/in.^{2}	Crack Progression Rate	R^2	Number of Cycles to Failure
1	Average	639	7.5	1.7	0.34	1.0	521
	Median	648	7.6	1.7	0.34	1.0	538
	Std Dev	24	0.4	0.1	0.02	0.0	139
	COV	**4%**	**5%**	**5%**	**6%**	**0%**	**27%**
2	Average	496	4.0	0.9	0.54	1.00	121
	Median	496	4.1	0.9	0.50	1.00	117
	Std Dev	14	0.4	0.1	0.11	0.00	66
	COV	**3%**	**10%**	**10%**	**20%**	**0%**	**54%**
3	Average	977	8.9	2.0	2.14	1.0	7
	Median	977	8.9	2.0	2.14	1.0	7
	Std Dev	6	0.5	0.1	0.02	0.0	0
	COV	**1%**	**5%**	**5%**	**1%**	**0%**	**0%**

Table B17 Characteristics for SP-C Mixes

Mix ID	Sample Size	Year	Aggregate Type	Asphalt Grade	Asphalt Source	Asphalt Content	Anti-Strip	Anti-Strip, %
1	3	2012	Limestone	PG70-22	Alon	5.0	None	None
2	3	2012	Limestone	PG64-22	Alon	6.5	N/P	N/P
3	3	2012	Limestone and Gravel	PG70-22	Alon	5.7	None	None
4	3	2012	Limestone	PG70-22	N/P	5.1	N/P	N/P
5	3	2012	N/P	N/P	N/P	N/P	N/P	N/P
6	3	2014	Limestone	PG70-22	Valero	5.7	None	None
7	3	2014	Igneous	PG76-22	Lion	5.2	None	None
8	3	2014	Limestone	PG70-22	Alon	5.2	None	None
9	2	2015	N/P	PG70-22	N/P	4.5	N/P	N/P
10	3	2015	N/P	PG70-22	N/P	5.2	N/P	N/P
11	3	2015	Igneous	PG 76-22	Lion	5.0	None	None
12	3	2015	N/P	N/P	N/P	N/P	N/P	N/P
13	3	2015	Limestone	PG70-22	Alon	5.1	None	None
14	3	2015	Gravel	PG64-22	N/P	5.7	N/P	N/P
15	3	2015	Igneous	PG76-22	Lion	5.1	None	None
16	3	2015	Limestone	PG 70-22	Alon	4.9	None	None
17	3	2015	Gravel	PG 70-22	Alon	6.0	Liquid	1

N/P stands for Not Provided

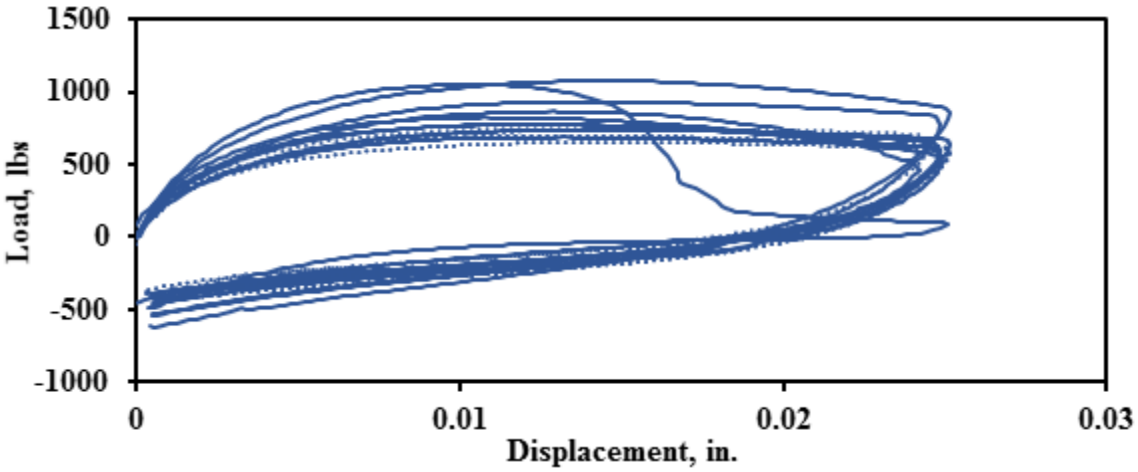

Figure B21 Average First Hysteresis Loops for SP-C Mixes

Table B18 Results from SP-C Mixes

Mix ID	Parameter	Max Load, lbs	Work of Fracture, in.-lbs	Critical Fracture Energy, in.-lbs/in.^{2}	Crack Progression Rate	R^2	Number of Cycles to Failure
1	Average	933	10.1	2.2	0.51	1.0	102
	Median	921	10.0	2.2	0.50	1.0	101
	Std Dev	62	1.3	0.3	0.04	0.0	17
	COV	**7%**	**13%**	**13%**	**8%**	**0%**	**17%**
2	Average	825	6.9	1.5	0.96	1.0	19
	Median	830	7.0	1.6	0.81	1.0	22
	Std Dev	42	0.5	0.1	0.23	0.0	6
	COV	**5%**	**7%**	**7%**	**24%**	**0%**	**31%**
3	Average	775	7.6	1.7	0.55	1.00	88
	Median	790	8.0	1.8	0.53	1.00	94
	Std Dev	43	0.7	0.2	0.04	0.00	13
	COV	**6%**	**10%**	**10%**	**7%**	**0%**	**15%**
4	Average	689	7.3	1.6	0.37	1.0	561
	Median	720	7.5	1.7	0.38	1.0	463
	Std Dev	65	0.3	0.1	0.03	0.0	315
	COV	**9%**	**4%**	**4%**	**8%**	**0%**	**56%**
5	Average	776	7.1	1.6	0.66	1.0	61
	Median	789	7.3	1.6	0.69	1.0	38
	Std Dev	54	0.7	0.2	0.11	0.0	38
	COV	**7%**	**10%**	**10%**	**16%**	**0%**	**62%**
6	Average	1057	8.7	1.9	2.40	0.9	6
	Median	1054	8.9	2.0	2.45	1.0	6
	Std Dev	35	0.3	0.1	0.23	0.0	0
	COV	**3%**	**4%**	**4%**	**10%**	**0%**	**7%**
7	Average	741	8.8	1.9	0.40	1.0	445
	Median	716	9.0	2.0	0.39	1.0	401
	Std Dev	39	0.7	0.2	0.03	0.0	114
	COV	**5%**	**8%**	**8%**	**7%**	**0%**	**26%**
8	Average	1082	12.4	2.8	0.74	1.0	44
	Median	1023	11.2	2.5	0.76	1.0	29
	Std Dev	134	2.4	0.5	0.10	0.0	24
	COV	**12%**	**19%**	**19%**	**13%**	**0%**	**55%**
9	Average	1055	9.3	2.1	1.44	1.0	9
	Median	1055	9.3	2.1	1.44	1.0	9
	Std Dev	2	1.1	0.2	0.20	0.0	3
	COV	**0%**	**12%**	**12%**	**14%**	**1%**	**29%**

Table B18 Results from SP-C Mixes (Continued)

10	Average	700	7.4	1.6	0.46	1.0	210
	Median	670	6.7	1.5	0.47	1.0	219
	Std Dev	58	1.3	0.3	0.03	0.0	53
	COV	**8%**	**17%**	**17%**	**6%**	**0%**	**25%**
11	Average	744	10.5	2.3	0.40	1.0	590
	Median	742	10.3	2.3	0.38	1.0	551
	Std Dev	6	1.3	0.3	0.06	0.0	195
	COV	**1%**	**12%**	**12%**	**14%**	**0%**	**33%**
12	Average	655	7.9	1.7	0.43	1.0	485
	Median	663	8.1	1.8	0.45	1.0	259
	Std Dev	18	0.5	0.1	0.04	0.0	365
	COV	**3%**	**7%**	**7%**	**10%**	**0%**	**75%**
13	Average	908	9.6	2.1	0.81	1.0	33
	Median	919	10.2	2.3	0.71	1.0	41
	Std Dev	31	1.1	0.2	0.19	0.0	15
	COV	**3%**	**11%**	**11%**	**24%**	**0%**	**44%**
14	Average	698	7.5	1.7	0.41	1.0	195
	Median	739	7.9	1.8	0.41	1.0	209
	Std Dev	68	1.0	0.2	0.04	0.0	68
	COV	**10%**	**14%**	**14%**	**9%**	**1%**	**35%**
15	Average	880	10.1	2.2	0.67	1.0	42
	Median	879	9.8	2.2	0.64	1.0	40
	Std Dev	13	1.2	0.3	0.06	0.0	12
	COV	**1%**	**12%**	**12%**	**9%**	**0%**	**27%**
16	Average	986	10.0	2.2	0.83	1.0	36
	Median	973	9.8	2.2	0.76	1.0	44
	Std Dev	134	1.4	0.3	0.12	0.0	11
	COV	**14%**	**14%**	**14%**	**14%**	**0%**	**31%**
17	Average	756	8.4	1.9	0.40	1.0	409
	Median	757	8.4	1.9	0.40	1.0	383
	Std Dev	43	0.3	0.1	0.01	0.0	38
	COV	**6%**	**4%**	**4%**	**2%**	**0%**	**9%**

Table B19 Characteristics for SP-D Mixes

Mix ID	Sample Size	Year	Aggregate Type	Asphalt Grade	Asphalt Source	Asphalt Content	Anti-Strip	Anti-Strip %
1	3	2014	Limestone	PG70-22	Alon	5.2	Liquid	1
2	3	2014	Limestone	PG70-22	Alon	N/P	N/P	N/P
3	3	2014	Gravel	PG76-22	Valero	5.5	Lime	1
4	3	2014	Limestone	PG64-22	Valero	5.2	Lime	1
5	2	2014	Limestone	PG70-22	Heartland	N/P	Liquid	0.75
6	3	2014	Gravel	PG70-22	Alon	6.1	N/P	N/P
7	3	2015	Limestone	PG 76-22	Alon	N/P	N/P	N/P
8	3	2015	Igneous	PG76-22	Lion	5.4	N/P	N/P
9	3	2015	Limestone	PG76-22	Heartland	6.1	N/P	N/P
10	2	2015	Limestone	PG70-22	Alon	5.8	Liquid	1
11	3	2015	N/P	PG70-22	N/P	N/P	N/P	N/P
12	3	2015	Limestone	PG70-22	Alon	6.3	Liquid	1
13	3	2015	Gravel	PG76-22	Lion	5.5	Lime	1
14	3	2015	Gravel	PG70-22	Alon	6.2	N/P	N/P
15	3	2015	N/P	PG70-22	N/P	N/P	N/P	N/P

N/P stands for Not Provided

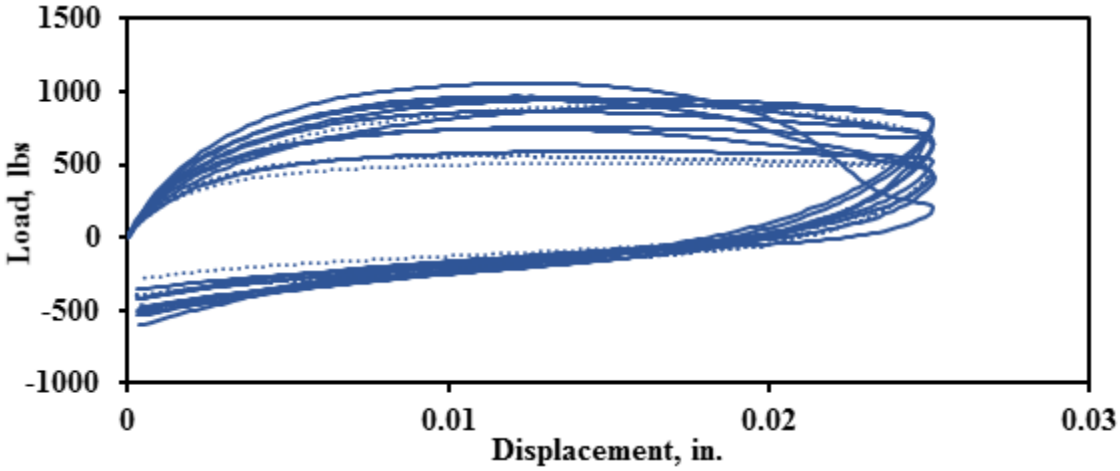

Figure B22 Average First Hysteresis Loops for SP-D Mixes

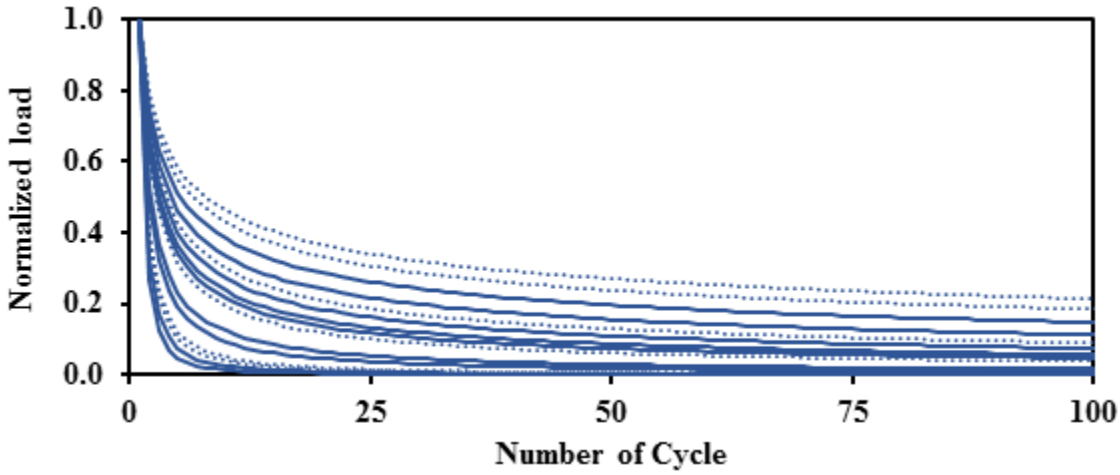

Figure B23 Average Normalized Load Reduction Curves for SP-D Mixes

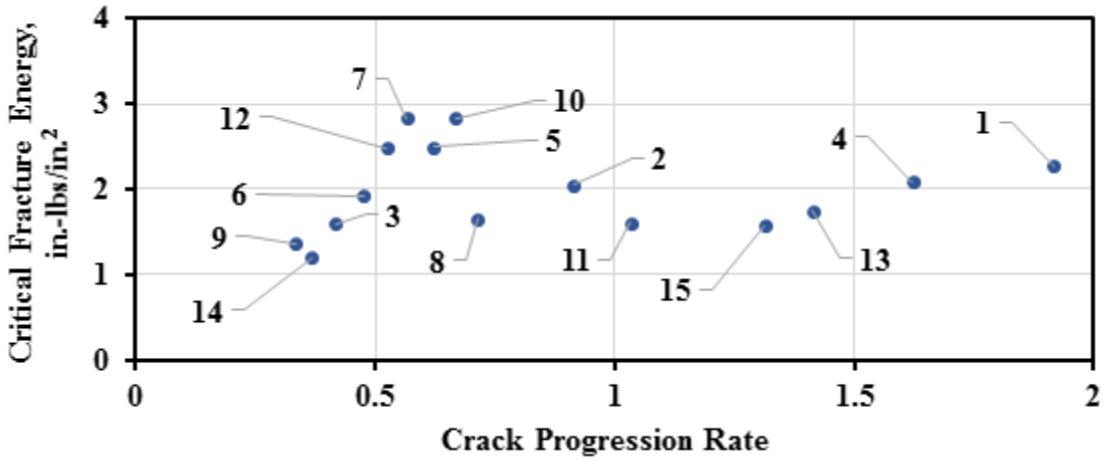

Figure B24 Cracking Performance of SP-D Mixes on Design Interaction Plot

Table B20 Results from SP-D Mixes

Mix ID	Parameter	Max Load, lbs	Work of Fracture, in.-lbs	Critical Fracture Energy, in.-lbs/in.^{2}	Crack Progression Rate	R^2	Number of Cycles to Failure
1	Average	1059	10.2	2.3	1.92	1.0	8
	Median	1042	10.2	2.3	2.02	1.0	7
	Std Dev	33	0.1	0.0	0.22	0.0	1
	COV	**3%**	**1%**	**1%**	**11%**	**1%**	**12%**
2	Average	972	9.2	2.1	0.91	1.0	26
	Median	963	9.6	2.1	0.89	1.0	25
	Std Dev	17	1.2	0.3	0.13	0.0	8
	COV	**2%**	**13%**	**13%**	**14%**	**0%**	**30%**
3	Average	590	7.21	1.60	0.42	0.99	134
	Median	584	7.03	1.56	0.45	1.00	141
	Std Dev	46	1.13	0.25	0.07	0.00	19
	COV	**8%**	**16%**	**16%**	**16%**	**0%**	**14%**
4	Average	955	9.4	2.1	1.62	1.0	9
	Median	924	8.5	1.9	1.63	1.0	9
	Std Dev	65	2.1	0.5	0.01	0.0	0
	COV	**7%**	**23%**	**23%**	**1%**	**1%**	**0%**
5	Average	1001	11.2	2.5	0.62	1.0	72
	Median	960	11.2	2.5	0.61	1.0	59
	Std Dev	75	0.1	0.0	0.04	0.0	32
	COV	**8%**	**1%**	**1%**	**6%**	**0%**	**44%**
6	Average	868	8.7	1.9	0.48	1.0	184
	Median	878	8.5	1.9	0.44	1.0	127
	Std Dev	48	0.4	0.1	0.08	0.0	112
	COV	**6%**	**5%**	**5%**	**18%**	**0%**	**61%**
7	Average	1012	12.7	2.8	0.57	1.0	363
	Median	1078	12.7	2.8	0.65	1.0	53
	Std Dev	105	0.6	0.1	0.18	0.0	451
	COV	**10%**	**4%**	**4%**	**31%**	**0%**	**124%**
8	Average	714	7.4	1.7	0.71	1.0	37
	Median	655	6.9	1.5	0.69	1.0	40
	Std Dev	86	1.3	0.3	0.08	0.0	9
	COV	**12%**	**17%**	**17%**	**11%**	**1%**	**25%**
9	Average	510	6.1	1.4	0.33	1.0	1000
	Median	507	6.4	1.4	0.33	1.0	1000
	Std Dev	26	0.5	0.1	0.02	0.0	0
	COV	**5%**	**9%**	**9%**	**5%**	**0%**	**NA**

Table B20 Results from SP-D Mixes (Continued)

10	Average	911	12.7	2.8	0.67	1.0	47
	Median	911	12.7	2.8	0.67	1.0	47
	Std Dev	97	0.0	0.0	0.10	0.0	13
	COV	**11%**	**0%**	**0%**	**15%**	**0%**	**27%**
11	Average	747	7.2	1.6	1.03	1.0	24
	Median	728	7.0	1.6	1.02	1.0	21
	Std Dev	65	0.7	0.2	0.20	0.0	10
	COV	**9%**	**10%**	**10%**	**19%**	**0%**	**43%**
12	Average	889	11.2	2.5	0.52	1.0	98
	Median	899	11.4	2.5	0.53	1.0	86
	Std Dev	126	1.0	0.2	0.12	0.0	45
	COV	**14%**	**9%**	**9%**	**24%**	**0%**	**46%**
13	Average	838	7.9	1.8	1.41	1.0	16
	Median	838	7.5	1.7	1.19	1.0	17
	Std Dev	3	0.7	0.1	0.49	0.0	7
	COV	**0%**	**8%**	**8%**	**35%**	**1%**	**44%**
14	Average	560	5.4	1.2	0.37	1.0	309
	Median	545	5.2	1.1	0.36	1.0	315
	Std Dev	25	0.6	0.1	0.02	0.0	44
	COV	**4%**	**11%**	**11%**	**5%**	**0%**	**14%**
15	Average	808	7.1	1.6	1.31	1.0	12
	Median	805	6.8	1.5	1.12	1.0	13
	Std Dev	16	0.8	0.2	0.41	0.0	6
	COV	**2%**	**12%**	**12%**	**32%**	**1%**	**46%**

Table B21 Characteristics for Type-C Mixes

Mix ID	Sample Size	Year	Aggregate Type	Asphalt Grade	Asphalt Source	Asphalt Content	Anti-Strip	Anti-Strip, %
1	3	2012	N/P	PG76-22	N/P	N/P	N/P	N/P
2	3	2012	Limestone	PG64-22	Jebro	4.8	Lime	1
3	3	2012	N/P	PG76-22	N/P	5.0	N/P	1
4	3	2013	Limestone	PG70-22	Gary-Williams	4.2	Liquid	1
5	2	2013	N/P	N/P	Valero	4.6	Lime	1
6	3	2013	Limestone and Gravel	PG64-22	Valero	4.7	Lime	N/P
7	3	2013	N/P	PG70-22	N/P	N/P	N/P	N/P
8	3	2014	N/P	PG70-22	N/P	N/P	N/P	N/P
9	3	2015	N/P	PG70-22	N/P	N/P	N/P	N/P
10	3	2015	Igneous	PG70-22	Lion	4.8	N/P	N/P
11	3	2015	Igneous	PG76-22	N/P	N/P	N/P	N/P
12	3	2015	Limestone	PG 70-22	Valero	4.7	EVOTHERM	0.4

N/P stands for Not Provided

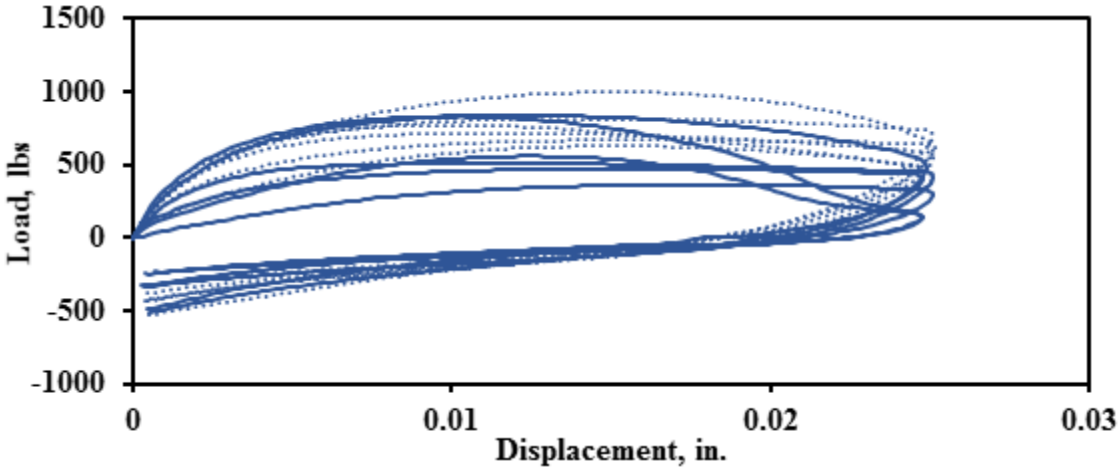

Figure B25 Average First Hysteresis Loops for Type-C Mixes

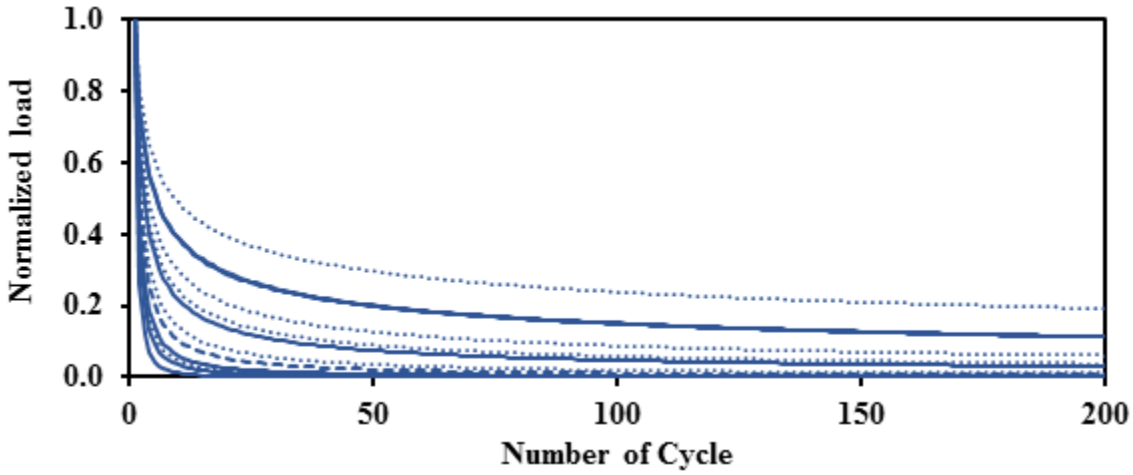

Figure B26 Average Normalized Load Reduction Curves for Type-C Mixes

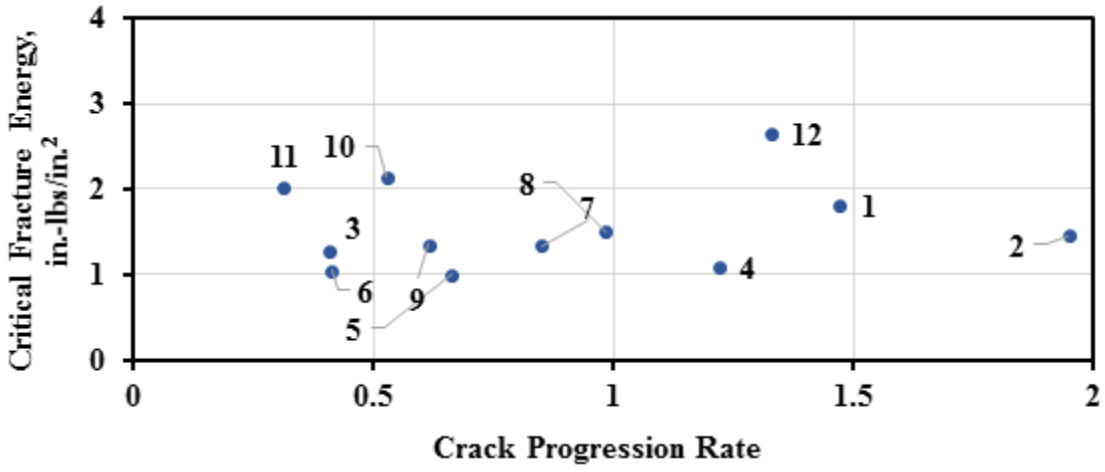

Figure B27 Cracking Performance of Type-C Mixes on Design Interaction Plot

Table B22 Results from Type-C Mixes

Mix ID	Parameter	Max Load, lbs	Work of Fracture, in.-lbs	Critical Fracture Energy, in.-lbs/in.^{2}	Crack Progression Rate	R^2	Number of Cycles to Failure
1	Average	841	8.2	1.8	1.47	1.0	9
	Median	845	7.9	1.8	1.34	1.0	9
	Std Dev	10	0.7	0.1	0.25	0.0	2
	COV	**1%**	**8%**	**8%**	**17%**	**0%**	**24%**
2	Average	834	6.5	1.5	1.95	1.0	4
	Median	832	6.8	1.5	1.92	1.0	4
	Std Dev	13	0.4	0.1	0.12	0.0	0
	COV	**2%**	**6%**	**6%**	**6%**	**0%**	**11%**
3	Average	473	5.8	1.3	0.41	1.00	423
	Median	471	5.5	1.2	0.41	1.00	484
	Std Dev	9	0.5	0.1	0.04	0.00	209
	COV	**2%**	**8%**	**8%**	**10%**	**0%**	**49%**
4	Average	559	4.9	1.1	1.22	1.0	11
	Median	555	4.8	1.1	1.20	1.0	11
	Std Dev	30	0.2	0.0	0.09	0.0	2
	COV	**5%**	**4%**	**4%**	**7%**	**1%**	**15%**
5	Average	365	4.5	1.0	0.66	1.0	58
	Median	365	4.5	1.0	0.66	1.0	58
	Std Dev	33	0.0	0.0	0.06	0.0	20
	COV	**9%**	**1%**	**1%**	**9%**	**0%**	**34%**
6	Average	510	4.7	1.0	0.41	1.0	223
	Median	487	4.9	1.1	0.39	1.0	254
	Std Dev	36	0.5	0.1	0.05	0.0	86
	COV	**7%**	**12%**	**12%**	**11%**	**0%**	**39%**
7	Average	773	6.0	1.3	0.85	1.0	34
	Median	766	6.0	1.3	0.80	1.0	35
	Std Dev	33	0.7	0.2	0.10	0.0	9
	COV	**4%**	**11%**	**11%**	**11%**	**1%**	**25%**
8	Average	632	6.8	1.5	0.98	1.0	16
	Median	632	6.4	1.4	1.03	1.0	16
	Std Dev	28	0.7	0.2	0.07	0.0	1
	COV	**4%**	**11%**	**11%**	**7%**	**0%**	**8%**

Table B22 Results from Type-C Mixes (Continued)

9	Average	720	6.1	1.4	0.62	1.0	122
	Median	726	6.3	1.4	0.59	1.0	79
	Std Dev	20	0.3	0.1	0.16	0.0	98
	COV	**3%**	**5%**	**5%**	**26%**	**0%**	**80%**
10	Average	816	9.7	2.1	0.53	1.0	112
	Median	817	9.3	2.1	0.54	1.0	112
	Std Dev	25	1.2	0.3	0.05	0.0	32
	COV	**3%**	**12%**	**12%**	**10%**	**0%**	**29%**
11	Average	672	9.1	2.0	0.31	1.0	1000
	Median	651	9.2	2.0	0.31	1.0	1000
	Std Dev	34	0.6	0.1	0.01	0.0	0
	COV	**5%**	**6%**	**6%**	**3%**	**0%**	**NA**
12	Average	1013	11.9	2.6	1.33	1.0	14
	Median	1006	11.0	2.4	1.21	1.0	14
	Std Dev	20	1.4	0.3	0.42	0.0	4
	COV	**2%**	**12%**	**12%**	**32%**	**1%**	**33%**

Table B23 Characteristics for Type-D Mixes

Mix ID	**Sample Size**	**Year**	**Aggregate Type**	**Asphalt Grade**	**Asphalt Source**	**Asphalt Content**	**Anti-Strip**	**Anti-Strip, %**
1	3	2012	N/P	N/P	N/P	N/P	Lime	1
2	3	2012	N/P	PG70-22	N/P	N/P	N/P	N/P
3	2	2012	Igneous	PG76-22	Lion	5.1	None	0
4	3	2013	N/P	PG76-22	Valero	5.5	Lime	1
5	3	2013	Gravel	PG70-22	Valero	5.1	Lime	1
6	3	2013	Gravel	PG70-22	N/P	5.1	Lime	1
7	3	2013	Limestone	PG76-22	Valero	5	N/P	N/P
8	3	2013	Limestone	PG70-22	Martin Asphalt	4.8	N/P	N/P
9	3	2013	Limestone	PG70-22	Valero	5.1	N/P	N/P
10	3	2015	Limestone	PG70-22	Valero	5.4	N/P	N/P
11	3	2015	Sandstone	PG70-22	Lion	5	Liquid	0.5
12	3	2015	Igneous	PG76-22	Heartland	6.9	Lime	1
N/P stands for Not Provided								

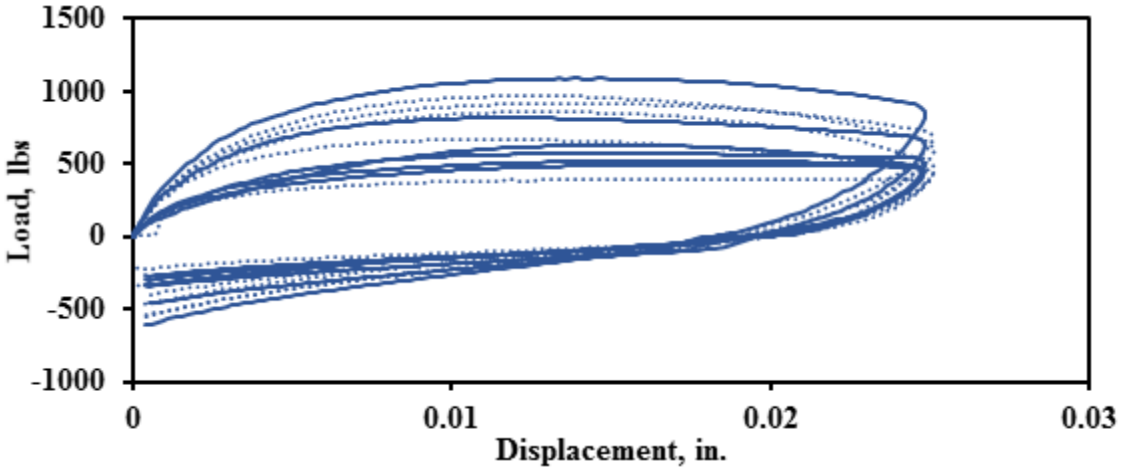

Figure B28 Average First Hysteresis Loops for Type-D Mixes

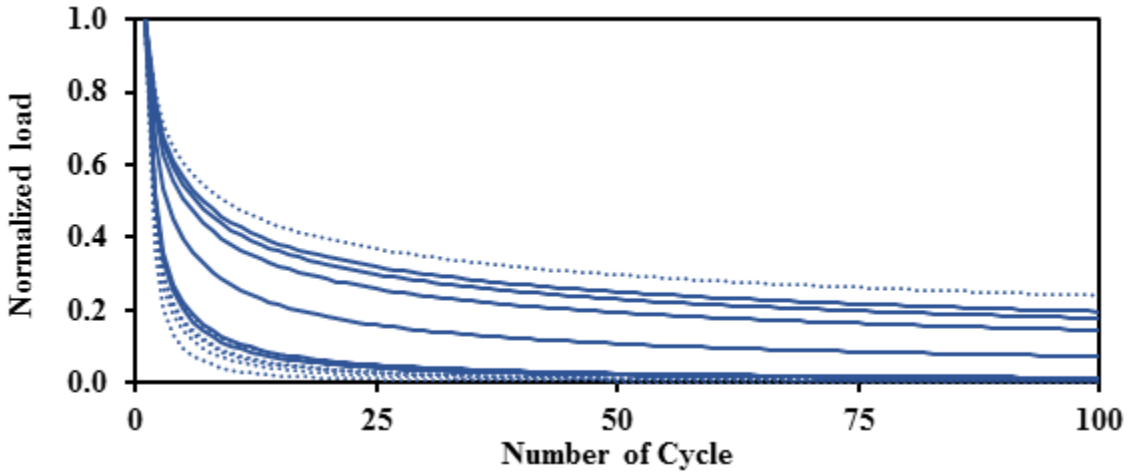

Figure B29 Average Normalized Load Reduction Curves for Type-D Mixes

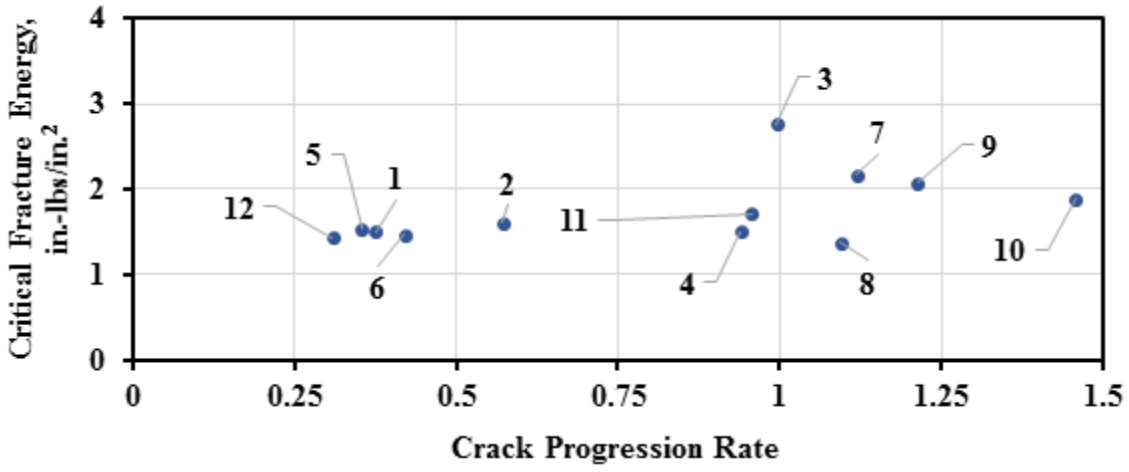

Figure B30 Cracking Performance of Type-D Mixes on Design Interaction Plot

Table B24 Results from Type-D Mixes

Mix ID	Parameter	Max Load, lbs	Work of Fracture, in.-lbs	Critical Fracture Energy, in.-lbs/in.^{2}	Crack Progression Rate	R^2	Number of Cycles to Failure
1	Average	574	6.8	1.5	0.38	1.0	452
	Median	580	6.8	1.5	0.37	1.0	412
	Std Dev	20	0.8	0.2	0.01	0.0	156
	COV	**3%**	**11%**	**11%**	**4%**	**0%**	**34%**
2	Average	818	7.2	1.6	0.57	1.0	104
	Median	803	6.9	1.5	0.57	1.0	65
	Std Dev	37	0.7	0.2	0.10	0.0	75
	COV	**5%**	**10%**	**10%**	**17%**	**0%**	**72%**
3	Average	1090	12.43	2.76	0.99	1.00	19
	Median	1090	12.43	2.76	0.99	1.00	19
	Std Dev	12	0.32	0.07	0.05	0.00	3
	COV	**1%**	**3%**	**3%**	**5%**	**0%**	**14%**
4	Average	630	6.8	1.5	0.94	1.0	22
	Median	646	6.8	1.5	0.92	1.0	21
	Std Dev	27	0.1	0.0	0.10	0.0	7
	COV	**4%**	**1%**	**1%**	**11%**	**0%**	**30%**
5	Average	499	6.9	1.5	0.35	1.0	380
	Median	518	7.3	1.6	0.35	1.0	320
	Std Dev	31	0.6	0.1	0.00	0.0	120
	COV	**6%**	**8%**	**8%**	**1%**	**0%**	**32%**
6	Average	534	6.6	1.5	0.42	1.0	224
	Median	515	7.2	1.6	0.42	1.0	181
	Std Dev	58	1.0	0.2	0.00	0.0	74
	COV	**11%**	**15%**	**15%**	**1%**	**0%**	**33%**
7	Average	919	9.8	2.2	1.12	1.0	17
	Median	908	10.0	2.2	1.21	1.0	14
	Std Dev	29	0.4	0.1	0.20	0.0	6
	COV	**3%**	**4%**	**4%**	**18%**	**0%**	**36%**
8	Average	668	6.2	1.4	1.09	1.0	18
	Median	660	5.9	1.3	1.05	1.0	17
	Std Dev	25	0.8	0.2	0.20	0.0	6
	COV	**4%**	**14%**	**14%**	**19%**	**0%**	**32%**

Table B24 - Results from Type-D Mixes (Continued)

9	Average	970	9.3	2.1	1.21	1.0	14
	Median	996	8.8	2.0	1.15	1.0	15
	Std Dev	40	0.7	0.2	0.14	0.0	2
	COV	**4%**	**8%**	**8%**	**12%**	**1%**	**15%**
10	Average	861	8.5	1.9	1.46	1.0	11
	Median	835	8.4	1.9	1.47	1.0	10
	Std Dev	68	1.0	0.2	0.14	0.0	2
	COV	**8%**	**12%**	**12%**	**10%**	**1%**	**16%**
11	Average	823	7.7	1.7	0.96	1.0	21
	Median	824	7.5	1.7	0.98	1.0	17
	Std Dev	8	0.8	0.2	0.18	0.0	9
	COV	**1%**	**11%**	**11%**	**19%**	**0%**	**43%**
12	Average	396	6.5	1.4	0.31	1.0	1000
	Median	389	6.5	1.4	0.31	1.0	1000
	Std Dev	19	0.1	0.0	0.00	0.0	0
	COV	**5%**	**2%**	**2%**	**1%**	**0%**	**NA**

Appendix C: Proposed OT Test Method and Specifications

Table C1 Results Obtained from Version 2014 Gluing Method

Specimen	Air Voids, %	Max Load, lbs	Work of Fracture, in-lbs	Critical Fracture Energy, in.-lbs/in.^{2}	Crack Progression Rate	R^2	Number of Cycles to Failure
1	6.8	358	4.8	1.1	0.35	1.00	375
2	6.1	334	6.6	1.5	0.34	1.00	404
3	6.1	467	6.8	1.5	0.40	1.00	363
4	7.1	330	5.2	1.2	0.33	1.00	449
5	7.5	556	7.0	1.6	0.61	1.00	79
Average	6.7	409	6.1	1.4	0.41	1.00	334
Std Dev	0.6	89	0.9	0.2	0.11	0.00	146
COV	**8%**	**22%**	**15%**	**15%**	**26%**	**NA**	**44%**

Table C2 Results Obtained from Proposed Gluing Method

Specimen	Air Voids, %	Max Load, lbs	Work of Fracture, in-lbs	Critical Fracture Energy, in.-lbs/in.^{2}	Crack Progression Rate	R^2	Number of Cycles to Failure
1	7.6	470	4.8	1.1	0.47	1.00	312
2	7.9	439	5.1	1.1	0.48	1.00	198
3	7.4	469	5.7	1.3	0.41	1.00	483
4	7.6	497	4.3	1.0	0.46	1.00	370
5	7.2	461	4.9	1.1	0.43	1.00	389
Average	7.5	467	5.0	1.1	0.45	1.00	350
Std Dev	0.2	19	0.5	0.1	0.03	0.00	94
COV	**3%**	**4%**	**9%**	**9%**	**6%**	**NA**	**27%**

Modifications to Specimen Preparation Process and Performance Indices Calculations for Proposed OT Method

6. PROCEDURE

6.1 *Sample Preparation:*

6.1.1 Obtain three cylindrical molded specimens according to Section 4.

Note 8—Test roadway cores for informational purposes only.

6.2 *Trimming of Cylindrical Samples:*

6.2.1 Refer to the sawing device manufacturer's instructions for trimming specimens when using a double blade saw

6.2.2 When using a single blade saw, use a cutting template on the top surface of the sample and trace the location of the first two cuts by drawing lines using paint or permanent marker. Refer to Figure 1. Trim the sides of the sample by cutting the sample perpendicular to the top surface. Follow the traced lines drawn. Cut the sides so the trimmed sample is 3 ± 0.02 in. (76 ± 0.5 mm) thick. Discard the cut pieces. Refer to Figure 2.

Figure 2—Trimmed Sample

6.2.3 Rotate the sample, and trim the top and bottom part of the sample to produce one specimen with a height of 1.5 ± 0.02 in. (38.1 ± 0.5 mm). Discard the top and bottom parts of the sample. Refer to Figure 3.

Figure 3—Trimmed OT Specimen

6.2.4 Measure the relative density of the trimmed laboratory-molded specimen in accordance with Tex-207-F.

Note 9–Do not measure the relative density of the trimmed PFC specimens.

6.2.4.1 Calculate the weight of the specimens in water.

6.2.4.2 Calculate the saturated surface dry weight (SSD) first then the dry weight of the specimen.

6.2.4.3 Dry the trimmed specimens using one of the following methods:

- Air-dry the specimen to remove excess moisture and then use a vacuum device to dry the specimen.
- Oven-dry the specimen at 104 ± 5°F (40 ± 3°C) to constant weight.

Note 10—It normally takes 8 hours to oven-dry the specimen. Do not oven-dry the specimen for more than 24 hr.

6.2.5 Density for the trimmed specimen must be 93 ± 1%. Discard and prepare a new specimen if the trimmed specimen does not meet the density requirement.

Note 11—The density for specimens trimmed from roadway cores is for informational purpose only. Trimmed PFC specimens do not have a density requirement.

6.3 *Mounting Trimmed Specimen:*

6.3.1 Prepare the materials required to mount the specimen. Follow the gluing process for each specimen individually (See Figure 4).

Figure 4—Materials required to mount specimens

6.3.2 Ensure the space bar and base plates are clean. Remove any dirt and epoxy from previous specimens.

6.3.3 Mount and secure the base plates to the mounting jig. Place the space bar between the plates as shown in Figure 5.

Note 12—It is recommended to have individual mounting jigs for the base plates to avoid dragging epoxy residuals between specimens.

Figure 5—Base Plates on Mounting Jig with Space Bar

6.3.4 Draw a line along the middle of the trimmed specimen to guide the placement of the tape as shown in Figure 6.

Figure 6—Middle Line Drawn with Permanent Marker

6.3.5 Place a piece of 4-mm wide tape along the middle of the trimmed specimen to cover the gap (apply a small amount of grease between the tape and the specimen to facilitate the tape removal once the specimen is mounted onto the base plates). See Figure 7.

Figure 7—Grease (Petroleum Jelly) on Specimen and Tape Placed on Center Line

6.3.6 Prepare two containers with 8 g of the two-part epoxy on each, following the manufacturer's instructions. Prepare epoxy only for one specimen in one batch. Refer to Figure 8.

Figure 8—Epoxy on Containers for a Single Specimen

6.3.7 Pour each container on each half of the specimen and spread evenly avoiding contact with the 4-mm wide tape. See Figure 9.

Figure 9—Pouring and Spreading Epoxy

6.3.8 Mount the specimen on the base plates while ensuring that the specimen is centered and aligned with the edges of the base plates. See Figure 10.

Figure 10—Centering and Alignment the Specimen

6.3.9 Add a 5-lb weight on top of the specimen to ensure contact between the specimen and the base plates. See Figure 11.

Figure 11—5-lb Weight on Top of Specimen

6.3.10 Remove the excess epoxy glue accumulated on the sides of the mounted specimen with a razor to ensure a uniform bond only between the specimen and the plates. See Figure 12.

Figure 12—Excess Epoxy Removed from Sides

6.3.11 Carefully remove the tape and the spacer bar while preventing the specimen from moving. See Figure 13.

Note 13—No more than 2 minutes should pass from spreading the epoxy onto the specimen to removing the tape and space bar.

Figure 13—Tape and Space Bar Removal

6.3.12 Allow the epoxy to cure for sufficient bonding strength as per manufacturer's recommendations. The mounted specimen is depicted in Figure 14.

Note 14—Usually overnight is an adequate curing period for the epoxy.

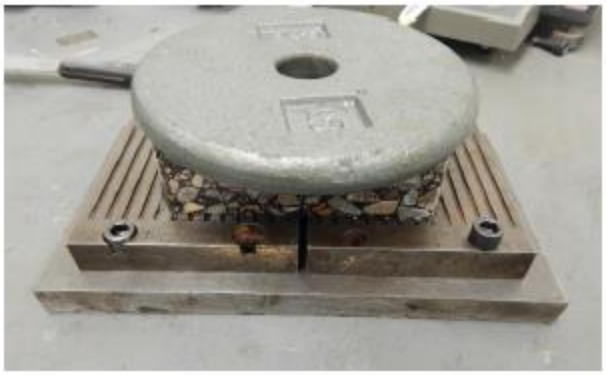

Figure 14—Mounted Specimen

6.3.13 Remove the weight from the specimen after the epoxy has cured.

6.4 Place the test sample assembly (specimen and plates) in a temperature chamber or oven at 77 ± 1°F (25 ± 0.5°C) for a minimum of 1 hour before testing.

6.5 *Starting Testing Device:*

6.5.1 Turn on the OT. Turn on the computer and wait at least 5 minutes to establish communication with the OT before starting the OT software.

6.5.2 Turn on the hydraulic pump by using the OT software.

6.6 *Mounting Specimen Assembly to Testing Device:*

6.6.1 Enter the required test information into the OT software.

6.6.2 Clean the bottom base plates and the top of the testing machine blocks before placing the specimen assembly into the blocks.

Note 15—The machine, the specimen, or the base plates may be damaged when tightening the base plates if not all the surfaces are clean.

6.6.2.1 Mount the specimen assembly onto the machine according to the manufacturer's instructions and the following additional steps. Ensure machine is in load mode while assembling specimen.

6.6.2.2 Put the specimen assembly in the machine ensuring that minimum stress is applied to the specimen.

6.6.2.3 Use the torque wrench to apply 15 lbs-ft of torque for each bolt to fasten the base plates to the machine. Use a similar torqueing pattern for all the replicate specimens. The pattern shown in Figure 15 is recommended.

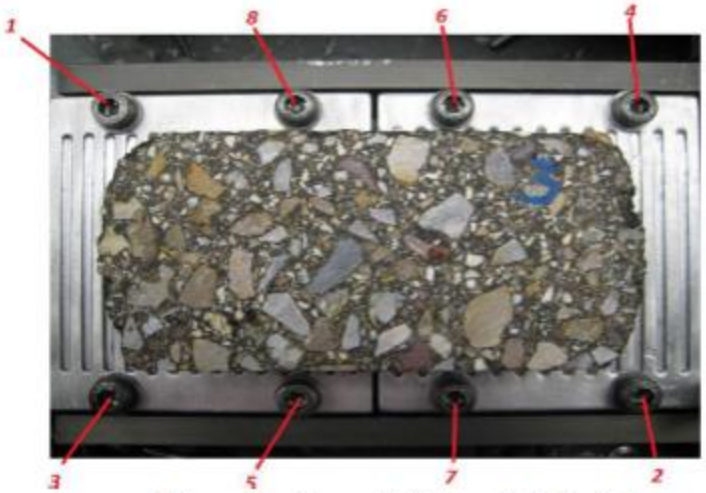

Figure 15—Suggested Pattern for Tying Bolts

6.7 *Testing the Specimen:*

6.7.1 Test all replicate specimens within the same day to minimize the variability in the test results. Test specimens within 5 days from the day of molding.

6.7.2 Perform testing at a constant temperature of 77 ± 1°F (25 ± 0.5°C).

Note 16—Ensure temperature of trimmed test specimen is 77 ± 1°F (25 ± 0.5°C).

6.7.3 Start the test by enabling the start button in the program.

Note 17—It is recommended to add a minimum of 10 minutes relaxation period prior testing each specimen. The test will automatically start after the specimen relaxation and temperature stabilization sequence is completed.

Note 18—The test should continue until a 95% reduction of the maximum positive load occurs, when measured from the first cycle. If a 95% load reduction is not reached within 200 cycles, the OT will stop the test.

6.7.4 Remove the specimen assembly upon completion of the test. Turn off the OT machine if needed.

7. CALCULATIONS

7.1 Figure 16 illustrates a graphical representation of the critical fracture energy. Calculate the critical fracture energy up to the maximum peak load using the load-displacement curve response curve of the first cycle using the following equation:

$$G_c = \frac{W_c}{b*h}$$

where, G_c is the critical fracture energy in lbs-in./in.^{2} (kN-mm/mm^2), W_c is the fracture area, lbs-in. (kN-mm), b is the width of OT specimen, (3 in., 76.2 mm), and h is the height of OT specimen, (1.5 in., 38.1 mm)

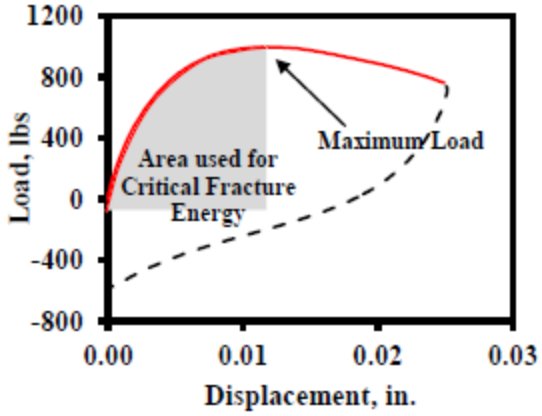

Figure 16—Area Used for Calculation of Critical Fracture Energy

7.2 Calculate the Crack Progression Rate by fitting a power equation to the peak load versus number of cycle curve as depicted in Figure 17.

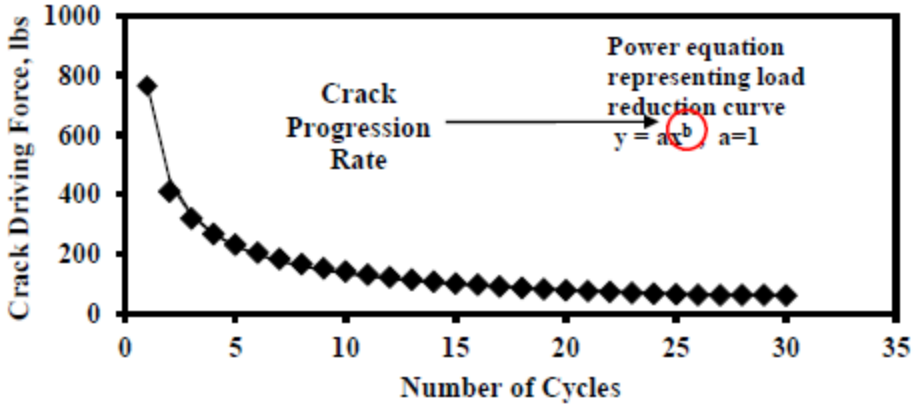

Figure 17—Calculation of Crack Progression Rate

AC Mix-Design Summary Sheets for Rigorous Evaluation of Proposed OT Method

	AGGREGATE BIN FRACTIONS													"RECYCLED MATERIALS"							
	Bin No.1		Bin No.2		Bin No.3		Bin No.4		Bin No.5		Bin No.6		Bin No.7	Bin No.8		Bin No.9		Bin No.10			
Aggregate Source:	Sandstone		Limestone_Dolom		Limestone_Dolom															Material Type	
Aggregate Pit:	Brownlee		Marble Falls		Feld															Material Source	
Aggregate Number:	1402704		1402702		1424602															RAS Type	
Sample ID:	Grade 5		F		Dry Screenings															Sample ID	
														Recycled Asphalt Binder (%)							
Hydrated Lime?:															% of Tot. Mix		% of Tot. Mix		% of Tot. Mix	Total Bin	Combined Gradation
Individual Bin (%):	60.0	Percent	20.0	Percent	20.0	Percent		Percent		Percent		Percent			% of Aggreg.		% of Aggreg.		% of Aggreg.	100.0%	Lower & Upper Specification Limits
Sieve Size:	Cum.% Passing	Wtd Cum. %	Cum.% Passing	Wtd Cum. %	Cum.% Passing	Wtd Cum. %	Cum.% Passing	Wtd Cum. %	Cum.% Passing	Wtd Cum. %	Cum.% Passing	Wtd Cum. %	Cum.% Passing	Wtd Cum. %	Cum.% Passing	Wtd Cum. %	Cum.% Passing	Wtd Cum. %	Cum.% Passing	Wtd Cum. %	Cum. % Passing	Lower	Upper	Within Spec's
1/2"	100.0	60.0	100.0	20.0	100.0	20.0															100.0	100.0	100.0	Yes
3/8"	98.1	58.9	100.0	20.0	100.0	20.0															98.9	85.0	100.0	Yes
No. 4	21.3	12.8	72.7	14.5	99.9	20.0															47.3	40.0	60.0	Yes
No. 8	2.7	1.6	6.7	1.3	94.4	18.9															21.8	17.0	27.0	Yes
No. 16	1.5	0.9	2.6	0.5	75.2	15.0															16.5	5.0	27.0	Yes
No. 30	1.3	0.8	1.7	0.3	58.8	11.8															12.9	5.0	27.0	Yes
No. 50	1.3	0.8	1.3	0.3	47.7	9.5															10.6	5.0	27.0	Yes
No. 200	1.1	0.7	0.8	0.2	27.4	5.5															6.3	5.0	9.0	Yes

Ratio of Recycled to Total Binder, % (based on binder percent (%) entered below in this worksheet): 0.0

(Bold Italic) Not within specifications *(Bold Italic)* Not within specifications- Restricted Zone *(Italic)* Not cumulative

Lift Thickness, in:		Binder Substitution?	No	Binder Originally Specified	PG 76-22	Substitute Binder		
Asphalt Source:			Binder Percent, (%):	6.5	Asphalt Spec. Grav.:	1.033		
Antistripping Agent:			Percent, (%):					

Figure C1 TOM Mix Design Summary Sheet

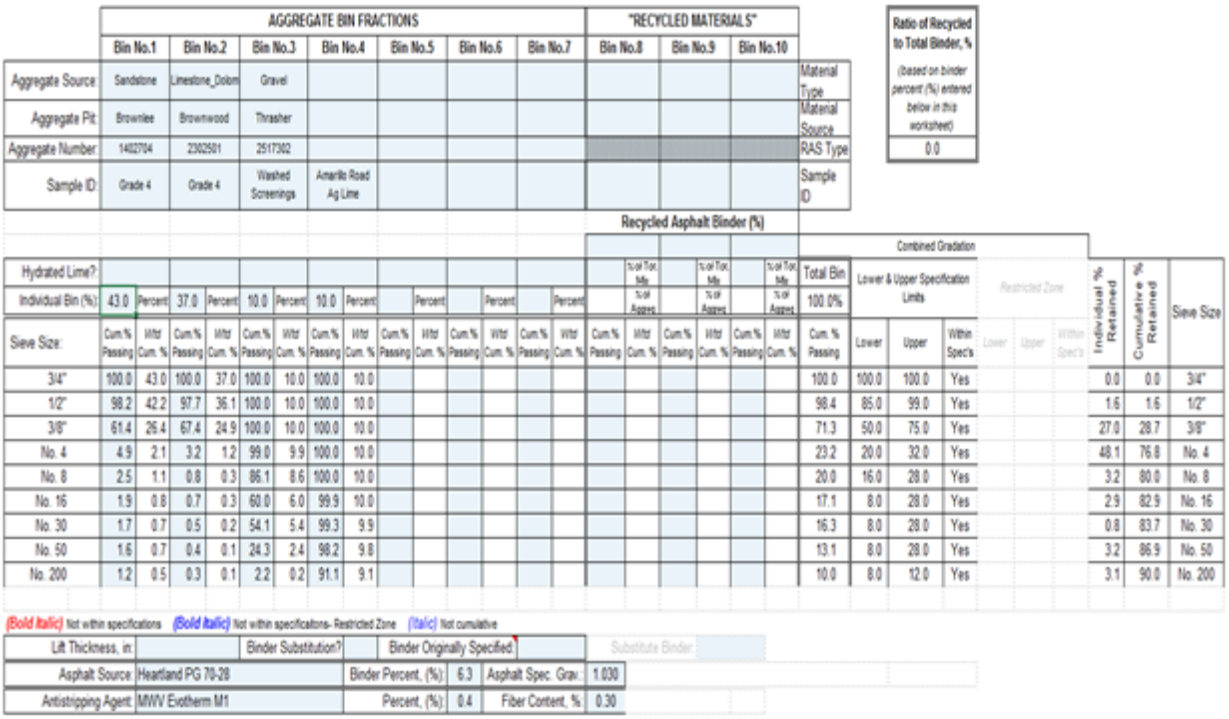

AGGREGATE BIN FRACTIONS								"RECYCLED MATERIALS"			
	Bin No.1	Bin No.2	Bin No.3	Bin No.4	Bin No.5	Bin No.6	Bin No.7	Bin No.8	Bin No.9	Bin No.10	
Aggregate Source	Sandstone	Limestone_Dolom	Gravel								Material Type
Aggregate Pit	Brownlee	Brownwood	Thrasher								Material Source
Aggregate Number	1402704	2302501	2517302								RAS Type
Sample ID	Grade 4	Grade 4	Washed Screenings	Amarillo Road Ag Lime							Sample ID
Hydrated Lime?											
Individual Bin (%)	43.0	37.0	10.0	10.0							100.0%

Ratio of Recycled to Total Binder, % (based on binder percent (%) entered below in this worksheet): 0.0

Recycled Asphalt Binder (%)

Sieve Size	Cum.% Passing	Wtd Cum. %	Cum.% Passing	Wtd Cum. %	Cum.% Passing	Wtd Cum. %	Cum.% Passing	Wtd Cum. %	Cum.% Passing	Wtd Cum. %	Cum.% Passing	Wtd Cum. %	Cum.% Passing	Wtd Cum. %	Cum.% Passing	Wtd Cum. %	Cum.% Passing	Wtd Cum. %	Cum.% Passing	Wtd Cum. %	Cum.% Passing	Wtd Cum. %	Combined Gradation Total Bin Cum. % Passing	Lower	Upper	Within Spec's	Restricted Zone Lower	Restricted Zone Upper	Restricted Zone Within Spec's	Individual % Retained	Cumulative % Retained	Sieve Size
3/4"	100.0	43.0	100.0	37.0	100.0	10.0	100.0	10.0															100.0	100.0	100.0	Yes				0.0	0.0	3/4"
1/2"	98.2	42.2	97.7	36.1	100.0	10.0	100.0	10.0															98.4	85.0	99.0	Yes				1.6	1.6	1/2"
3/8"	61.4	26.4	67.4	24.9	100.0	10.0	100.0	10.0															71.3	50.0	75.0	Yes				27.0	28.7	3/8"
No. 4	4.9	2.1	3.2	1.2	99.0	9.9	100.0	10.0															23.2	20.0	32.0	Yes				48.1	76.8	No. 4
No. 8	2.5	1.1	0.8	0.3	86.1	8.6	100.0	10.0															20.0	16.0	28.0	Yes				3.2	80.0	No. 8
No. 16	1.9	0.8	0.7	0.3	60.0	6.0	99.9	10.0															17.1	8.0	28.0	Yes				2.9	82.9	No. 16
No. 30	1.7	0.7	0.5	0.2	54.1	5.4	99.3	9.9															16.3	8.0	28.0	Yes				0.8	83.7	No. 30
No. 50	1.6	0.7	0.4	0.1	24.3	2.4	98.2	9.8															13.1	8.0	28.0	Yes				3.2	86.9	No. 50
No. 200	1.2	0.5	0.3	0.1	2.2	0.2	91.1	9.1															10.0	8.0	12.0	Yes				3.1	90.0	No. 200

(Bold Italic) Not within specifications (Bold Italic) Not within specifications- Restricted Zone (Italic) Not cumulative

Lift Thickness, in:		Binder Substitution?		Binder Originally Specified:	
Asphalt Source:	Heartland PG 70-28		Binder Percent, (%):	6.3	Asphalt Spec. Grav: 1.030
Antistripping Agent:	MWV Evotherm M1		Percent, (%):	0.4	Fiber Content, %: 0.30

Figure C2 SMA-D Mix Design Summary Sheet

AGGREGATE BIN FRACTIONS								"RECYCLED MATERIALS"			
	Bin No.1	Bin No.2	Bin No.3	Bin No.4	Bin No.5	Bin No.6	Bin No.7	Bin No.8	Bin No.9	Bin No.10	
Aggregate Source	Gravel	Gravel		Gravel	Limestone_Dolom			Fractionated RAP			Material Type
Aggregate Pit	Beaver	Beaver		Beaver	CM_Jasmine						Material Source
Aggregate Number	141539	141540		141543	141542						RAS Type
Sample ID	Grade 3	Grade 4	Grade 5	Grade 6	Grit-Man Sand	Field Sand					Sample ID
Hydrated Lime?								6.3			
Individual Bin (%)	10.0	26.0	23.0	8.0	2.0	1.0		30.0			100.0%

Ratio of Recycled to Total Binder, % (based on binder percent (%) entered below in this worksheet): 30.2

Recycled Binder exceeds maximum allowable %

Recycled Asphalt Binder (%)

Sieve Size	Cum.% Passing	Wtd Cum. %	Cum.% Passing	Wtd Cum. %	Cum.% Passing	Wtd Cum. %	Cum.% Passing	Wtd Cum. %	Cum.% Passing	Wtd Cum. %	Cum.% Passing	Wtd Cum. %	Cum.% Passing	Wtd Cum. %	Cum.% Passing	Wtd Cum. %	Cum.% Passing	Wtd Cum. %	Cum.% Passing	Wtd Cum. %	Combined Gradation Total Bin Cum. % Passing	Lower	Upper	Within Spec's	Restricted Zone Lower	Restricted Zone Upper	Restricted Zone Within Spec's	Individual % Retained	Cumulative % Retained	Sieve Size
1"	100.0	10.0	100.0	26.0	100.0	23.0	100.0	8.0	100.0	2.0	100.0	1.0									100.0	100.0	100.0	Yes				0.0	0.0	1"
3/4"	100.0	10.0	100.0	26.0	100.0	23.0	100.0	8.0	100.0	2.0	100.0	1.0									100.0	98.0	100.0	Yes				0.0	0.0	3/4"
1/2"	93.4	9.3	100.0	26.0	100.0	23.0	100.0	8.0	100.0	2.0	100.0	1.0									100.0	90.0	100.0	Yes				0.7	0.7	1/2"
3/8"	21.1	2.1	86.3	22.4	99.4	22.9	100.0	8.0	100.0	2.0	99.8	1.0									97.5	29.3								11.7	12.3	3/8"
No. 4	4.2	0.4	8.1	2.1	42.4	9.8	94.3	7.5	100.0	2.0	99.8	1.0									80.4	24.1								46.7	53.1	No. 4
No. 8	3.1	0.3	3.3	0.9	13.7	3.2	72.7	5.8	91.1	1.8	99.5	1.0									63.2	19.0								31.9	28.0	58.0	Yes	39.1	39.1	Yes	15.0	68.1	No. 8
No. 16	2.8	0.3	2.8	0.7	7.2	1.7	53.5	4.3	66.5	1.3	98.6	1.0									48.6	14.6								23.8	2.0	58.0	Yes	25.6	31.6	Yes	8.1	76.2	No. 16
No. 30	2.7	0.3	2.7	0.7	5.3	1.2	40.0	3.2	50.1	1.0	94.3	0.9									38.2	11.5								18.8	2.0	58.0	Yes	19.1	23.1	Yes	5.0	81.2	No. 30
No. 50	2.5	0.3	2.5	0.7	4.5	1.0	29.2	2.3	38.0	0.8	66.0	0.7									28.4	8.5								14.2	2.0	58.0	Yes	15.5	15.5	Yes	4.6	85.8	No. 50
No. 200	2.5	0.3	2.0	0.5	3.0	0.7	15.6	1.2	24.3	0.5	8.4	0.1									12.4	3.7								7.0	2.0	10.0	Yes				7.2	93.0	No. 200

(Bold Italic) Not within specifications (Bold Italic) Not within specifications- Restricted Zone (Italic) Not cumulative

Lift Thickness, in:		Binder Substitution?		Binder Originally Specified:	PG 70-22
Asphalt Source:	Valero PG 64-22		Binder Percent, (%):	6.3	Asphalt Spec. Grav: 1.033
Antistripping Agent:	None		Percent, (%):		

Figure C3 SP-C Mix Design Summary Sheet

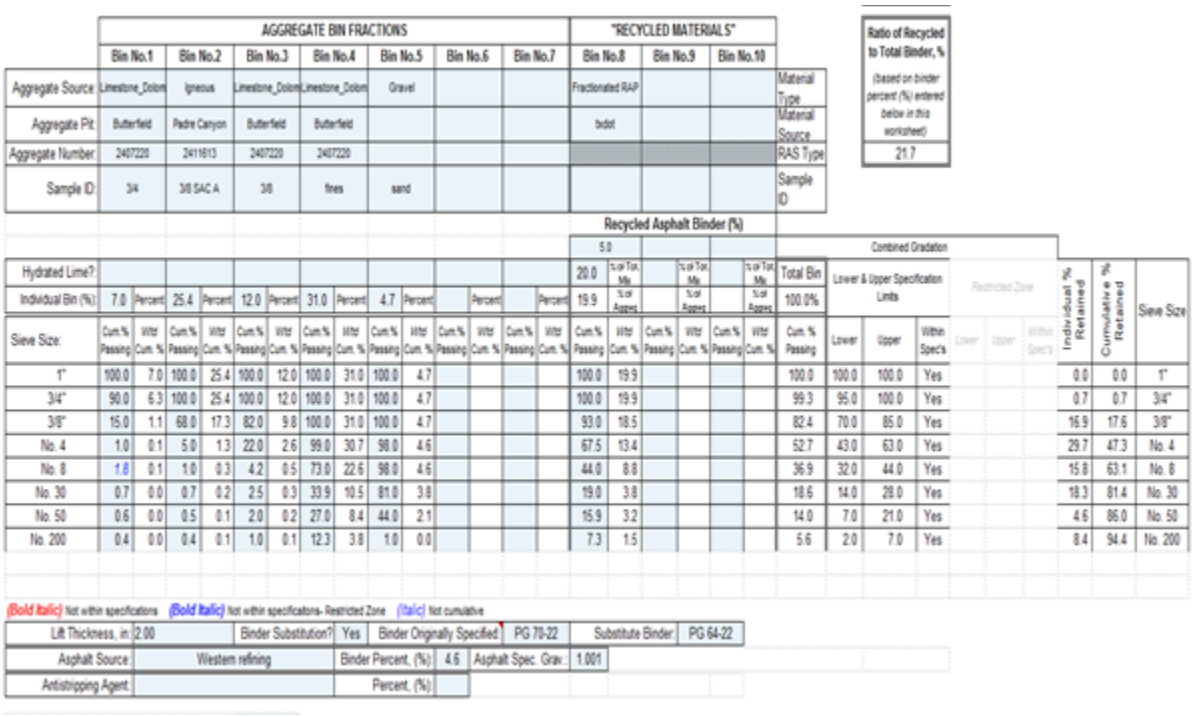

	AGGREGATE BIN FRACTIONS							"RECYCLED MATERIALS"			
	Bin No.1	Bin No.2	Bin No.3	Bin No.4	Bin No.5	Bin No.6	Bin No.7	Bin No.8	Bin No.9	Bin No.10	
Aggregate Source	Limestone_Dolom	Igneous	Limestone_Dolom	Limestone_Dolom	Gravel			Fractionated RAP			Material Type
Aggregate Pit	Butterfield	Padre Canyon	Butterfield	Butterfield				txdot			Material Source
Aggregate Number	2407220	2411613	2407220	2407220							RAS Type
Sample ID	3/4	3/8 SAC A	3/8	fines	sand						Sample ID

Ratio of Recycled to Total Binder, % (based on binder percent (%) entered below in this worksheet): 21.7

Recycled Asphalt Binder (%): 5.0

Combined Gradation

Hydrated Lime?																		20.0	% of Tot. Mix			% of Tot. Mix			% of Tot. Mix	Total Bin	Lower & Upper Specification Limits			Restricted Zone			Individual % Retained	Cumulative % Retained	Sieve Size
Individual Bin (%)	7.0	Percent	25.4	Percent	12.0	Percent	31.0	Percent	4.7	Percent		Percent		Percent				19.9	% of Aggres			% of Aggres			% of Aggres	100.0%									
Sieve Size:	Cum.% Passing	Wtd Cum. %	Cum.% Passing	Wtd Cum. %	Cum.% Passing	Wtd Cum. %	Cum.% Passing	Wtd Cum. %	Cum.% Passing	Wtd Cum. %	Cum.% Passing	Wtd Cum. %	Cum.% Passing	Wtd Cum. %				Cum.% Passing	Wtd Cum. %	Cum.% Passing	Wtd Cum. %	Cum.% Passing	Wtd Cum. %			Cum. % Passing	Lower	Upper	Within Spec's	Lower	Upper	Within Spec's			
1"	100.0	7.0	100.0	25.4	100.0	12.0	100.0	31.0	100.0	4.7								100.0	19.9							100.0	100.0	100.0	Yes				0.0	0.0	1"
3/4"	90.0	6.3	100.0	25.4	100.0	12.0	100.0	31.0	100.0	4.7								100.0	19.9							99.3	95.0	100.0	Yes				0.7	0.7	3/4"
3/8"	15.0	1.1	68.0	17.3	82.0	9.8	100.0	31.0	100.0	4.7								93.0	18.5							82.4	70.0	85.0	Yes				16.9	17.6	3/8"
No. 4	1.0	0.1	5.0	1.3	22.0	2.6	99.0	30.7	98.0	4.6								67.5	13.4							52.7	43.0	63.0	Yes				29.7	47.3	No. 4
No. 8	1.0	0.1	1.0	0.3	4.2	0.5	73.0	22.6	98.0	4.6								44.0	8.8							36.9	32.0	44.0	Yes				15.8	63.1	No. 8
No. 30	0.7	0.0	0.7	0.2	2.5	0.3	33.9	10.5	81.0	3.8								19.0	3.8							18.6	14.0	28.0	Yes				18.3	81.4	No. 30
No. 50	0.6	0.0	0.5	0.1	2.0	0.2	27.0	8.4	44.0	2.1								15.9	3.2							14.0	7.0	21.0	Yes				4.6	86.0	No. 50
No. 200	0.4	0.0	0.4	0.1	1.0	0.1	12.3	3.8	1.0	0.0								7.3	1.5							5.6	2.0	7.0	Yes				8.4	94.4	No. 200

(Bold Italic) Not within specifications (Bold Italic) Not within specifications- Restricted Zone (Italic) Not cumulative

Lift Thickness, in:	2.00	Binder Substitution?	Yes	Binder Originally Specified	PG 70-22	Substitute Binder	PG 64-22
Asphalt Source:	Western refining			Binder Percent, (%)	4.6	Asphalt Spec. Grav.	1.001
Antistripping Agent:				Percent, (%)			

Figure C4 Type-C Mix Design Summary Sheet

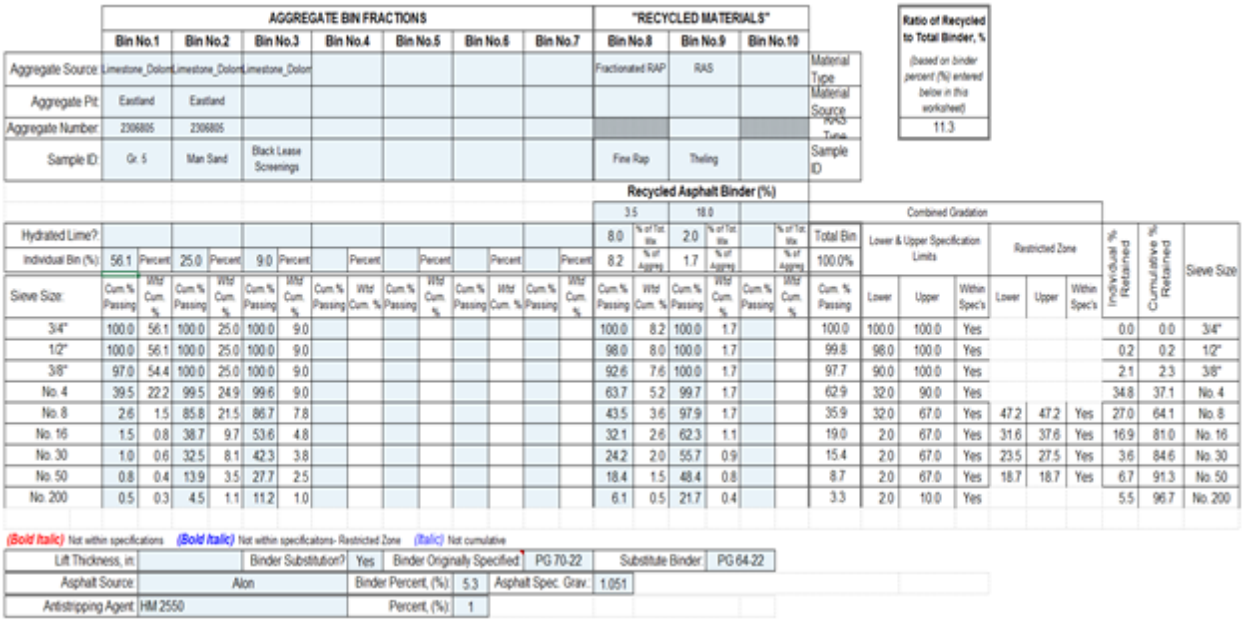

	AGGREGATE BIN FRACTIONS							"RECYCLED MATERIALS"			
	Bin No.1	Bin No.2	Bin No.3	Bin No.4	Bin No.5	Bin No.6	Bin No.7	Bin No.8	Bin No.9	Bin No.10	
Aggregate Source	Limestone_Dolom	Limestone_Dolom	Limestone_Dolom					Fractionated RAP	RAS		Material Type
Aggregate Pit	Eastland	Eastland									Material Source
Aggregate Number	2306805	2306805									RAS Type
Sample ID	Gr. 5	Man Sand	Black Lease Screenings					Fine Rap	Theling		Sample ID

Ratio of Recycled to Total Binder, % (based on binder percent (%) entered below in this worksheet): 11.3

Recycled Asphalt Binder (%): 3.5 | 18.0

Combined Gradation

Hydrated Lime?																		8.0	% of Tot. Mix	2.0	% of Tot. Mix		% of Tot. Mix	Total Bin	Lower & Upper Specification Limits			Restricted Zone			Individual % Retained	Cumulative % Retained	Sieve Size
Individual Bin (%)	56.1	Percent	25.0	Percent	9.0	Percent		Percent		Percent		Percent		Percent				8.2	% of Aggres	1.7	% of Aggres		% of Aggres	100.0%									
Sieve Size:	Cum.% Passing	Wtd Cum. %	Cum.% Passing	Wtd Cum. %	Cum.% Passing	Wtd Cum. %	Cum.% Passing	Wtd Cum. %	Cum.% Passing	Wtd Cum. %	Cum.% Passing	Wtd Cum. %	Cum.% Passing	Wtd Cum. %				Cum.% Passing	Wtd Cum. %	Cum.% Passing	Wtd Cum. %	Cum.% Passing	Wtd Cum. %			Cum. % Passing	Lower	Upper	Within Spec's	Lower	Upper	Within Spec's			
3/4"	100.0	56.1	100.0	25.0	100.0	9.0												100.0	8.2	100.0	1.7			100.0	100.0	100.0	Yes				0.0	0.0	3/4"
1/2"	100.0	56.1	100.0	25.0	100.0	9.0												98.0	8.0	100.0	1.7			99.8	98.0	100.0	Yes				0.2	0.2	1/2"
3/8"	97.0	54.4	100.0	25.0	100.0	9.0												92.6	7.6	100.0	1.7			97.7	90.0	100.0	Yes				2.1	2.3	3/8"
No. 4	39.5	22.2	99.5	24.9	99.6	9.0												63.7	5.2	99.7	1.7			62.9	32.0	90.0	Yes				34.8	37.1	No. 4
No. 8	2.6	1.5	85.8	21.5	86.7	7.8												43.5	3.6	97.9	1.7			35.9	32.0	67.0	Yes	47.2	47.2	Yes	27.0	64.1	No. 8
No. 16	1.5	0.8	38.7	9.7	53.6	4.8												32.1	2.6	62.3	1.1			19.0	2.0	67.0	Yes	31.6	37.6	Yes	16.9	81.0	No. 16
No. 30	1.0	0.6	32.5	8.1	42.3	3.8												24.2	2.0	55.7	0.9			15.4	2.0	67.0	Yes	23.5	27.5	Yes	3.6	84.6	No. 30
No. 50	0.8	0.4	13.9	3.5	27.7	2.5												18.4	1.5	48.4	0.8			8.7	2.0	67.0	Yes	18.7	18.7	Yes	6.7	91.3	No. 50
No. 200	0.5	0.3	4.5	1.1	11.2	1.0												6.1	0.5	21.7	0.4			3.3	2.0	10.0	Yes				5.5	96.7	No. 200

(Bold Italic) Not within specifications (Bold Italic) Not within specifications- Restricted Zone (Italic) Not cumulative

Lift Thickness, in:		Binder Substitution?	Yes	Binder Originally Specified	PG 70-22	Substitute Binder	PG 64-22
Asphalt Source:	Alon			Binder Percent, (%)	5.3	Asphalt Spec. Grav.	1.051
Antistripping Agent:	HM 2550			Percent, (%)	1		

Figure C5 SP-D 1 Mix Design Summary Sheet

TEXAS DEPARTMENT OF TRANSPORTATION

HMACP MIXTURE DESIGN : SUMMARY SHEET

File Version: 08/21/13 13:35:17

SAMPLE ID:	D Jeb 70-22 (64-22) RR	SAMPLE DATE:	7-11-14
LOT NUMBER:	Mix Design	LETTING DATE:	
SAMPLE STATUS:		CONTROLLING CSJ:	
COUNTY:		SPEC YEAR:	2004
SAMPLED BY:	Brian E. Clough, SET	SPEC ITEM:	3224 / 3268
SAMPLE LOCATION:		SPECIAL PROVISION:	
MATERIAL CODE:		MIX TYPE:	SS3268_D_Fine_Surface
MATERIAL NAME:	D Jebro 64-22 for 70-22 RAP/RAS 2014		
PRODUCER:	Vulcan Materials - Brownwood		
AREA ENGINEER:		PROJECT MANAGER:	

COURSE\LIFT:	Surface	STATION:		DIST. FROM CL:		CONTRACTOR DESIGN # :	DJEB6422RR2014

Target Density, %:	96.5
Number of Gyrations:	

Note: This mix design requires an asphalt content of at least 4.0% to meet the Maximum Ratio of Recycled to Total Binder requirement.

TEST SPECIMENS								Mixture Evaluation @ Optimum Asphalt Content			
									Hamburg Wheel Tracking Test		
Asphalt Content (%)	Binder Ratio (%)	Specific Gravity Of Specimen (Ga)	Maximum Specific Gravity (Gr)	Effective Gravity (Ge)	Theo. Max. Specific Gravity (Gt)	Density from Gt (Percent)	VMA (Percent)	Indirect Tensile Strength (psi)	Number of cycles	Rut depth (mm)	Overlay Tester Min. Number of Cycles
4.0	20.0	2.371	2.544	2.711	2.548	93.0	16.2	174.3	15,553	12.5	
4.5	17.8	2.401	2.526	2.712	2.529	94.9	15.6				
5.0	16.0	2.415	2.517	2.725	2.510	96.2	15.5				
5.5	14.5	2.435	2.496	2.722	2.491	97.8	15.3				
6.0	13.3	2.456	2.466	2.708	2.472	99.4	15.0				

Effective Specific Gravity:	2.716
Optimum Asphalt Content :	5.1
Binder Ratio @ OAC:	15.7
VMA @ Optimum AC:	15.5

Interpolated Values	
Specific Gravity (Ga):	2.419
Max. Specific Gravity (Gr):	2.513
Theo. Max. Specific Gravity (Gt):	2.506

Estimated Percent of Stripping, %:	0

Mixing Temp,°F:	300
Molding Temp,°F:	275

Remarks:

Additional Mixture Evaluation			
Test	AC%	Number of cycles	Rut depth (mm)

Figure C6 Type-D Mix Design Summary Sheet

Results from Rigorous Evaluation of Proposed OT Test Method

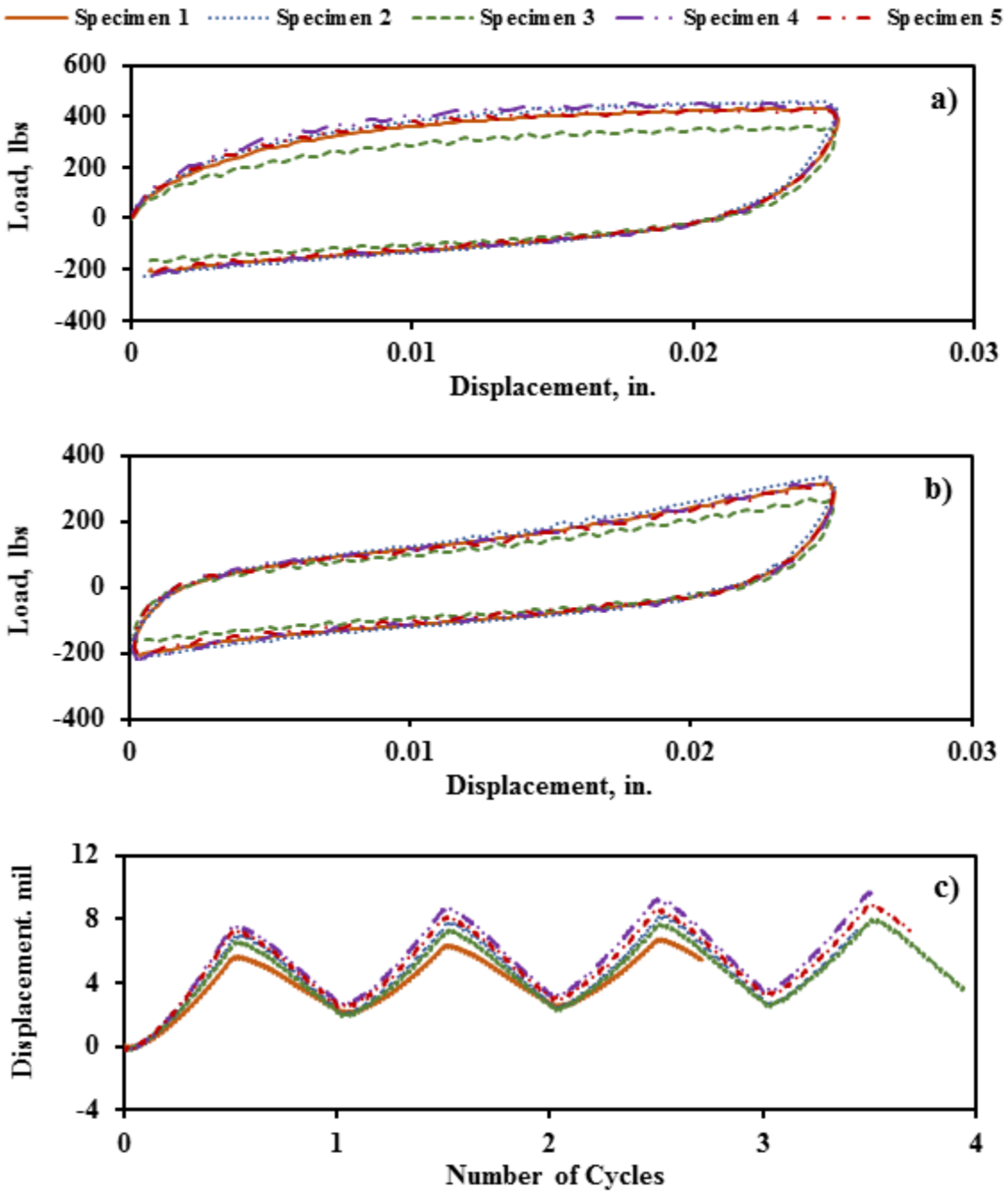

Figure C7 Results for SMA-D Mix: a) First Cycle Hysteresis Loop, b) Second Cycle Hysteresis Loop, and c) Displacement of Top LVDT

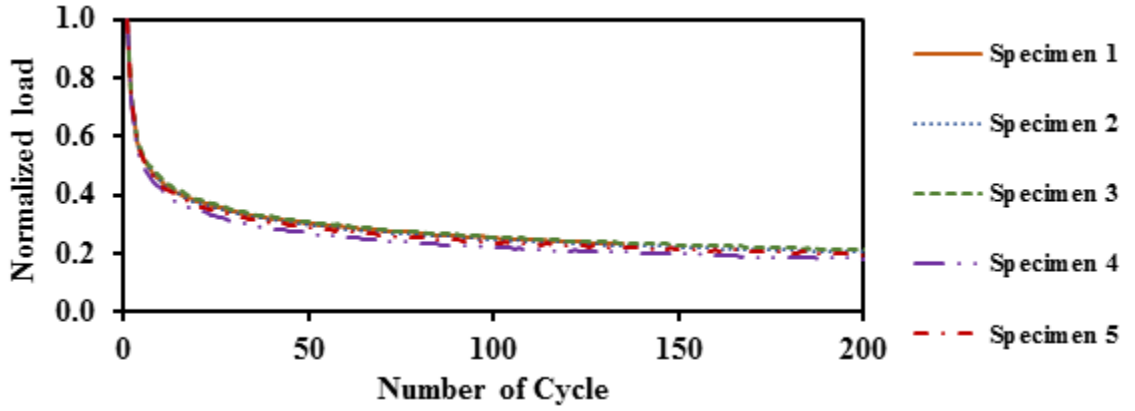

Figure C8 Normalized Load Reduction Curves for SMA-D Mix

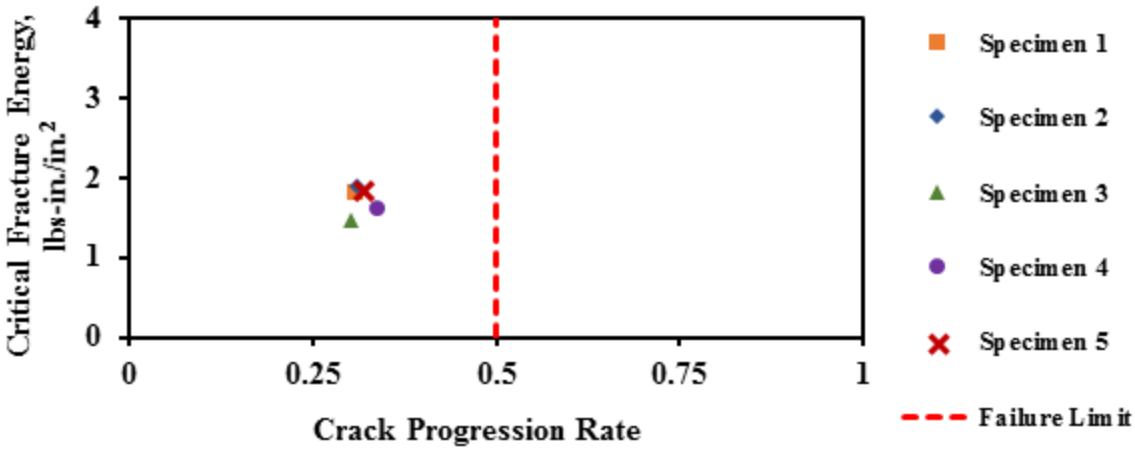

Figure C9 Performance of SMA-D on Design Interaction Plot

Table C3 Summary of Results for SMA-D Mix

Specimen	Air Voids, %	Max Load, lbs	Work of Fracture, in-lbs	Critical Fracture Energy, in.-lbs/in.^{2}	Crack Progression Rate	R^2	Number of Cycles to Failure
1	6.9	429	8.2	1.8	0.31	1.00	1000
2	7.7	457	8.6	1.9	0.31	1.00	1000
3	6.6	362	6.7	1.5	0.30	1.00	1000
4	6.4	452	7.3	1.6	0.34	1.00	1000
5	6.2	428	8.3	1.8	0.32	1.00	1000
Average	6.8	426	7.8	1.7	0.32	1.00	1000
Std Dev	0.5	34	0.7	0.2	0.01	0.00	0
COV	**8%**	**8%**	**9%**	**9%**	**4%**	**NA**	**NA**

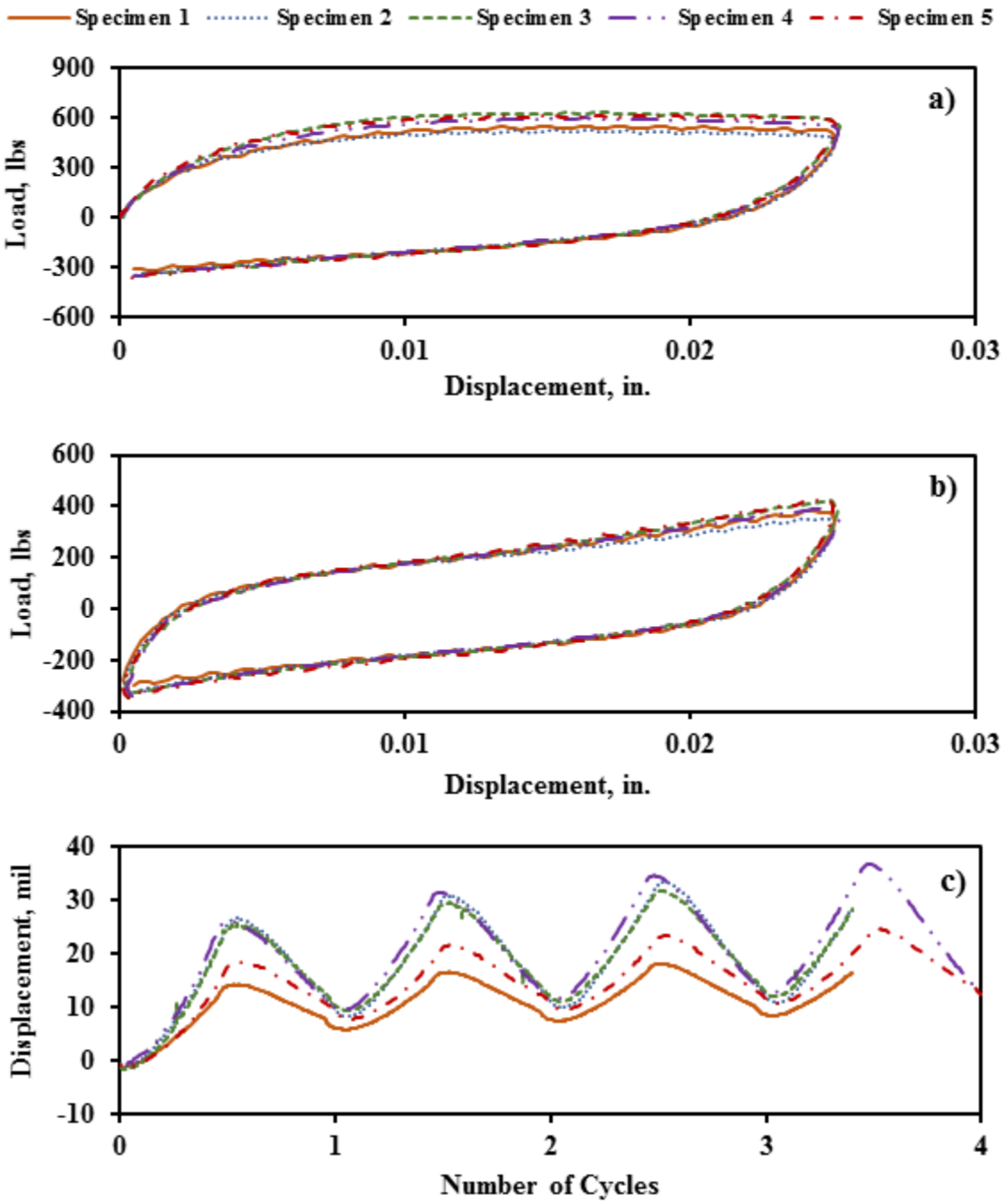

Figure C10 Results for SP-C Mix: a) First Cycle Hysteresis Loop, b) Second Cycle Hysteresis Loop, and c) Displacement of Top LVDT

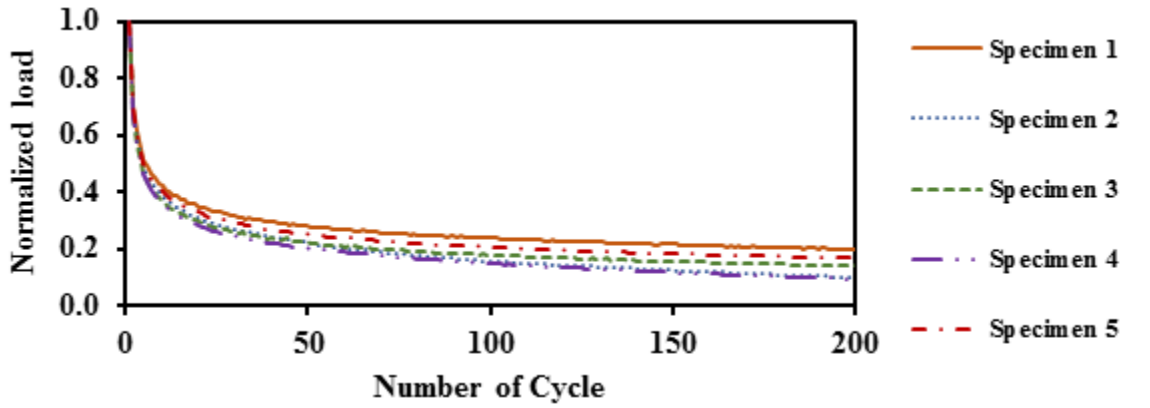

Figure C11 Normalized Load Reduction Curves for SP-C Mix

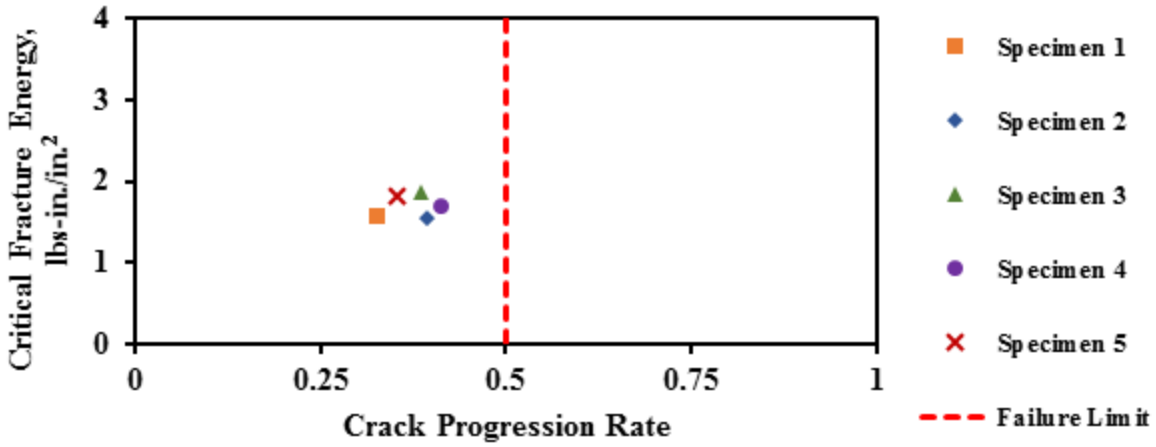

Figure C12 Performance of SP-C on Design Interaction Plot

Table C4 Summary of Results for SP-C Mix

Specimen	Air Voids, %	Max Load, lbs	Work of Fracture, in-lbs	Critical Fracture Energy, in.-lbs/in.^{2}	Crack Progression Rate	R^2	Number of Cycles to Failure
1	7.0	550	7.1	1.6	0.33	1.00	1000
2	6.9	523	7.0	1.6	0.39	1.00	253
3	6.8	628	8.4	1.9	0.39	1.00	714
4	7.4	595	7.7	1.7	0.41	1.00	298
5	6.6	615	8.2	1.8	0.35	1.00	1000
Average	6.9	582	7.7	1.7	0.37	1.00	653
Std Dev	0.3	40	0.6	0.1	0.03	0.00	326
COV	**4%**	**7%**	**8%**	**8%**	**8%**	**0%**	**50%**

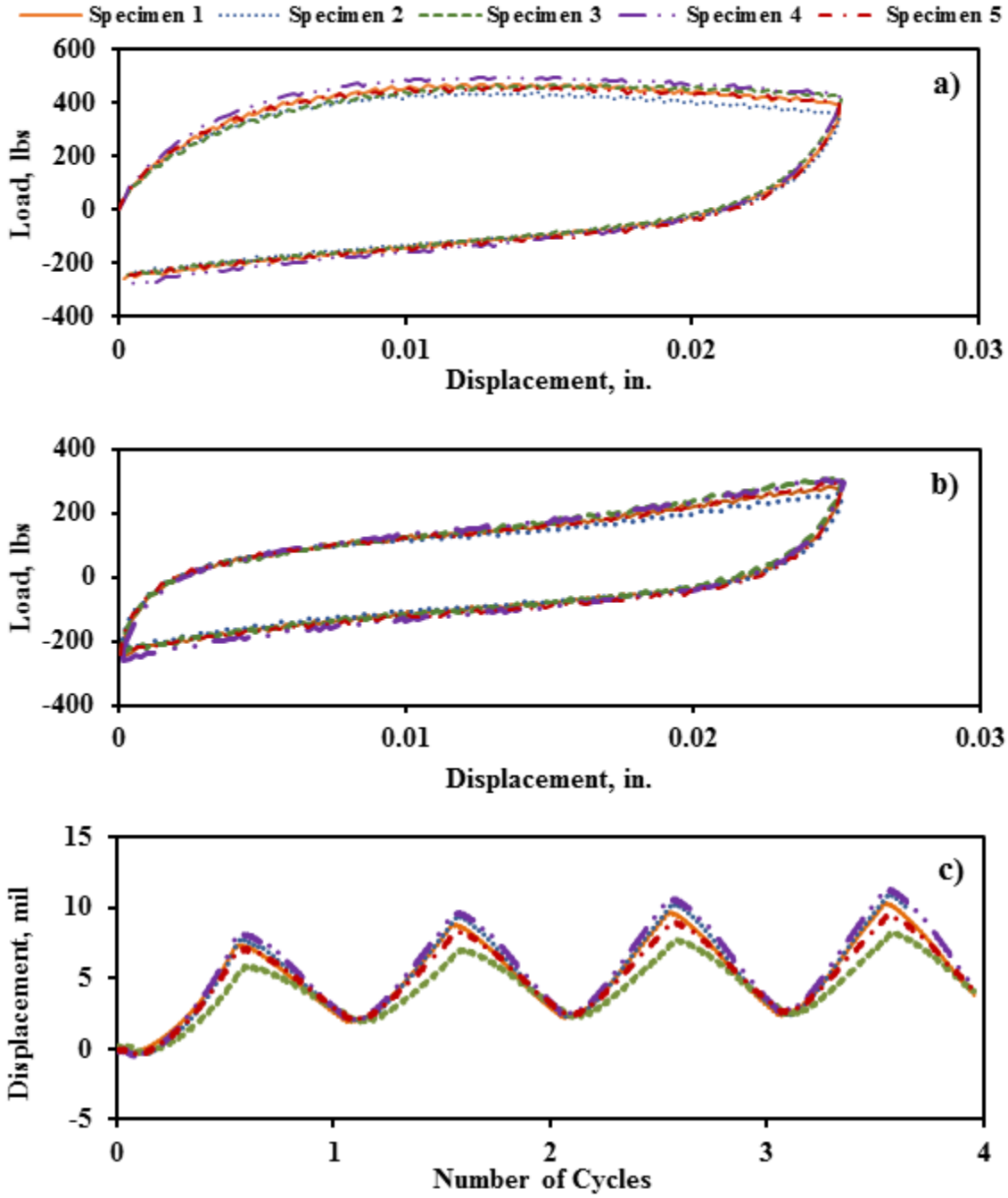

Figure C13 Results for Type-C Mix: a) First Cycle Hysteresis Loop, b) Second Cycle Hysteresis Loop, and c) Displacement of Top LVDT

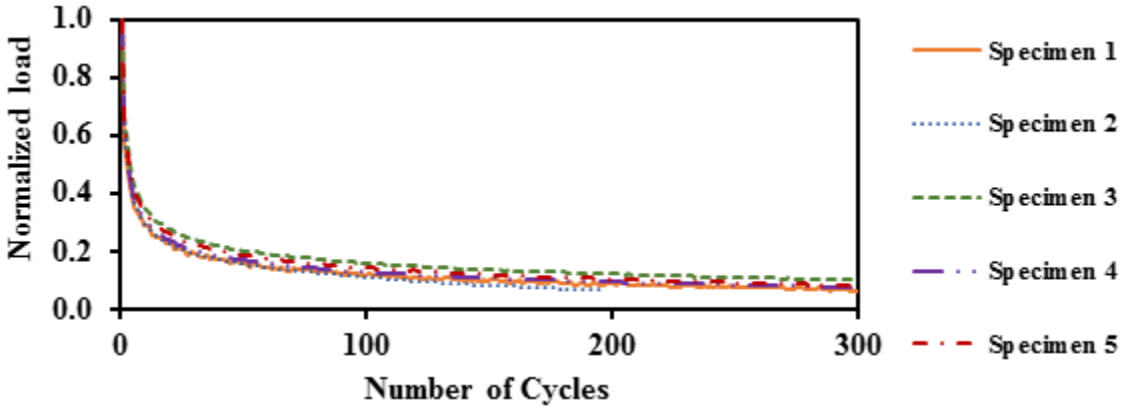

Figure C14 Normalized Load Reduction Curves for Type-C Mix

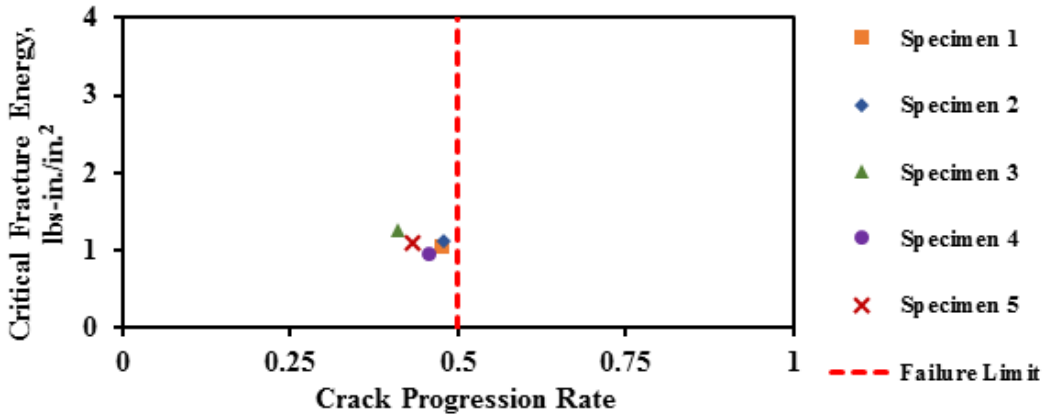

Figure C15 Performance of Type-C on Design Interaction Plot

Table C5 Summary of Results for Type-C Mix

Specimen	Air Voids, %	Max Load, lbs	Work of Fracture, in-lbs	Critical Fracture Energy, in.-lbs/in.^{2}	Crack Progression Rate	R^2	Number of Cycles to Failure
1	7.6	470	4.8	1.1	0.47	1.00	312
2	7.9	439	5.1	1.1	0.48	1.00	198
3	7.4	469	5.7	1.3	0.41	1.00	483
4	7.6	497	4.3	1.0	0.46	1.00	370
5	7.2	461	4.9	1.1	0.43	1.00	389
Average	7.5	467	5.0	1.1	0.45	1.00	350
Std Dev	0.2	19	0.5	0.1	0.03	0.00	94
COV	**3%**	**4%**	**9%**	**9%**	**6%**	**NA**	**27%**

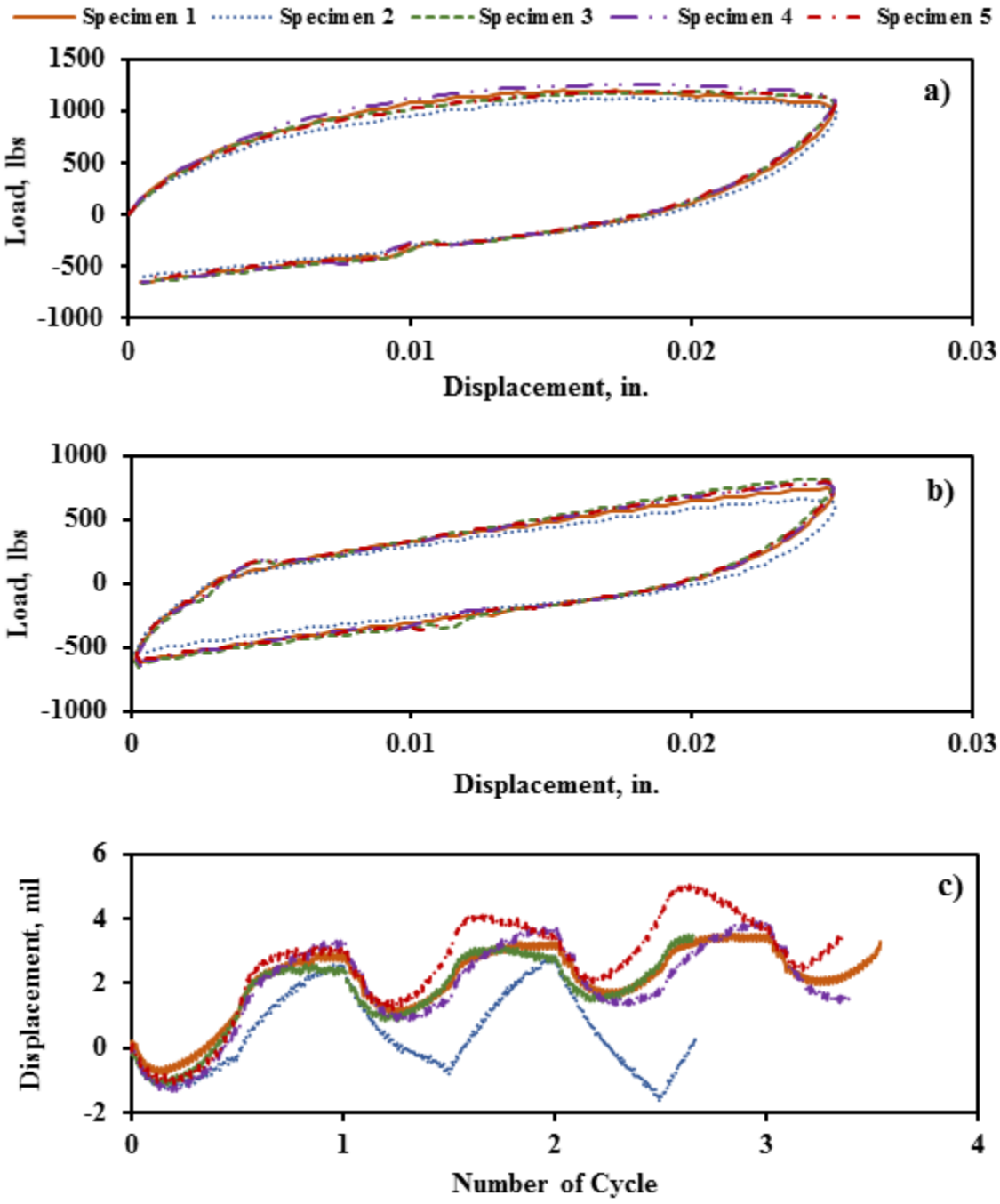

Figure C16 Results for SP-D 1 Mix: a) First Cycle Hysteresis Loop, b) Second Cycle Hysteresis Loop, and c) Displacement of Top LVDT

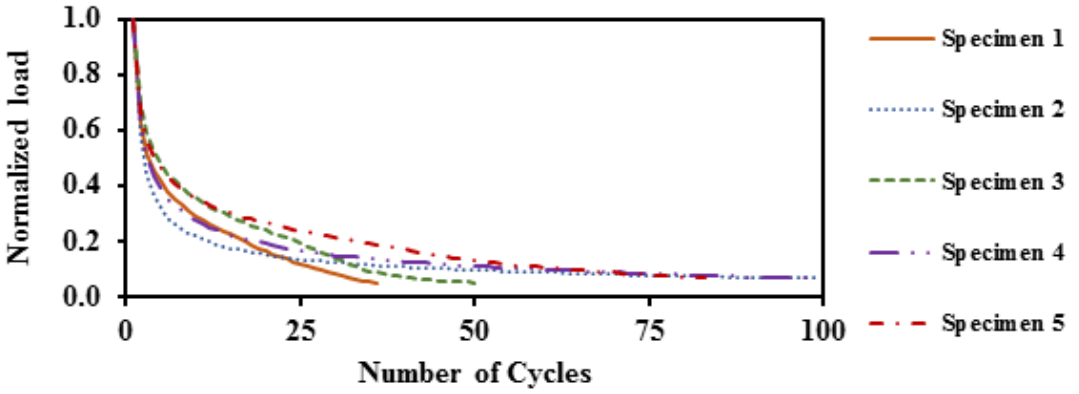

Figure C17 Normalized Load Reduction Curves for SP-D 1 Mix

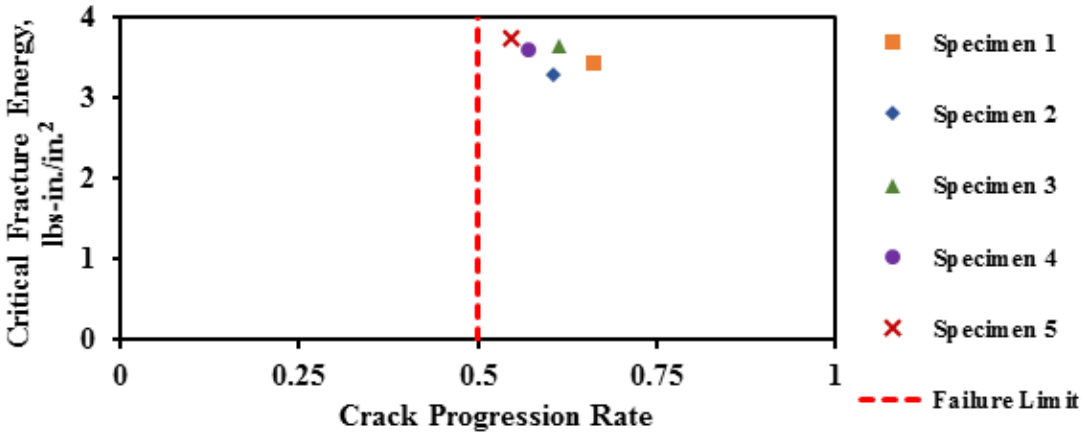

Figure C18 Performance of SP-D 1 on Design Interaction Plot

Table C6 Summary of Results for SP-D 1 Mix

Specimen	Air Voids, %	Max Load, lbs	Work of Fracture, in-lbs	Critical Fracture Energy, in.-lbs/in.2	Crack Progression Rate	R^2	Number of Cycles to Failure
1	7.9	1193	15.5	3.4	0.66	0.98	36
2	7.4	1125	14.8	3.3	0.60	1.00	99
3	7.6	1186	16.4	3.7	0.62	0.97	50
4	7.4	1258	16.2	3.6	0.57	1.00	99
5	7.5	1190	16.9	3.7	0.55	0.99	83
Average	7.6	1190	16.0	3.5	0.60	0.99	73
Std Dev	0.2	42	0.7	0.2	0.04	0.01	26
COV	**2%**	**4%**	**5%**	**5%**	**7%**	**1%**	**35%**

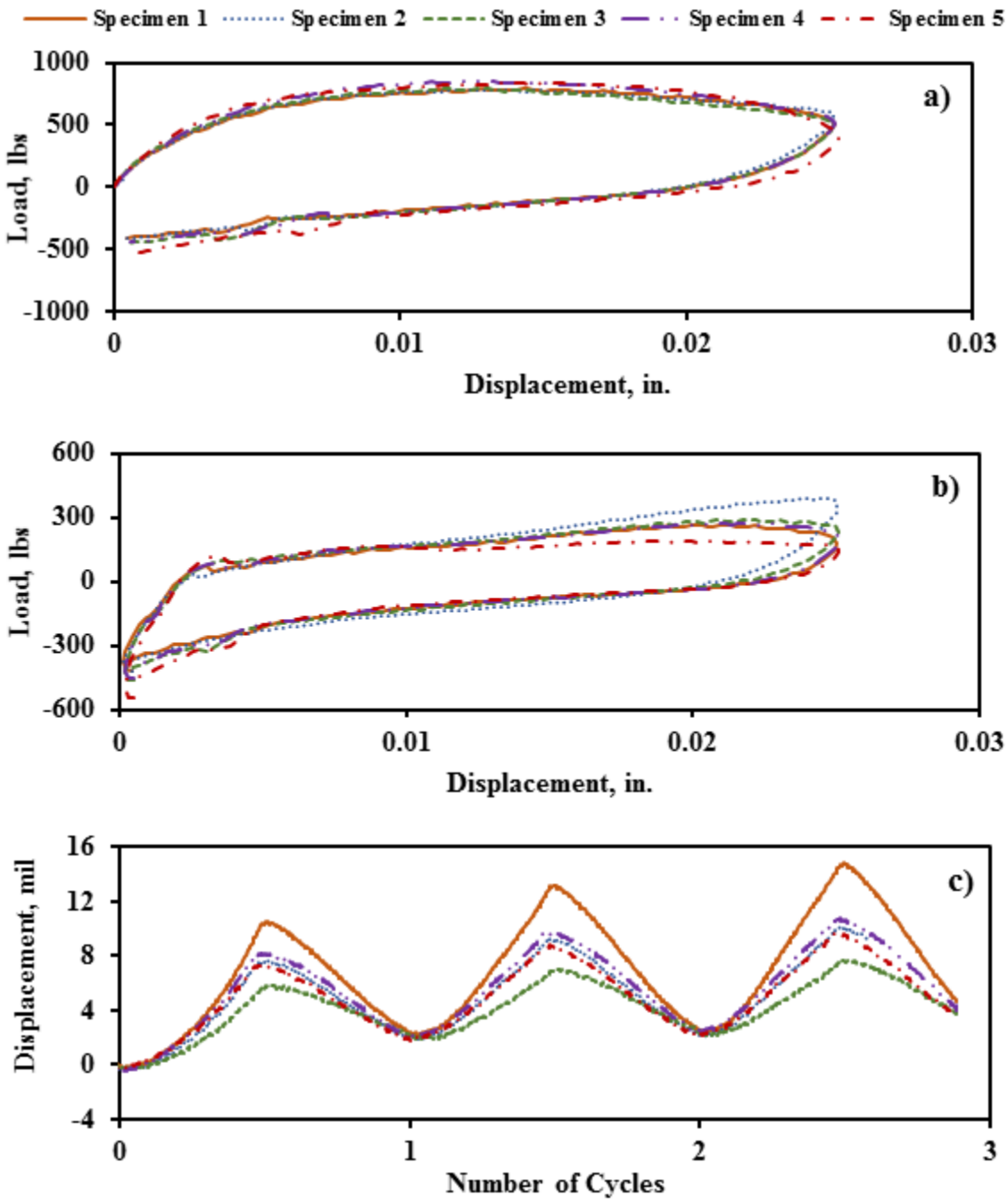

Figure C19 Results for SP-D 2 Mix: a) First Cycle Hysteresis Loop, b) Second Cycle Hysteresis Loop, and c) Displacement of Top LVDT

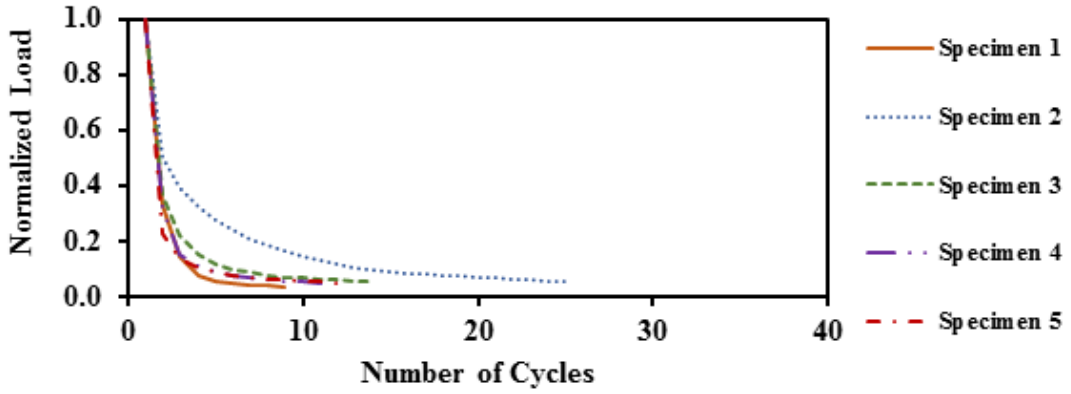

Figure C20 Normalized Load Reduction Curves for SP-D 2 Mix

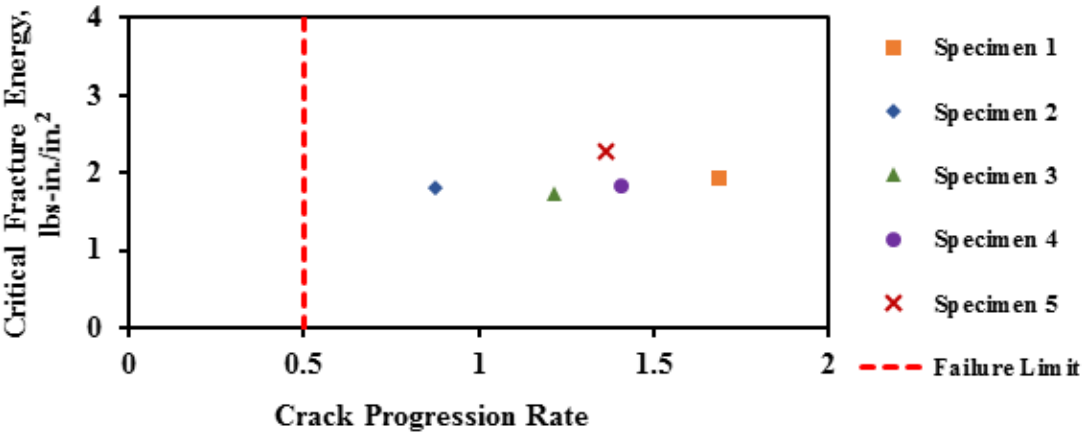

Figure C21 Performance of SP-D 2 on Design Interaction Plot

Table C7 Summary of Results for SP-D 2 Mix

Specimen	Air Voids, %	Max Load, lbs	Work of Fracture, in-lbs	Critical Fracture Energy, in.-lbs/in.^{2}	Crack Progression Rate	R^2	Number of Cycles to Failure
1	7.2	789	8.7	1.9	1.68	1.00	25
2	7.1	780	8.2	1.8	0.88	1.00	9
3	7.3	789	7.8	1.7	1.21	1.00	14
4	7.3	849	8.2	1.8	1.41	0.99	11
5	7.3	835	10.3	2.3	1.36	0.98	12
Average	7.2	809	8.6	1.9	1.31	0.99	14
Std Dev	0.1	28	0.9	0.2	0.26	0.01	6
COV	**1%**	**3%**	**10%**	**10%**	**20%**	**1%**	**40%**

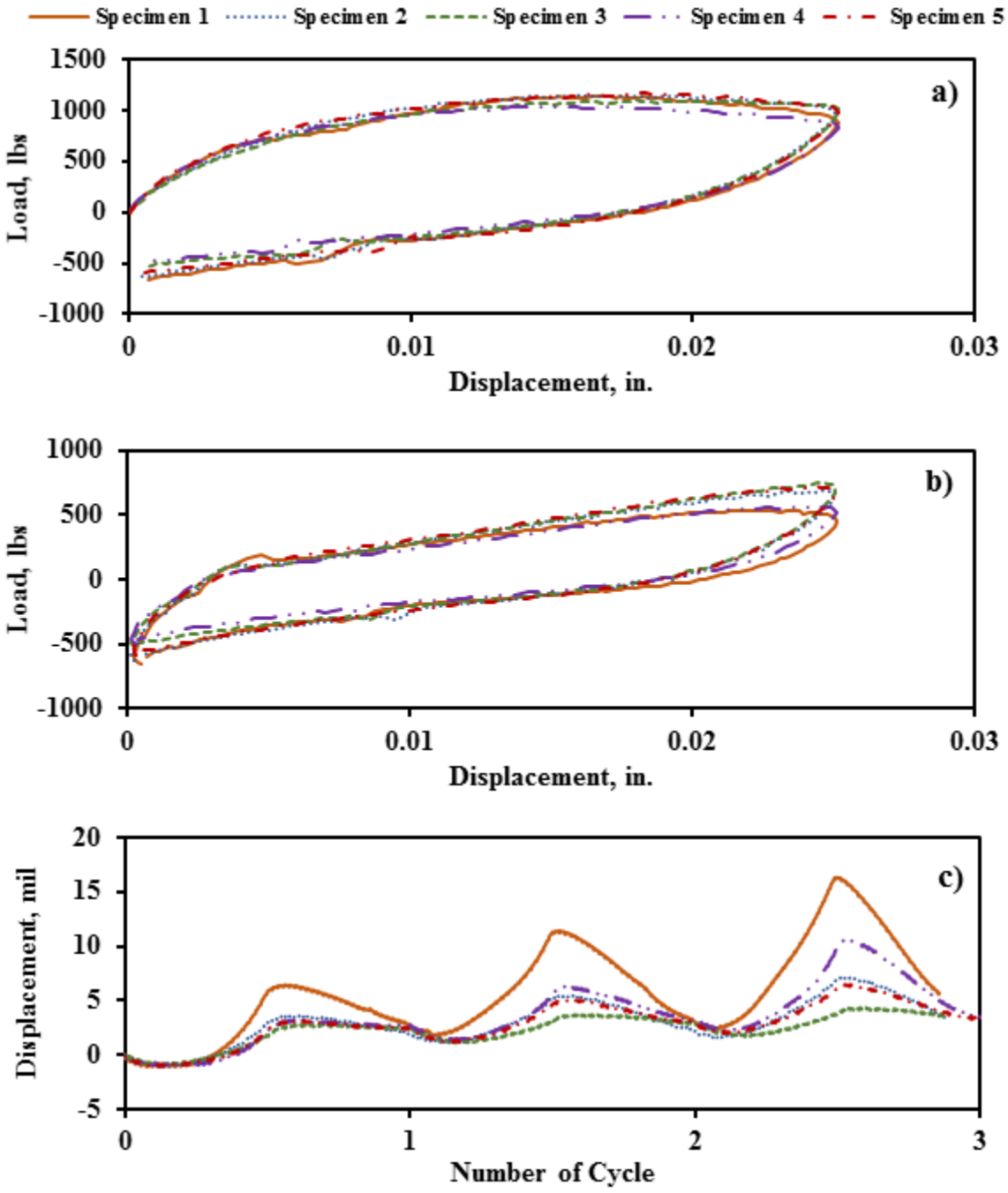

Figure C22 Results for Type-D Mix: a) First Cycle Hysteresis Loop, b) Second Cycle Hysteresis Loop, and c) Displacement of Top LVDT

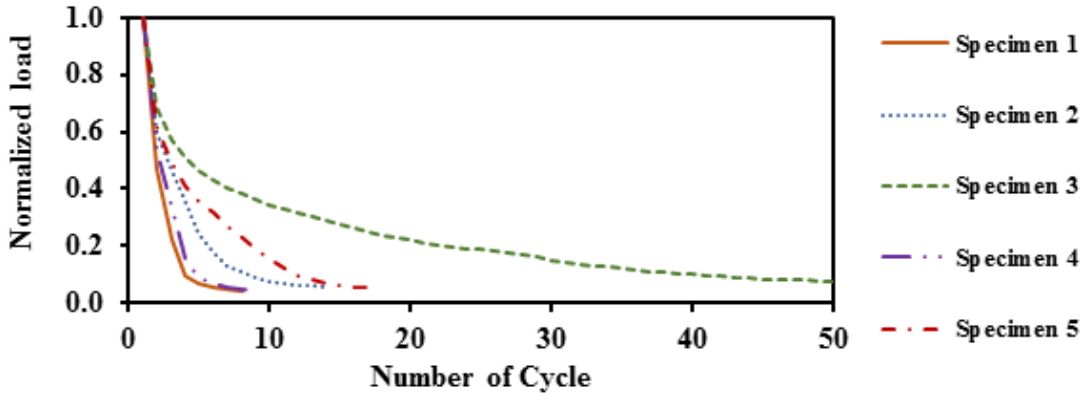

Figure C23 Normalized Load Reduction Curves for Type-D Mix

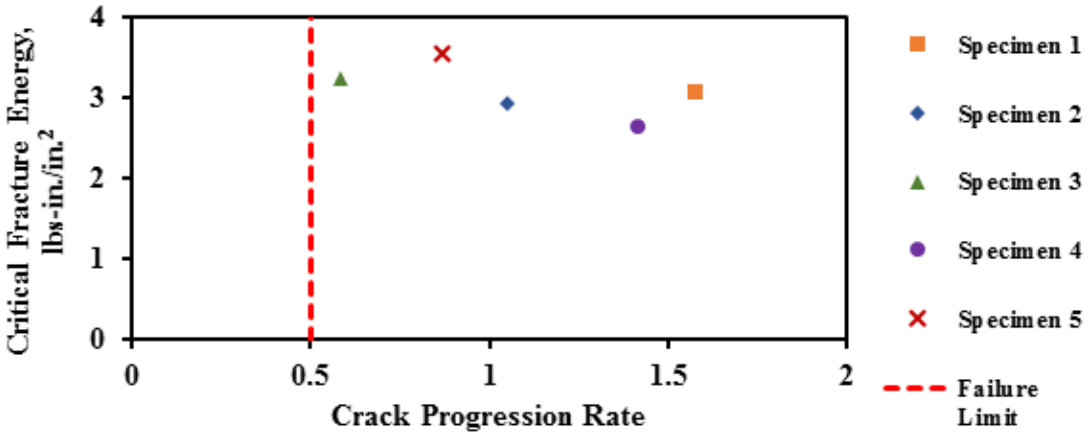

Figure C24 Performance of Type-D on Design Interaction Plot

Table C8 Summary of Results for SP-C Mix

Specimen	Air Voids, %	Max Load, lbs	Work of Fracture, in-lbs	Critical Fracture Energy, in.-lbs/in.^{2}	Crack Progression Rate	R^2	Number of Cycles to Failure
1	7.6	1141	14	3.1	1.58	0.99	8
2	7.9	1145	13	2.9	1.05	0.99	14
3	7.4	1091	15	3.3	0.58	0.99	55
4	7.6	1036	12	2.6	1.42	0.99	9
5	7.2	1168	16	3.5	0.87	0.97	17
Average	7.5	1116	14	3.1	1.10	0.99	21
Std Dev	0.2	47	1	0.3	0.36	0.01	18
COV	**3%**	**4%**	**10%**	**10%**	**33%**	**1%**	**85%**

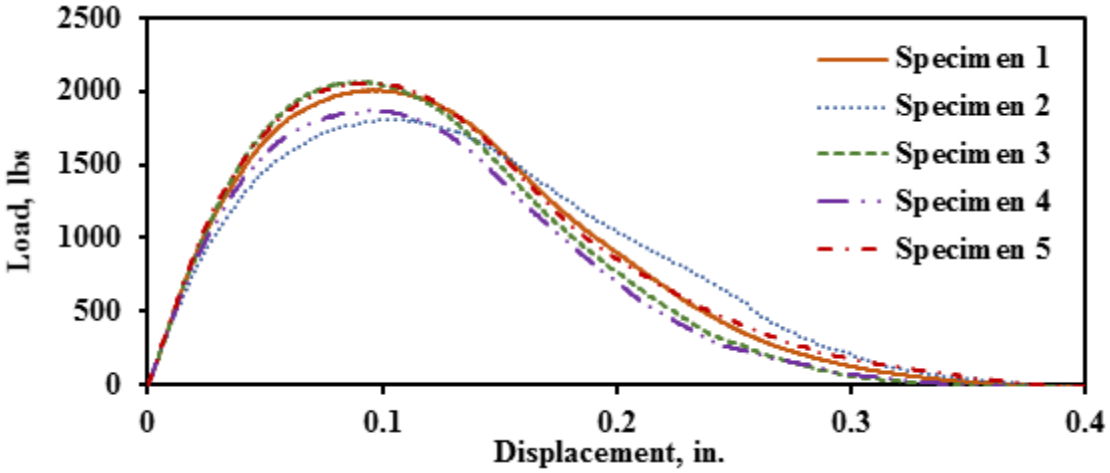

Figure C25 IDT Load-displacement Response Curves for TOM Mix

Table C9 Summary of IDT Results for TOM Mix

Specimen	Air Voids, %	Maximum Load, lbs	Tensile Modulus, psi	Tensile Strength, psi	Strain at Peak Load, %
1	6.7	2007	14339	159	2.3
2	6.8	2061	13667	163	2.2
3	7.0	1867	13479	148	2.2
4	7.2	2056	14317	163	2.3
5	7.1	2045	12977	162	2.5
Average	7.0	2007	13756	159	2.3
Std Dev	0.2	81	580	6	0.1
COV	**3%**	**4%**	**4%**	**4%**	**5%**

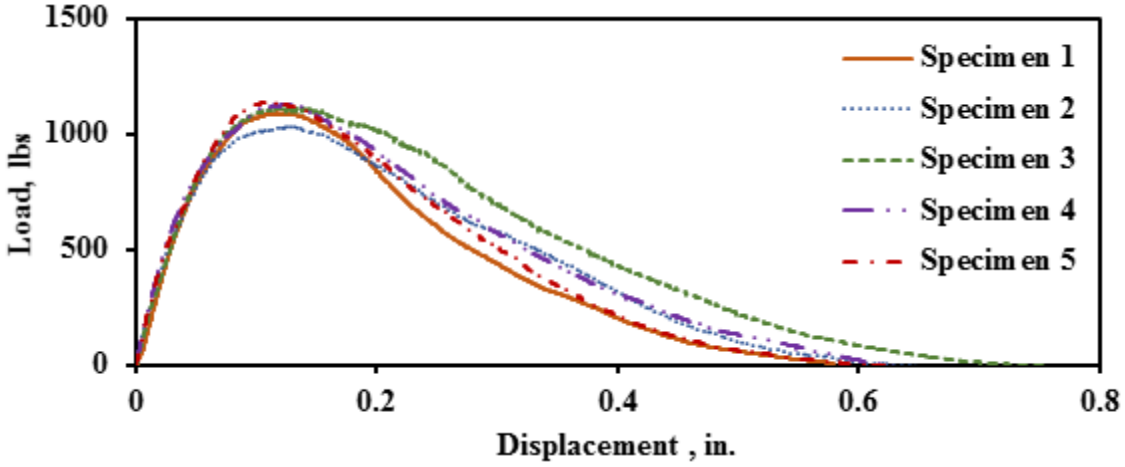

Figure C26 IDT Load-displacement Response Curves for SMA-D Mix

Table C10 Summary of IDT Results for SMA-D Mix

Specimen	Air Voids, %	Maximum Load, lbs	Tensile Modulus, psi	Tensile Strength, psi	Strain at Peak Load, %
1	7.5	1088	5963	86	2.9
2	7.0	1075	4810	85	3.6
3	7.2	1110	5361	88	3.0
4	6.8	1128	6074	89	3.0
5	7.7	1138	6229	90	2.7
Average	7.2	1108	5687	88	3.0
Std Dev	0.4	26	590	2	0.3
COV	**5%**	**2%**	**10%**	**2%**	**11%**

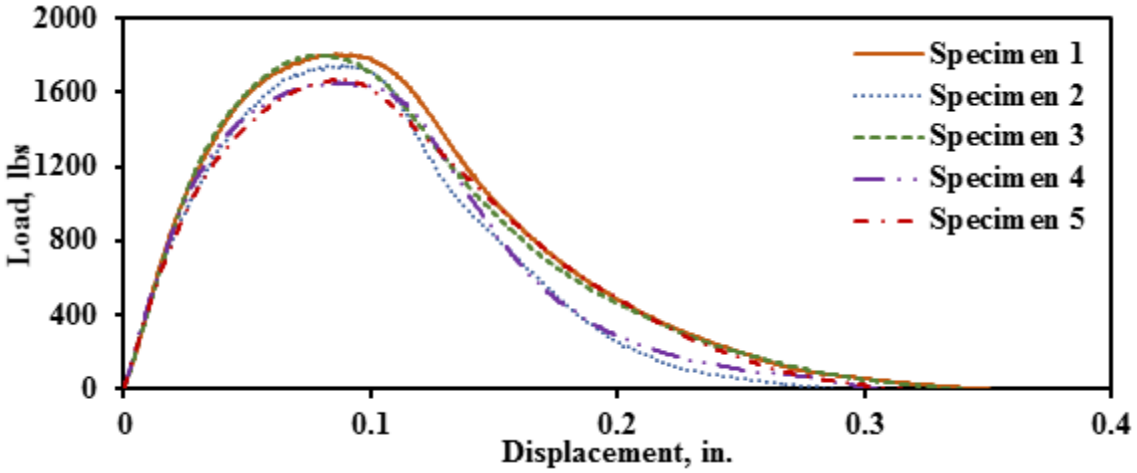

Figure C27 IDT Load-displacement Response Curves for Type-C Mix

Table C11 Summary of IDT Results for Type-C Mix

Specimen	Air Voids, %	Maximum Load, lbs	Tensile Modulus, psi	Tensile Strength, psi	Strain at Peak Load, %
1	6.5	1806	14540	143	2.1
2	6.8	1746	13947	138	2.1
3	6.9	1803	14018	142	1.8
4	7.0	1655	14190	130	2.1
5	6.6	1672	13084	132	2.0
Average	6.8	1736	13956	137	2.0
Std Dev	0.2	71	539	6	0.1
COV	**3%**	**4%**	**4%**	**4%**	**5%**

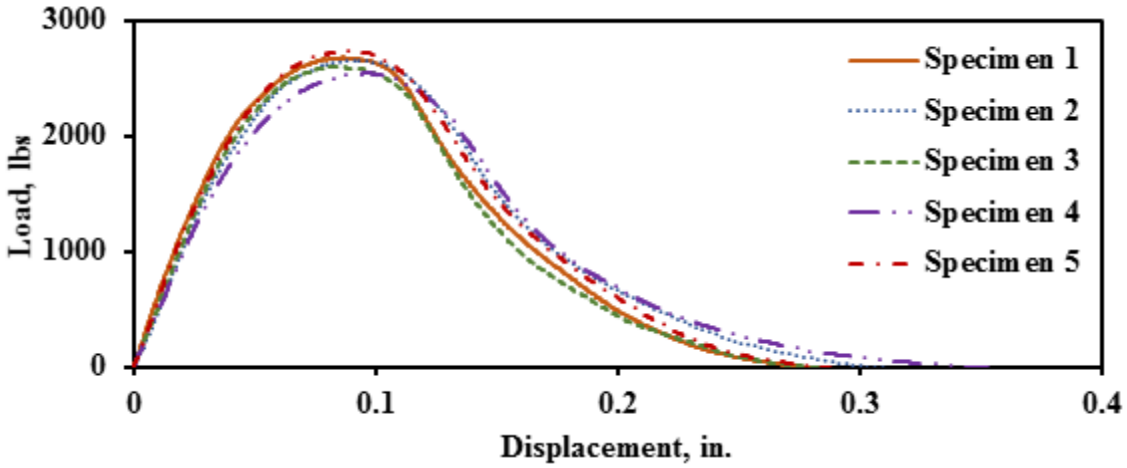

Figure C28 IDT Load-displacement Response Curves for SP-D 1 Mix

Table C12 Summary of IDT Results for SP-D 1 Mix

Specimen	Air Voids, %	Maximum Load, lbs	Tensile Modulus, psi	Tensile Strength, psi	Strain at Peak Load, %
1	7.7	2674	18433	212	2.0
2	6.7	2657	16369	211	2.2
3	6.8	2594	16943	205	2.0
4	7.3	2542	14989	201	2.3
5	6.7	2738	17595	217	2.1
Average	7.0	2641	16866	209	2.1
Std Dev	0.4	75	1300	6	0.1
COV	**6%**	**3%**	**8%**	**3%**	**6%**

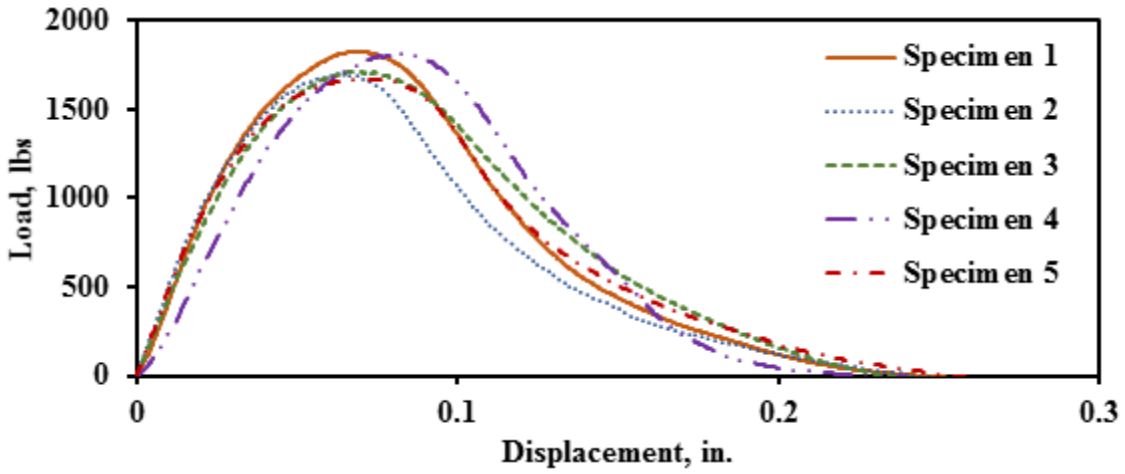

Figure C29 IDT Load-displacement Response Curves for SP-D 2 Mix

Table C13 Summary of IDT Results for SP-D 2 Mix

Specimen	Air Voids, %	Maximum Load, lbs	Tensile Modulus, psi	Tensile Strength, psi	Strain at Peak Load, %
1	7.4	1825	14913	144	1.6
2	7.8	1698	15402	134	1.5
3	7.2	1712	13249	135	1.6
4	7.4	1809	10704	144	2.0
5	7.0	1671	13898	132	1.7
Average	7.4	1743	13633	138	1.7
Std Dev	0.3	69	1842	6	0.2
COV	**4%**	**4%**	**14%**	**4%**	**11%**

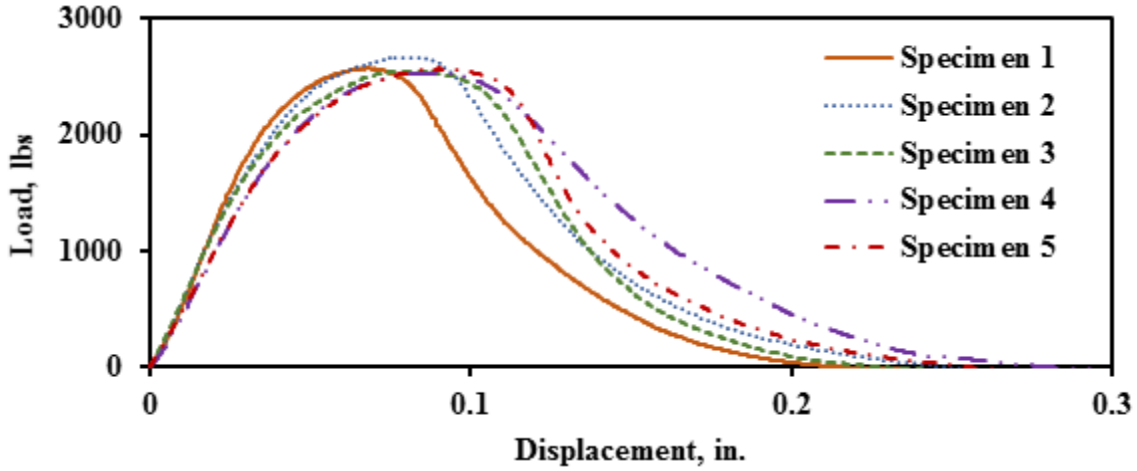

Figure C30 IDT Load-displacement Response Curves for Type-D Mix

Table C14 Summary of IDT Results for Type-D Mix

Specimen	Air Voids, %	Maximum Load, lbs	Tensile Modulus, psi	Tensile Strength, psi	Strain at Peak Load, %
1	6.5	2572	20716	204	1.5
2	6.0	2670	19505	211	1.9
3	6.7	2548	18850	202	2.0
4	6.5	2535	16251	201	2.1
5	6.0	2573	15946	204	2.2
Average	6.3	2580	18253	204	1.9
Std Dev	0.3	53	2081	4	0.2
COV	**5%**	**2%**	**11%**	**2%**	**13%**

Appendix D: Information and Conditions of Field Pavement Sections

Figure D1 Field Core from Section 1

Figure D2 Field Core from Section 2

Figure D3 Field Core from Section 3

Figure D4 Field Core from Section 4

Figure D5 Field Core from Section 5

Figure D6 Field Core from Section 6

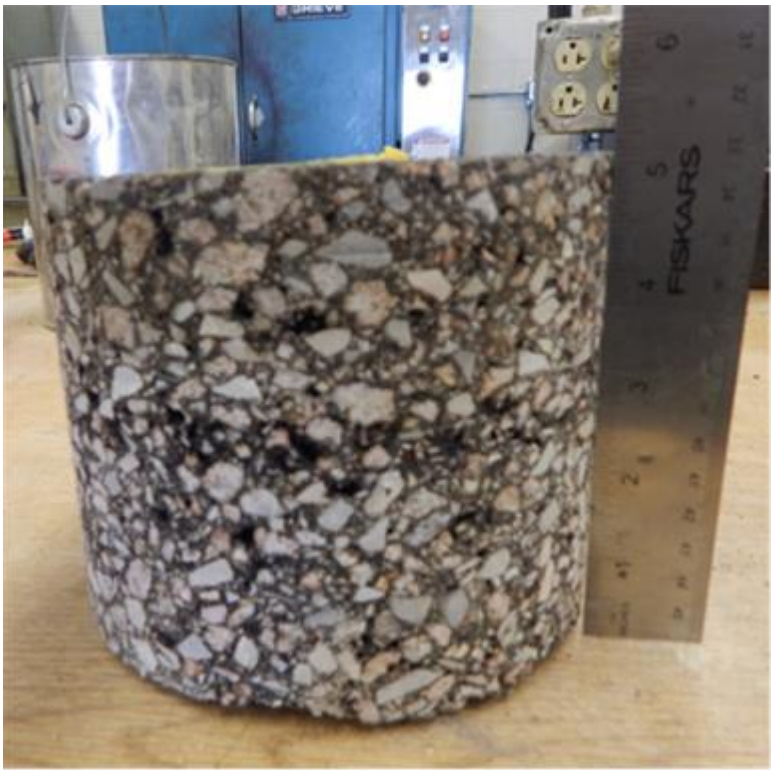

Figure D7 Field Core from Section 7

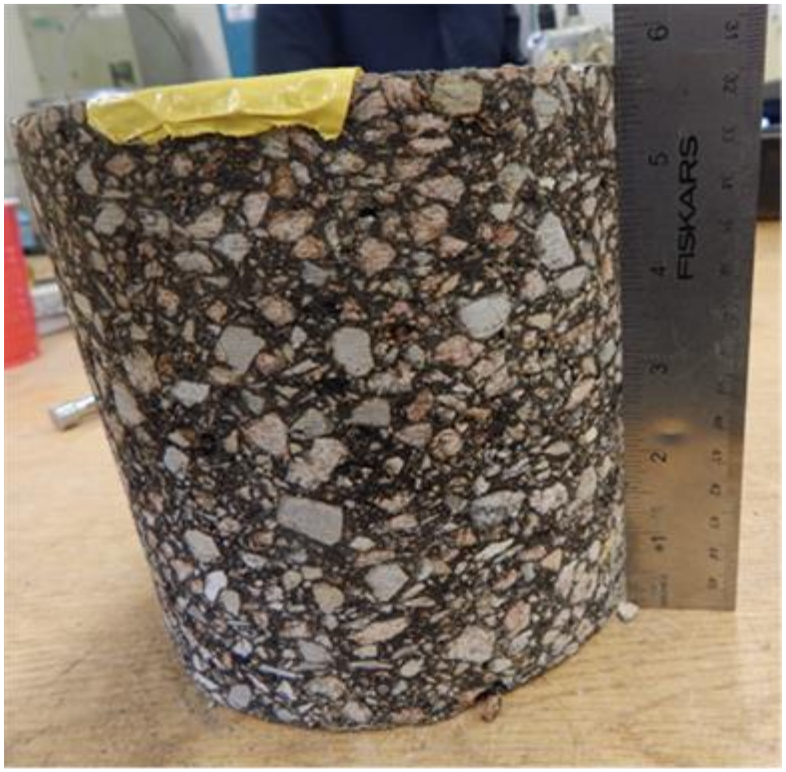

Figure D8 Field Core from Section 8

Figure D9 Field Core from Section 9

Figure D10 Field Core from Section 10

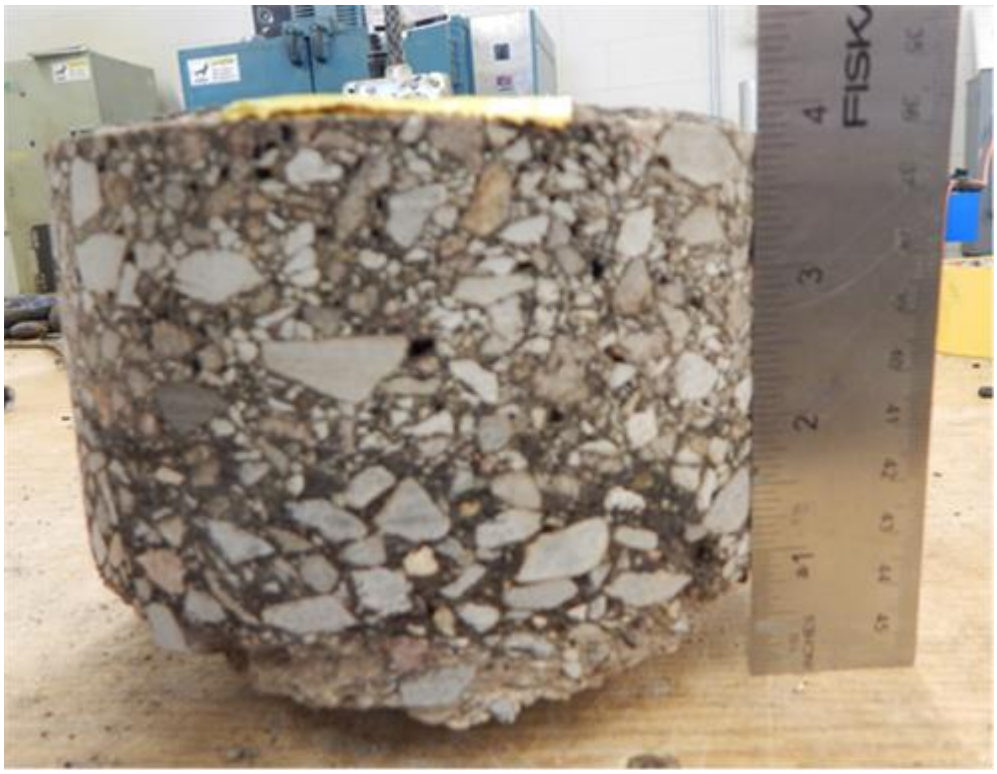

Figure D11 Field Core from Section 11

Figure D12 Field Core from Section 12

Figure D13 Field Core from Section 13

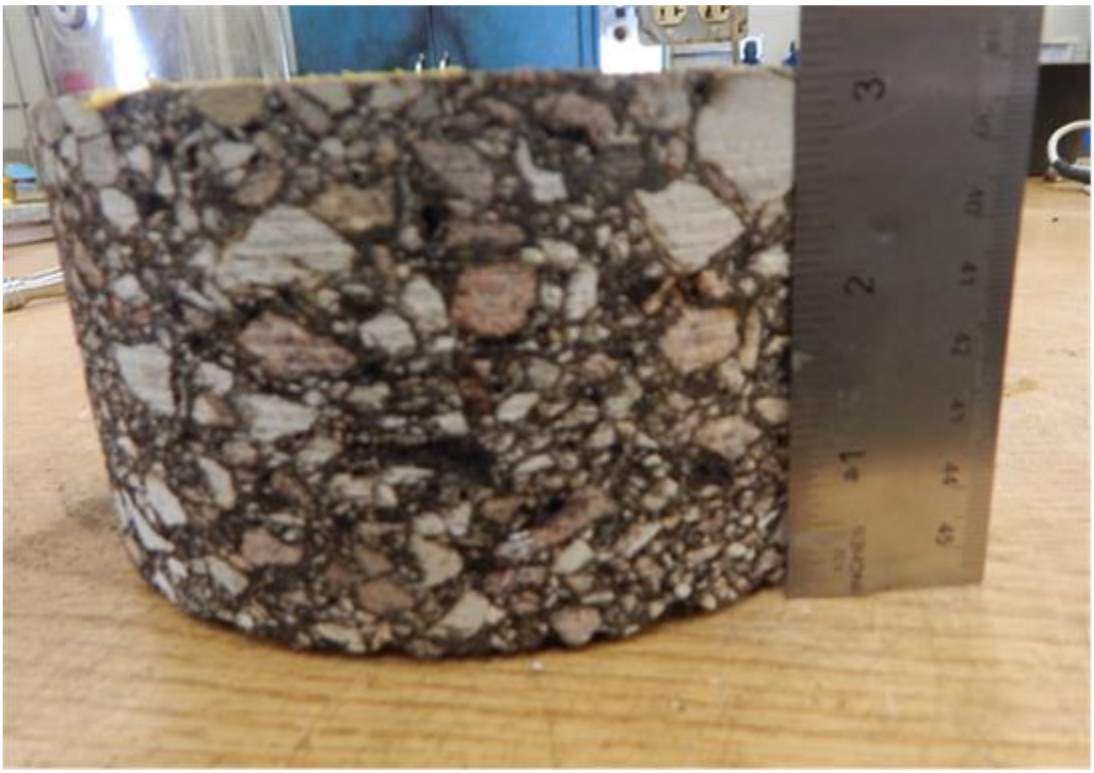

Figure D14 Field Core from Section 14

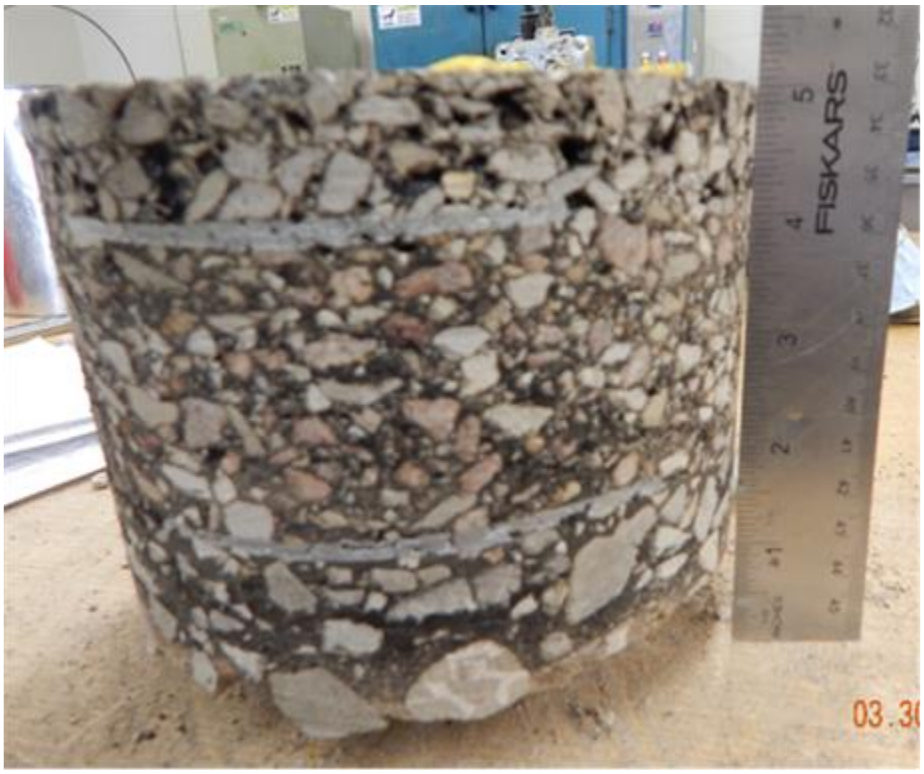

Figure D15 Field Core from Section 15

Figure D16 Field Core from Section 16

Figure D17 Field Cores from Section 17: a) Reflection Crack and b) Regular

Figure D18 Section Condition for Section 7: a) View of Pavement Section and b) Typical Cracking Distress

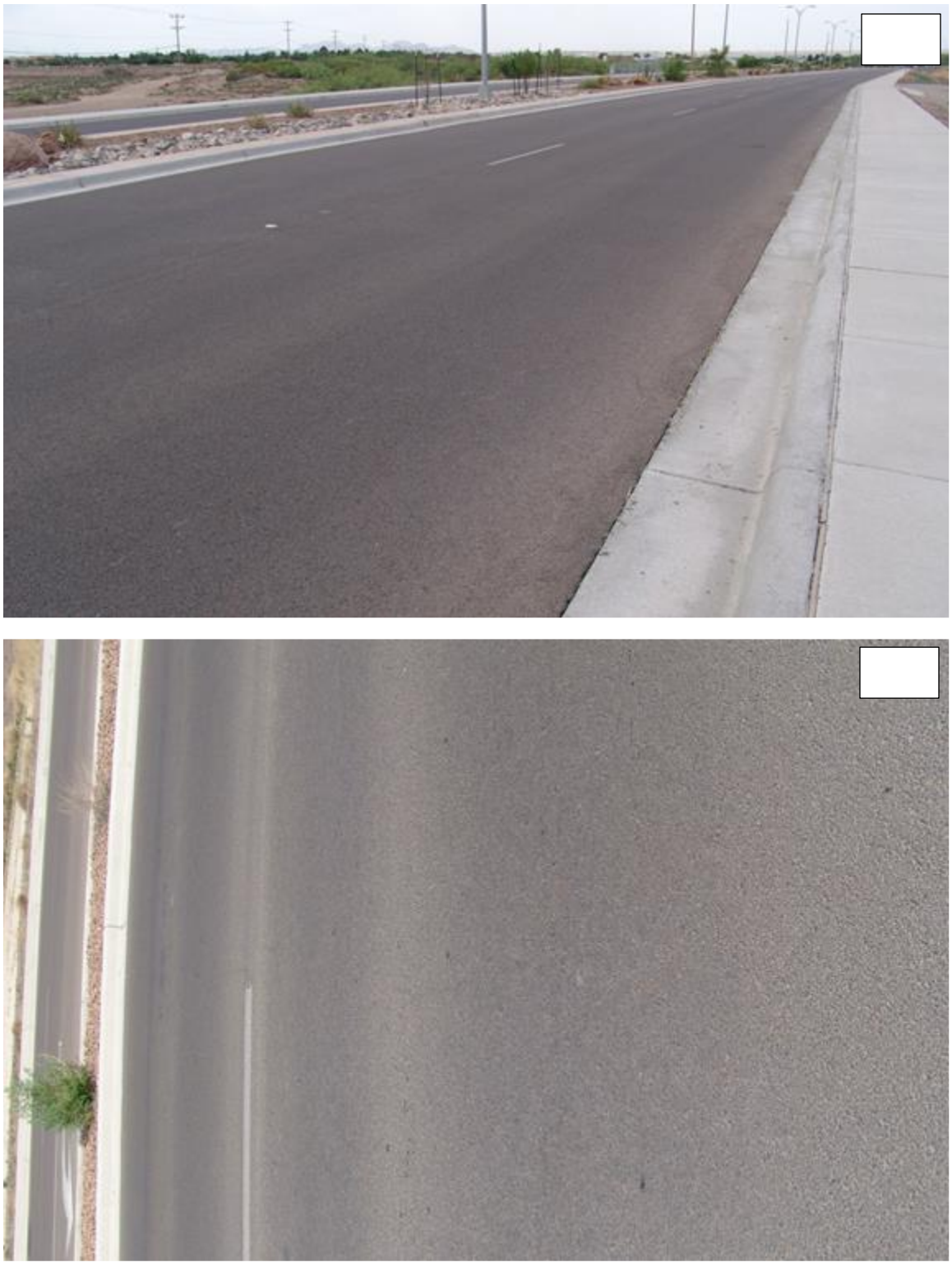

Figure D19 Section Condition for Section 8: a) View of Pavement Section and b) Typical Cracking Distress

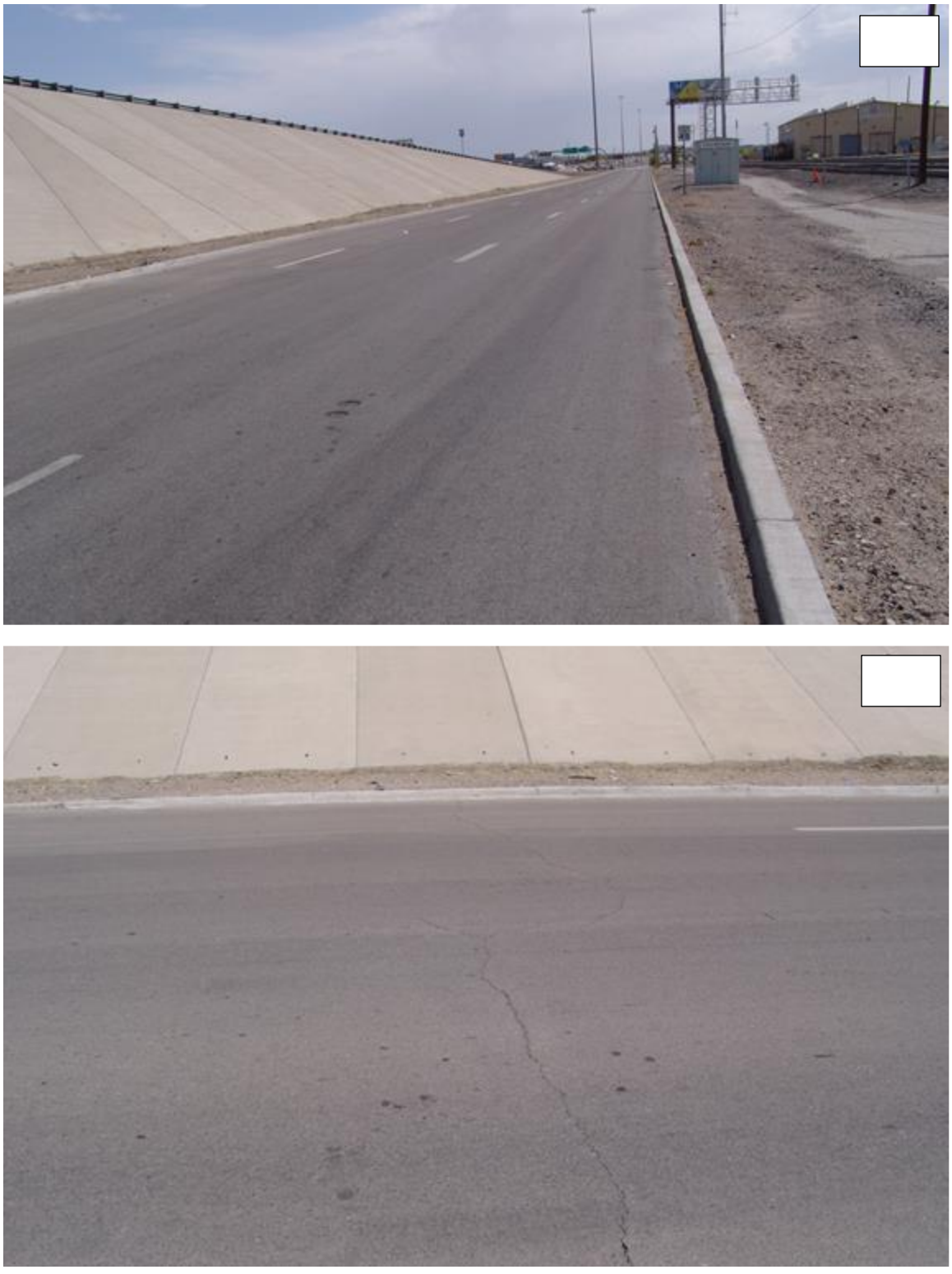

Figure D20 Section Condition for Section 9: a) View of Pavement Section and b) Typical Cracking Distress

Figure D21 Section Condition for Section 10: a) View of Pavement Section and b) Typical Cracking Distress

Figure D22 Section Condition for Section 11: a) View of Pavement Section and b) Typical Cracking Distress

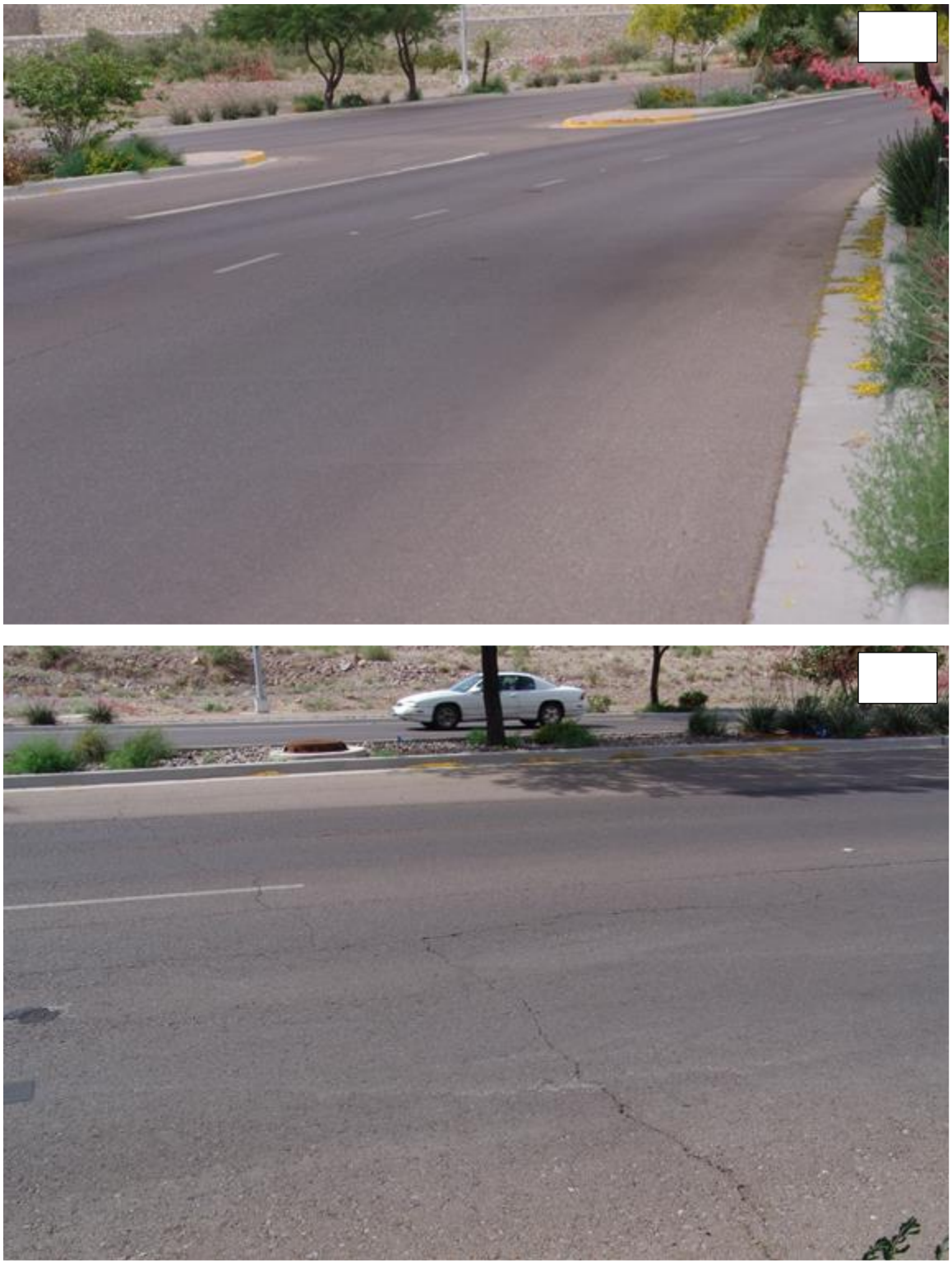

Figure D23 Section Condition for Section 12: a) View of Pavement Section and b) Typical Cracking Distress

Figure D24 Section Condition for Section 13: a) View of Pavement Section and b) Typical Cracking Distress

Figure D25 Section Condition for Section 14: a) View of Pavement Section and b) Typical Cracking Distress

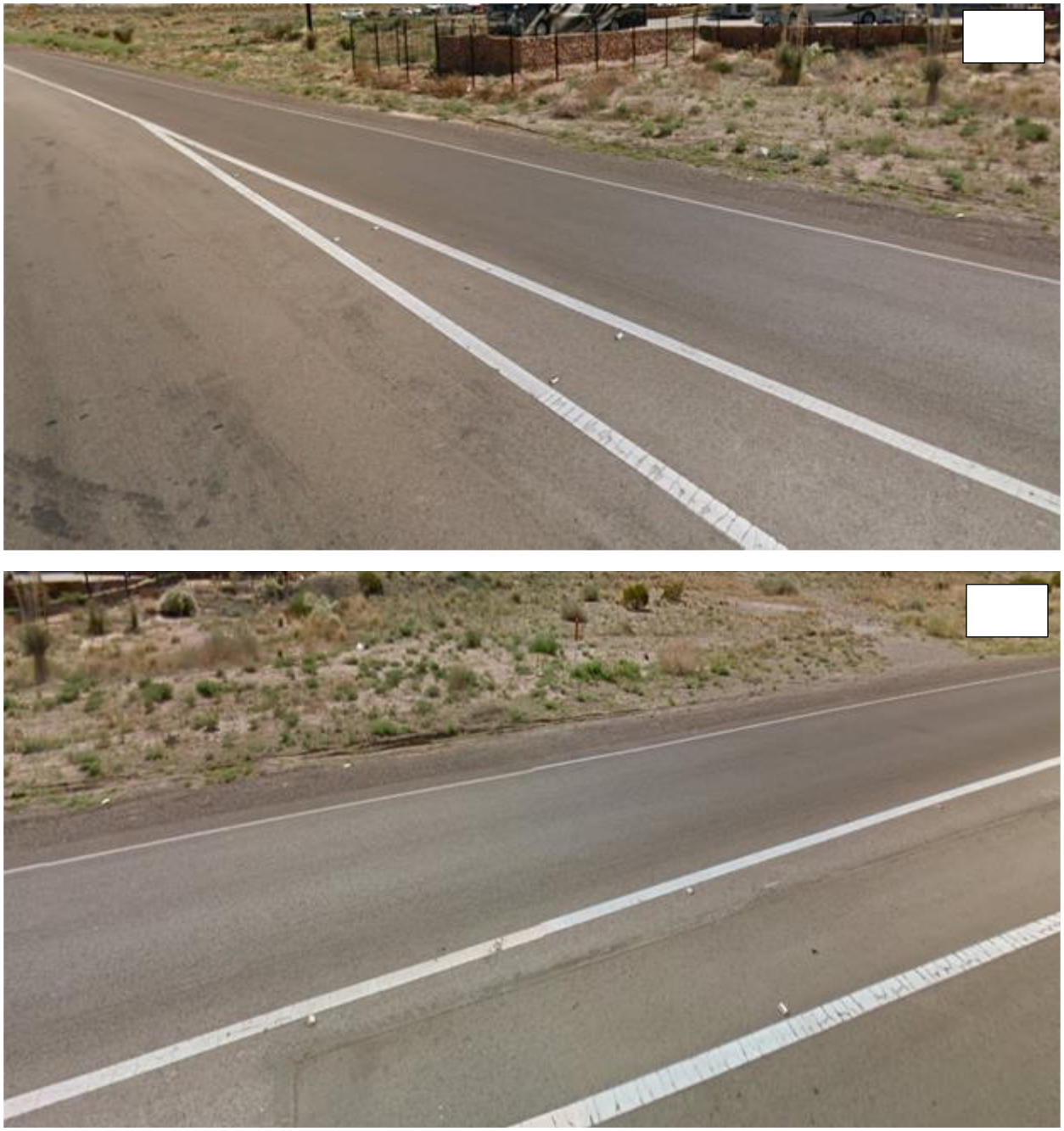

Figure D26 Section Condition for Section 15: a) View of Pavement Section and b) Typical Cracking Distress

Figure D27 Section Condition for Section 16: a) View of Pavement Section and b) Typical Cracking Distress

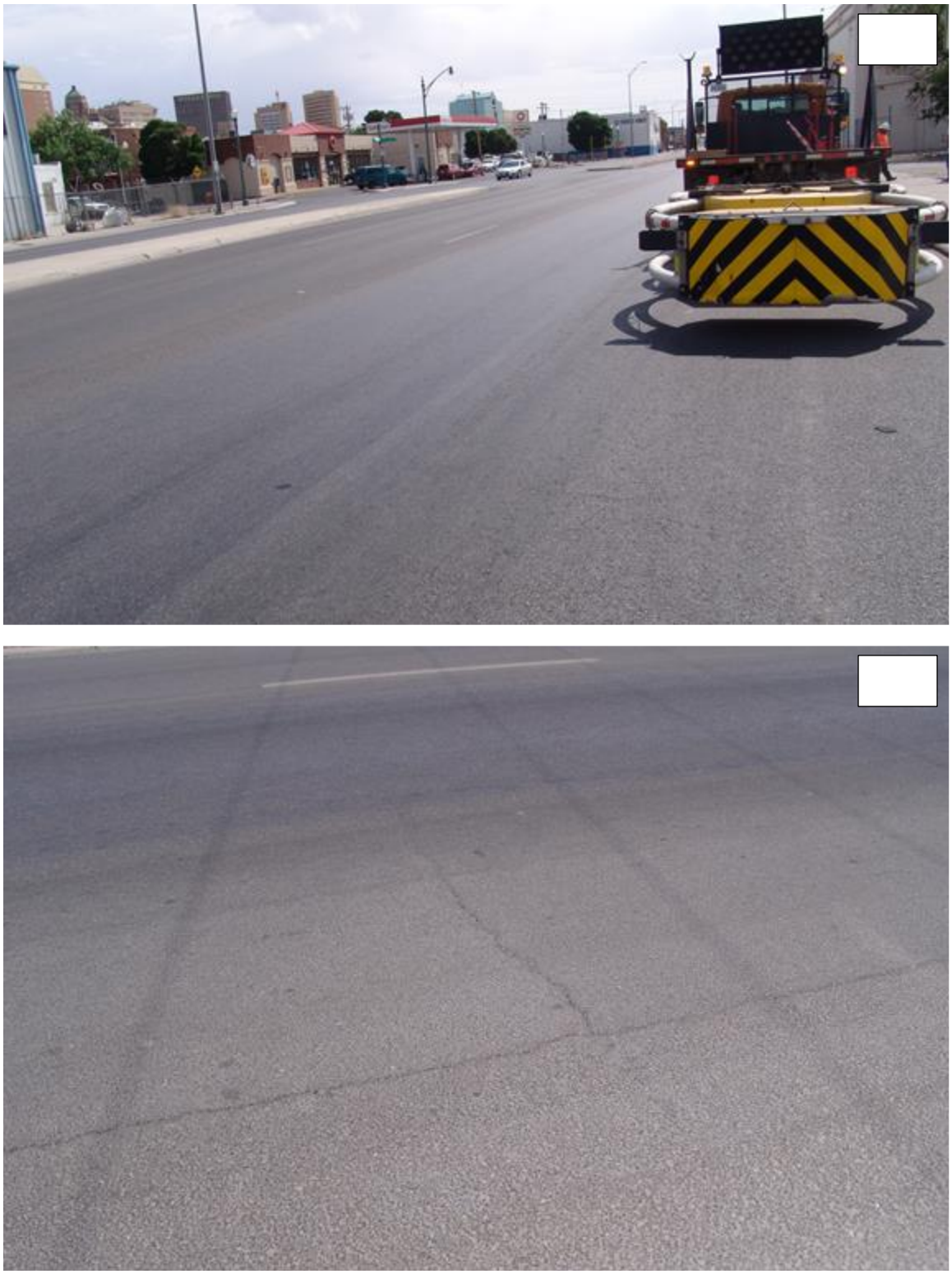

Figure D28 Section Condition for Section 17: a) View of Pavement Section and b) Typical Cracking Distress

Table D1 Results from Lab Specimens for Section 1

Specimen	Max Load, lbs	Work of Fracture, in.-lbs	Critical Fracture Energy, in.-lbs/in.^{2}	Crack Progression Rate	R^2	Number of Cycles to Failure
1	745	10.7	2.4	0.36	1.00	540
2	730	10.9	2.4	0.33	1.00	1000
3	683	10.4	2.3	0.32	1.00	1000
Average	719	10.7	2.4	0.34	1.00	847
Std Dev	26	0.2	0.1	0.01	0.00	217
COV	**4%**	**2%**	**2%**	**4%**	**NA**	**26%**

Table D2 Results from Lab Specimens for Section 2 and 3

Specimen	Max Load, lbs	Work of Fracture, in.-lbs	Critical Fracture Energy, in.-lbs/in.^{2}	Crack Progression Rate	R^2	Number of Cycles to Failure
1	680	12.3	2.7	0.30	1.00	1000
2	628	11.7	2.6	0.30	1.00	1000
Average	654	12.0	2.7	0.30	1.00	1000
Std Dev	26	0.3	0.1	0.00	0.00	0
COV	**4%**	**2%**	**2%**	**NA**	**NA**	**NA**

Table D3 Results from Lab Specimens for Section 4

Specimen	Max Load, lbs	Work of Fracture, in.-lbs	Critical Fracture Energy, in.-lbs/in.^{2}	Crack Progression Rate	R^2	Number of Cycles to Failure
1	478	6.7	1.5	0.37	1.00	635
2	522	5.0	1.1	0.36	1.00	897
3	499	5.5	1.2	0.40	1.00	1000
Average	500	5.7	1.3	0.38	1.00	844
Std Dev	18	0.7	0.2	0.01	0.00	154
COV	**4%**	**12%**	**12%**	**4%**	**NA**	**18%**

Table D4 Results from Lab Specimens for Section 5

Specimen	Max Load, lbs	Work of Fracture, in.-lbs	Critical Fracture Energy, in.-lbs/in.^{2}	Crack Progression Rate	R^2	Number of Cycles to Failure
1	982	10.9	2.4	0.65	1.00	57
2	1012	12.2	2.7	0.69	0.97	31
Average	997	11.6	2.6	0.67	0.99	44
Std Dev	15	0.7	0.2	0.02	0.01	13
COV	**2%**	**6%**	**6%**	**4%**	**1%**	**30%**

Table D5 Results from Lab Specimens for Section 6

Specimen	Max Load, lbs	Work of Fracture, in.-lbs	Critical Fracture Energy, in.-lbs/in.^{2}	Crack Progression Rate	R^2	Number of Cycles to Failure
1	358	6.4	1.4	0.28	1.00	700
2	450	8.2	1.8	0.29	1.00	1000
Average	404	7.3	1.6	0.28	1.00	850
Std Dev	46	0.9	0.2	0.01	0.00	150
COV	**11%**	**12%**	**12%**	**2%**	**NA**	**18%**

Table D6 Results from Lab Specimens for Section 7 and 8

Specimen	Max Load, lbs	Work of Fracture, in.-lbs	Critical Fracture Energy, in.-lbs/in.^{2}	Crack Progression Rate	R^2	Number of Cycles to Failure
1	519	3.6	0.8	0.91	0.99	29
2	528	4.6	1.0	0.98	1.00	20
3	438	3.4	0.7	0.83	1.00	34
4	459	3.7	0.8	1.06	0.99	19
Average	486	3.8	0.8	0.95	0.99	26
Std Dev	38	0.5	0.1	0.08	0.00	6
COV	**8%**	**12%**	**12%**	**9%**	**NA**	**25%**

Table D7 Results from Lab Specimens for Section 9

Specimen	Max Load, lbs	Work of Fracture, in.-lbs	Critical Fracture Energy, in.-lbs/in.^{2}	Crack Progression Rate	R^2	Number of Cycles to Failure
1	533	5.4	1.2	0.55	1.00	128
2	572	5.7	1.3	0.42	1.00	223
3	585	5.5	1.2	0.53	1.00	114
Average	563	5.5	1.2	0.50	1.00	155
Std Dev	22	0.2	0.0	0.06	0.00	48
COV	**4%**	**3%**	**3%**	**11%**	**NA**	**31%**

Table D8 Results from Lab Specimens for Section 10

Specimen	Max Load, lbs	Work of Fracture, in.-lbs	Critical Fracture Energy, in.-lbs/in.^{2}	Crack Progression Rate	R^2	Number of Cycles to Failure
1	381	3.6	0.8	0.61	0.99	192

Table D9 Results from Lab Specimens for Section 11

Specimen	Max Load, lbs	Work of Fracture, in.-lbs	Critical Fracture Energy, in.-lbs/in.^{2}	Crack Progression Rate	R^2	Number of Cycles to Failure
1	507	5.3	1.2	0.54	1.00	268
2	887	8.7	1.9	0.41	1.00	350
3	647	7.8	1.7	0.46	1.00	367
Average	680	7.3	1.6	0.47	1.00	328
Std Dev	157	1.4	0.3	0.05	0.00	43
COV	**23%**	**20%**	**20%**	**11%**	**NA**	**13%**

Table D10 Results from Lab Specimens for Section 12

Specimen	Max Load, lbs	Work of Fracture, in.-lbs	Critical Fracture Energy, in.-lbs/in.^{2}	Crack Progression Rate	R^2	Number of Cycles to Failure
1	686	5.0	1.1	0.61	0.99	121
2	1104	9.0	2.0	1.34	0.99	12
3	951	5.8	1.3	0.76	0.98	58
Average	914	6.6	1.5	0.90	0.99	64
Std Dev	173	1.7	0.4	0.32	0.01	45
COV	**19%**	**26%**	**26%**	**35%**	**1%**	**70%**

Table D11 Results from Lab Specimens for Section 13 and 14

Specimen	Max Load, lbs	Work of Fracture, in.-lbs	Critical Fracture Energy, in.-lbs/in.^{2}	Crack Progression Rate	R^2	Number of Cycles to Failure
1	893	7.8	1.7	1.28	0.99	13
2	892	6.5	1.4	2.34	0.96	6
3	670	4.7	1.0	0.99	0.98	24
Average	819	6.3	1.4	1.54	0.98	14
Std Dev	105	1.3	0.3	0.58	0.01	7
COV	**13%**	**21%**	**21%**	**38%**	**1%**	**52%**

Table D12 Results from Lab Specimens for Section 15

Specimen	Max Load, lbs	Work of Fracture, in.-lbs	Critical Fracture Energy, in.-lbs/in.^{2}	Crack Progression Rate	R^2	Number of Cycles to Failure
1	226	4.2	0.9	0.31	1.00	1000
2	175	3.0	0.7	0.35	0.99	139
Average	201	3.6	0.8	0.33	0.99	570
Std Dev	26	0.6	0.1	0.02	0.01	431
COV	**13%**	**17%**	**17%**	**7%**	**1%**	**76%**

Table D13 Results from Lab Specimens for Section 16 and 17

Specimen	Max Load, lbs	Work of Fracture, in.-lbs	Critical Fracture Energy, in.-lbs/in.^{2}	Crack Progression Rate	R^2	Number of Cycles to Failure
1	682	8.7	1.9	0.37	1.00	354
2	680	7.3	1.6	0.37	1.00	339
3	681	8.6	1.9	0.40	1.00	253
Average	681	8.2	1.8	0.38	1.00	315
Std Dev	1	0.6	0.1	0.02	0.00	44
COV	**0%**	**7%**	**7%**	**4%**	**NA**	**14%**

Vita

Victor Garcia was born in the United States, but spent eighteen years living and studying in Mexico until his high school graduation in 2009. He received his Bachelors of Science in Civil Engineering from The University of Texas at El Paso (UTEP) in December 2014. In summer 2013, he collaborated on a research project funded by the U.S.-Brazil Universities of the Future Consortium to develop sustainable and regenerative engineering solutions for Iracambi research center. During his senior year, he engaged in transportation research at a nationally recognized University Transportation Center (UTC) under prominent civil engineering researcher and mentor, Dr. Soheil Nazarian. He successfully published a paper as a first author on a first tier research journal: *Journal of the Transportation Research Record*. He was also selected as a Transportation Research Board Minority Scholar and a Dwight D. Eisenhower Transportation Fellow.

Mr. Garcia completed a Master's Degree in Civil Engineering in August 2016. While a graduate student, he contributed and developed research projects for Texas Department of Transportation (TxDOT). He has been the author of technical articles that deal with evaluating and developing test protocols to characterize the cracking resistance of asphalt concrete mixtures. He is a member of different student organizations such as, American Society of Civil Engineering (ASCE), and Chi Epsilon National Civil Engineering and Tau Beta Pi Engineering Honor Societies. To pursue his master's degree, Victor Garcia was fortunate to receive funding from a merit-based National Science Foundation (NSF) scholarship, the NSF-S-STEM Graduate Bridge Program for Highly Achieving Engineering and Computer Science from UTEP.

Contact Information: vmgarcia5@utep.edu

This thesis was typed by Victor M Garcia.